# Contents

ASM Sc. J.
Volume 2(1), 2008

## RESEARCH ARTICLES



*Continued on the inside of the back cover.*

ISSN 1823-6782

ASM Science Journal 2(1) 2008

# ASM Science JOURNAL

In Pursuit of Excellence in Science

Vol. 2, No. 1, June 2008 • ISSN : 1823-6782

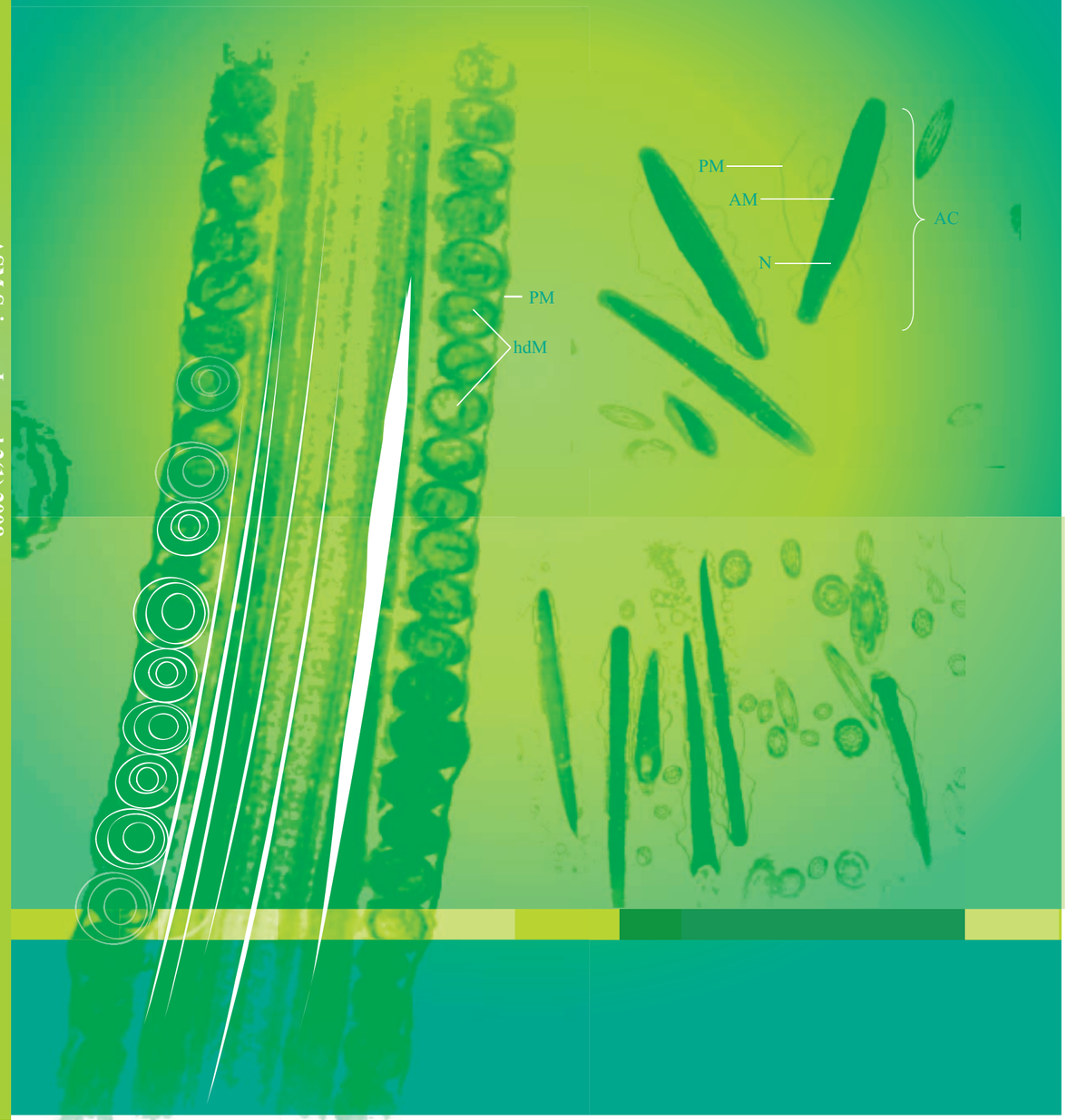

ASM Science
JOURNAL

# Editorial

The *ASM Sc. J.* has come of age. With a total of nearly 300 pages of text in three issues, it is now in the second year of publication. In this first issue of the second volume, there is again evidence of a multi-disciplinary blend of articles/topics on medicine, expert systems for diagnosis of breast diseases, ultra-wideband signals, chemical reaction analysis, application of nanotechnology, nanoporous materials, growth and production of biosurfactants, carbon nanotubes, goat sperm morphology, speech recognition algorithms, alkaline hydrolysis of *N*-(2'-hydroxyphenyl)phthalimide, and mathematics (fractional integral operator)—all contained in a concise manner, contributed by 30 scientists in collaborative R&D work.

The varied and increasing role of computers, computer-based systems, expert and knowledge-based systems, simulation and mathematical modelling in industry, science and medicine is also evident in various articles in this issue.

The next issue *(ASM Sc. J.*, vol. 2, no. 2) will contain 10 articles on photonics—this being a feature in this Journal, as mentioned in the *Editorial* of the maiden issue, where periodically there will be a concentration of articles on particular thematic subject areas.

In attracting and insuring the publication of a wide variety of articles on scientific topics, the Academy of Science Malaysia continues to fulfil its objective of promoting and harnessing science, technology and innovation for the progress of humanity at large. Research opens up wide horizons and new data crowds upon us swiftly. Sharing this knowledge is not only desirable but also vital for knowledge is international and indivisible. The Academy of Science Malaysia continues, therefore, to stress on the importance of publishing research findings.

Md. Ikram Mohd Said
Editor-in-Chief/Chairman, Editorial Board *ASM Sc. J.*

**Cover:**

Design adapted from transmission electron microscopy *Figures 2–4* of article entitled "Ultrastructural Assessment of Fresh, Capacitated and Acrosome-reacted Jermasia Goat Sperm...", pp. 65–73.

Scientists from the Centre for Foundation Studies in Science and the Institute of Biological Sciences, University of Malaya compared the ultrastructural changes in the plasma and acrosomal membranes, mitochondria and axonemal complexes of fresh, capacitated and acrosome-reacted Jermasia goat sperm. Findings provided a general understanding of the complex interrelationships between the sperm movement characteristic with fertilization rate and might possibly provide good guidance to the fertilizability of the sperm.

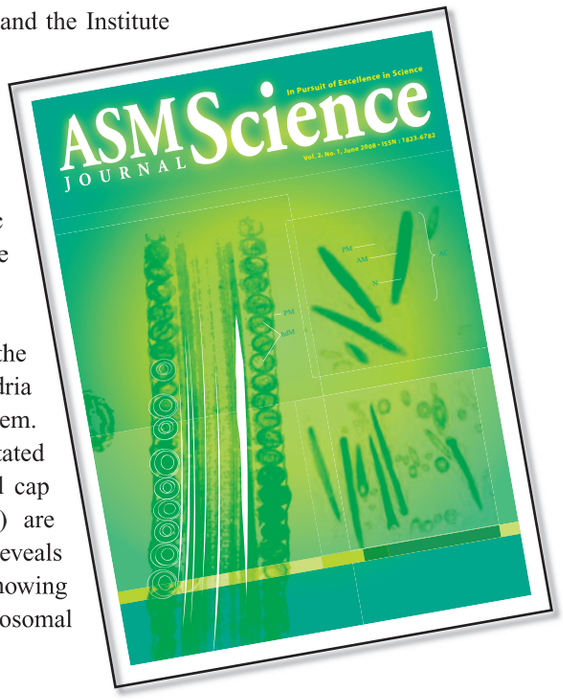


The enlarged design on the left shows the longitudinal section of the fresh sperm midpiece showing rounded and hooded mitochondria (hdM) with plasma membrane (PM) closely juxtaposed to them. Figure on the top right shows a longitudinal section of the capacitated sperm head. The nucleus (N) is surrounded by the acrosomal cap (AC). The plasma (PM) and acrosomal membranes (AM) are swollen. The electron microscopy figure on the bottom right reveals the longitudinal section of the acrosome-reacted sperm head showing dispersion of the acrosomal matrix, ruptured plasma, and acrosomal membranes.

# The Academy of Sciences Malaysia (ASM)

The Academy of Sciences Malaysia (ASM) was established, under the *Academy of Sciences Act 1994* which came into force on 1 February 1995, with the ultimate aim to pursue excellence in science. Thus the mission enshrined is to pursue, encourage and enhance excellence in the field of science, engineering and technology for the development of the nation and the benefit of mankind.

The functions of the Academy are as follows:

- To promote and foster the development of science, engineering and technology
- To provide a forum for the interchange of ideas among scientists, engineers and technologists
- To promote national awareness, understanding and appreciation of the role of science, engineering and technology in human progress
- To promote creativity among scientists, engineers and technologists
- To promote national self-reliance in the field of science, engineering and technology
- To act as a forum for maintaining awareness on the part of the Government of the significance of the role of science, engineering and technology in the development process of the nation and for bringing national development needs to the attention of the scientists, engineers and technologists
- To analyse particular national problems and identify where science, engineering and technology can contribute to their solution and accordingly to make recommendations to the Government
- To keep in touch with developments in science, engineering and technology and identify those developments which are relevant to national needs to bring such developments to the attention of the Government
- To prepare reports, papers or other documents relating to the national science, engineering and technology policy and make the necessary recommendations to the Government
- To initiate and sponsor multi-disciplinary studies related to and necessary for the better understanding of the social and economic implications of science, engineering and technology
- To encourage research and development and education and training of the appropriate scientific, engineering and technical man power
- To establish and maintain relations between the Academy and overseas bodies having the same or almost similar objectives in science, engineering and technology as the Academy
- To advise on matters related to science, engineering and technology as may be requested by the Government from time to time; and
- To carry out such other actions that are consistent with the *1994 Academy of Sciences Act* as may be required in order to facilitate the advancement of science, engineering and technology in Malaysia, and the well being and status of the Academy.

The Academy is governed by a Council. Various Working Committees and Task Forces are charged with developing strategies, plans and programmes in line with the Academy's objectives and functions.

The functions of the Council are:

- To formulate policy relating to the functions of the Academy
- To administer the affairs of the Academy
- To appoint such officers or servants of the Academy as are necessary for the due administration of the Academy
- To supervise and control its officers and servants
- To administer the Fund; and
- To convene general meetings of the Academy to decide on matters which under this Act are required to be decided by the Academy.

The Academy has Fellows and Honorary Fellows. The Fellows comprise Foundation Fellows and Elected Fellows. The Academy Fellows are selected from the ranks of eminent Malaysian scientists, engineers and technocrats in the fields of medical sciences, engineering sciences, biological sciences, mathematical and physical sciences, chemical sciences, information technology and science and technology development and industry.

## The Future

Creativity and innovation are recognised the world over as the key measure of the competitiveness of a nation. Within the context of K-Economy and the framework of National Innovation System (NIS), ASM will continue to spearhead efforts that will take innovation and creativity to new heights in the fields of sciences, engineering and technology and work towards making Malaysia an intellectual force to be reckoned with.



Published by the Academy of Sciences Malaysia

ASM Sci. J., **2(1)**, 1–11

# ROC Analysis of MAMMEX and SOUNDEX — Expert Systems for the Diagnoses of Breast Diseases

U.K. Ngah[1], S.A. Aziz[1], M.E. Aziz[2], M. Murad[2], N.M.N. Mahdi[2], A.Y.M. Shakaff[3], N.A.M. Isa[1], M.Y. Mashor[3] and M.R. Arshad[1]

The incidences of breast cancer have been rising at an alarming rate. Mass breast screening programmes involving mammography and ultrasound in certain parts of the world have also proven their benefits in early detection. However, radiologists may be confronted with increased workload. An attempt has been made in this paper to rectify part of the problems faced in this area. Expert systems based on the interpretation of mammographic and ultrasound images for classifying patient cases could be utilized by doctors (expert and non-expert) in screening. These softwares consist of MAMMEX (for mammogram) and SOUNDEX (for breast ultrasound) could be used to deduce cases according to Breast Imaging Recording and Data System (BI-RADS), based on patients' history, physical and clinical assessment, mammograms and breast ultrasound images. A total of 179 retrospective cases from the Radiology Department, hospital of the University of Science Malaysia, Kubang Kerian, Kelantan were used in this study. A receiver operating characteristic (ROC) curve analysis was implemented, based on the usage of a two-class forced choice of classifying suspicious and malignant findings as positive with normal, benign and probably benign classified as negative. Results yielded an area under the curve (AUC) of 0.997 with the least standard error value of 0.003 for MAMMEX while an AUC of 0.996 with the least standard error of 0.004 was accomplished for SOUNDEX. A system which very closely simulated radiologists was also successfully developed in this study. The ROC curve analysis indicated that the expert systems developed were of high performance and reliability.

**Key words:** expert systems; knowledge-based systems; mammograph; ultrasound, breast cancer; SOUNDEX; MAMMEX; BI-RADS

Breast cancer ranks second to lung cancer, is the most common form of malignancy and leading cause of death amongst women (CAD Breast Cancer 2006). Almost 4000 newly diagnosed cases were recorded in Malaysia in the year 2000. In 2002, out of the 26 089 diagnosed with cancer in Peninsula Malaysia, 55% were cancers among women, of which 30.4% were breast cancer (National Cancer Institute 2003).

Although mechanisms such as prevention, detection and treatment are the steps that may be taken to control the disease, early detection is the most successful method of dealing with the disease. Breast screening is synonymous with early detection (Boyle *et al.* 2005).

Breast screening is not without its problems. The implementation of mass screening would result in increased work load for radiologists which would in turn, result in improper diagnosis. Diagnosticians with the training and experience to interpret mammographic images and breast ultrasounds are scarce. This is further aggravated by the requirement of having two radiologists reading a case in certain practices (Astley 2005). In addition to this, mammography reading is a very arduous skill to learn, requiring years of experience and frequent scrutinizing (Caulkin *et al.* 2000). Training in radiology traditionally involves viewing large numbers of films and a high throughput (approximately 7000 cases per year) needs to be maintained in order for the radiologists to perform well in reading and interpreting the mammograms (Caulkin *et al.* 2000). Issues such as sensitivity and specificity are very crucial and the accuracy of interpreting lesions should be improved (Hadjiiski *et al.* 2004).

Routine and repetitive use of computer-based systems developed for experiments would certainly bring several benefits. Radiologists could be trained to evaluate the perceptual features appropriately (D'Orsi *et al.*1992). The

[1] School of Electrical and Electronic Engineering, Universiti Sains Malaysia, Engineering Campus, 14300 Nibong Tebal, Penang, Malaysia
[2] Radiology Department, Hospital Universiti Sains Malaysia, Kubang Kerian, Kelantan, Malaysia
[3] School of Computer and Communication Engineering, Universiti Malaysia Perlis, Jalan Kangar-Arau, Jejawi, Perlis, Malaysia
* Corresponding author (e-mail: umi@eng.usm.my)

existence of an expert system would make diagnostic expertise more widely and readily available in the clinical community. The availability of this system would facilitate computer-aided study and learning. This system would also prove to be useful in the training of radiologists in the early part of their career. The archiving of knowledge gathered in this area with numerous patient cases would also promote the interpretation of images in a more consistent and standard manner and it may be used periodically as references.

However, a moderate expert system needs about five to ten man-years to build (Negnevitsky 2005). The most crucial stage in the technology is in the process of knowledge acquisition. Focused efforts need to be geared towards the identification of facts that amalgamate the whole knowledge base. Another factor is the arduous task that clinicians and health providers need to undergo in the process of knowledge dissipation. This involves the process of transferring systematically the sketches that are in their minds and eventually documenting it. This would ultimately become knowledge which would form algorithms to culminate in diagnosis.

Numerous studies (Cook & Fox 1987; Wu *et al.*1993; Floyd *et al.*1994; Baker *et al.*1995; Lo *et al.*1999; Chen *et al.*1999; Floyd *et al.* 2000) have been done but none quite exactly fit into what this study is intended to achieve.

## METHODOLOGY

The lack of standardized description and categorization of breast assessment of patients (Elmore *et al.*1994; Baker *et al.* 1999; Berg *et al.* 2000), has contributed towards the existence of the 'Breast Imaging Reporting and Data System', referred to as BI-RADS (D'Orsi 1996; American College of Radiology 1998). Its routine use started in 1997 (Orel 1999) and it was intended to standardize the terminology in reporting, beginning with the mammogram report. This effort was then extended into the other modalities.

On the basis of the level of suspicion, detected lesions or abnormalities could be placed into one of the BI-RADS assessment categories, with the appropriate recommendations for each of the categories (Table 1). Even though its introduction was to help standardize feature analysis and final management of breast modality findings, continued efforts to educate radiologists to promote maximum consistency still need to be done (Lehman *et al.* 2002).

Although tedious, certain guidelines may be adopted that can eventually prove to ease the entire process. The knowledge acquisition process involves three steps which are shown as in Figure 1. These steps are acquiring explanations from the experts, the actual capturing of the knowledge and the organizing of the knowledge. The capturing stage may comprise of the process of documenting the objects, the relations and actions that make up the knowledge. The organization stage would be the process of ordering the knowledge into a form so as to accommodate certain mappings into the knowledge base being developed. The knowledge explanation phase might include conducting interviews, maintaining a healthy interview environment and the awareness of certain do's and dont's that need to be abided by the interviewers. This may also extend into efforts of obtaining knowledge existing in written forms and their capture.

Table 1. The categorization of BI-RADS for breast imaging modalities and the corresponding interpretation categories.

| Classification | BI-RADS Category | Suggested action |
|---|---|---|
| Negative | 1 | Routine examination according to age |
| Benign finding | 2 | Routine examination according to age |
| Probably benign finding | 3 | Follow-up examination within six months |
| Suspicious abnormality | 4 | Biopsy is needed |
| Highly suggestive of a malignancy | 5 | Biopsy is needed |


Figure 1. The knowledge acquisition process, involving three steps.

Knowledge acquisition through a human expert is a delicate task and need to be conducted deliberately. It is therefore paramount that knowledge engineers be equipped with a thorough and well thought out plan. Experience proved that the process would certainly be typically lacking in any organizational format to guide the entire activity. Figure 2 illustrates the complexity of the process of arriving at the domain definition.

The development of the knowledge base is the most important task that the knowledge engineer needs to perform. Hence, stringent and diligent processes are required to produce a systematic, thoughtful procedure in the knowledge-base construction. In this study, the process of knowledge acquisition and knowledge representation proceeded virtually hand in hand. The complete knowledge base or expert system was then gradually developed in an incremental manner. As the system development was based on production rules, decision tables were considered. Different modalities with their associated features form the basis of the formation of rules.

In this study, the BI-RADS classification by the radiologists was used as a benchmark against which MAMMEX and SOUNDEX was tested and the Builder C++ language environment was used.

## THE DEVELOPMENT OF A PROTOTYPE

The process of interpreting mammograms and ultrasounds involved a multifaceted medical decision-making task (Moskowitz 1992). There was a constellation of characteristics, a plethora of features to be considered before a certain conclusion or decision could be made. This required a more thorough investigation of all possibilities and procedures. In addition, there was a poorly structured collection of many isolated facts and it was unclear what kinds of distinctions between the facts were the important ones. The inclusion of heuristic or appropriate methods which did not require perfect data was sometimes necessary. Varying degrees of certainties were also proposed as eventual solutions derived by the systems. Explanations may also be important to infer how the expert system arrived at the answer and for justifications of the knowledge itself. It was therefore preferred that the knowledge be represented through the usage of rules.

Frequent discussions with practicing clinicians and radiologists were necessary for the creation of the rule base. Other efforts in establishing the rules included references through journals and texts on established practices on patients who present themselves with complaints or for routine assessment.

To describe a typical consultation session, questions pertaining to the patient history, clinical and physical assessment, mammographic features and eventually, ultrasound features were displayed when the system was run. These would facilitate decision making at the end, i.e. after the software had obtained all the necessary data. A multiple-choiced type of question displayed a statement ending in a verb. To complete the sentence, the user would be requested to enter the number of the correct choice from amongst the numbered list of possible choice available, with a click on the mouse. Depending on the path designated by the choice of answers, a barrage of questions will continue to be displayed. For example, subsequent questions pertaining to mammogram mass would be deleted if the user found that there was no mass present on mass assessment. Instead, questions pertaining to the next subject matter involving other features (such as calcifications, for example) would ensue.

All questions displayed by the system needed to be answered appropriately. Ultimately, the system would provide the user with a conclusion listing the categories of the BI-RADS for the particular modality. The answer returned by the system will be the highest numeric value from the list associated with the particular category.

The consultation was essentially a search through a tree of goals. The top goal at the root of the tree was the action part of the goal rule, i.e. the suspicious level returned. Subgoals further down the tree included determining the other features involved and seeing if they were significant. Subgoals might in turn have subsubgoals of their own (such as for mammographic features, for example, which would

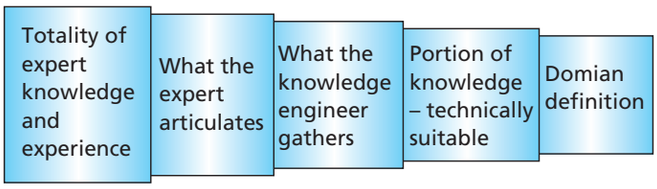


Figure 2. The knowledge acquisition process from the expert.

have questions pertaining to the presence of mass and its details). This special kind of structure called the tree was very useful for representing the way in which goals can be expanded into subgoals by a program. The basic idea was that the root node of the tree represented the main goals, the terminal nodes represented primitive actions that could be carried out and the non-terminal nodes represented subgoals that were susceptible for further analysis.

To facilitate the natural way of designing expert systems for analysis and interpretation, the Forward Chaining Search and Inference Technique with pruning were taken as the technical term to describe the search strategy implied in this study. This meant that the process began with certain data concerning the category that was most likely; for example, its mass features (if any), calcification features (if any) and so on. These data, along with the constraints, served to highlight the potential alternatives and to decimate the unlikely ones. This was consistent with the way a domain expert would react when confronted with patients' cases as they arrive at the hospital for check-up. The expert first will need to gather some information and then try to infer whatever that may be inferred from the information. Thus the search would ultimately arrive at a listing from which a final selection was made based upon the highest score. The pruning process resulted in a reduction in search requirements.

An attempt had also been made to incorporate patients' images to be included in the expert system developed to allow for image manipulations and processing.

## KNOWLEDGE ACQUISITION AND ENGINEERING

The consensus of three radiologists (one being the head of radiology department; another, the head of the mammography unit and the other, an intern) were obtained comprising the premises suggested in Tables 2, 3, 4 and 5. The premises used in the classifier system for patient history are listed in Table 2 while the premises used in the physical and clinical assessment are shown in Table 3. The premises concerning the mammographic assessment are listed in Table 4. Lastly, the premises for the ultrasound assessment are laid out in Table 5.

Each modality and its various features required a substantial amount of digging and fact-finding efforts numerous papers were mined. To determine reasonable

Table 2. The premises used in the classifier system for a patient's history.

| Concensus of radiologists | Premises |
|---|---|
| 1. | The patient's age is — (20–29, 30–39, 40–49, 50–59, greater than 60, not available) |
| 2. | Patient's age of menarche — (9–10, 11–12, 13–14, 15–16, greater than 17, not available) |
| 3. | Patient has menopause — (yes, no, not available) |
| 4. | If patient is menopause than age of onset — (30–39, 40–49, 50–59, not available) |
| 5. | Patient's marital status — (married, single, divorced) |
| 6. | Number of children that patient has is (none, less than 5, more than 5, not available) |
| 7. | Patient has history of breast feeding — (yes, no, uncertain) |
| 8. | Patient lactating or nursing recently — (yes, no, not known) |
| 9. | Patient has other family members with history of cancer i.e. ovarian, prostate cancer — (yes, no, uncertain) |
| 10. | Patient has previous abnormal breast biopsy i.e. atypical ductal hyperplasia — (yes, no, uncertain) |
| 11. | Patient has previous history of breast trauma — (Yes, no, uncertain) |
| 12. | Patient has previous breast surgery/implant — (yes, no, uncertain) |
| 13. | If patient has had history of breast surgery, then surgery is — (mastectomy, lumpectomy, others) |
| 14. | Patient is on hormone replacement therapy ('HRT') — (yes, no, not available)) |
| 15. | Patient had an oophorectomy or TAHBSO done — (yes, no, not available)) |
| 16. | Patient is on contraceptive pills — (yes, no, not available) |
| 17. | Patient has history of extramammary malignancy — (yes, no, not available) |

numerical values associated with each and every factor making up the sections in MAMMEX and SOUNDEX. Each and every piece of information relating to the main modalities had to be investigated and unearthed. A more reliable numerical value could then be found and used in the eventual knowledge-based system to be developed.

### Use of Decision Tables and Collating Past Work

Prior to actually embarking on fact finding, decision tables were developed. The decision tables accommodated the various previous studies that were based on each and every characteristic of the overall processes involved in breast assessment. Considering the case for the mammographic feature assessment and referring to Table 6, for example, the presence of mass which related to the mass margin would entail the search for facts in previous work related to it. Then, these premises would be listed in the left hand side of the table, making up the rows. The top headers of the table would be in the form of columns whereby resources and previous studies found to support evidences on the characteristics mentioned, would be recorded.

For each of the previous studies, the positive predictive values (PPV) for the associated benign and malignant features mentioned in the resources for the associated premises were entered accordingly in the appropriate cells of the decision table. While certain studies focused on benign features only, some studies dealt mainly with the malignant features while others scrutinized on a much broader basis, enveloping the benign as well as the malignant features.

The means of the positive predictive values were then calculated for the benign and malignant values after 'exhaustive' searching previous works. Eventually, values pertaining to the benign and malignant cases began to surface. These emerging values were then taken to represent the possible range of certainty values for the benign and malignant values, each differing in the different features for the different modalities. Table 6 depicts this transparently, showing a sub-section of the eventual whole decision table.

The decision table in its entirety represented a method for visualizing the large number of possible situations in a single table. From the decision table, rules could then be created directly, allowing the knowledge base or expert system to be constructed and developed. This accommodated certainty values to be formulated based upon the fact findings from the collection of referred papers on the various parameters. Work then ensued in the direction of determination of the framework of the knowledge-based system i.e. constructing the backbone of the entire system in the set of decision tables.

Table 3. The premises used in the classifier system for the physical and clinical assessment of a patient.

| Concensus of radiologists | Premises |
|---|---|
| 1. | The lump is palpable — (yes, vague lump, no, uncertain) |
| 2. | The nature of the lump is — (firm, hard, soft, uncertain) |
| 3. | The lump is mobile — (yes, no, mobility is uncertain) |
| 4. | The location of the lump is — (upper outer-quadrant, upper inner-quadrant, lower outer-quadrant, lower inner-quadrant, retroareolar, inner-middle, outer-middle, upper-middle, lower-middle, uncertain) |
| 5. | There is nipple retraction — (yes, no, uncertain) |
| 6. | Presence of nipple discharge — (yes, no, uncertain) |
| 7. | If there is nipple discharge then discharge is — (from one breast and one orifice, not from one breast one orifice, uncertain from one breast, one orifice) |
| 8. | If there is nipple discharge, then discharge is — (white, yellowish, greenish-grey, clear serous, bloody, uncertain) |
| 9. | Discharge is with pus — (yes, no, not available) |
| 10. | Mass is present in axilla — (yes, no, uncertain) |
| 11. | There is breast tenderness/pain — (yes, no, not available) |
| 12. | If there is breast tenderness/pain then it is — (localized, diffused, uncertain) |
| 13. | There is/are skin changes — (yes, no, not available) |
| 14. | If there is skin change then skin change is — (retraction/puckering, skin oedema, ulcer, others) |

## RECEIVER OPERATING CHARACTERISTICS CURVES

The receiver operating characteristics (ROC) was chosen for analysis because it is the state-of-the-art method for testing diagnostic tools especially in the medical field (Ifeachor *et al.* 2004; Obuchowski 2004; Obuchowski 2003). Moreover, it is independent of the size of the sample data.

An important performance indicator of the ROC curve is the area under the curve (AUC). The AUC provides a measure of the performance independent of any threshold and indicates that the larger its value, the better the diagnostic examination. Another factor to be taken into consideration is the standard error (SE). The smaller the standard error, the better is the performance for the test in question. ROC curves allow the diagnosis given by an intelligent system to be compared to a 'bench mark' diagnosis or 'gold standard' provided by clinical experts.

The graph plots, the AUC and SE for this study were conducted using the SPSS software version 14, based upon the five category scales (Langlotz 2003) of the BI-RADS.

Table 4. The premises used in the classifier system pertaining to mammogramic features.

| Concensus of radiologists | Premises |
|---|---|
| 1. | Mass/Masses present is — (positive, negative, uncertain) |
| 2. | The location of the mass is — (upper outer quadrant, upper inner quadrant, lower outer quadrant, lower inner quadrant, retroareolar, inner-middle, outer-middle, upper-middle, lower-middle, uncertain location) |
| 3. | The margin of the mass is — (well defined, sharp halo, microlobulated, macrolobulated, ill-defined, irregular, obscured, uncertain) |
| 4. | The shape of the mass is — (round, oval, irregular, stellate, uncertain) |
| 5. | The size is — (less than 1.0 cm, equal to 1.0 cm, greater than 1.0 cm, uncertain) |
| 6. | The density of the mass — (fat density, low density, isodense, high, has central lucency) |
| 7. | The mass are — (multicentered, multifocused, multicentred/multifocused, uncertain) |
| 8. | If the mass is multicentred or multifocused, then they are also bilateral — (yes, no) |
| 9. | There is no architectural distortion — (yes, no, uncertain) |
| 10. | There is skin thickening — (yes, no, uncertain) |
| 11. | There is nipple retraction/abnormality — (yes, no, uncertain) |
| 12. | Calcifications are present — (yes, no, uncertain) |
| 13. | The calcification is — [micro, macro, mixed (micro, macro), uncertain] |
| 14. | The morphology of calcifications are — (lucent-centered, parallel tracks/linear tubular, coarse/popcorn like, large rod-like, round, eggshell/rim, milk of calcium, suture calcifications, dystrophic, punctate, amorphous/indistinct, granular sand-like, pleomorphic/heterogeneous/granular, fine linear/fine linear branching/casting) |
| 15. | The calcification distribution is — (grouped/cluster, linear, segmental, regional, diffused/scattered) |
| 16. | The number of calcifications per cubic cm is — (1, less than 5, greater than 5, uncertain) |
| 17. | There is presence of node in axilla — (yes, no, uncertain) |
| 18. | There are multiple nodes — (yes, no, uncertain) |
| 19. | The shape of node in axilla is — (round, ovoid/ellipsoid, bean-shaped, slightly lobulated, spiculated, uncertain) |
| 20. | The margins of node is well-circumscribed — (yes, no, uncertain) |
| 21. | Nodes are bilateral — (yes, no, uncertain) |
| 22. | Size of node is — (less than 2.0 cm, more than 2.0 cm, is uncertain) |
| 23. | Node has central lucency — (yes, no, uncertain) |

## CASE STUDIES

In this study, data were obtained from the Radiology Department of Hospital Universiti Sains Malaysia (HUSM), Health Campus, Kubang Kerian, Kelantan. These were then tested on MAMMEX and SOUNDEX and the results analyzed using the ROC curve analysis, to ascertain whether the diagnostic tools were good or unworthy.

A total of 179 cases (mammographic cases with corresponding ultrasounds) were gathered i.e. cases from the years 2003 until the year 2005, ages between 30 and 60, multiracial background, each with its respective patient history, clinical and physical assessment particulars, mammographic images and their corresponding ultrasound images. Prior to these years, the database of patient images and cases in DICOM format were non-existent.

## RESULTS

Out of the 179 cases, radiologists had classified 52 cases as normal (BI-RADS 1), 73 as benign (BI-RADS 2), 22 as probably benign (BI-RADS 3), 24 as suspicious (BI-RADS 4) and 8 cases as malignant

Table 5. The premises used in the classifier system pertaining to the ultrasound features.

| Concensus of radiologists | Premises |
|---|---|
| 1. | The mass is detected on the ultrasound image — (yes, no, uncertain) |
| 2. | Location of breast mass is — (on the upper outer-quadrant, upper inner-quadrant, lower outer-quadrant, lower inner-quadrant, retroareolar, inner-middle, outer-middle, upper-middle, lower-middle, uncertain) |
| 3. | The shape of the mass is — (round, ovoid/ellipsoid, irregular, lobular, spiculated, uncertain) |
| 4. | The orientation of axis of the mass is — (taller than wide, wider than tall, is almost equal, uncertain) |
| 5. | Overall mass margin is — (smooth/well-circumscribed, gentle lobulations, radial/ductal extension, branch pattern, angular margin, uncertain) |
| 6. | The number of lobulations are — (less than 3, greater than 3, uncertain) |
| 7. | Echo pattern of mass is — (anechoic, hypoechoic, hyperechoic, isoechoic, mixed, uncertain) |
| 8. | Posterior to the mass — (there is acoustic enhancement, normal/no enhancement/shadowing, complete shadowing, uncertain) |
| 9. | The lesion has calcifications — (yes, no, uncertain) |

Table 6. A subset of the decision table.

| Mammogram features | Benign/malignant features | | | | | | | | |
|---|---|---|---|---|---|---|---|---|---|
| | Dronkers *et al.* (2002) | | Hong *et al.* (2005) | Average Benign (1–10) | Average Malignant (1–100) | Liberman *et al.* (1998) | | | Hong *et al.* (2005) |
| Mass margin | | .. | | | | | | | |
| Well defined | 9.00 | .. | 10.00 | 8.30 | 0.39 | 0.90 | .. | | 0 |
| Sharp halo | 9.00 | | | 9.32 | 0.14 | | .. | .. | |
| Micro-lobulated | | .. | 5.00 | 2.67 | 5.65 | 1.70 | | .. | 5.00 |
| Macro-lobulated | | | | 6.60 | 1.50 | | .. | | |
| Ill-defined | 1.00 | .. | 4.00 | 2.83 | 6.77 | 4.40 | | .. | 6.00 |
| Irregular | 1.00 | | | 1.00 | 6.50 | | | .. | |
| Spiculated | | .. | 0.30 | 0.60 | 8.82 | 8.10 | .. | | 9.70 |
| Obscured | | .. | 8.40 | 8.40 | 4.60 | 3.30 | | .. | 1.60 |

(BI-RADS 5) according to the mammographic features assessment. Radiologists also had classified 63 cases as normal (BI-RADS 1), 90 as benign (BI-RADS 2), 12 as probably benign (BI-RADS 3), 8 as suspicious (BI-RADS 4) and 6 as malignant (BI-RADS 5) categories accordingly for the ultrasound features assessment. The screen displays of MAMMEX and SOUNDEX are shown as in Figures 3 and 4.

ROC curve analyses were then conducted. The two-class forced choice classes are grouped along the following positivity thresholds as suggested by Obuchowski (2004) which were:

- Classifying probably benign, suspicious and malignant findings as positive and classifying normal and benign findings as negative (i.e. noted as B1B2 versus B3B4B5 or from now on is known as A); and
- Classifying suspicious and malignant findings as positive with normal, benign and probably benign as negative (i.e. noted as B1B2B3 versus B4B5 or from now on known as known B).

Other positivity thresholds were as suggested by the Head of Radiology Department, HUSM. These were:

- Classifying benign, probably benign, suspicious and malignant findings as positive i.e. abnormal against normal findings as negative (noted as B1 versus B2B3B4B5, known as C),
- Excluding the normal cases and taking suspicious and malignant findings as positive and benign, probably benign as negative (noted as XB1 B2 versus B3B4B5, known as D); and
- Excluding the normal cases and taking the probably benign, suspicious and malignant findings as positive and benign cases only as negative (noted as XB1 B2B3 versus B4B5, known as E).

The results based upon the above mentioned positivity thresholds are tabled as shown in Table 7 for MAMMEX and SOUNDEX.

## DISCUSSIONS

For all the ROC plots, the curves rose well above the diagonal line connecting the points (0,0) and (1,1). These indicated the performance standards of MAMMEX and SOUNDEX.

Evaluations of the AUC also showed favourable outcome. The greatest value for AUC for MAMMEX was for the schema used in category B (AUC value being 0.997, in Table 7) with the least standard error value (0.003). This meant that the ROC curve analysis indicated that the best combination of the two-class forced choice is the B1B2B3 versus B4B5 i.e. classifying suspicious and malignant

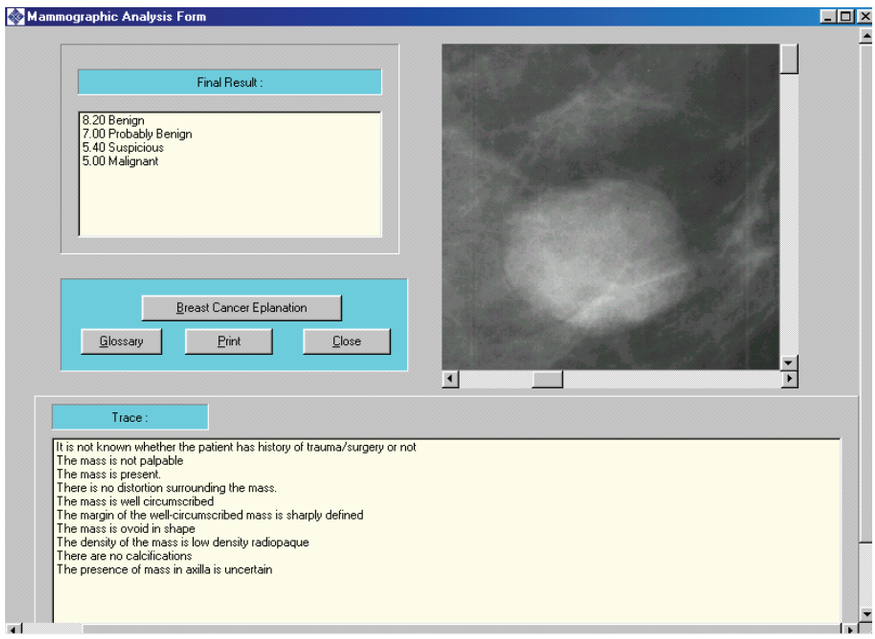


Figure 3. The screen display of MAMMEX.

findings as positive with normal, benign and probably benign as negative. This also indicated that the performance of MAMMEX was best used to distinguish between the normal, benign and probably benign from the suspicious and malignant cases.

For SOUNDEX, the greatest value for the AUC was in category E with zero standard error. This may sound a bit too over-confident. The reason may be because the features distinguishing the normal from the abnormal cases were clear cut and straightforward as the chances of not detecting a lesion on ultrasound was quite remote. The situation for MAMMEX was quite different because the presence of mass and added to it, the possibility of finding microcalcifications was always there. Therefore, the next best result was taken. Again, referring to Table 7 and looking at the next highest AUC category would be schema B having an AUC value of 0.996 which also had the least standard error value (0.004). This ROC curve analysis also indicated that the best combination of the two-class forced choice for SOUNDEX was the B1B2B3 versus B4B5 i.e. classifying suspicious and malignant findings as positive with normal, benign and probably benign as negative. Similarly therefore, the performance of SOUNDEX was best used to distinguish between the normal, benign and probably benign from the suspicious and malignant cases.

For comparison purposes, the performances of other studies were noted. These were namely, the mammographic image analysis study by Cook and Fox (1987); Wu *et al.* (1993); Floyd *et al.* (1994); Baker *et al.* (1995); Lo *et al.* (1999); Chen *et al.* (1999) who all used Artificial Neural Networks (ANN) in their studies. The works by FIoyd *et al*. (2000) who used Cased Based Reasoning (CBR) and Burnside *et al*. (2006) who used Bayesian Network (BN) were also referred. A table listing the performances is shown in Table 8.

Table 7. Tabulation of the AUCs and SE for the different cut-offs in the categories for MAMMEX and SOUNDEX.

| Different curves | AUC for MAMMEX | SE (AUC MAMMEX) | AUC for SOUNDEX | SE (AUC SOUNDEX) |
|---|---|---|---|---|
| A | 0.962 | 0.015 | 0.981 | 0.014 |
| B | 0.997 | 0.003 | 0.996 | 0.004 |
| C | 0.975 | 0.013 | 1.000 | 0.000 |
| D | 0.937 | 0.024 | 0.968 | 0.023 |
| E | 0.996 | 0.005 | 0.993 | 0.006 |

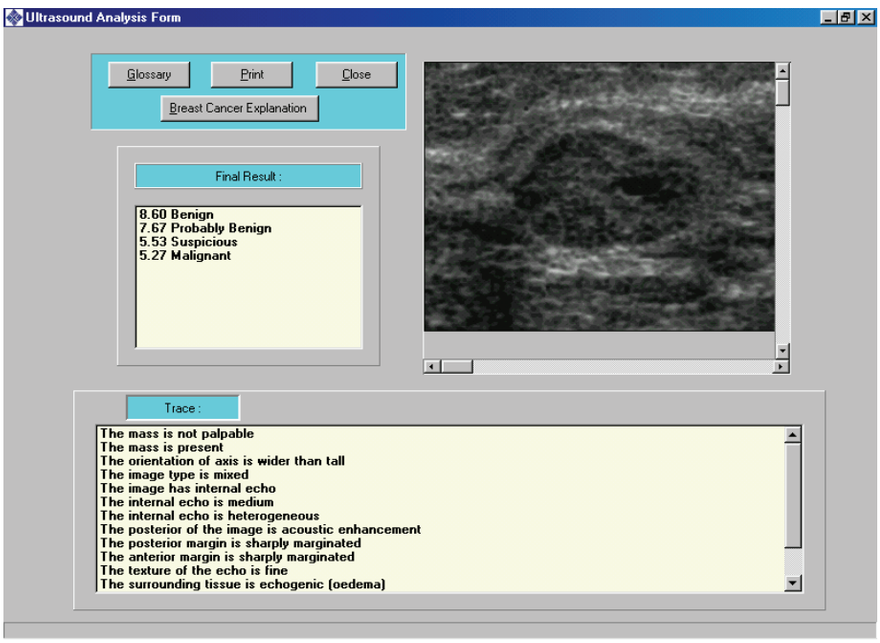


Figure 4. The screen display of SOUNDEX.

Table 8. Comparison of the performance of MAMMEX and SOUNDEX with previous studies.

| Work/Study | Approach | AUC for ROC / Accuracy |
|---|---|---|
| Cook & Fox (1987) | ES | Accuracy of 75% |
| Wu *et al.* (1993) | ANN | 0.95 |
| Floyd *et al.* (1994) | ANN | 0.94 (±0.01) |
| Baker *et al.* (1995) | ANN | 0.89 (±0.02) |
| Lo *et al.* (1999) | ANN | 0.91 (±0.03) |
| Chen *et al.* (1999) | ANN | Accuracy of 95.0% |
| FIoyd *et al.* (2000) | CBR | 0.83 |
| Burnside *et al.* (2006) | BN | 0.919 |
| MAMMEX | ES | Accuracy of 97%, AUC 0.997 (±0.003) |
| SOUNDEX | ES | Accuracy of 99%, AUC 0.996 (±0.004) |

It may be observed that the performances of MAMMEX and SOUNDEX are comparable to the other studies.

## CONCLUSION

A BI-RADS based mammographic and ultrasound expert system for breast diseases was successfully developed in this study (MAMMEX and SOUNDEX). The ROC curve analysis indicated that the expert systems developed were of high performance and reliability.

## ACKNOWLEDGEMENT

The authors wish to thank Universiti Sains Malaysia (USM) for the RU grant 1001.pelect.814012 and the Ministry of Science, Technology and Innovations of Malaysia (MOSTI) for providing the necessary grant (IRPA 06-02-05-2188EA007) for this work.

*Date of submission: March 2007*
*Date of acceptance: March 2008*

## REFERENCES

American College of Radiology 1998, *Breast imaging reporting and data system (BI-RADS)*, 3rd edn. Restem.

Astley, SM 2005, 'Evaluation of Computer-Aided Detection (CAD) prompting techniques for mammography', *British Journal of Radiology*, Special Issue, vol. 78, S20–S25.

Baker, JA, *et al.* 1999, 'Sonography of solid breast lesions: observer variability of lesion description and assessment', *Am. J. Roentgenol.*, vol. 172, no. 6, pp. 1621–1625.

Baker, JA, *et al.* 1995, 'Breast cancer: prediction with artificial neural network based on B-RADS standardized lexicon', *Radiology,* vol. 196, pp. 817–822.

Berg, WA, *et al.* 2000, 'Breast imaging reporting and data system: inter- and intraobserver variability in feature analysis and final assessment', *American Journal of Roentgenology,* vol. 174, pp. 1769–1777.

Boyle, UVP, Goldhirsch, A, Orecchia, R, & Viale, G 2005, 'Breast cancer', *The Lancet,* vol. 365, pp. 1727–1741.

Burnside, ES, *et al.* 2006, 'Bayesian network to predict breast risk of mammographic microcalcifications and reduce number of benign biopsy results: initial experience', *Radiology*, vol. 240, pp. 666–673.

CAD Breast Cancer 2006, viewed December 2007, <http://www2.enelucalgary.ca/People/Ranga/cadmam.html>.

Caulkin, SJ & Astley, SM 2000, 'Generating realisitic spiculated lesions in digital mammograms', in *5th. International Workshop on Digital Mammography (IWDM 2000),* Ed. MJ Yafe, Toronto, Canada, Medical Physics Publishing, Madison, Wisconsin, pp. 713–720.

Chen, DR, Chang, RF & Huang, YL 1999, 'Computer-aided diagnosis applied to US of solid breast nodules by using neural networks', *Radiology*, vol. 213, pp. 407–412.

Cook, HM & Fox, MD 1987, 'Artificial intelligence applied to mammographic image analysis', *Electronic imaging,* Boston, USA.

D'Orsi, CJ 1996, 'The american college of radiology mammography lexicon: an initial attempt to standardize terminology', *Am. J. Roentgenol.,* vol. 166, pp. 779–780.

D'Orsi, CJ, *et al.* 1992, 'Reading and decision aids for improved standardization of mammographic diagnosis', *Radiology,* vol. 184, pp. 619–622.

Elmore, G, *et al.* 1994, 'Variability in radiologists' interpretations of mammograms', *The New England Journal of Medicine*, Dec. 1994, pp. 1493–1439.

Floyd, CE, Lo, J Y & Tourassi, GD 2000, 'Case-based reasoning computer algorithm that uses mammographic findings for breast biopsy decisions', *Am. J. Roentgenol.,* vol. 175, pp. 1347–1352.

Floyd, CE, *et al.* 1994, 'Prediction of breast cancer malignancy using an artificial neural network', *Cancer,* vol. 74, no. 11, pp. 2944–2948.

Hadjiiski, L, *et al.* 2004, 'Improvements in radiologists' characterization of malignant and benign breast masses on serial mammograms with computer-aided diagnosis: an ROC study', *Radiology*, vol. 233, pp. 255–265.

Ifeachor, EC & Hamadicharef, B 2004, 'ROC analysis in the evaluation of intelligent medical systems', in *1st European Workshop on the Assessment of Diagnostic Performance*, viewed August 2004, <http://www.tech.plym.ac.uk/spmc/brahim/pdf/EWARDP2004.PAPER02.P#_#@.IFEACHOR.pdf>.

Langlotz, CP 2003, 'Fundamental measures of diagnostic examination performance: usefulness for clinical decision making and research', *Radiology,* vol. 228, pp. 3–9.

Lehman, C, *et al.* 2002, 'Use of the American college of radiology bi-rads guidelines by community radiologists: concordance of assessments and recommendations assigned to screening mammograms', *Am. J. Roentgenol.*, vol. 179, pp. 15–20.

Lo, JY, *et al.* 1999, 'Predicting breast cancer invasion with artificial neural networks on the basis of mammographic features', *Radiology,* vol. 203, pp. 159–163.

Moskowitz, M 1992, 'Positive predictive values for mammographically detected carcinomas', Letters, *Am. J. Roentgenol.,* vol. 158, pp. 688.

National Cancer Institute 2003, viewed September 2007, <http://jncicancerspectrum.oupjournals.org/cgi/content/full/jnci;95/171>.

Negnevitsky, M 2005, *Artificial intelligence – a guide to intelligent systems*, 2nd edn, Addison Wesley, Essex, England.

Obuchowski, NA 2003, 'Receiver operating characteristic curve and their use in radiology', *Radiology*, vol. 229, pp. 3–8.

Obuchowski, NA 2004, 'Fundamentals of clinical research for radiologists', *Am. J. Roentgenol.,* vol. 184, pp. 364–372.

Orel, SG, *et al.* 1999, 'BI-RADS categorization as a predictor of malignancy', *Radiology*, vol. 211, no. 3, pp. 845–850.

SPSS 2005, SPSS version 14, SPSS Inc, <http://spss.com>.

Wu, Y, *et al.* 1993, 'Artificial neural in mammography: application to decision making in the diagnosis of breast cancer', *Radiology*, vol. 187, pp. 81–67.

ASM Sci. J., **2(1)**, 13–22

# Performance of Ultra-wideband Systems in the Presence of WiFi and 3G Signals

A.S. Rashid[1], S. Khatun[1], B.M. Ali[1] and A.M. Khazani[1]

An analysis of the power spectral density of ultra-wideband (UWB) signals is presented in order to evaluate the effects of cumulative interference from multiple UWB devices on victim narrowband systems in their overlay bands like WiFi (i.e. IEEE802.11a) and 3rdG systems (Universal mobile telecommunications system/ wideband code division multiple access). In this paper, the performances are studied through the bit-error-rate as a function of signal-to-noise ratio as well as signal-to-interference power ratio using computer simulation and exploiting the realistic channel model (i.e. modified Saleh-Valenzuela model). Several modifications of a generic Gaussian pulse waveform with lengths in the order of nanoseconds were used to generate UWB spectra. Different kinds of pulse modulation (i.e. antipodal and orthogonal) schemes were also taken into account.

**Key words:** ultra-wideband; co-existence; in-band interference; UMTS/WCDMA; WiFi; Federal Communications Commission

Ultra-wideband (UWB) technology plays a key role in short-range wireless connectivity. This is due to the potential advantages of UWB transmissions such as low power consumption, very high data rate, immunity to multipath fading, less complex transceiver hardware, and location capabilities. UWB systems spread the transmitted signal power over an extremely large frequency band (minimum 528 MHz), and the power spectral density of the signal is very low (maximum –41dBm/MHz). As a result, UWB systems operate over dedicated spectrum bands already occupied by other narrowband (NB) systems (Sadler & Swami 2004). In April 2002 the Federal Communications Commission (FCC) released UWB emission masks and introduced the concept of co-existence with traditional and protected radio services in the frequency spectrum which allowed the operation of UWB systems mainly in the 3.1 GHz to 10.6 GHz band, limiting the power level emission to –41dBm/MHz (Federal Communications Commission 2002). In March 2005, the FCC granted the waiver request filed by the Multiband OFDM Alliance (MBOA) approving the change in measurement for the all UWB technologies (neutral approach)(Federal Communications Commission 2005). The FCC's waiver grant effectively removes the previous transmitting power penalties for both frequency-hopping and gated UWB technologies (TH and DS) which can transmit at higher power levels and then sit quiet, as long as they still meet the same limits for average power density. Table 1 shows the new FCC waiver rules (Tao, Yong & Kangsheng 2003).

There are many parameters that influence how a UWB system would interfere with a narrowband system. In particular, it was found that the UWB modulation, pulse repetition frequency (PRF), center frequency of the narrowband system, and the structure of narrowband receiver (i.e. matched filter) influenced the impact of the UWB system on narrowband receiver performance (Bora & Jana 2003).

This paper focuses on the unlicensed WiFi 5.3 GHz industrial, scientific and medical (ISM) bands and UMTS/ WCDMA (in frequency domain FDD uplink allocated between 1.92 GHz and 1.98 GHz) as narrowband systems, both overlapping the FCC UWB spectrum which evaluate into accurate methods for bit error-ratio (BER) calculation as given for different modulation schemes under the Rayleigh multipath channel model. The result was verified by Monte Carlo simulations. Furthermore, in our work, we gave guidance on the configuration of co-existing UWB signals with NB systems as future work.

## UWB SYSTEM MODEL

### Signal Model

There are many UWB pulse waveform candidates (i.e. Hermite, Prolate Spheroidal Wave Functions, etc.). In our work we adopted the Gaussian doublet, a pair of separated narrow Gaussian's monocycles, which contain a positive

[1] Department of Computer and Communications Systems Engineering, Engineering Faculty, Universiti Putra Malaysia, 43400 UPM, Serdang, Selangor, Malaysia

* Corresponding author (e-mail: eng_Rashid@ieee.org)

pulse followed by a negative pulse. This offer two degrees of freedom, time separation between the two pulses in the doublet and time separation between doublets.

The 2nd Gaussian derivative $P_{G2}(t)$ could be expressed as:

$$P_{G2}(t) = A_{G2} \frac{1-(t-\mu)^2/\sigma^2}{\sqrt{2\pi\sigma^2}} \exp\left(-\frac{(t-\mu)^2}{2\sigma^2}\right) \quad (1)$$

where, the parameter σ determined the monocycle width $T_p$. The effective time duration of the waveform that contained 99.99% of the total monocycle energy was $T_p = 7\sigma$ centered at $\mu = 3.5\sigma$. The factor $A_{G2}$ was introduced so that the total energy of the monocycle was normalized to unity, i.e. $\int p_{G2}^2(t)dt = 1$ (the time domain shown in Figure 1and frequency domain shown in Figure 2).

The null frequencies of the Gaussian doublet could be controlled by regulating the position of the second Gaussian pulse (the first pulse $p_0(t)$ began at $t = 0$, the second one $p_1(t)$ began at $t = T_n$). With spectrum analysis, we had:

$$p(t) = p_0(t) - p_1(t) \quad (2)$$

The energy spectral density (ESD) is:

$$|P(\omega)|^2 = 4\pi e.(wt_p^2)^2.e^{-(\omega t_p)^2}.[1-\cos\omega T_n] \quad (3)$$

Since $\omega = 2\pi f$, the null frequencies in ESD were $\pi(2fT_n) = 0, 2\pi,.., 2k\pi..$, then $f = (k/T_n)$, where k = 1, 2....

Conceptually, a pulse-train (which may be dithered to reduce spectral lines, to accommodate user codes, to represent data via pulse position modulation (PPM), and so on) is convolved with the pulse-shape, so that the power

Table 1. Pre- and post-FCC waiver ruling effects.

| FCC new rules | Power requirement | Method of measurement |
|---|---|---|
| Pre-waiver ruling | – 41 dBm/MHz | Power measured in always-on mode |
| Post-waiver ruling | – 41 dBm/MHz | Only average power measured; systems now allowed to burst and then sit quiet |
| Effect | No change; spectrum holders still protected from interference | Both FH and gated UWB systems benefit |

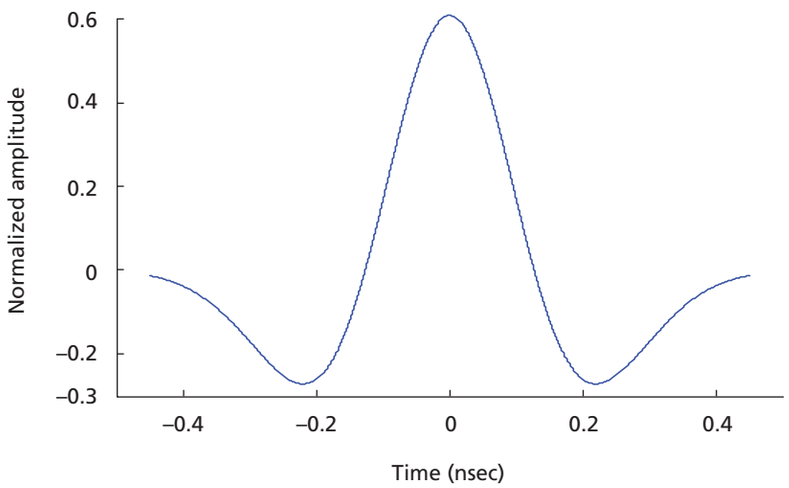


Figure 1. Second derivative of Gaussian pulse.

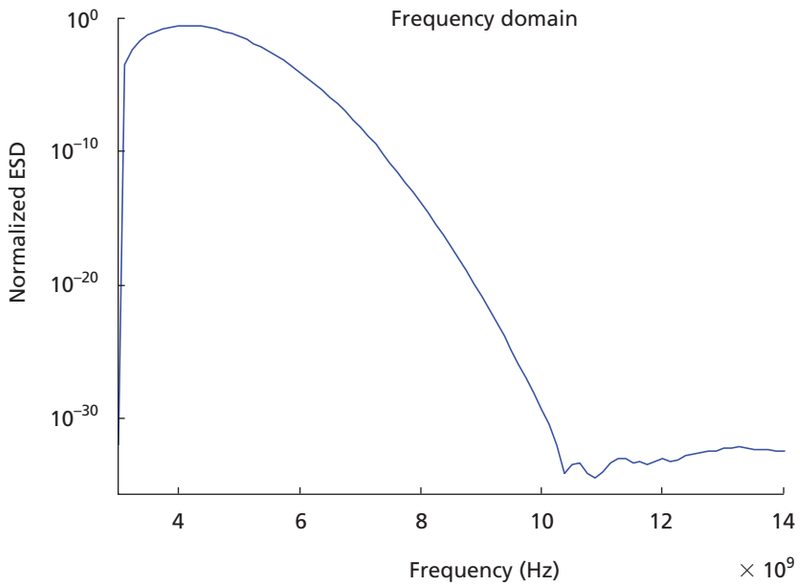


Figure 2. Energy spectral density for second derivative of Gaussian pulse.

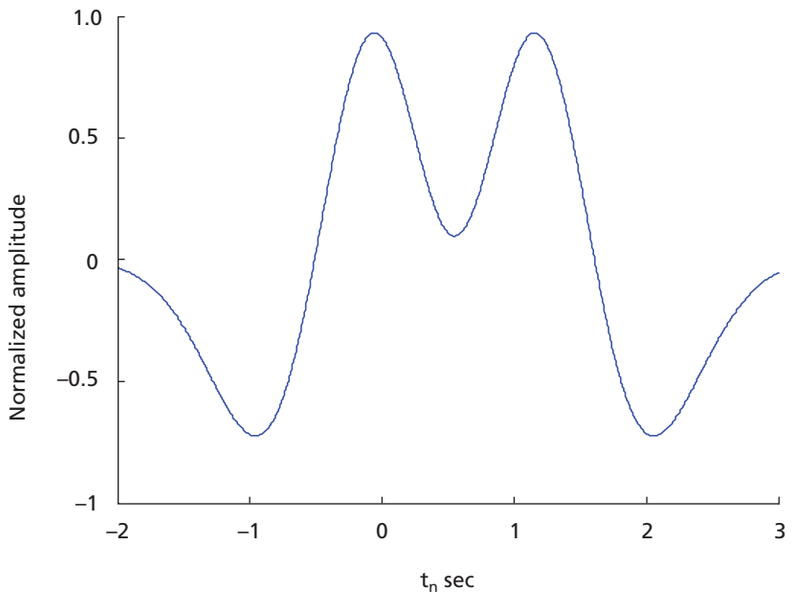


Figure 3. Gaussian doublets with $T_n = 1.1e^{-9}$ sec.

spectrum of the transmitted UWB signal is essentially given by $|P(f)|^2$ (Han & Nguyen 2002). The effect of dithering makes the modulation zero-mean and removes periodicities in the data, so that the PSD = log ESD has no spectral lines. The pulse $p(t)$ and its 'PSD' $|P(f)|^2$ are shown in Figures 3 and 4; notice that the PSD is skewed. It is depicted from Figure 4 that there were notch spectral in the doublet waveform which could be used to mitigate interference to other systems.

The transmitted signal was then given by:

$$x(t) = \sum_{l=-\infty}^{\infty} b_{[l/N_b]} a_{[l/N_{ds}]} \Psi(t - lT_f - c_{[l/N_{th}]} T_c), \quad (4)$$

Where, $N_b$ is the number of consecutive pulses modulated by each data symbol $b_i$, $T_f$ is the pulse repetition period (PRP); $T_c$ is the chip duration which is the unit of additional time shift provided by the TH sequence and $[.], \lfloor . \rfloor$ denote the integer division reminder operation and the floor operation, respectively. The pseudorandom TH sequence $\{c_l\}_{l=0}^{N_{th}-1}$ has length $N_{th}$ where each $c_l$ took integer values between 0 and $N_{th}-1$, where $N_{th}$ less than the number of chips per frame was $N_f = T_f/T_c$. The DS sequence $\{a_l\}_{l=0}^{N_{ds}-1}$ has the length $N_{ds}$ with each $a_l$ taking the value +1 or –1.

## Channel Model and Received Signal

UWB system performance was studied in the case of a fading channel by using the modified Saleh-Valenzuela (SV) model (Molisch, Foerster & Pendergrass 2003), which was adopted by IEEE 802.15.3 as a reference model for UWB link-level studies. The model was based on empirical measurements in indoor environment. These measurements showed that the replicas of the signal (multipath) arrived in clusters. Due to this phenomenon, the proposed model was derived from the original Saleh-Valenzuela model by using a lognormal distribution rather than a Rayleigh distribution for the magnitude of multipath gain. Independent fading was assumed for each cluster as well as each ray within the cluster.

The phase of the channel impulse response could be either 0 or π. Therefore, the model contained no imaginary component.

Analytically, the impulse response could be written as:

$$h_i(t) = V_i \sum_{l=0}^{L} \sum_{k=0}^{K} \alpha_{k,l}^{i} \delta(t - T_l^i - \tau_{k,l}^i) \quad (5)$$

where,

$\alpha_{k,l}^i$ = the gain coefficient of the $k^{th}$ multipath of the $l^{th}$ cluster related to the $i^{th}$ channel realization
$T_l^i$ = the arrival time of the first path of the $l^{th}$ cluster
$\tau_{k,l}^i$ = the delay of the $k^{th}$ multipath component relative to the cluster arrival time $T_l^i$
$V_i$ = a lognormal random value that takes into account the shadowing effect.

Imposing $\tau_{0,l}^i$, for any channel realization $i$ (the superscript was removed in the next formulae) the

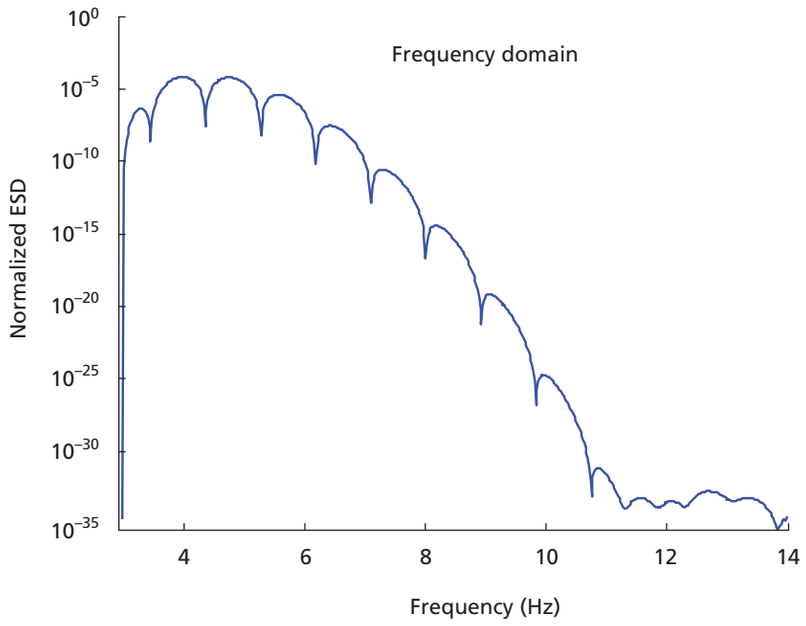


Figure 4. Energy Spectral Density Gaussian doublet pulse.

distributions of cluster arrival time and ray arrival time were given by:

$$p(T_l|T_{l-1}) = \Lambda \exp[-\Lambda(T_l|T_{l-1})], \quad \ell > 0$$
$$p(T_{k,l}|T_{(k-1),l}) = \lambda \exp[-\lambda(T_{k,l}|T_{(k-1),l})], \quad k > 0 \tag{6}$$

where,

$\Lambda$ = the cluster arrival rate

$\lambda$ = the ray arrival rate, i.e., the arrival rate of the paths within each cluster.

The channel coefficients were unit normalized values defined as:

$$\alpha_{k,l} = p_{k,l}\xi_l\beta_{k,l} \tag{7}$$

where,

$\beta_k$ and $\beta_{k,l}$ = stochastic processes with lognormal distribution

$p_{k,l}$ = a stochastic variable which can assume values +1 and −1, taking into account signal inversion due to reflections.

The received signal from a single user could then be expressed as:

$$r(t) = \sum_{l=-\infty}^{\infty} b_{[l/N_b]} a_{[l/N_{ds}]} p(t - lT_f - c_{[l/N_{th}]}T_c - \tau) + n(t), \tag{8}$$

where:

$$p(t) = \sum_{k=0}^{N_{sp}-1} h_k \psi_k(t - t_k), \tag{9}$$

is the received waveform corresponding to a single pulse. The duration of the received pulse $T_p$ is assumed to be less than the chip duration $T_c$. The propagation delay is denoted by $\tau$ and $n(t)$ is a zero mean noise process. Given the received signal, the acquisition system attempts to retrieve the timing offset $\tau$.

## PERFORMANCE EVALUATION

### Effect of NB Receive Filter

In a typical NB radio, using digital modulation, the same symmetric baseband pulse-shape was used at both the transmitter and the receiver, namely the root-raised cosine filter (RRCF) with transfer function $H_{rrcf}(f)$ with nominal bandwidth $W$, roll-off factor or excess bandwidth parameter denoted by $\Omega\ (0 \le \Omega \le 1)$, and overall bandwidth $W(1+\Omega)$ (Proakis 2001).

Taking into account the fact that the front-end band-pass filter and the low-pass filter following the demodulator typically had larger bandwidth than the RRCF transfer function $H_{rrcf}(f)$, we note the overall filter for the UWB impulse-train was given by:

$$G(f) = 0.5[P(f - f_c) + P(f + f_c)]H_{rrcf}(f)$$
$$= \overline{P}(f)H_{rrcf}(f) \tag{10}$$

where,

$P(f)$ = the Fourier transform of the Gaussian monocycle

$f_c$ = the carrier frequency for the NB system.

### Bit Error-ratio Analysis

Let $r(t)$ denote the received signal as in Equation 8, after down-conversion to baseband. Consider the usual matched filter (MF) plus threshold receiver for binary phase shift keying (BPSK) signal which was optimal for the AWGN channel. In the $k^{th}$ symbol interval, Equation 8 could be written as (Padgett, Koshy & Triolo 2003):

$$r(t) = \sqrt{E_b} b_k s(t) + n(t) + i(t) \tag{11}$$

where,

$s(t)$ = the unit energy signal waveform with duration $T$ (corresponding to $H_{rrcf}(f)$, $E_b$ is the energy per bit

$b_k\{-1, 1\}$ = the unknown bit

$N(t)$ =AWGN with two-sided PSD $N_o/2$

$i(t)$ = the interference.

Applying the MF, we have:

$$z = \int_0^T \left[\sqrt{E_b} b_k s(t) + n(t) + i(t)\right] s(t)dt$$
$$= \sqrt{E_b} b_k + \tilde{n} + \upsilon(\varsigma) \tag{12}$$

Here $\tilde{n}$ represented the 'noise' term and is zero-mean Gaussian, with variance $N_o/2$. The term $\upsilon(\varsigma)$ represent the interference. Assuming that the interfering pulse $i(t)$ is completely contained within the symbol period and has a relative delay of $\varsigma$, we have:

$$\upsilon(\varsigma) = \int_0^T i(t)s(t)dt = \sqrt{E_p}\int_{-\infty}^{\infty} \overline{P}(-f)S(f)e^{j2\pi f\varsigma}df \tag{13}$$

$E_b$ is the energy in the received UWB pulse. For an NB $S(f)$, $\overline{P}(f)$ essentially constant over the bandwidth of $S(f)$, so that:

$$\upsilon(\varsigma) \approx \sqrt{E_p} P(f_c)s(\varsigma) \tag{14}$$

To define the $SNR$ impairment factor, we have:

$$\delta = \sqrt{\frac{E_p}{E_B}} P(f_c)s(\varsigma) \tag{15}$$

Conditioned on a given time offset ς, the interference term, $\upsilon(\varsigma)$ in Equation 14 acts as a fixed bias in the decision statistic of Equation 12. Conditioned on the interference, the decision variable Z in Equation 12 is Gaussian with mean and variance $N_o/2$; the MF receiver uses a threshold of zero and the BER is then given by:

$$P(\delta) = 0.25erfc\left(\sqrt{\frac{E_b}{N_o}}(1+\delta)\right) + 0.25erfc\left(\sqrt{\frac{E_b}{N_o}}(1-\delta)\right) \quad (16)$$

Here we assumed NB BPSK modulation for simplicity, but clearly the result is readily generalized to other modulation formats such as M-ary PAM, PPM and Q-PSK.

If the UWB pulse rate, $R_p$ is very small, not every NB symbol is affected by the interference. With $T_s$ denoting the NB symbol duration, the probability that interference is present is given by $\gamma = T_s R_p$ ; the average BER is then given by:

$$P_e = \gamma E_\delta\{P_e(\delta)\} + 0.5(1-\gamma)erfc\left(\sqrt{\frac{E_b}{N_o}}\right) \quad (17)$$

Equation 17 is simulated by using MATLAB 2007b and the resulting discussions is given below.

## SIMULATION RESULTS AND DISCUSSION

### Pulse Shape

Figure 5 shows the UWB doublet waveforms with different pulse widths. From the figure it was obvious that there were some nulls in the ESD spectrum; the null frequencies could be used to mitigate interference to/from different narrowband signals. For example when we consider WiFi (IEEE 802.11a) with carrier frequency $f$ = 5.3 GHz) in the FCC permitted UWB transmission frequency band (3.1 GHz~10.6 GHz), it would be better to adjust the pulse so as to be null in this band.

### Modulation Techniques Effect

Pulse position modulation has been widely used with UWB; however, PPM has discrete spectra that can cause interference to other systems while pulse amplitude modulation (PAM) and binary phase shift keying (BPSK) have continuous spectra. Figures 6 and 7 show some modulation types with different signal-to-interference-ratios (SIR), where M-ary PAM overcomes other types of modulation. However in Figure 7 BPSK outperforms other modulations when SIR ≥ 7 dB.

In Figure 8, the used modulation scheme was still BPSK; The curves are parameterized by different SIRs

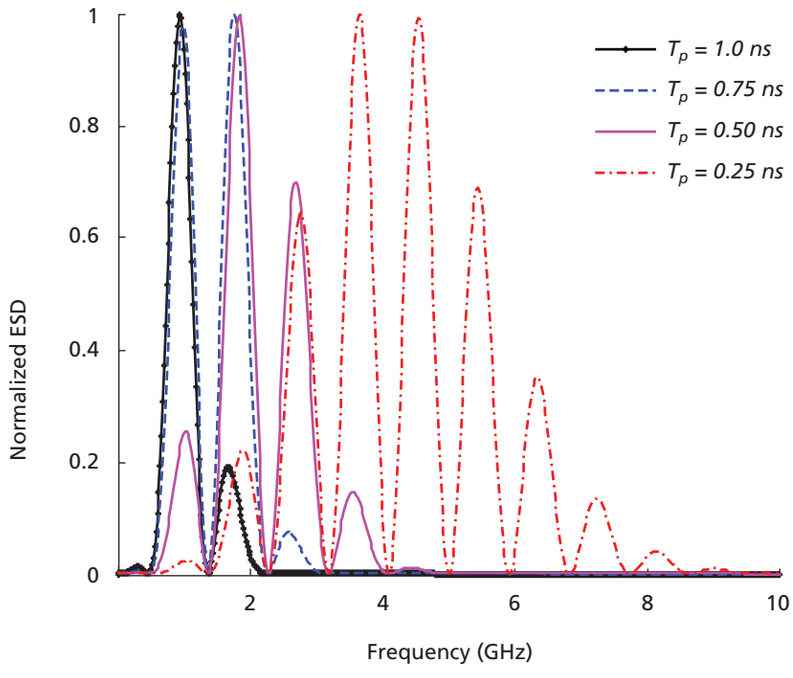


Figure 5. Energy spectral density UWB doublet pulse curves for different pulse widths.

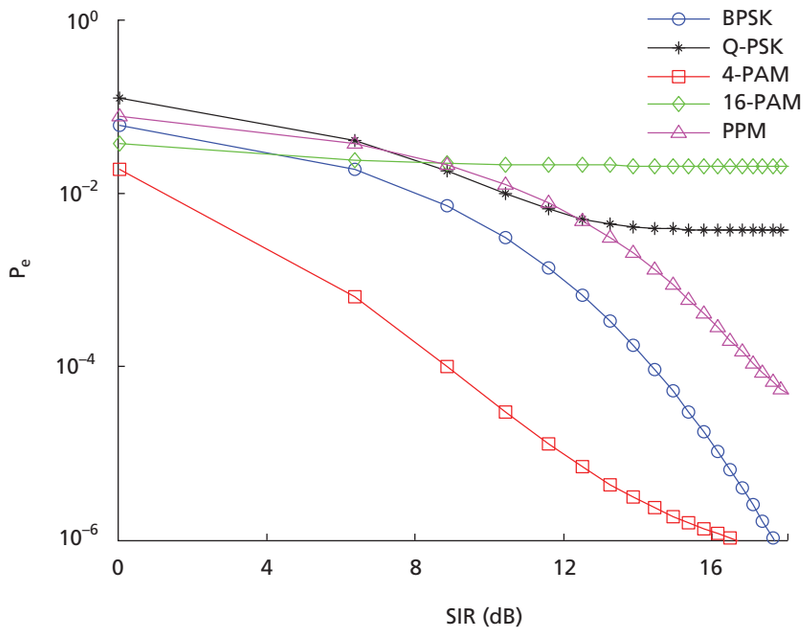


Figure 6. Error probability for different types of modulation using $E_b/N_o$ = 15 dB and $\gamma$ = 0.25.

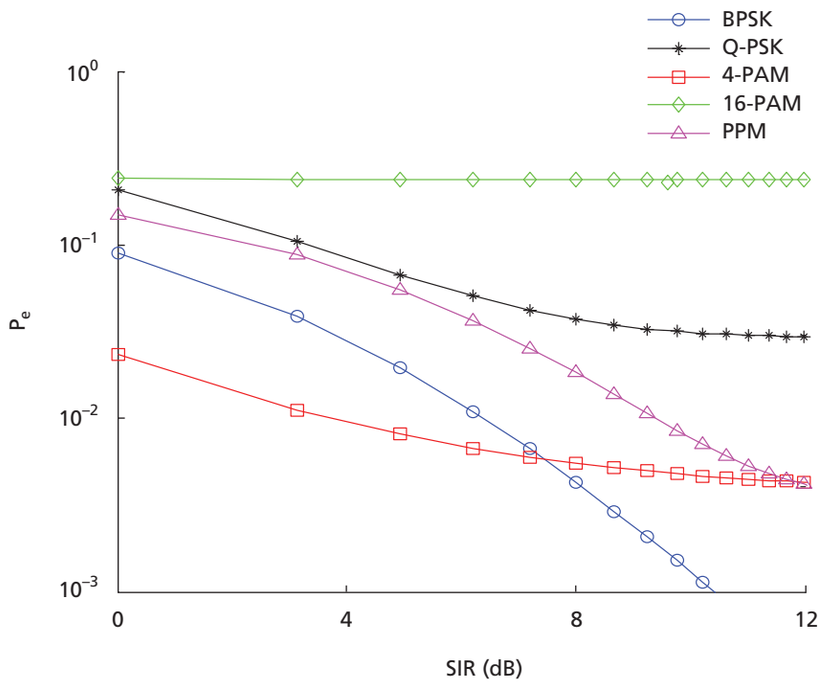


Figure 7. Error probability for different types of modulation using $E_b/N_o$ = 10 dB and duty cycle $\gamma$ = 0.75.

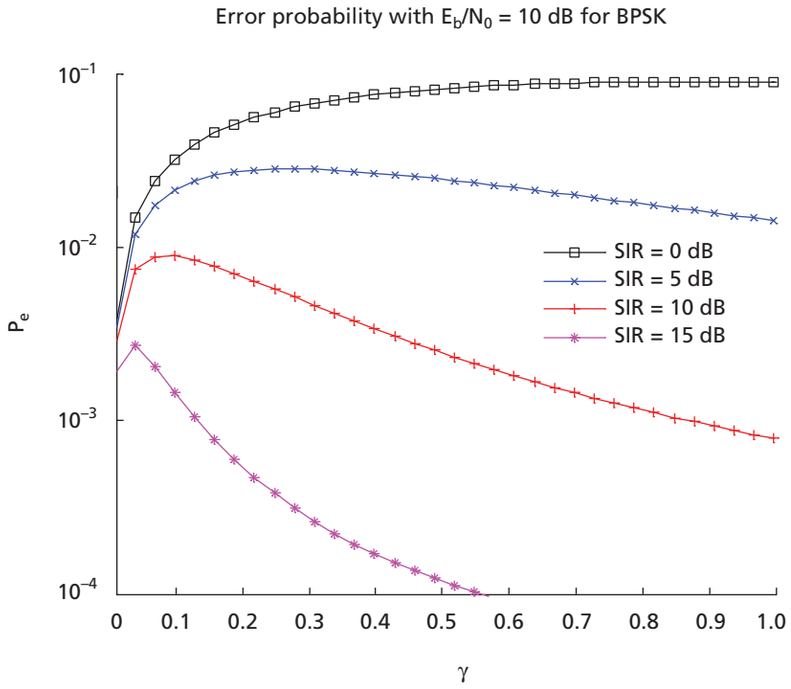


Figure 8. UWB-BPSK error probability at Saleh-Valenzuela channel with different signal-to-noise-ratio and duty cycle (γ).

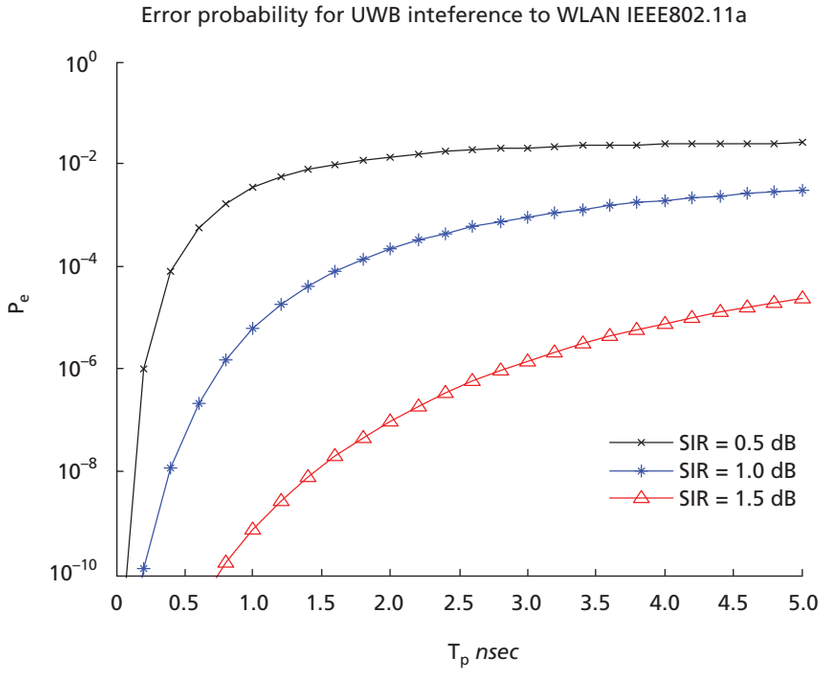


Figure 9. Error probability for UWB interference to WiFi using different pulse widths and different interfering power levels.

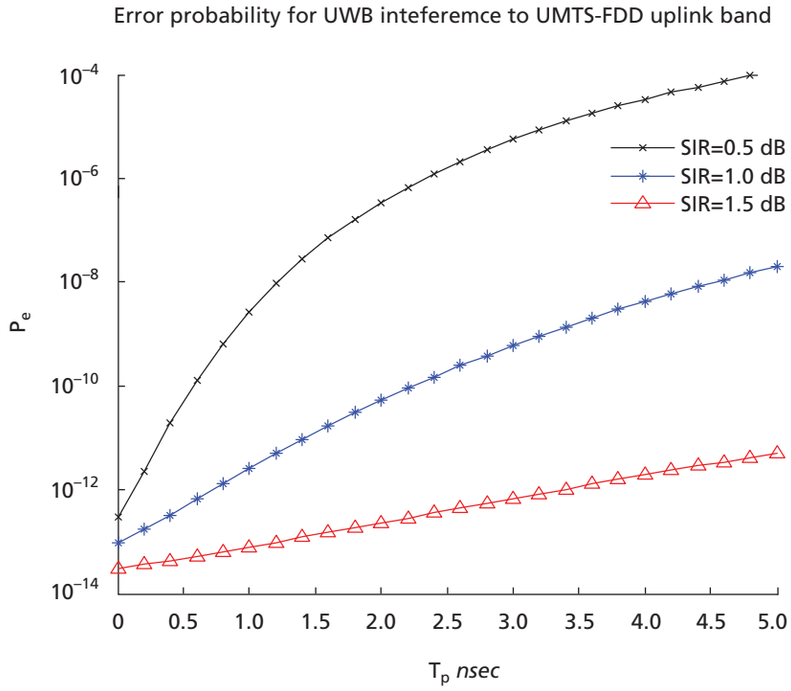


Figure 10. Error probability for UWB interference to UMTS-FDD uplink band using different pulse widths and different interfering power levels.

corresponding to target $E_b/N_o$ of 10 dB. Note that as $\gamma$ becomes small, $P_e$ goes to 0.002.

### Interference to Narrowband Systems

This section introduces the effect of UWB on the WiFi and 3rdG (i.e. UMTS/WCDMA) systems degradation. Error probability curves are presented for different signal-to-interference ratios utilizing the waveforms from Figure 3 with different pulse widths. In the presence of a UWB signal, WiFi and 3rdG systems performance could be improved by selecting proper pulse width for fixed waveform. The change of the pulse width shifted the spectrum in the frequency domain. In Figures 9 and 10, the waveforms were doublet Gaussian that were produced by the 2nd derivative of Gaussian monopulse but the pulse width was changed.

## FUTURE WORK

For smarter interference mitigation and co-existence with other conventional systems, UWB cognitive radio (CR) can be employed. The concept of CR is that performance can be improved and interference reduced if UWB transmissions have the ability to sense spectrum usage by neighbouring devices, change operating frequency, adjust output power and even alter transmission parameters and characteristics (Federal Communications Commission 2002). A CR takes an expanded view of the channel by managing and adapting time, frequency, space, power, and coding parameters.

This technology can lead to the advent of smarter unlicensed devices that make greater use of the spectrum than possible today—without interfering with licensed users. It may also provide licensees with innovative ways to use their current spectrum more efficiently.

## CONCLUSION

In this paper we have studied the performance of the different single band UWB systems through bit-error-rate simulations in the modified Saleh-Valenzuela model in the presence of interference coming from the UNII bands, 802.11 WiFi that will operate at 5.3 GHz, and 3rdG (i.e. UMTS/WCDMA) uplinks for different modulation schemes under Rayleigh multipath channel model.

*Date of submission: October 2006*
*Date of acceptance: June 2008*

## REFERENCES


Borah, DK, Jana, R, Stamoulis, A 2003, 'Performance evaluation of IEEE 802.11a wireless LANs in the presence of ultra-wideband interference,' in *Proc. IEEE WCNC,* pp. 83–87.

Čabrićl, D, Mubaraq, S, Willkomm, D, Brodersen1, R & Wolisz, A 2005, 'A cognitive radio approach for usage of virtual unlicensed spectrum', in *2005 Joint UWBST & IWUWBS,* pp. 50–54.

Federal Communications Commission, 2002, 'Revision of Part 15 of the Commission's rules regarding ultra-wideband transmission systems,' *First Report and Order, FCC-02-48.*

Freescale Semiconductor 2005, 'Ultra-wideband opportunities under the new FCC waiver', *Document Number: UWBOPPFCCWVRWP, Rev 1, March 2005.*

Han, J & Nguyen, C 2002, 'A new ultra-wideband, ultra-short monocycle pulse generator with reduced ringing,' *IEEE Microwave and Wireless Components Letters,* vol. 12, no. 6, pp. 206–208.

Molisch, AF, Foerster, JR & Pendergrass, M 2003, 'Channel models for ultra-wideband personal area networks,' *IEEE Wireless Communications Magazine,* vol. 10, no. 6, pp. 14–21.

Padgett, JE, Koshy, JC, Triolo, AA 2003, 'Physical-layer modeling of UWB interference effects,' *Telcordia Report to DARPA NETEX Program*, Jan. 2003.

Proakis, JG 2001, *Digital Communications*, chap 6, McGraw Hill Inc, California.

Sadler, M & Swami, A 2004, 'On the performance of episodic UWB and direct-sequence communication systems,' in *IEEE Trans. Wireless Comms. 2004.*

Tao, W, Yong, W & Kangsheng, C 2003, 'Analyzing the interference power of narrowband jamming signal on UWB systems,' in *Proc. IEEE PIMRC*, pp. 612—15.

ASM Sci. J., **2(1)**, 23–33

# Chemical Reaction and Variable Viscosity Effect on Mixed Heat and Mass Transfer Convection for Hiemenz Flow over a Porous Wedge with Heat Radiation

R. Kandasamy[1]*, Azme[1], I. Hashim[2] and M. Ismoen[1]

The effect of chemical reaction and variable viscosity on mixed convection heat and mass transfer for Hiemenz flow over a porous wedge plate was studied in the presence of heat radiation. The wall of the wedge was embedded in a uniform Darcian porous medium to allow for possible fluid wall suction or injection and had a power-law variation of both the wall temperature and concentration. The fluid was assumed to be viscous and incompressible. Numerical calculations were carried out for different values of dimensionless parameters and an analysis of the results obtained showed that the flow field was influenced appreciably by the buoyancy ratio between species, thermal diffusion and suction/injection at wall surface. The effects of these major parameters on the transport behaviours were investigated methodically and typical results illustrated to reveal the tendency of the solutions. Representative results are presented for the velocity, temperature, and concentration distributions. Comparisons with previously published works were performed and excellent agreement between the results were obtained. It is predicted that this research might prove to be useful for study of the movement of oil or gas and water through the reservoir of an oil or gas field, in the migration of underground water, in filtration, and water purification processes.

**Key words:** buoyancy ratio; chemical reaction; heat radiation; Hiemenz flow; porous medium; oil field; gas field; reservoir; underground water; filtration; purification

The present trend in the field of chemical reaction analysis is to give a mathematical model for the system to predict the reactor performance. A large amount of research work has been reported in this field. In particular, the study of heat and mass transfer with chemical reactions is of considerable importance in chemical and hydrometallurgical industries. Chemical reactions can be classified as either heterogeneous or homogeneous processes (Figure 1). This depends on whether they occur at an interface or as a single phase volume reaction. A few representative fields of interest in which combined heat and mass transfer with variable viscosity and chemical reaction effects play important roles, are design of chemical processing equipment, formation and dispersion of fog, distribution of temperature and moisture over agricultural fields and groves of fruit trees, damage of crops due to freezing, food processing and cooling towers. Cooling towers are the cheapest way to cool large quantities of water. For example, formation of smog is a first order homogeneous chemical reaction. Consider the emission of $NO_2$ from automobiles and other smoke-stacks. This $NO_2$ reacts chemically in the atmosphere with unburned hydrocarbons (aided by sunlight) and produces peroxyacetylnitrate, which forms an envelope of what is termed as photochemical smog.

Frequently the transformations proceed in a moving fluid, a situation encountered in a number of technological fields. Simultaneous heat and mass transfer from different geometrics embedded in porous media has many engineering and geophysical applications such as geothermal reservoirs, drying of porous solids, thermal insulation, enhanced oil recovery, packed-bed catalytic reactors, cooling of nuclear reactors, and underground energy transport. A very significant area of research in radiative heat transfer, at the present time is the numerical simulation of combined radiation and convection/conduction transport processes. The effort has arisen largely due to the need to optimize industrial systems such as furnaces, ovens and boilers; the interest in our environment and in non-conventional energy sources, such as the use of salt-gradient solar ponds for energy collection and storage. In particular, natural convection induced by the simultaneous action of buoyancy forces resulting from thermal and mass diffusion is of considerable interest in nature and in many

[1] Science Studies Centre, KUITTHO, 86400, Parit Raja, Batu Pahat, Johor, Malaysia
[2] School of Mathematical Sciences, Universiti Kebangsaan Malaysia, 43600, UKM, Bangi, Selangor, Malaysia
* Corresponding author (e-mail: kandan_kkk@yahoo.co.in)

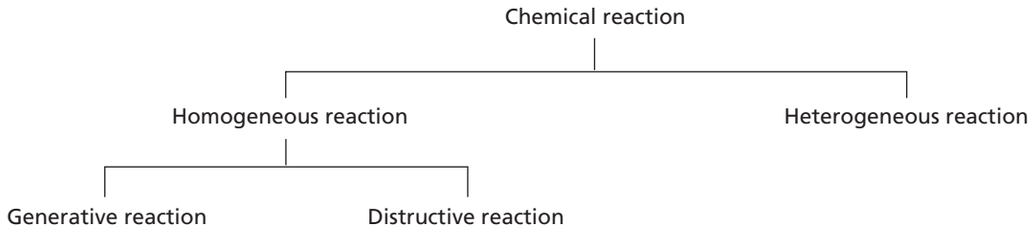


Figure 1. Classification of chemical reactions.

industrial applications such as geophysics, oceanography, drying processes, solidification of binary alloy and chemical engineering. Stagnation flows are found in many applications such as flows over the tips of rockets, aircrafts, submarines and oil ships. The study of the stagnation flow problem was started by Hiemenz (1911) who developed an exact solution to the Navier–Stokes governing equations for the forced convection case. Later, Eckert (1942) studied a similar solution for both the momentum and energy governing equations excluding the effect of buoyancy forces. Ariel (1994) considered the stagnation-point flow of electrically-conducting fluids in the presence of large transverse magnetic field strengths. Yih (1998a) reported on the effects of uniform suction or blowing and magnetic field on the heat transfer characteristics of the Hiemenz problem in porous media.

Frequently the transformations proceed in a moving fluid, a situation encountered in a number of technological fields. In previous investigations, Chambre and Acrivos (1956) analyzed catalytic surface reactions in hydro-dynamic flows. The paper was concerned with its counterpart, namely, an investigation of a certain special class of homogeneous volume reactions in flow systems. Chambre and Acrivos (1957) had studied the diffusion of a chemically reactive species in a laminar boundary layer flow. Acrivos (1960) analyzed the laminar forced convection mass transfer with homogeneous chemical reaction. A unified boundary layer analysis was applied to the problem of steady state mass transfer of a chemical species, diffusing from a surface and reacting isothermally in a linear fluid stream.

Stagnation flows are found in many applications such as flows over the tips of rockets, aircrafts, submarines and oil ships. In these types of problems, the well known Falkner-Skan transformation is used to reduce boundary-layer equations into ordinary differential equations for similar flows. It can also be used for non-similar flows for convenience in numerical work because it reduces, even if it does not eliminate, dependence on the x-coordinate. The solutions of the Falkner-Skan equations are sometimes referred to as wedge-flow solutions with only two of the wedge flows being common in practice. The dimensionless parameter $\beta_1$ plays an important role in such type of problems because it denotes the shape factor of the velocity profiles. It has been shown by Schlichting (1979) that when $\beta_1 < 0$ (increasing pressure), the velocity profiles have a point of inflexion whereas when $\beta_1 > 0$ (decreasing pressure), there is no point of inflexion. This fact is of great importance in the analysis of the stability of laminar flows with a pressure gradient.

Yih (1998b) presented an analysis of the forced convection boundary layer flow over a wedge with uniform suction/blowing, whereas Watanabe (1990) investigated the behaviour of the boundary layer over a wedge with suction or injection in forced flow. Recently, magnetic fluid dynamics (MHD) laminar boundary layer flow over a wedge with suction or injection had been discussed by many authors: Kafoussias and Nanousis (1997); Kumari (1998); Kuo Bor-Lih (2005); Cheng and Lin (2002), and Anjali Devi and Kandasamy (2001a, 2001b). Chamkha and Khaled (2001) investigated the problem of coupled heat and mass transfer by MHD free convection from an inclined plate in the presence of internal heat generation or absorption. For the problem of coupled heat and mass transfer in MHD free convection, the effects of viscous dissipation and Ohmic heating with chemical reaction were not studied in the above investigation. However, it was more realistic to include these effects to explore the impact of the magnetic field on thermal transport in the buoyancy layer. With this awareness, the effect of Ohmic heating on the MHD free convection heat transfer has been examined for a Newtonian fluid (Hossain 1992) and for a micro-polar fluid (Hakiem *et al.* 1999). Pantokratoras (2006) discussed the Falkner – Skan flow with constant wall temperature and variable viscosity. Hossain *et al.* (1999) analyzed the effects of radiation on free convection from a porous plate. These effects on combined heat and mass transfer in mixed convection flow past a wedge in the presence of suction or injection have not yet been studied. The similarity solutions for mixed convection heat and mass transfer for Hiemenz flow through porous media was explained by Chamkha and Khaled (2000). This study is therefore initiated to investigate the problem of mixed convection flow over a

wedge, taking into consideration the effects of viscous dissipation and heat radiation.

Since no attempt has been made to analyze the effects of chemical reaction, heat and mass transfer on Hiemenz flow over a porous wedge surface with heat radiation in the presence of suction or injection, we have investigated it in this article. The similarity transformation has been utilized to convert the governing partial differential equations into ordinary differential equations and then the numerical solution of the problem is drawn using Runge Kutta Gill method (Gill 1951). This method has the following advantages over other available methods: (i) it utilizes less storage registers; (ii) it controls the growth of rounding errors and is usually stable, and (iii) it is computationally economical. Numerical calculations up to third levels of truncation were carried out for different values of dimensionless parameters of the problem under consideration for the purpose of illustrating the results graphically. Examination of such flow models revealed the influence of chemical reaction, heat radiation and buoyancy ratio on velocity, temperature and concentration profiles. The analysis of the results obtained showed that the flow field was influenced appreciably by the presence of heat radiation and buoyancy ratio in the presence of suction or injection at the wall of the wedge. It is hoped that the results obtained will not only provide useful information for applications, but also serve as a complement to the previous studies.

## MATHEMATICAL ANALYSIS

Two dimensional laminar boundary layer flow of an incompressible, viscous and Boussinesq fluid over a wall of the wedge with suction or injection was considered. The x-axis was taken parallel to the wedge and y-axis taken normal to it as cited in Figure 2. The fluid was assumed to be Newtonian, heat generation or absorbing and its property variations due to temperature were limited to density and viscosity. The density variation and the effects of the buoyancy were taken into account in the momentum equation (Boussinesq's approximation) and the concentration of species far from the wall, $C_\infty$, was infinitesimally small (Byron Bird *et al.* 1992). The chemical reactions took place in the flow and a constant suction or injection was imposed at the wedge surface (see Figure 2). In the following equations, the governing boundary layer equations of momentum, energy and diffusion for the flow under Boussinesq's approximation (Kuo 2005; Ibrahim *et al.* 2006; Cheng & Lin 2002) are:

$$\frac{\partial u}{\partial x} + \frac{\partial v}{\partial y} = 0 \tag{1}$$

$$u\frac{\partial u}{\partial x} + v\frac{\partial v}{\partial y} = v\frac{\partial^2 u}{\partial x^2} + U\frac{dU}{dx} - [g\beta(T - T_\infty) + g\beta^*(C - C_\infty)] + \cos\frac{\Omega}{2} + \frac{v}{K}(u - U) \tag{2}$$

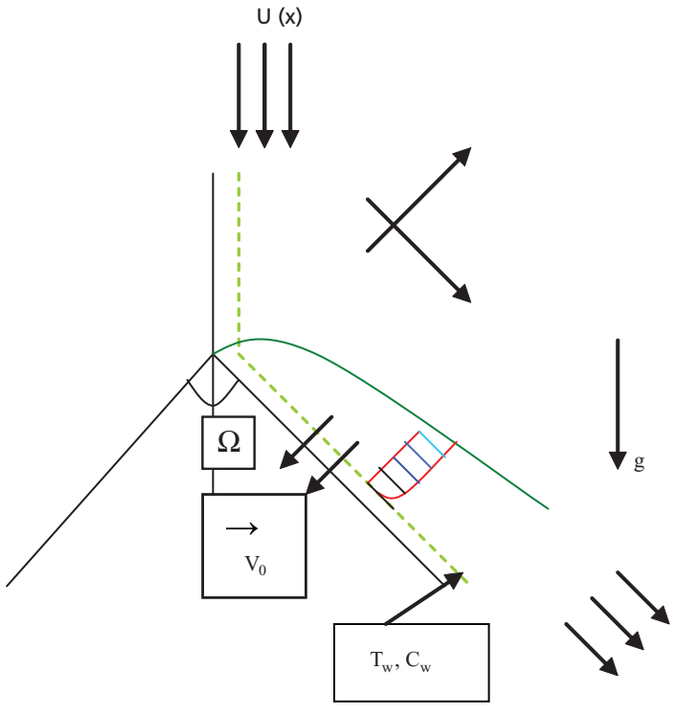


Figure 2. Hiemenz flow analysis along the wall of the wedge.

$$u\frac{\partial T}{\partial x}+v\frac{\partial T}{\partial y}=\alpha_e\frac{\partial^2 T}{\partial y^2}-\frac{\partial q_r}{\partial y}+Q(T_\infty-T)+Q_1(C_\infty-C) \quad (3)$$

$$u\frac{\partial C}{\partial x}+v\frac{\partial C}{\partial y}=D\frac{\partial^2 C}{\partial y^2}-k_1C \quad (4)$$

where,

$u$ ,v are velocity components in $x$ and $y$ direction

$u$ is the flow velocity of the fluid away from the wedge

$g$ is the acceleration due to gravity

$\beta$ is the coefficient of thermal expansion

$k_1$ is the rate of chemical reaction

$K$ is the permeability of the porous medium

$T$ is the temperature of the fluid

$T_w$ is the temperature of the wall

$T_\infty$ is the temperature of the fluid far away from the wall

$\beta^*$ is the coefficient of expansion with concentration

$C$ is the species concentration of the fluid

$C_w$ is the species concentration of the fluid along the wall

$C_\infty$ is the species concentration of the fluid away from the wall

$Q_1$ is the coefficient of proportionality for the absorption of radiation

$Q$ is the dimensional heat absorption coefficient

$\rho$ is the density of the fluid

$\sigma$ is the Stefan-Boltzman constant

$\alpha$ is the thermal diffusivity.

The boundary conditions are:

$$u=0,\ v=v_0,\ C=C_w,\ T=T_w \text{ at } y=0 \quad (5)$$

$$u=U(x),\ C=C_\infty,\ T=T_\infty \text{ at } y\to\infty \quad (6)$$

By using the Rosseland diffusion approximation (Hossain *et al.* 1999; Rapits 1998), the radiative heat flux $q_r$ is given by $q_r=-\frac{4\sigma}{3\mu}\frac{\partial T^4}{\partial y}$ and the term $Q(T_\infty-T)$ is assumed to be the amount of heat generated/absorbed per unit volume. $Q$ is a constant, which may take on either positive or negative values. When the wall temperature $T_w$ exceeds the free stream temperature $T_\infty$, the source term represents the heat source when $Q<0$ and heat sink when $Q>0$. For the condition that $T_w<T_\infty$ the opposite relationship is true and $D$ is the effective diffusion coefficient. Assuming that the temperature differences within the flow are sufficiently small, $T^4$ may be expressed as a linear function of temperature:

$$T^4\cong 4T_\infty^{\ 3}-3T_\infty^{\ 4} \quad (7)$$

Following the lines of Yih (1998b) and Bansal (1986), the following change of variables are introduced:

$$\Psi(x,y)=\sqrt{\frac{2U\alpha_e x}{1+m}}\,f(x,\eta) \text{ where } \eta(x,y)=y\sqrt{\frac{(1+m)U}{2\alpha_e x}},$$
$$\theta=\frac{T-T_\infty}{T_w-T_\infty},\ \phi=\frac{C-C_\infty}{C_w-C_\infty} \quad (8)$$

where $\alpha_e$ is the effective thermal diffusivity of the porous medium $(\alpha_e=\frac{k_e}{\rho c_p})$. The variations of viscosity are written (Elbashbeshy & Ibrahim 1993) in the form: $\frac{\mu}{\mu_0}=e^{-\alpha\theta}$, where $\mu_0$ is the viscosity at temperature $T_w$ and $\alpha$ is the viscosity parameter.

Under this consideration, the potential flow velocity can be written as:

$$U(x)=Ax^m,\ \beta_1=\frac{2m}{1+m} \quad (9)$$

where $A$ is a constant and $\beta_1$ is the Hartree pressure gradient parameter that corresponds to $\beta_1=\frac{\Omega}{\pi}$ for a total angle $\Omega$ of the wedge. In this work, temperature and concentration variation of the surface are assumed to have power-law variation (Kandasamy *et al.* 2005) forms as shown by the following equations:

$$T_w=T_\infty+c_1x^n \text{ and } C_w=T_\infty+c_2x^n$$

where $c_1$ and $c_2$ are constants and $n$ is the power of index of the wall temperature and concentration. Both the wall temperature and concentration are assumed to have the same power index $n$.

The continuity Equation 1 is satisfied by the stream function $\Psi(x, y)$ defined by:

$$u=\frac{\partial\Psi}{\partial y} \text{ and } v=-\frac{\partial\Psi}{\partial x} \quad (10)$$

Transform Equations 2, 3 and 4 into a set of ordinary differential equations as:

$$\frac{\mathrm{Pr}}{e^{\alpha\theta}}\frac{\partial^3 f}{\partial\eta^3}=-f\frac{\partial^2 f}{\partial\eta^2}-\frac{2m}{1+m}\left[1-\left(\frac{\partial f}{\partial\eta}\right)^2\right]+\frac{2}{1+m}\frac{N\phi+\theta}{1+N}\cos\frac{\Omega}{2}+\frac{2x}{1+m}\left(\frac{\partial f}{\partial\eta}\frac{\partial^2 f}{\partial x\partial\eta}\right)-\frac{\partial f}{\partial x}\frac{\partial^2 f}{2\eta^2}-\frac{2}{m+1}\lambda\left(\frac{\partial f}{\partial\eta}-1\right) \quad (11)$$

$$(1+\frac{1}{R})\frac{\partial^2\theta}{\partial\eta^2} = -\Pr\frac{\partial\theta}{\partial\eta} + \frac{2\Pr}{1+m}\theta\frac{\partial f}{\partial\eta} + \Pr\frac{2x}{1+m}(\frac{\partial f}{\partial\eta}\frac{\partial\theta}{\partial x} - \frac{\partial f}{\partial x}\frac{\partial\theta}{\partial\eta} - \frac{2\Pr}{m+1}(\delta\theta - \phi Q^*) \quad (12)$$

$$\frac{\partial^2\phi}{\partial\eta^2} = -Sc f\frac{\partial\phi}{\partial\eta} + \frac{2\,Sc\,x}{1+m}\gamma\phi + \frac{2Sc}{1+m}\phi\frac{\partial f}{\partial\eta} + \frac{2xSc}{1+m}(\frac{\partial f}{\partial\eta}\frac{\partial\phi}{\partial x} - \frac{\partial f}{\partial\eta}\frac{\partial\phi}{\partial x}) \quad (13)$$

Where, the Grashof number, the modified Grashof number, the buoyancy ratio (N), the Prandtl number (Pr), the Schmidt numbers, the suction (S) or injection parameter, the chemical reaction parameter, the internal heat generation or absorption coefficient, the dimensionless porous medium ($\lambda$) parameter, $Q^*$ is the absorption of radiation parameter and the radiation parameter are defined as:

$$\mathrm{Gr}_1 = \frac{\nu g\beta(T-T_\infty)}{U^3},\ \mathrm{Gc}_1 = \frac{\nu g\beta^*(T-T_\infty)}{U^3},\ N = \frac{\beta^*(C_w-C_\infty)}{\beta(T_w-T_\infty)},$$
$$\Pr = \frac{\nu}{\alpha},\ \mathrm{Sc} = \frac{\nu}{D},\ S = -v_0\sqrt{\frac{(1+m)x}{2\nu U}},\ \gamma = \frac{\nu k_1}{U^2},$$
$$\delta = \frac{Q}{A\rho c_p},\ \lambda = \frac{\alpha}{KA},\ Q^* = \frac{\nu Q_1(C_w-C_\infty)}{(T_w-T_\infty)}$$
$$\text{and } R = \frac{3k\nu}{16\sigma T_\infty^3} \quad (14)$$

The boundary conditions can be written as:

$$\eta = 0: \frac{\partial f}{\partial\eta} = 0, \frac{f}{2}(1+\frac{x}{U}\frac{dU}{dx}) + x\frac{\partial f}{\partial x} = -v_0\sqrt{\frac{(1+m)x}{2\nu U}},\ \theta = 1,\ \phi = 1$$
$$\eta \to \infty: \frac{\partial f}{\partial\eta} = 1,\ \theta = 0,\ \phi = 0 \quad (15)$$

where, $v_0$ is the velocity of suction if $v_0 < 0$ and injection if $v_0 > 0$ and $\mathrm{Gr} = \mathrm{Gr}_1 + \mathrm{Gc}_1$

Equations 11 to 13 and boundary conditions Equation 15 can be written as:

$$\frac{\Pr}{e^{\alpha\theta}}\frac{\partial^3 f}{\partial\eta^3} = (f+\frac{1-m}{1+m}\xi\frac{\partial f}{\partial\xi})\frac{\partial^2 f}{\partial\eta^2} - \frac{1-m}{1+m}\xi\frac{\partial^2 f}{\partial\xi\partial\eta}\frac{\partial f}{\partial\eta} + \frac{2m}{1+m}\left(1-(\frac{\partial f}{\partial\eta})^2\right) - \frac{2}{1+m}\frac{N\phi+\theta}{1+N}\cos\frac{\Omega}{2} + \frac{2}{m+1}\lambda(\frac{\partial f}{\partial\eta}-1) = 0 \quad (16)$$

$$(1+\frac{1}{R})\frac{\partial^2\theta}{\partial\eta^2} + \Pr(f+\frac{1-m}{1+m}\xi\frac{\partial f}{\partial\xi})\frac{\partial\theta}{\partial\eta} - \frac{2\Pr}{1+m}\theta\frac{\partial f}{\partial\eta} - \frac{1-m}{1+m}\xi\frac{\partial\theta}{\partial\xi}\frac{\partial f}{\partial\eta} + \frac{2\Pr}{m+1}(\delta\theta-\phi Q^*) = 0 \quad (17)$$

$$\frac{\partial^2\phi}{\partial\eta^2} + \mathrm{Sc}\,f\frac{\partial\phi}{\partial\eta} - \frac{2\mathrm{Sc}}{1+m}\xi^2\gamma\phi + \mathrm{Sc}\frac{1+m}{1-m}(\frac{\partial\phi}{\partial\eta}\xi\frac{\partial f}{\partial\xi} - \frac{\partial f}{\partial\eta}\xi\frac{\partial\phi}{\partial\xi}) - \frac{2\mathrm{Sc}}{1+m}\phi\frac{\partial f}{\partial\eta} = 0 \quad (18)$$

$$\eta = 0: \frac{\partial f}{\partial\eta} = 0, \frac{(1+m)f}{2} + \frac{1-m}{2}\xi\frac{\partial f}{\partial\xi} = S,$$
$$\theta = 1,\ \phi = 1\quad \eta\to\infty: \frac{\partial f}{\partial\eta} = 1, \theta = 0,\ \phi = 0 \quad (18a)$$

where, S is the suction parameter if $S > 0$ and injection if $S < 0$ and $\xi = kx^{\frac{1-m}{2}}$ (Kafoussias & Nanousis 1997), is the dimensionless distance along the wedge ($\xi > 0$). In this system of equations $f(\xi, \eta)$ is the dimensionless stream function; $\theta(\xi, \eta)$ be the dimensionless temperature; $\phi(\xi, \eta)$ be the dimensionless concentration; Pr, the Prandtl number; $\mathrm{Re}_x$, Reynolds number etc. which are defined in Equations 10 – 20. So, following the lines of Kafoussias and Nanousis (1997), the parameter $\xi$ indicates the dimensionless distance along the wedge ($\xi > 0$). It is obvious that to retain the $\xi$-derivative terms, it is necessary to employ a numerical scheme suitable for partial differential equations for the solution. In addition, owing to the coupling between adjacent stream-wise locations through the $\xi$-derivatives, a locally autonomous solution, at any given stream-wise location can not be obtained. In such a case, an implicit marching numerical solution scheme is usually applied preceding the solution in the $\xi$-direction, i.e., calculating unknown profiles at $\xi_\iota + 1$ when the same profiles at $\xi_\iota$ are known. The process starts at $\xi_\iota = 0$ and the solution proceeds from $\xi_\iota$ to $\xi_{\iota+1}$ but such a procedure is time consuming.

However, the level of truncation (Anjali Devi & Kandasamy 2001a), when the terms involving $\frac{\partial f}{\partial\xi}$, $\frac{\partial\theta}{\partial\xi}$ and $\frac{\partial\phi}{\partial\xi}$ their $\eta$ derivatives are deleted, the resulting system of equations resembles, in effect, a system of ordinary differential equations for the functions $f$, $\theta$ and $\phi$ with $\xi$ as a parameter and the computational task is simplified. Further-more, a locally autonomous solution for any given $\xi$ can be obtained because the stream wise coupling is severed. So, following the lines of Gill (1951) and Shooting numerical solution scheme are utilized for obtaining the solution of the problem. Now, due to the above mentioned factors and for small value of $\xi$, the Equations 16 – 18 are changed to:

$$f''' + \frac{e^{\alpha\theta}}{\Pr} f\, f'' + \frac{2m}{1+m}\frac{e^{\alpha\theta}}{\Pr}(1 - f'^2) - \frac{2m}{1+m}\frac{e^{\alpha\theta}}{\Pr}\frac{N\phi + \theta}{1 + N}\cos\frac{\Omega}{2} - \frac{e^{\alpha\theta}}{\Pr}\frac{2}{1+m}\lambda(f' - 1) = 0 \quad (19)$$

$$\left(1 + \frac{1}{R}\right)\theta'' + \Pr f\,\theta' - \frac{2\Pr}{1+m} f'\theta' + \frac{2\Pr}{1+m}(\delta\theta - \phi Q^*) = 0 \quad (20)$$

$$\phi'' + \mathrm{Sc}\, f\,\theta' - \frac{2\,\mathrm{Sc}}{1+m} f'\phi + \frac{2\,\mathrm{Sc}}{1+m}\xi^2\gamma\phi = 0 \quad (21)$$

with boundary conditions:

$$\eta = 0: \mathrm{f}(0) = \frac{2}{1+m} S, f'(0) = 0, \theta(0) = 1, \phi(0) = 1$$

$$\eta \to \infty: f'(\infty) = 1, \theta(\infty) = 0, \phi(\infty) = 0 \quad (22)$$

The mass diffusion Equation 21 can be adjusted to meet these circumstances if one takes (i) $k_1 > 0$ for destructive reaction, (ii) $k_1 = 0$ for no reaction and (iii) $k_1 < 0$ for generative reaction.

## NUMERICAL SOLUTION

The set of non-linear ordinary differential Equations 19–21 with boundary conditions (Equation 22) have been solved by using the Gill method (Gill 1951) along with the Shooting Technique with $\alpha$, $\gamma$, $\Omega$, Pr, Sc, R and N as prescribed parameters. The numerical solution was done using Matlab computational software. A step size of $\Delta\eta = 0.001$ was selected to be satisfactory for a convergence criterion of $10^{-7}$ in nearly all cases. The value of $\eta_\infty$ was found for each iteration loop by assignment statement $\eta_\infty = \eta_\infty + \Delta\eta$ . The maximum value of $\eta_\infty$ for each group of the parameters $\alpha$, $\gamma$, $\Omega$, Pr, Sc, R and N was determined when the values of unknown boundary conditions at $\eta = 0$ did not change to a successful loop, with error less than $10^{-7}$. Effects of chemical reaction, heat and mass transfer were studied for different values of suction at the wall of the wedge and the strength of heat radiation.

## RESULTS AND DISCUSSION

The computations have been carried out for various values of variable viscosity ($0 \leq \alpha \geq 1$), chemical reaction ($\gamma$), Schmidt's number (Sc), Prandtl number (Pr), heat radiation (R), porous medium ($\lambda$), buoyancy ratio (N) and power index of the wall temperature (n). The edge of the boundary layer $\eta_\infty = 8$ depending on the values of parameters.

In the absence of energy and diffusion equations, in order to ascertain the accuracy of our numerical results, the present study was compared with the available exact solution in literature. The velocity profiles for different values of $m$ were compared with the available exact solution of Schlichting (1979), is shown in Figure 3. It is observed that agreement with the theoretical solution of velocity profile is excellent.

The effects of chemical reactions with heat source play very important roles in the concentration field. The dimensionless velocity, temperature and concentration distribution for different destructive chemical reactions are shown in Figure 4. It is seen from the figure that the concentration of the fluid decreased with increase of destructive chemical reaction ($\gamma > 0$) while the velocity and temperature of the fluid are not significantly altered with increase of destructive reaction. It is also observed that the concentration of the fluid decreased uniformly near the wall of the wedge.

Figure 5 depicts the dimensionless velocity profiles $f'(\eta)$ for different values of viscosity. Due to the uniform suction with fixed angle of inclination of the wall of the wedge, the effect of increase of viscosity was to increase the velocity component of the fluid along the wall of the wedge, while the temperature and concentration were not significantly altered with increase of viscosity. The results presented demonstrate quite clearly that $\alpha_1$, which is an indicator of the variation of viscosity with temperature, has a substantial effect on fluid motion within the boundary layer over a heat surface as well as the drag and heat transfer characteristics.

Effects of the buoyancy parameter on velocity, temperature and concentration profiles are shown through Figure 6. It is interesting to note that the velocity of the fluid decreased whereas the temperature and concentration of the fluid were not significantly altered with increase of the buoyancy parameter.

Figure 7 represents the dimensionless velocity, temperature and concentration profiles for different values of heat radiation. In the presence of uniform viscosity, it is clear that the velocity and the concentration of the fluid changed while the temperature of the fluid decreased with increase of heat radiation. All these physical behaviour were due to the combined effect of buoyancy ratio between species and thermal diffusion and the strength of the viscosity of the fluid.

Figure 8 illustrates the influence of the suction parameter S on the velocity, temperature and concentration profiles, respectively. The imposition of wall fluid suction for this problem had the effect of increasing the entire hydrodynamic and reducing the thermal and concentration boundary layers causing the fluid velocity to increase while decreasing its temperature and concentration. The decrease in thickness of the concentration layer was caused by two effects: (i) the direct action of suction, and (ii) the indirect action

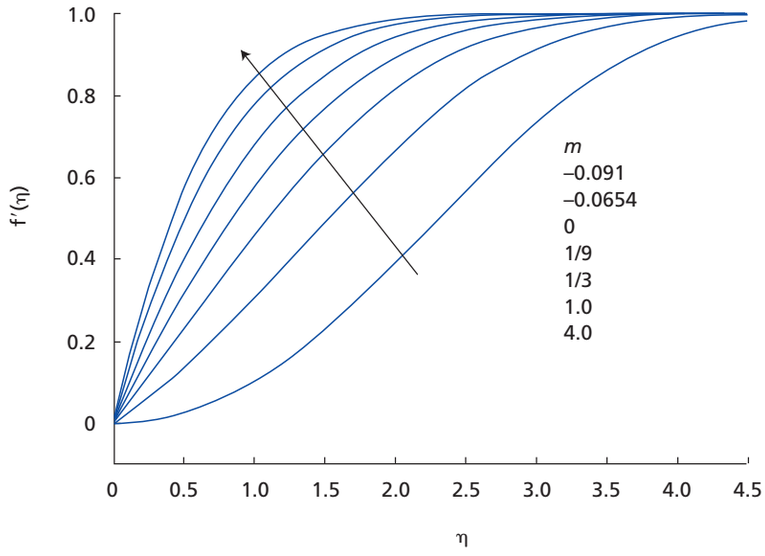


Figure 3. Effects of *m* on the velocity distribution in laminar flow past a wedge.

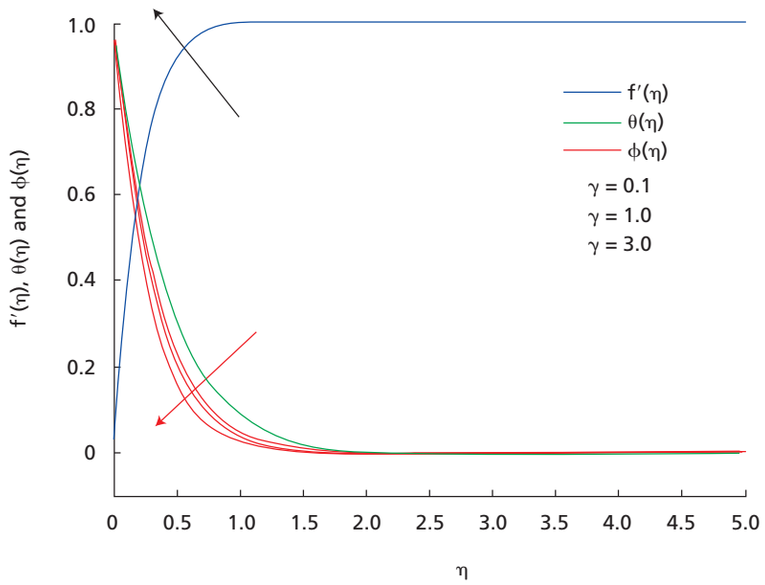


Figure 4. Chemical reaction effect on dimensionless velocity, temperature and concentration profile: Pr = 1; N = 1; $\xi^2 = Q^* = 1$; $\lambda = 0.1$; Sc = 0.62; R = 1; S = 2; $\delta = 0.1$; $\Omega = 30°$ and $\alpha = 0.1$.

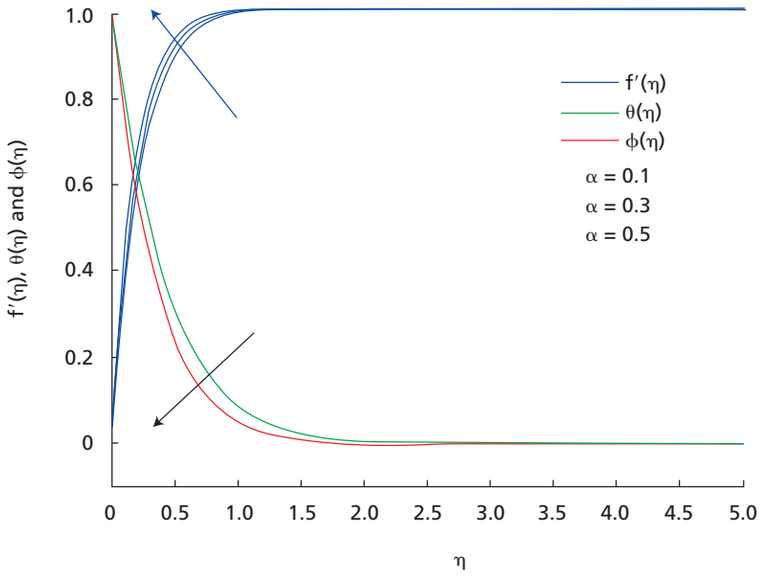


Figure 5. Viscosity effect on dimensionless velocity, temperature and concentration profile: Pr = 1; N = 1; $\xi^2 = Q^* = 1$; $\lambda = 0.1$; Sc = 0.62; R = 1; S = 2; $\delta = 0.1$; $\Omega = 30°$ and $\alpha = 0.1$.

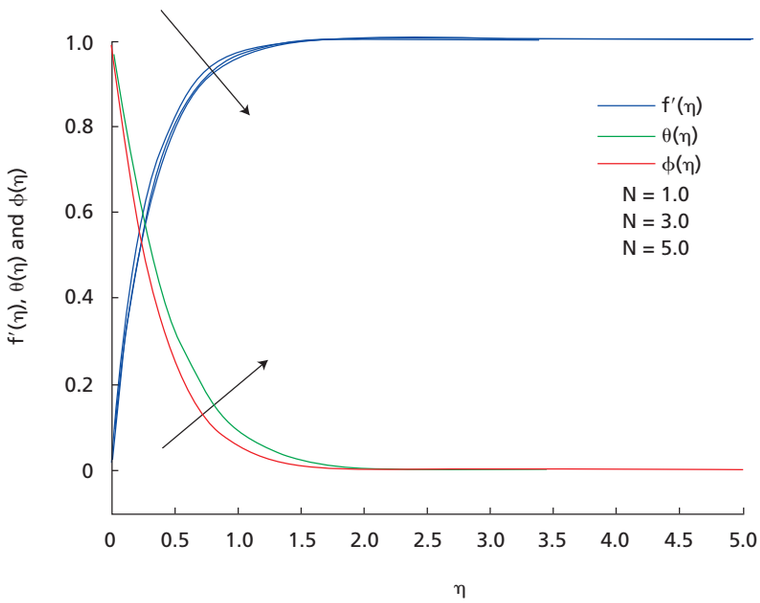


Figure 6. Buoyancy effect on dimensionless velocity, temperature and concentration profile: Pr = 1; N = 1; $\xi^2 = Q^* = 1$; $\lambda = 0.1$; Sc = 0.62; R = 1; S = 2; $\delta = 0.1$; $\Omega = 30°$ and $\alpha = 0.1$.

of suction causing a thicker thermal boundary layer which corresponded to a lower temperature gradient, a consequent increase in the thermophoretic force and a higher concentration gradient.

Effects of the Schmidt's number on velocity, temperature and concentration profiles are shown through Figure 9. It is seen from this figure that the concentration of the fluid decreased and the velocity of the fluid increased with increase of Schmidt's number, whereas the profiles for temperature were not significantly different with increase in Schmidt's number. It is clear that the concentration decreased tremendously in the presence of Schmidt's number.

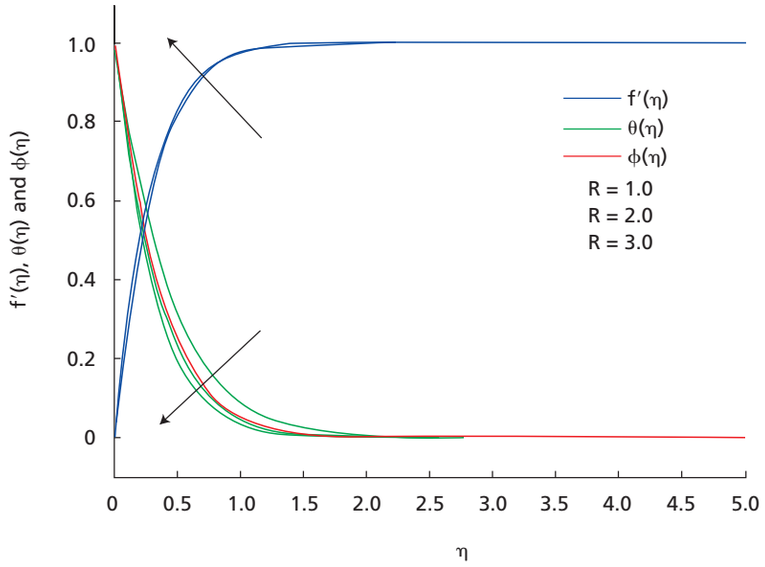


Figure 7. Heat radiation effect on dimensionless velocity, temperature and concentration profile: Pr = 1; N = 1; $\xi^2 = Q^* = 1$; $\lambda = 0.1$; Sc = 0.62; R = 1; S = 2; $\delta = 0.1$; $\Omega = 30°$ and $\alpha = 0.1$.

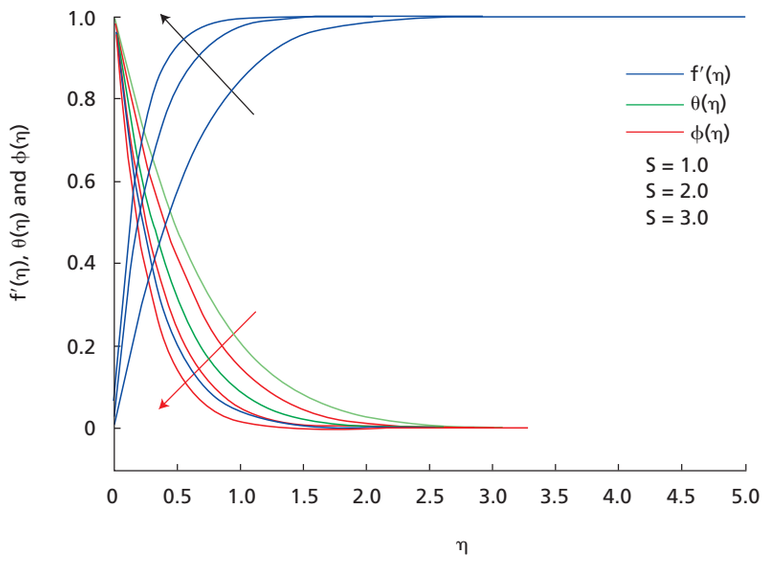


Figure 8. Suction effect on dimensionless velocity, temperature and concentration profile: Pr = 1; N = 1; $\xi^2 = Q^* = 1$; $\lambda = 0.1$; Sc = 0.62; R = 1; S = 2; $\delta = 0.1$; $\Omega = 30°$ and $\alpha = 0.1$.

## CONCLUSION

In this study the problem of the effect of the chemical reaction and variable viscosity on mixed heat and mass transfer convection for Hiemenz flow over a porous wedge in the presence of heat radiation was investigated. The governing equations were approximated to a system of non-linear ordinary differential equations by similarity transformation. Comparisons with previously published work were performed and excellent agreement with the results were obtained. The results are presented graphically and the conclusion drawn indicated that the flow field and other quantities of physical interest were significantly influenced by these parameters. From the investigation, it was noticed that the increase in strength of viscosity, buoyancy and heat radiation parameter were expected to alter the momentum and thermal boundary layers significantly. Particularly, it was seen that the chemical reaction with suction have a substantial effect on the flow field and thus on the concentration boundary layer from the wall of the wedge to the fluid. It was interesting to note that the decrease of concentration field due to increase in Sc showed that it increased gradually as we replaced hydrogen (Sc = 0.32) by water vapour (Sc = 0.62) and ammonia (Sc = 1.0) in the said sequence. It is expected that this research may prove to be useful for the study of the movement of oil or gas and water through the reservoir of an oil or gas field, in the migration of underground water and in filtration and water purification processes. It is hoped that the results obtained will not only provide useful information for applications, but also serve as a complement to previous studies.

## ACKNOWLEDGEMENT

The authors wish to express their cordial thanks to the Vice-chancellor and the Director of Science Studies Centre, UTHM, Malaysia for their encouragement and acknowledge the financial support received from FRGS 00405- 406/2007.

*Date of submission: December 2006*
*Date of acceptance: June 2008*

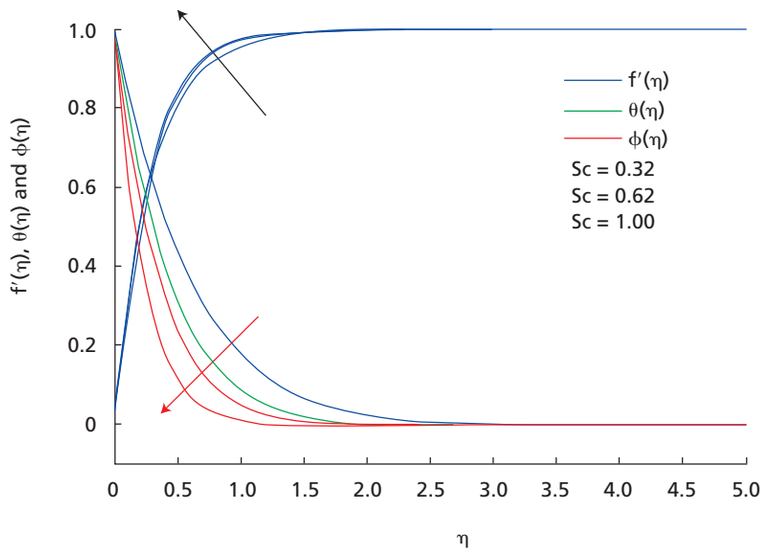


Figure 9. Effect of Schmidt's number on dimensionless velocity, temperature and concentration profile: Pr = 1; N = 1; $\xi^2 = Q^* = 1$; $\lambda = 0.1$; Sc = 0.62; R = 1; S = 2; $\delta = 0.1$; $\Omega = 30°$ and $\alpha = 0.1$.

## REFERENCES


Acrivos, A 1960, 'Analysis of the laminar forced convection mass transfer with homogeneous chemical reaction', *Amer. Inst. Chem. Engrs.*, vol. 6, no. 1, pp. 410–419.

Anjali Devi, SP & Kandasamy, R 2001a, 'Thermal stratification effects on laminar boundary layer flow over a wedge with suction or injection', *Mechanics Research Communications*, vol. 28, no. 3, pp. 349–354.

Anjali Devi, SP & Kandasamy, R 2001b, 'Effects of heat and mass transfer on MHD laminar boundary layer flow over a wedge with suction or injection', *Journal of Energy Heat and Mass Transfer,* vol. 23, no. 2, pp. 167–172.

Ariel, PD 1994, 'Hiemenz flow in hydromagnetic', *Acta Mech*., vol. 103, no.1, pp. 31–43.

Bansal, JL 1986, *Boundary layer theory* , chp 6, IBM Publishing Company, Oxford.

Byron Bird, R, Stewart, WE & Lightfoot, EN 1992, *Transport phenomena*, John Wiley and Sons, New York.

Chambre, PL & Acrivos, JD 1956, 'Analysis of catalytic surface reactions in hydrodynamic flows', *Journal of Applied Physic*s, vol. 27, no. 4, pp. 1322–1329.

Chambre, PL & Acrivos, A 1957, 'Diffusion of a chemically reactive species in a laminar boundary layer flow', *Indian Engng. Chem*, vol. 49, no. 1, pp. 1025–1031 .

Chamkha, AJ & Khaled, ARA 2001, 'Similarity solutions for hydro magnetic simultaneous heat and mass transfer', *Heat Mass Transfer*, vol. 37, no. 3, pp. 117–124.

Chamkha, AJ & Pop, I 2004, 'Effects of thermophoresis particle deposition in free convection boundary layer from a vertical flat plate embedded in a porous medium', *Int. Comm. Heat Mass Transfer,* vol. 31, no. 2, pp. 421–430.

Cheng, WT & Lin, HT 2002, 'Non-similarity solution and correlation of transient heat transfer in laminar boundary layer flow over a wedge', I*nternational Journal of Engineering Science*, vol. 40, no. 3, pp.531–539.

Cheng, P & Minkowycz, WJ 1977, 'Free convection about a vertical flat embedded in a saturated porous medium with application to heat transfer from a dike', *Journal of Geophysical Research,* vol. 82, no. 1, pp. 2040–2044.

Chamkha, AJ & Khaled, AA 2000, 'Similarity solutions for hydromagnetic mixed convection heat and mass transfer for Hiemenz flow through porous media', *Int. J. Numer. Math. Heat Fluid Flow*, vol. 10, no.3, pp. 94–115.

Eckert, ERG 1942, 'Die berechnung des warmeubergangs in der laminaren grenzschung auf dem gebiete des ingenierwesens', *VDI Forschungsheft*, vol. 416, no. 1, pp. 1.

Elbashbeshy, EMA & Ibrahim, FN 1993, 'Steady free convection flow with variable viscosity and thermal diffusivity along a vertical plate', *J. Phys. D: Appl. Phys.*, vol. 26, pp. 2137–2143.

Gill, S 1951, 'A process for the step-by-step integration of differential equatiuons in an automatic digital computing machine', in Proceeding of Cambridge Philosophical Society*,* vol. 47, no. 1, pp. 96–108.

Hakiem, MAEL, Mohammadeian, AA, Kaheir, SMMEL & Gorla, RSR 1999, 'Joule heating effects on Magnetohydrodynamic free convection flow of a micro polar fluid', *International Communications Heat Mass Transfer,* vol. 26, no. 2, pp. 219–227.

Hiemenz, K 1911, 'Die grenzschicht an einem in den gleichformigen flussigkeitsstrom eingetauchten geraden kreiszylinder', *Dingl Poltech Journal,* vol. 326, no. 1, pp. 321–410.

Hossain, MA, Alim, MA & Rees, DAS 1999, 'The effects of radiation on free convection from a porous plate', *Int. J. Heat Mass Transfer,* vol. 42, no. 2, pp.181–191.

Hossain, MA 1992, 'Viscous and Joule heating effects on MHD free convection flow with variable plate temperature', *International Journal of Heat and Mass Transfer*, vol. 35, no. 1, pp. 3485–3492.

Ibrahim, FS, 'Elaiw, AM & Bakr, AA 2008, 'Effect of the chemical reaction and radiation absorption on the unsteady MHD free convection flow past a semi infinite vertical permeable moving plate with heat source and suction', *Communication in Nonlinear Science and Numerical Simulation*, vol. 13, no. 1, pp. 1056–1066.

Kandasamy, R, Periasamy, K & Sivagnana Prabhu, KK 2005, 'Chemical reaction, heat and mass transfer on MHD flow over a vertical stretching surface with heat source and thermal stratification effects', *International Journal of Heat Mass Transfer,* vol. 48, no. 3, pp. 4557–4561.

Kafoussias, NG & Nanousis, ND 1997, 'Magnetohydrodynamic laminar boundary layer flow over a wedge with suction or injection', *Canadian Journal of Physics*, vol.75, no. 2, pp. 733–745.

Kumari, M 1998, 'Effect of large blowing rates on the steady laminar incompressible electrically conducting fluid over an infinite wedge with a magnetic field applied parallel to the wedge', *International Journal of Engng. Sci.,* vol. 36, no. 1, pp. 299–306.

Kuo Bor-Lih 2005, 'Heat transfer analysis for the Falkner-Skan wedge flow by the differential transformation method', *International Journal of Heat Mass Transfer,* vol. 48, no. 2, pp. 5036–5046.

Pantokratoras, A 2006, 'The Falkner- Skan flow with constant wall temperature and variable viscosity', *International Journal of Thermal Sciences,* vol. 45, no. 3, pp. 378–389.

Raptis, A 1998, 'Flow of a micro polar fluid past a continuously moving plate by the presence of radiation', *Int. J. Heat Mass Transfer,* vol. 41, no. 1, pp. 2865–2866.

Schlichting, H 1979, *Boundary layer theory*, trans. J Kestin, McGraw Hill Inc, New York , chap 9.

Yih, KA 1998a, 'The effect of uniform suction/blowing on heat transfer of Magnetohydrodynamic Hiemenz flow through porous media', *Acta Mech.,* vol. 130, no. 1, pp. 147–158.

Yih, KA 1998b, 'Uniform suction/blowing effect on force convection about wedge, *Acta Mech*., vol. 128, no. 2, pp.173–181.

Watanabe, T 1990, 'Thermal boundary layer over a wedge with uniform suction or injection in forced flow', *Acta Mechanica,* vol. 83, no. 1, pp.119–126.

ASM Sci. J., **2(1)**, 35–44

# Methane Adsorption on Structurally Different Zeolites

K.S.N. Kamarudin[1]*, Y.Y. Chieng[1], H. Hamdan[2] and H. Mat[1]

The importance of zeolite surface area and pore volume in adsorption processes has been much reported in literature. In addition to that, structural framework and pore network system may also influence the adsorption capacity and selectivity of methane on zeolite. This paper discusses the characteristics of methane adsorption based on several physical properties of the adsorbents such as surface area, pore volume, pore network system and its interaction with adsorbate. The study, using FTIR spectroscopy showed that the adsorbed methane at room temperature was detected in the FTIR region between 3200 $cm^{-1}$ – 1200 $cm^{-1}$. Based on the physical properties of the adsorbents and the FTIR spectra of adsorbed methane, the surface area was not the only factor that determined methane adsorption; in fact the type of pore network system of the adsorbent also affected the interaction, thus affecting the adsorption of methane in zeolite.

**Key words:** methane adsorption; FTIR spectroscopy; adsorbent; adsorbate interaction; zeolite; surface area; pore network; characterization

The rapid development in nanotechnology over the last decade has led to the creation of nanoporous materials which has attracted a great deal of attention from researchers of various fields. The understanding of the properties of these materials is indispensable in the development of superior catalytic and separation characteristics (Ghorai *et al*. 2006). Silica-type is ranked as one of the prominent materials that have been employed due to the possibility of having an enormous amount of nano-sized pores created therein per unit mass of silica (Esparza *et al*. 2005). Zeolite, a crystalline hydrated silica-alumina porous material forms a large family with a framework based on an extensive three dimensional structure of $TO_4$ tetrahedra (T = Si or Al) which has long been used in chemical industries as a catalyst or separation agent (Barrer *et al.* 1978; Barrer 1982; Roozeboom *et al.* 1983; Suzuki 1990; van Bekkum *et al.* 1991). The applications of zeolites as adsorbents and catalysts are related to the exceptional extension of their solid-liquid interface, accessible through a perfectly defined pore structure (Bebon *et al.* 2002). Other potential applications includes adsorptive gas storage (Matranga *et al.* 1992; Bileo *et al.* 2001; Nijkamp *et al.* 2001), gas and chemical sensors (Mintova & Bein 2001; Szabo 2003), and semiconductor metal-doped zeolites (Simoncic & Ambruster 2004).

Eventually, natural gas recovery using zeolite adsorbent for the separation of gaseous nitrogen and carbon dioxide from methane is also becoming increasingly important (Bülow *et al.* 1996; Jayaraman *et al.* 2004; Melo *et al.* 2006; Li & Tezel 2007). The potential use of zeolite material for high energy density gas storage technology also requires such an adsorbent to have high capacity and selectivity for methane gas, a major component in natural gas (Weikamp 1996; Nishimaya *et al.* 2001; Njikamp *et al.* 2001). Among more than 150 types of synthetic zeolites, those with high surface area and regular cavity properties become important nanomaterial as catalysts for petrochemical applications and promising adsorbents in gas adsorption and separation processes (Kusakabe *et al*. 1998; Hasegawa *et al*. 2001; Mizukami *et al*. 2001; Harlick & Tezel, 2004; Sultana *et al.* 2004).

Various observations were reported regarding adsorption of gases onto zeolites. Choudhary and Mayadevi (1996) and Hernandez-Huesca *et al*. (1999) have reported that the chemical composition of zeolites influenced the adsorption characteristics. However, other studies have indicated that adsorption was influenced by the accessibility of adsorbates and it was determined by the size of cations at the pore opening (Ackley & Yang 1991; Chen *et al.* 1999; Suzuki 1999; Kurama *et al.* 2002). In many cases, the relationship between the zeolite structure and its gas adsorption characteristics towards methane is still unclear even though zeolites have shown their own possibility as gas adsorbent. The adsorption characteristics and interaction of methane-zeolites have not yet comprehensively elucidated and analyzed particularly adsorption at room temperature.

[1] Advanced Material and Process Engineering Research Group, Faculty of Chemical and Natural Resources Engineering, Universiti Teknologi Malaysia, 81310 Skudai, Johor, Malaysia
[2] Zeolite and Porous Material Group, Ibnu Sina Institute for Fundamental Science Studies, Universiti Teknologi Malaysia, 81310 Skudai, Johor, Malaysia
* Corresponding author (e-mail: sozana@fkkksa.utm.my)

In this study, several types of synthetic zeolites were used in order to unveil the relationship between the zeolite's physical properties (surface area, pore volume, and pore network system) and adsorbate-adsorbent interaction. The zeolites were divided into two main groups according to the pore network systems, uniform channel-like system and interconnected cage-like system.

At present, various techniques and methods have evolved for identifying and characterizing materials and measuring the adsorption of gases in order to understand the adsorption phenomena. Apart from volumetric and gravimetric measurements, methods such as FTIR, Raman spectroscopy and NMR are also being used to study the adsorption characteristics of gases on zeolites. In this study, FTIR spectroscopy was used for characterizing the adsorbate-adsorbent interaction and evaluating the diffusion of interacting molecules to the inner part of zeolite pores. Their corresponding differences of FTIR spectra were compared to determine the effect of different structural framework, pore size, and surface area to the methane adsorptive properties. However, since methane is a very weak base, it is expected that interaction with zeolite cations and protons of acidic sites do not lead to a strong perturbance of adsorbed molecules. The measurement of adsorption isotherm and the FTIR spectra will provide an insight on the gas adsorption characteristics of different zeolite structural frameworks.

## MATERIALS AND METHOD

### Materials

A powdered form of zeolite NaY, NaX, ZSM-5, mordenite, ferrierite and zeolite beta (Zeolyst Intl.), and NaX (Aldrich Chemical) were used as adsorbents. The methane gas (99.9 %) used in the adsorption study was obtained from Southern Industrial Gas (M) Sdn Bhd and used without any further treatment.

### Experimental Procedures

*Zeolite characterization*. The structural properties of zeolites were determined using a Bruker X-ray diffractometer with $CuK\alpha_1$ radiation of $\lambda = 1.5418$ Å at 40 kV and 20 mA in the range of $2\theta = 5^o - 50^o$ at a scanning speed of 0.05º per second. The porosity of the samples was determined by measuring nitrogen adsorption at 77 K by using a Micromeritics analyzer (ASAP Model 2000). The total surface area was calculated using BET method, while the external surface area and micropore volume were calculated using the t-plot method.

*Methane adsorption*. An adsorption cell with $CaF_2$ as infrared window, integrated to the FTIR instrument was used to study methane adsorption on different zeolites (Figure 1). A thin self-supported sample wafer was prepared, placed inside the adsorption cell, and outgassed (activated) in a dynamic vacuum (residual pressure $< 2 \times 10^{-3}$ kPa) for 2 h at about 700 K to remove moisture and other components, if any, adsorbed on the zeolite. The adsorption cell was then isolated by closing the valves, allowed to cool to room temperature (298 K), and the FTIR spectrum recorded using the spectroscopic instrument Spectrum One-Perkin Elmer. This FTIR spectrum was designated as the background spectrum of the zeolite wafer. Methane was then introduced at 137 kPa, and the gas allowed to adsorb on the zeolite sample at 300 K for 2 h which was sufficient to achieve the adsorption equilibrium. The valve was closed and the FTIR spectrum was again measured using the same FTIR instrument. The FTIR spectra obtained were compared against the background spectrum of zeolite wafer.

## RESULTS AND DISCUSSIONS

### Characterization of Zeolite

In order to elucidate the effect on structurally different zeolites of methane adsorption, the selected zeolite was divided into two categories; a uniform channel and an internal pore system of interconnected cage-like void named as channel-type zeolites and cage-type zeolites, respectively. The channel-type zeolites consist of ZSM-5, mordenite, ferrierite and beta zeolites, whereas the cage-type zeolite was represented by NaX and NaY zeolites (Figure 2).

Figure 3 shows the XRD spectra of channel and cage-type zeolites used in this study. The intensity of peaks indicated that ZSM-5, mordenite and ferrierite zeolites have relatively higher crystallinity than beta zeolite. The X-ray diffractograms of cage-type structures (NaX and NaY) were found to be similar. This might be due to the fact that both zeolites belong to faujasite structural group. The patterns exhibited low background signal and sharp reflection, indicating excellent crystallinity of sample.

As recommended by IUPAC, the first step to understand the behaviour of adsorption is to identify the isotherm type and hence the nature of the adsorption process (Sing 1984). Figure 4 shows the adsorption isotherms of nitrogen for channel and cage-type zeolites. The adsorption isotherms show a rapid increase in the amount adsorbed followed by a long nearly flat region at higher pressures. As reported by Khelifa *et al*. (2004), the volume of the adsorbed phase was limited by the volume of the microporosity at which the adsorption occurred. However, the adsorption isotherm of zeolite beta shows that it is rather similar to Type I, but as it reaches saturation, the adsorption rapidly increases to a higher value (Type IV). This indicates a shift of micropore-size distribution with

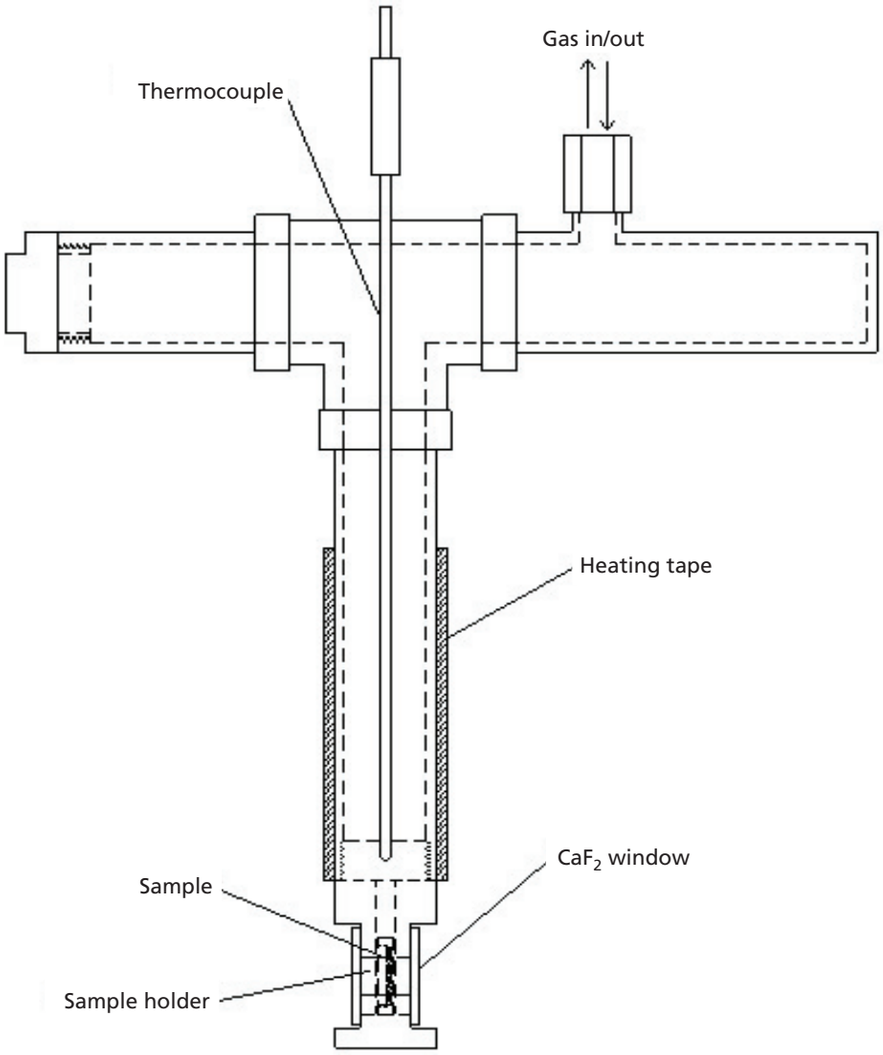


Figure 1. A schematic diagram of gas-zeolite interaction adsorption cell.

formation of larger micropores progressively filled at higher pressure. A slope at the end of the isotherm signifies the presence of mesoporous or external surface area (Carvalho *et al.* 1994).

In adsorption applications, the wide use of zeolites and other porous materials is based on the fundamental understanding that they have a high surface area and high pore volume. Table 1 shows surface area, micropore volume and pore diameter of channel-type and cage-type zeolites. Surface area and micropore volume were determined from $N_2$ adsorption isotherm data using t-plot and BET equation respectively. In general, zeolites with large pore diameter will allow more molecules to diffuse and adsorb on the inner surface. However, this study revealed that crystallinity and pore network system would also determine the surface area and pore volume of zeolites. For the channel-type zeolites, mordenite has higher surface area and micropore volume than ZSM-5, beta and ferrierite. However, the cage-type zeolites have even higher values. The supercages in NaY and NaX zeolites offers more advantages in term of surface area and pore volume as they provide more space for the adsorbates to accumulate and adsorb inside the cage.

## FTIR Spectra

*Methane spectra*. Methane gas has four fundamental vibrations in the gaseous phase; $v_3$ (3020 $cm^{-1}$) and $v_4$ (1306 $cm^{-1}$) are infrared active, while $v_1$ (2914 $cm^{-1}$) and $v_2$ (1526 $cm^{-1}$) are infrared inactive. The gas phase spectrum exhibits the characteristic shape of a rotation-vibration spectrum in the adsorbed samples. The gas phase methane as adsorbed species on zeolite surfaces was found at 3017 ± 1 $cm^{-1}$ (Seidel *et al.* 2000). FTIR spectra of adsorbed methane was observed in the region between 3200 $cm^{-1}$ – 1200 $cm^{-1}$. In the case of methane, it is a very weak base

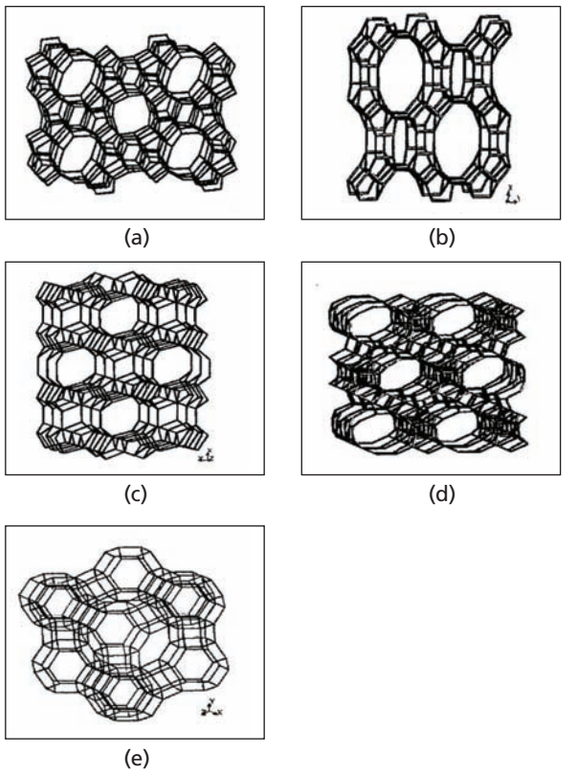


Figure 2. The structural framework of zeolites: (a) ZSM-5; (b) mordenite; (c) ferrierite; (d) zeolite beta and (e) Zeolite Y (International Zeolite Association 2000).

and its interactions with zeolite cations and protons of acidic sites do not lead to a strong perturbance of adsorbed molecules. Due to this fact and the small size and high symmetry of methane, FTIR spectra are easy to interpret. The interactions of adsorbed methane with cations present in the zeolite framework lead to the appearance of a band from the fully symmetric C-H stretching vibration ($v_1$), which is forbidden for methane molecules (Kazanskii *et al.* 2002). The two peaks that appeared in the region around 3020 $cm^{-1}$ and 1306 $cm^{-1}$ were assigned to asymmetric band ($v_3$) and symmetric band ($v_4$), respectively (Yoshida *et al.* 2000). However, a weaker band around 2900 $cm^{-1}$ assigned to $v_1$ (symmetric) band could only be observed at temperatures lower than 273 K (Yamazaki *et al.* 2000).

*Adsorption on channel-type zeolites*. Adsorption on a series of materials classified as channel-type zeolites demonstrated the effect of the pore network system on gas adsorption. FTIR spectra of methane molecules are shown in Figure 5. Although unique identification of the adsorbed molecule was difficult to be confirmed, some peaks attributed to specific interactions on the adsorbents could be observed. Figure 5 also shows the FTIR spectra of methane adsorbed on channel-type zeolites. The peak assigned to the $v_3$ of adsorbed $CH_4$ was observed in the region around 3015 $cm^{-1}$. It is a result of the free rotation of the adsorbed molecules around a single axis normal to the adsorbent surface (Yamazaki *et al.* 2000). There was another band in the region around 1300 $cm^{-1}$ that was assigned to $v_4$ band. The appearance of $v_4$ band was induced by the interaction of adsorbed molecules with the sites which created an electrical field at the surface. The peaks could not be clearly distinguished from other peaks that appeared in that region, with the exception of zeolite beta. It indicated that only weak interaction exist between the adsorbate and the channel-type zeolites. As shown in Figure 3, X-ray diffractograms of zeolite beta had low peak intensity with broad reflection. It indicated low crystallinity and a partial structural disorder of beta framework. However, the partial structural disorder could contribute to the formation of more active sites, thus the quantity of adsorption could be increased as shown by the area of $v_3$ and $v_4$ spectra in Table 2.

*Adsorption on cage-type zeolites*. The FTIR spectra of adsorbed methane on cage-type zeolites show that the peak ($v_3$ band) intensities for cage-type zeolites are higher and sharper than for channel-type zeolites. The peak positions have also shifted to the low-frequency side of methane gas which indicate that the adsorbed molecules experienced some perturbation. The presence of supercages within faujasite structures (NaX and NaY) would allow the larger freedom for the adsorbed molecules to rotate and experience a symmetrical field from the pore wall of the zeolites. The FTIR spectra of $v_4$ band for adsorbed methane in cage-type zeolites are also shown in Figure 5. The differences between those two zeolites are relatively small. This was due to similar zeolite structure as indicated by the XRD patterns (Figure 3).

However, as reported by Yamazaki *et al*. (2000), the peak area of FTIR spectra does not actually represent the amount of methane adsorbed, but only indicates the relative amount of methane adsorbed on each zeolite. As a comparison, Table 2 shows the peak areas of $v_3$ and $v_4$ for channel-type and cage-type zeolites. The peak areas of cage-type zeolites are larger than those of channel-type zeolites. The results demonstrated that cage-type zeolites had better adsorption capacity than the channel-type zeolites. Due to the confinement effect, more interactions between $CH_4$ and the walls of NaX and NaY zeolites structures occurred. The results also indicated that methane adsorbed in the supercages and smaller pores of NaX and NaY zeolites were physically adsorbed molecules. Both adsorption sites contributed to the high methane adsorption capacity. In addition, from the shape of the $v_3$ it also showed that rotational freedoms of an adsorbed methane molecule on the active adsorption sites adequately remained. It is therefore indicated that methane molecules in the pores underwent a symmetrical field from the pore wall.

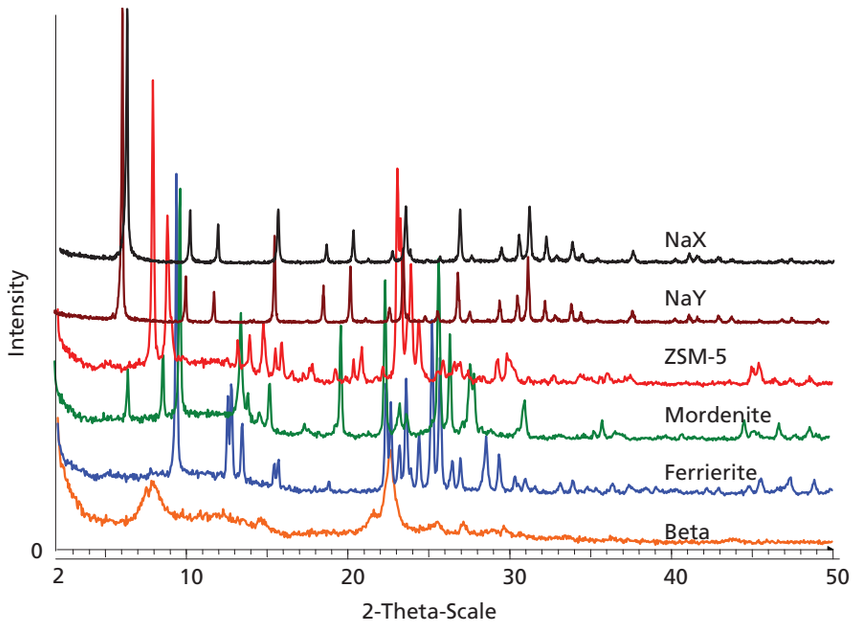


Figure 3. XRD diffractogram of channel-type and cage-type zeolites.

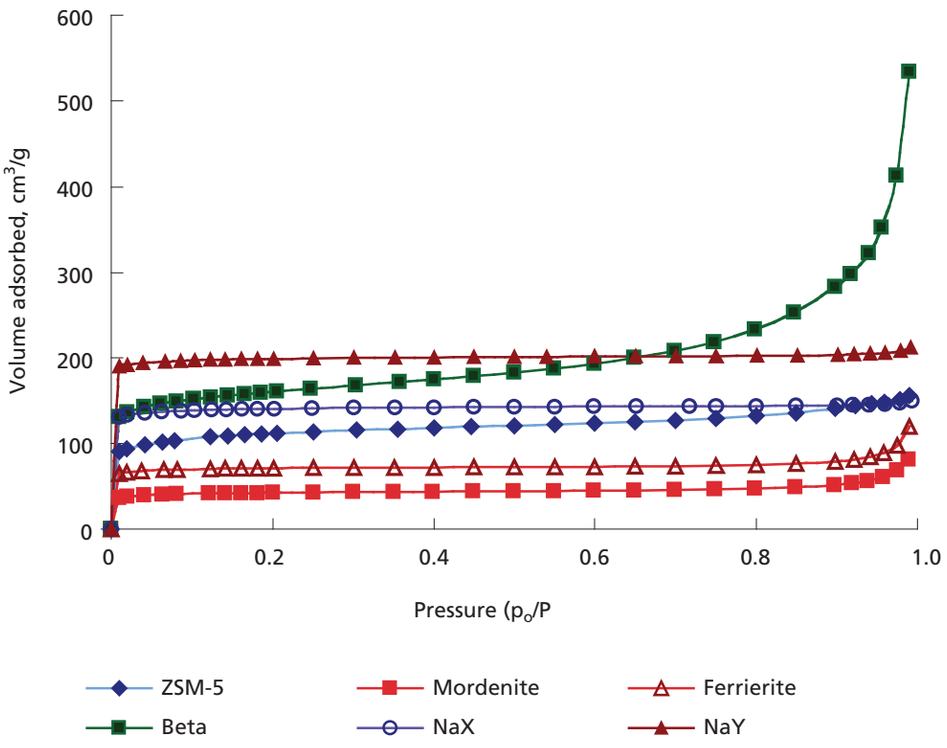


Figure 4. Nitrogen adsorption isotherm: (a) channel-type structure (ZSM-5, mordenite, ferrierite, and beta); and (b) cage-type structures (NaX and NaY).

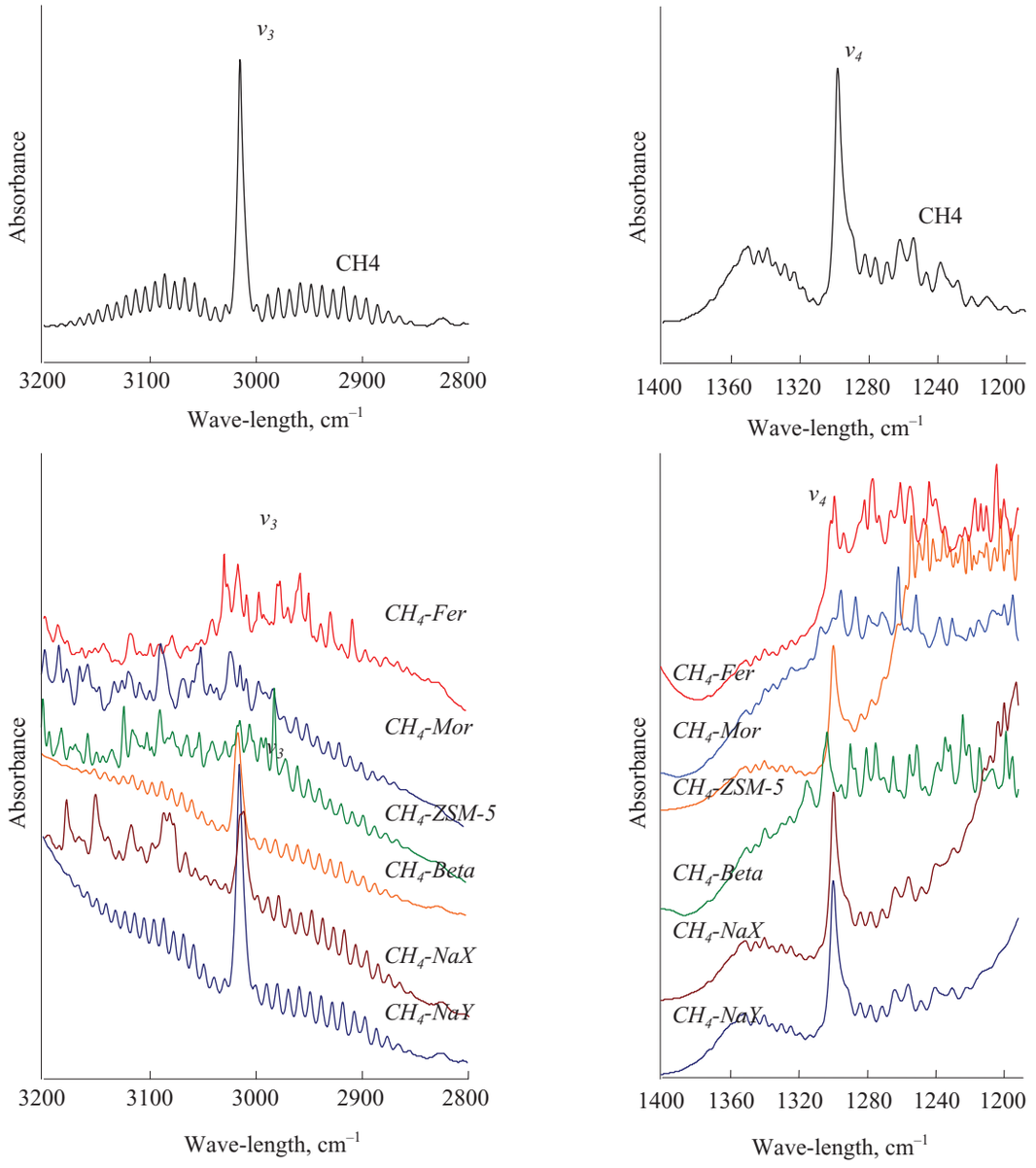


Figure 5. The FTIR spectra of methane, adsorbed methane on channel-type and cage-type zeolites zeolites at 293 K and 137 kPa.

## Methane-zeolite Interactions

Depending on the structure of the adsorbent, several types of diffusion mechanisms become dominant and sometimes two or three of them compete or co-operate (Suzuki 1990). The dominant mechanism also depends on a combination of adsorbate and adsorbent, and adsorption conditions used such as pressure, temperature, and concentration range. In microporous adsorbent such as zeolites, macropores usually act as a path for the adsorbate molecules to reach the interior part of the particle. Based on pore size of the zeolite, the diffusion is classified either as Knudsen or configurational. According to Xiao and Wei (2001), the configurational regime takes place when the ratio of molecular diameter (2r) to channel diameter (d) is greater than 0.8.

In general, there are several possible interactions between methane and zeolite structures. The electrostatic forces of methane-zeolite might exist between C — Na, H — O, and Si — C. The results of these interactions could be indicated in the FTIR spectra of asymmetric and symmetric bands of the adsorbates. Although unique identification of the adsorption spectra is difficult to perform, some peaks that attribute to specific interactions of the adsorbate on

Table 1. Surface area, micropore volume and pore diameter of channel-type and cage-type zeolites.

| Zeolite | Surface area ($m^2/g$) BET | Micropore volume ($cm^3/g$) | Pore diameter (nm) |
|---|---|---|---|
| ZSM-5 | 428.7 | 0.145 | 0.51 × 0.55 |
| Zeolite beta | 494.0 | 0.131 | 0.60 × 0.73, circular 0.5 |
| Mordenite | 520.4 | 0.180 | 0.70 × 0.65, 0.26 × 0.57 |
| Ferrierite | 290.7 | 0.106 | 0.54 × 0.42, 0.48 × 0.35 |
| NaY | 820.0 | 0.304 | 0.74 |
| NaX | 567.4 | 0.214 | 0.74 |

Table 2. The position of $v_3$ and $v_4$ FTIR bands and peak area of the adsorbed $CH_4$.

| Zeolite | $v_3$ band | | $v_4$ band | |
|---|---|---|---|---|
| | Peak position ($cm^{-1}$) | Area ($cm^2$) | Peak position ($cm^{-1}$) | Area ($cm^2$) |
| $CH_4$ | 3020 | | 1306 | |
| Channel: | | | | |
| Beta | 3015 (–5) | 14.80 | 1303 (–3) | 9.12 |
| ZSM-5 | 3013 (–7) | 3.23 | 1307 (+1) | 4.56 |
| Mordenite | 3011 (–9) | 0.95 | 1303 (–3) | 0.13 |
| Ferrierite | 3016 (–4) | 4.04 | 1303 (–3) | 4.50 |
| Cage: | | | | |
| NaY | 3015 (–5) | 18.52 | 1303 (–3) | 11.35 |
| NaX | 3012 (–8) | 9.67 | 1303 (–3) | 10.81 |

the adsorbent could be observed. The peak assigned to the $v_3$-band of adsorbed $CH_4$ observed in the region around 3015 $cm^{-1}$ is a result of free rotation of the adsorbed molecules around a single axis normal to the adsorbent surface (Yamazaki *et al.* 2000). For ZSM-5, mordenite and ferrierite, peaks in this region are relatively weak and the $v_3$-vibration band of methane split into several peaks. This finding indicated that the methane molecules experience a non-symmetrical field from the pore wall of the zeolites. However, zeolite beta and cage-type zeolites (NaX and NaY) have larger pore size (Table 1), thus the adsorbed molecules in the pore have a larger freedom of rotation and would experience a symmetrical field from the pore wall of the zeolites.

A weaker band in the spectra around 2900 $cm^{-1}$ assigned to the $v_1$ (symmetric) band actually represents the effect of the electrical field on the adsorption sites rather than a strong dispersion force at the surface of the zeolite. The peak could not be detected during the adsorption of methane on the zeolites. The appearance of $v_4$ bands induced by the interaction of adsorbed molecules with the sites created an electrical field at the surface shown in cage-type zeolites and beta zeolite. The peaks could not be clearly distinguished from other peaks in other channel-type zeolites. The stronger peak which appeared could be due to the unspecific interaction between methane and the pore which has a larger average pore diameter. As discussed in the previous section, the interaction between $CH_4$ and the wall of zeolite structure is not based on the active sites but it is more likely due to the confinement effect.

The magnitude of the $v$-peak shift is correlated with the strength of the interaction at the adsorption site (Barbosa *et al.* 2000). Table 2 shows that at 298 K and 137 kPa, the peaks are shifted to lower wavelength values. These phenomena indicate that there are some interactions between methane and zeolite even though they are only weak interactions. It also indicates that desorption could be easily achieved either by increasing the temperature or reducing the pressure of the adsorption system. It is also known that the band intensity represents the strength and the amount of molecules adsorbed on zeolites. However, the peak area does not actually represent in total the amount of methane adsorbed, but indicates the relative amount of adsorption in each zeolite.

Table 2 also shows that the integrated areas under of the $v_3$ and $v_4$ bands for cage-type structures are higher than for channel-type zeolites. Even though the large surface area might be the reason for higher adsorption, the amount adsorbed on mordenite with relatively high surface area (520 $m^2/g$) and pore volume (0.180 $cm^3/g$) does not follow the general assumption of adsorption. In fact, mordenite with it's high surface area and

micropore volume has lower integrated peak area than zeolite beta. For different structural framework, the integrated peak areas is in the order of NaY > NaX > beta > ferrierite > ZSM-5 > mordenite. Thus, this study indicates that the cage-type structure could be a better methane adsorbent than the channel-type zeolite. The presence of supercages and sodalite cages that encapsulated the methane molecules inside the structure contributed to higher adsorption of methane.

Even though channel-type structures might have limited adsorption sites, the channel itself acts as a channel for diffusion and site for the methane to adsorb. Adsorption of methane in a parallel channel (e.g. mordenite) is considered faster than the zig-zag channel, however once the channel is blocked, the adsorbate could not diffuse further into the adsorption sites. The zig-zag channels (e.g. ZSM-5) might encounter some problems at the intersection as any deposition could either partially or fully obstruct the pathway and thus, affect the adsorption of methane. The existence of zig-zag or sinusoidal channels may also affect the diffusivity of methane. Moreover, accessibility is also denied if pore blockage or any deposition occurred due to the collapse of the lattice structure. These explain the reasons for low adsorption of several types of zeolites. Thus, zeolite structures such as ZSM-5, mordenite and ferrierite might experience complex adsorption processes that result in less methane adsorption. The FTIR spectroscopy shows that there are several interactions between methane and zeolite. Hence, the possible electrostatic interaction between the adsorbate and zeolite are illustrated in Figure 6.

## CONCLUSION

A large number of different zeolite structures offer many possibilities for specific application. In order to choose the suitable adsorbent, adsorption characteristics of adsorbate-adsorbent need to be well understood. In this study, FTIR spectroscopy provided some information on the adsorption and interaction between methane and zeolites. The FTIR spectra revealed the effect of surface area, pore volume and different internal pore systems on methane adsorption. Even though the data obtained did not represent the absolute amount of adsorbate molecules adsorbed, it represented instead the relative amount of adsorbates that are attached to the active site. The information is important especially in the selection of potential zeolite adsorbent for specific applications such as adsorbed gas storage. This study showed that surface area was not the only factor to be considered when selecting the adsorbent of gases. Pore network system and structural arrangement might also influence the characteristics of adsorption processes. It also showed that cage-type zeolite could become potential methane adsorbent.

## ACKNOWLEDGEMENT

The authors would like to thank the Ministry of Science, Technology and Innovation, Malaysia and the Universiti Teknologi Malaysia for financing this project.

*Date of submission: November 2007*
*Date of acceptance: June 2008*

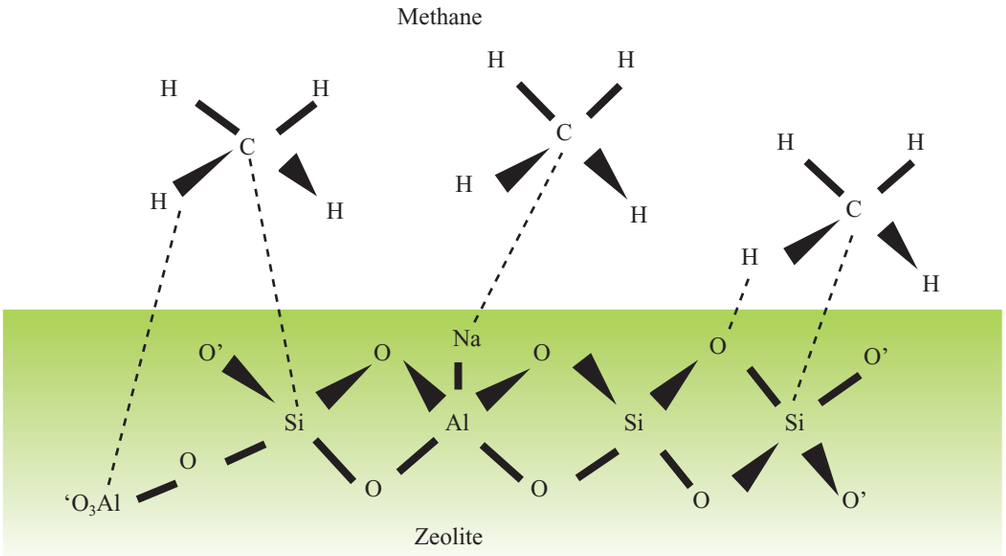


Figure 6. A schematic diagram indicates all possibilities of electrostatic interactions between methane and zeolite adsorbent.

## REFERENCES


Ackley, MW & Yang, RT 1991, 'Diffusion in ion-exchanged clinoptilolites', *American Institute of Chemical Engineering Journal*, vol. 37, pp. 1645 – 1656.

Barbosa LAMM, Zhidomirov GM, & van Santen, RA 2000, 'Theoretical study of methane adsorption on Zn(II) zeolites', *Physical Chemistry Chemical Physics*, vol. 2, pp. 3909–3918.

Barrer, RM 1982, *Hydrothermal Chemistry of Zeolites*, Academic Press, London.

Barrer, RM 1978 *Zeolites and Clay Minerals as Sorbents and Molecular Sieves*, Academic Press, London.

Bebon C, Colson D, Marrot B, Klein JP & Di Renzo, F 2002, 'Synthesis of zeolite: study and application of a new process of homogeneous shaking out of the medium to minimize the shear rate during crystallization', *Microporous and Mesoporous Materials*, vol. 53, pp. 13–20.

Bileo, S, Goetz, V, & Maurin, S 2001, 'Dynamic discharge and performance of a new adsorbent for Natural Gas', *American Institute of Chemical Engineering Journal*, vol. 47, pp. 2819–2830.

Bülow, M, Dao, L & Fitch, FR 1996, *Removal of carbon dioxide from gas streams*, U.S. Patent 5, 587,003.

Calvalho, MB, Carlvalho, AP, Ribeiro, FR, Florentino, A, Gnep, NS, & Guisnet, M 1994, 'Dealumination of zeolites: part V. Influence of the hydrothermal treatment of offretite on its pore structure and acid properties', *Zeolites*, vol. 14, pp. 217–224.

Chao, CC 1990, *Selective adsorption on magnesium-containing clinoptilolites*, U.S. Patent 4, 964,889.

Chen, H, Matsumoto, A, Nishimiya, N, & Tsutsumi, K 1999, 'Preparation and characterization of $TiO_2$ incorporated Y-zeolite', *Colloids and Surfaces A: Physicochemical and Engineering Aspects*, vol. 57, pp. 295–305.

Choudhary, VR & Mayadevi, S 1996, 'Adsorption of methane, ethane, ethylene and carbon dioxide in silicalite — I.', *Zeolites*, vol. 17, pp. 501–507.

Esparza, JM, Ojeda, ML, Campero, A, Hernandez, G, Felipe, C, Asomoza, M, Cordero, S, Kornhauser, I, & Rojas, F 2005, 'Development and sorption characteristion of some model mesoporous and microporous silica adsorbents', *Journal of Molecular Catalysis A: Chemical*, vol. 228, pp. 97–110.

Ghorai, PK, Sluiter, M, Yashonath, S, & Kawazoe, Y 2006, 'Intermolecular potential for methane in zeolite A and Y: adsorption isotherm and related properties', *Solid State Science*, vol. 8, pp 214–258.

Harlick, PJE & Tezel, FH 2004 'An experimental adsorbent screening study for $CO_2$ removal from $N_2$', *Microporous and Mesoporous Materials*, vol. 76, pp. 71–79.

Hasegawa, Y, Watanabe, K, Kusakabe, K & Morooka, S 2001, 'The separation of $CO_2$ using Y-type zeolite membranes ion-exchanged with alkali metal cations', *Separation and Purification Technology*, vol. 22–23, pp. 319–325.

Hernandez-Huesca, R, Diaz, L, & Aguilar-Armenta, G 1999, 'Adsorption equilibria and kinetics Of $CO_2$, $CH_4$, and $N_2$ in natural zeolites', *Separation and Purification Technology*, vol. 15, pp. 163–173.

Jayaraman, A, Yang, RT, Chinn, D, & Munson, CL 2004, 'Tailored clinoptilolites for nitrogen/methane separation', *Industrial & Engineering Chemistry Research*, vol. 44, pp. 5184–5192.

Kazanskii VB, Serykh, AI, & Bell, AT 2002, 'Diffuse-reflectance IR spectra of methane adsorbed on NaZSM-5 and HZSM-5 zeolites', *Kinetics and Catalysis*, vol. 43, pp. 419–426.

Khelifa, A, Benchehida, L, & Derriche, Z 2004, 'Adsorption of carbon dioxide by X zeolites exchanged with $ni^{2+}$, and $cr^{3+}$: isotherm and isosteric heat', *Journal of Colloid Interface Science*, vol. 278, pp. 9–17.

Kurama, H, Zimmer, A, & Reschetilowski, W 2002, 'Chemical modification effect on the sorption capacities of natural clinoptilolite', *Chemical Engineering Technology*, vol. 25, pp. 301–305.

Kusakabe, K, Kuroda T & Morooka, S 1998, 'Separation of carbon dioxide from nitrogen using ion-exchanged faujasite-type zeolite membranes formed on porous support tubes', *Journal of Membrane Science*, vol. 148, pp. 13–23.

Li, P & Tezel, FH 2007, 'Adsorption separation of $N_2$, $O_2$, $CO_2$ and $CH_4$ gases by β-zeolite', *Microporous and Mesoporous Materials*, vol. 98, pp. 94–101.

Matranga, KR, Myers, AL & Glandt, ED 1992, 'Storage of natural gas by adsorption on activated carbon', *Chemical Engineering Science*, vol. 47, pp. 1569–1579.

Melo, DMA, de Souza, JR, Melo, MAF, Martinelli, AE, Cachama, GHB & Cunha, JD, 2006, 'Evaluation of zinox and zeolite materials as adsorbents to remove $H_2S$ from natural gas', *Colloids and Surfaces A: Physicochemical and Engineering Aspects*, vol. 272, pp. 32–36.

Mintova, S & Bein, T 2001, 'Nanosized zeolite films for vapor sensing applications', *Microporous and Mesoporous Materials*, vol. 50, pp. 159–166.

Mizukami, K, Takaba, H, Kobayashi, Y, Oumi, Y, Belosludov, RV, Takami, S, Kubo, M & Miyamoto, A 2001, 'Molecular dynamics calculations of $CO_2/N_2$ mixture through the NaY type zeolite membrane', *Journal of Membrane Science*, vol. 188, pp. 21–28.

Nijkamp, MG, Raaymakers, JEMJ, van Dillen, AJ & Jong, KP 2001, 'Hydrogen storage using physisorption-materials demand', *Applied Physics A*, vol. 72, pp. 619–623.

Nishimaya, N, Kishi, T, Mizushima, T, Matsumoto, A & Tsutsumi, K 2001, 'Hyperstoichiometric hydrogen occlusion by palladium nanoparticles included in NaY Zeolite', *Journal of Alloys and Compound*, vol. 319, pp. 312–321.

Roozeboom, F, Robson, HE, & Chan, SS 1983 'Laser Raman study on the crystallization of zeolites A, X, and Y', *Zeolites*, vol. 3, pp. 321–328.

Seidel, U, Koch, M, Brunner, E, Staudte, B & Pfeifer, H 2000, 'NMR and IR studies on the adsorption of methane and trimethylgallium on zeolite HY', *Microporous and Mesoporous Materials*, vol. 35–36, pp. 341–347.

Simoncic, P & Armbruster, T 2004, 'Se incorporated into zeolite mordenite-Na: a single-crystal X-ray study', *Microporous and Mesoporous Materials*, vol. 71, pp. 185–198.

Sing, KSW 1984 'Reporting physisorption data for gas /liquid systems fundamental of adsorption: fundamental of adsorption', in *Proceedings of the Engineering Foundation Conference*, United Engineering Trustees Inc.

Sultana, A, Habermacher, DD, Kirschhock, CEA & Martens, JA 2004, 'Adsorptive separation of $NO_x$ in presence of $SO_x$ from gas mixture simulating lean burn engine exhaust by pressure swing process on Na-Y zeolite', *Applied Catalysis B: Environmental*, vol. 48, pp. 65–76.

Suzuki M 1990, *Adsorption Engineering*, Elsevier, Amsterdam.

Szabo, NF 2003, 'Development of harsh environment nitrogen oxides solid-state gas sensors', PhD thesis, Ohio State University.

van Bekkum H, Flanigen, EM, & Jansen, JC (eds) 1991, *Introduction to zeolite science and practice: studies in surface science and catalysis*, vol. 58, Elsevier, Amsterdam.

Weikamp, J 1996, *Zeolite as media for hydrogen storage*, Institute for Thermodynamic and Warmetechnic, University Stuttgart.

Xiao, J & Wei, J 2001, 'Diffusion mechanism of hydrocarbon in zeolites — I. theory', *Chemical Engineering Science*, vol. 47, pp. 1123–1141.

Yamazaki, T, Nishimura, H, & Ozawa, S 2000, 'Adsorption behavior of some gas molecules in Ω-zeolite pores', *Microporous and Mesoporous Materials*, vol. 38, pp. 187–196.

Yang, L, Trafford, Kresnawahjuesa, KO, Šepa, J & Gorte, RJ 2001, 'An examination of confinement effects in high-silica zeolites', *Journal of Physical Chemistry B*, vol. 105, pp. 1935–1942.

Yoshida, H, Yamazaki T & Ozawa, S 2000, 'IR spectra of CH4 physisorbed on an active carbon at low temperature', *Journal of Colloid and Interface Science*, vol. 224, pp. 261–264.

ASM Sci. J., **2(1)**, 45–56

# Effect of Nutritional Factors on the Growth and Production of Biosurfactant by *Pseudomonas aeruginosa* Strain 181

L. Al-Araji[1,2]*, R.N.Z.A. Rahman[1], M. Basri[1] and A. B. Salleh[1]

The growth and production of biosurfactant by *P. seudomonas aeruginosa* (181) was dependant on nutritional factors. Among the eleven carbon sources tested, glucose supported the maximum growth (0.25 g/L) with the highest biosurfactant yield and this was followed by glycerol. Glucose reduced the surface tension to 35.3 dyne/cm and gave an E24 reading of 62.7%. Butanol gave the lowest growth and had no biosurfactant production. For the nitrogen sources tested, casamino acid supported a growth of 0.21 g/L which reduced the surface tension to 41.1 dyne/cm and gave an E24 reading of 56%. Soytone was assimilated similarly, with good growth and high biosurfactant production. Corn steep liquor gave the lowest growth and did not show any biosurfactant activity.

**Key words:** growth; production; biosurfactant; *P. seudomonas aeruginosa*; carbon sources; glycerol; butanol; nitrogen sources; casamino; soytone; corn steep liquor

Biosurfactants are amphiphilic compounds containing hydrophobic and hydrophilic moieties that reduce surface tension and interfacial tension between individual molecules at the surface and interface, respectively. Biosurfactants have several advantages over chemical surfactants such as lower toxicity, better environmental compatibility, high selectivity and specific activity at extreme temperatures, pH, and salinity (Banat *et al*. 2000). Interest in microbial surfactants has increased considerably in recent years, especially due to their potential application in enhanced oil recovery. Their potential for enhanced oil recovery is based on their application as agents for rock wetting, micellar flooding, emulsification, de-emulsification, and viscosity reduction of heavy crude oil (Finnerty & Singer 1983). The biodegradative property of biosurfactants makes them ideal for environmental applications. Microbial surfactants have been used for hydrocarbon-contaminated site restoration (Ron & Rosenberg 2002). It has been reported that biosurfactants can enhance solubility and degradation of organic toxic compounds (Jordan *et al*. 1999).

One of the strategies used to stimulate biosurfactant production is to modify the nutritional conditions (Cooper *et al*. 1981; Guerra-Santos *et al*. 1984). It is important to understand the role of macro- and micro-nutrients for biosurfactants production by micro-organisms. For example, the addition of metals to medium had no effect on microbial surfactant production by *Torulopsis bombicola*, *Corynebacterium lepus* and *Nocardia amarae*, but, it has been shown that the addition of these can improve the yield of surfactin by *Bacillus subtilis* (Yu-Hong & I-Ming 1998). Some micro-organisms produce biosurfactants only when hydrophobic carbon sources such as hydrocarbons or vegetable oils are used, while others require carbohydrates, and several other carbon sources, either in combination or individually (Mulligan & Gibbs 1993). This study describes the effect of various carbon and nitrogen sources on the growth and biosurfactant production by bacterium identified as *P. seudomonas aeruginosa* strain 181.

## MATERIALS AND METHODS

### Bacteria

*P. seudomonas aeruginosa* strain 181 used in this study was isolated from soil (Ali 1998).

### Media and Growth Conditions

The basal medium used for this study was Bushnell and Hass medium (Difco). The pH of the medium was adjusted to 7.0 and it was autoclaved at 121ºC for 15 min. All the carbon sources used were of 2% (v/v) and filter-sterilized using 0.20 µm filter membrane, except for glycerol which was autoclaved together with the basal medium. Apart

[1] Enzyme and Microbial Technology Research, Faculty of Biotechnology and Biomolecular Sciences, Universiti Putra Malaysia, 43400 Serdang, Selangor, Malaysia

[2] Current address: Department of Basic Medical Sciences, Faculty of Nursing, International Islamic University Malaysia, 25100 Kuantan, Pahang, Malaysia

* Corresponding author (e-mail: laith@iiu.edu.my)

from corn steep liquor of (2% v/v), other nitrogen sources as of 2% (w/v) were each added to the basal medium and autoclaved. Different concentrations of metal ions were tested to optimize the basal medium. *P. aeruginosa* strain 181 was grown in nutrient broth at 37ºC for 18 h at 150 r.p.m. The culture was then added (10% v/v) to the medium from various carbon and nitrogen sources. The whole cell protein was determined by the method of Patel and Desai (1997) with modification. The cells were then briefly centrifuged at 8600 × g for 15 min and the protein was estimated by the method of Bradford (1976). Biosurfactant activity was determined by measuring the reduction in the surface tension of the culture supernatant using a Fisher surface tensiomat model 21. The E24 was determined by vortexing equal volumes of culture supernatant with hexadecane at high speed for 4 min and leaving it for 24 h. The E24 was calculated as the height of the emulsion layer/ total height × 100.

## RESULTS AND DISCUSSION

### Effect of Carbon Sources

The results showed that glucose supported the highest growth as measured by whole cell protein (0.24/0.25 g/l) (Figure 1), followed by glycerol and ethanol. Slight growth was observed with crude oil. Decreasing growth was observed with tetradecane, 1-propanol, 1-butanol, sucrose and maltose. Glucose yielded the highest biosurfactant production, reducing the surface tension to 35.3 dyne/cm. It was followed by glycerol, hexadecane and crude oil with surface tension reduction to 41.5, 45 and 49.5 dyne/cm, respectively. The highest emulsifying activity was 62.7% and 52% for glucose and glycerol, respectively. Hexadecane gave a significant emulsification index (E24), of 45.8% which correlated well with the increase in biomass. In an attempt to maximize the biosurfactant production from *P. aeruginosa* 181, the effects of several carbon sources on growth performances and biosurfactant production in a time course study were examined. Hexadecane was used slowly by the bacteria, growth was observed to delay, it might be due to the adaptation of the bacteria to the carbon source. This delay was expected since a number of different biochemical reactions are involved in alkane utilization including their terminal hydroxylation and the β-oxydation (Witholt *et al.* 1990). The result indicated that the biosurfactant production of *P. aeruginosa* 181 when grown in glucose, was growth dependent. However, even though ethanol supported good growth, the biosurfactant activity was lower compared to hexadecane. The surface tension dropped rapidly while the emulsification capacity continued to increase over the entire period of the experiment. This contrast might be due to the biosurfactant reaching its critical micelle concentration, beyond which constant surface tension was observed. Emulsification capacity, however, would continue to increase with further biosurfactant accumulation (Ghurye *et al*. 1994). Similar observations were reported by Kim *et al.* (1997) which showed that glucose gave the highest emulsification index (E24) among several carbon sources tested by *B. subtilis* C9. Production of biosurfactant by strain 181 appeared to be growth associated similar to that shown in the production of biosurfactant from *P. seudomonas putida* (Tuleva *et al*. 2002). Growth associated biosurfactant production was reported to have parallel relationships existing between growth, substrate utilization and biosurfactant production (Cooper & Goldenberg 1987). A number of studies have indicted that the type of media and growth conditions can influence the type and yield of the biosurfactant. The carbon sources influence the biosurfactant synthesis either via induction or repression. In some cases, addition of water-immiscible substrates results in induction of biosurfactant production (Cameotra & Makkar 1998).

### Effect of Nitrogen Sources

Nitrogen represents another important element in bacterial metabolism. To evaluate the influence of nitrogen sources on the growth and biosurfactant production by *P. aeruginosa* 181, batch cultures were conducted in media containing various nitrogen sources. Casamino acid supported the highest growth (0.25 g/l) followed by soytone, peptone, meat extract, yeast extract and tryptone (Figure 2). Casamino acid yielded the highest biosurfactant production, reducing the surface tension 41.1 dyne/cm. It was followed by soytone and malt extract, they reduced the surface tension to 36.13 and 41.1 dyne/cm, respectively. Meat extract, tryptone, peptone and yeast extract, reduced the surface tension to 38.4 dyne/cm, 45.1 dyne/cm, 46.4 dyne/cm and 50.4 dyne/cm, respectively. The highest emulsifying activity was 56% and 52% for casamino acid and soytone, respectively. Corn steep liquor was ineffective as a nitrogen source to promote the growth and biosurfactant production of *P. aeruginosa* 181. Apart from serving as a nitrogen source, corn steep liquor also provided several micronutrients, vitamins and growth-promoting factors. Nevertheless, its use was limited by its seasonal and inter-batch variability factors (Malathi & Chakraborty 1991). The results indicated that the biosurfactant production of *P. aeruginosa* 181 when grown in casamino acid and soytone was growth dependent. While meat extract, yeast extract and tryptone supported good growth of the microbe, their biosurfactant activity was lower than malt extract. Banat (1995) reported that 3.5% yeast extract could reduce the surface tension of culture-broth to 42 dynes/cm on *Rhodococcus* bacterium strain ST5. In another study Guerra-Santos *et al*. (1984) found that biosurfactant was poor when yeast extract was present in the medium. Based on these results, the use of complex medium additives, such as yeast extract in the basal medium should be avoided. With casamino acid and soytone, most of the biosurfactants were produced by *P. aeruginosa* 181 at the late exponential growth phase

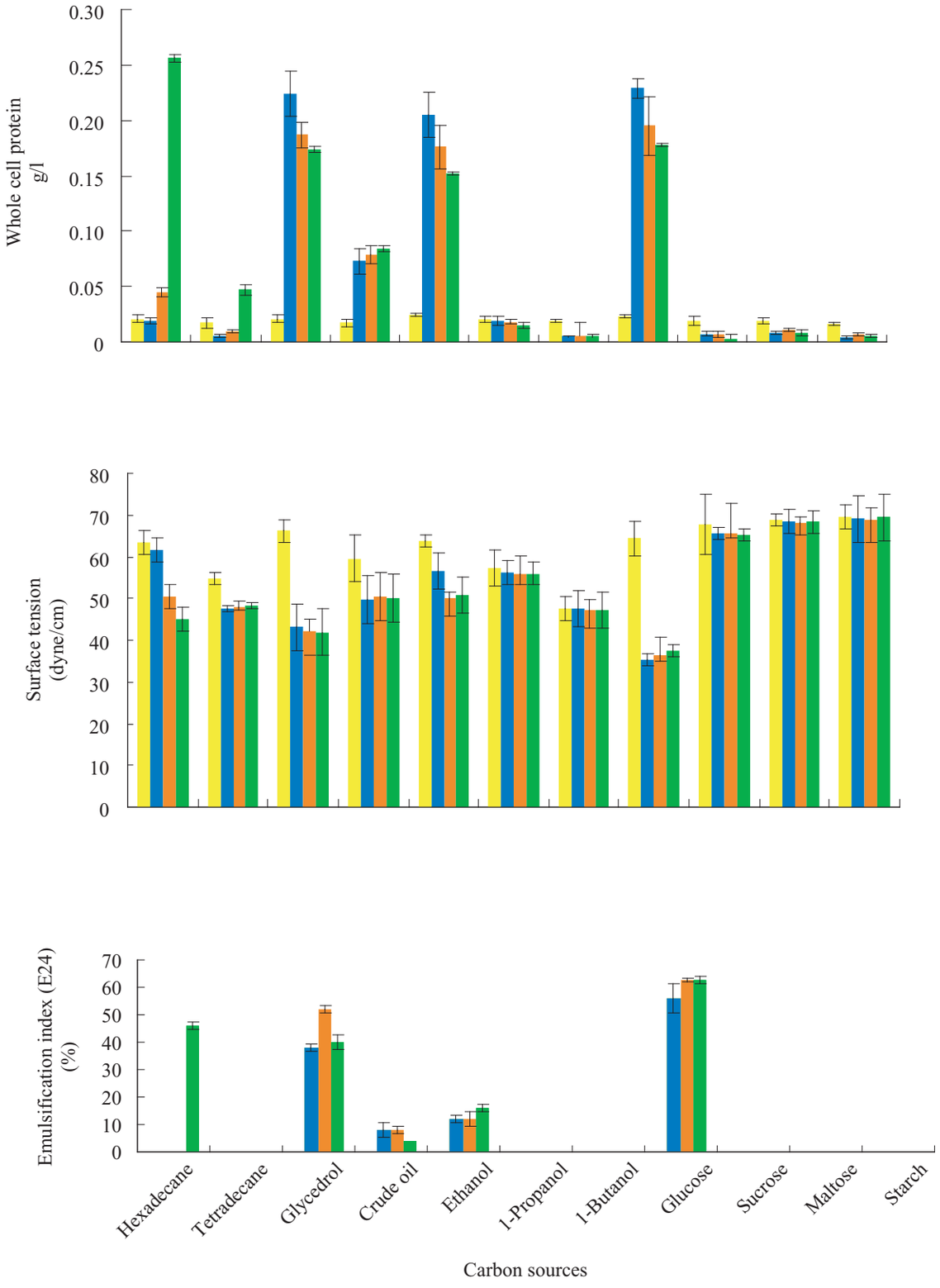


Figure 1. Effect of carbon sources on bacterial growth and biosurfactant production by *P. aeruginosa* 181 as determined by whole cell protein, surface tension reduction and emulsification index (E24). Different carbon sources: 2.0% (v/v) of hexadecane, tetradecane, glycerol, crude oil, ethanol, 1-propanol, 1-butanol, glucose, sucrose, maltose, starch were adde into basal media and at pH 7.0, 37°c for 0 day ( ), 7 days ( ), 14 days ( ) and 21 days ( ).

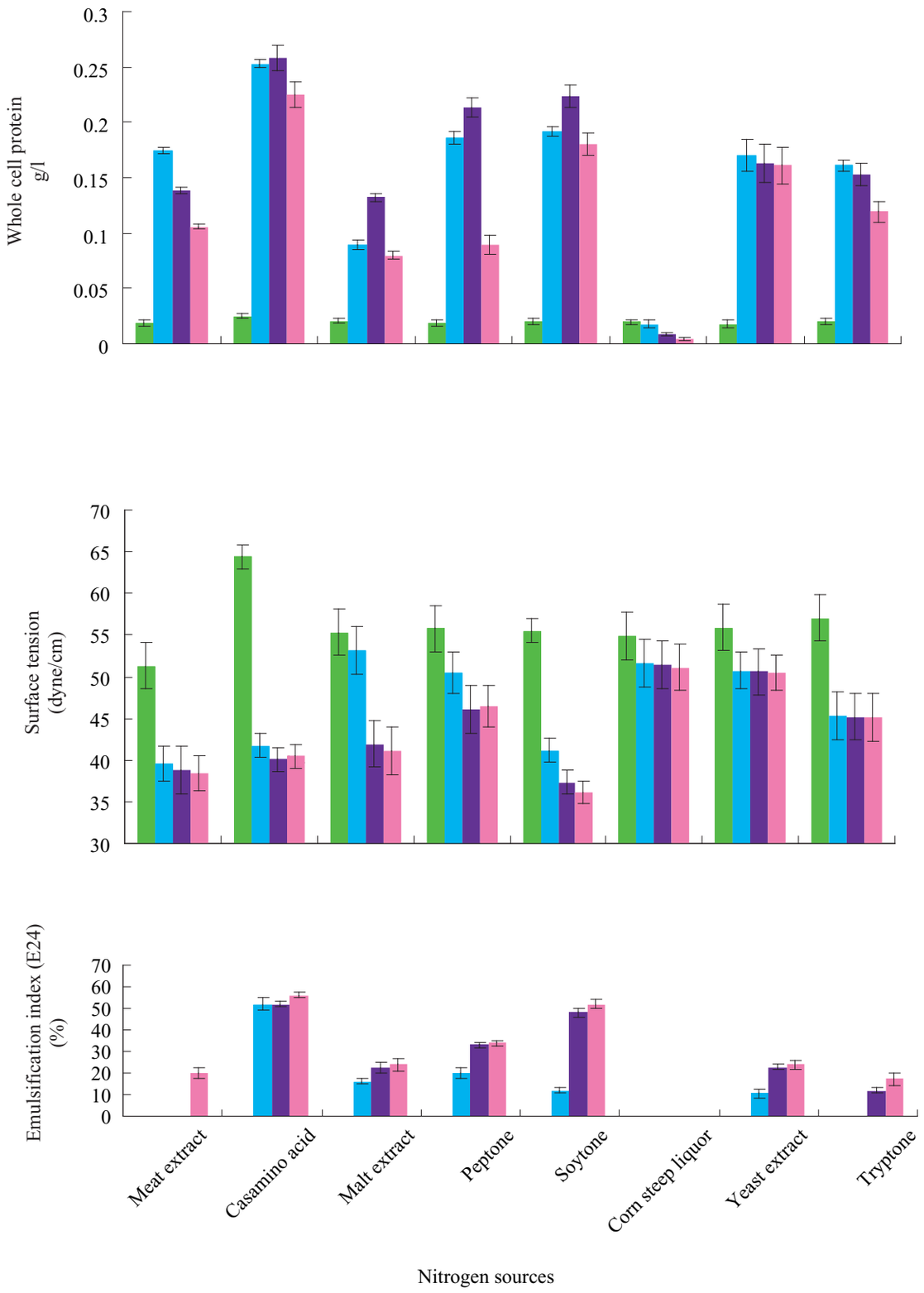


Figure 2. Effect of nitrogen sources on bacterial growth and biosurfactant production by *P. aeruginosa* 181 as determined by whole cell protein, surface tension reduction and emulsification index (E24). Different nitrogen sources: 2.0% (w/v) of yeast extract, tryptone, soytone, corn steep liquor, casamino acid, malt extract, peptone and meat extract were added into basal media at pH 7.0, 37°C for 0 day ( ), 7 days ( ), 14 days ( ), and 21 days ( ).

and the maximum level was obtained at the stationary growth phase. This is in agreement with the studies done by Ramana & Karanth (1989). They observed that the synthesis of biosurfactant for *P. aeruginosa* occurred only when the cells were in the stationary growth phase. The use of casamino acid as nitrogen sources in biosurfactant production has not been listed in published reports. In most of the studies, the levels of biosurfactant increase were marginal and were probably due to difference in the process condition, i.e. physicochemical and engineering parameters or nutritional factors. A nitrogen source was also understood to regulate secondary metabolite (Marwick *et al*. 1999; Haba *et al*. 2000).

## Effect of Different Metal Ions

*Effect of different concentrations of ferric chloride*. Luxuriant growth was observed in all concentrations (0 g/l – 0.3 g/l) of ferric chloride, increasing the concentrations (0 g/l – 0.1 g/l) of the ion in the media was shown to enhance the biosurfactant yield proportionally. A concentration of 0.05 g/l of ferric chloride maximized the biosurfactant production while higher concentrations considerably repressed the biosurfactant synthesis (Figure 3a). *P. aeruginosa* 181 exhibited a similar growth pattern in all concentrations of ferric chloride and it started to produce biosurfactant at the late-exponential phase, and maximum production was reached at the stationary phase. Currently, the molecular mechanism underlying metal ions regulation remains unknown. Many researchers have found that biosurfactant liberated in the presence of iron salts was more active and stable. Therefore based on cost effectiveness, availability, stability and the stimulating effects on surfactant actions, to optimize the biosurfactant of *P. aeruginosa* 181 ferric chloride should be added in the basal medium. Espuny *et al*. (1996) reported that the effect of iron concentration on biosurfactant production was greater than on cell growth from *Rhodococcus sp*. 51T7. On the other hand some researchers demonstrated the negative effect of iron. Zenaitis & Cooper (1994) showed that with iron concentrations of 0.4 p.p.b. and greater, no tetracycline was detected from *Streptomyces aureofaciens*.

*Effect of different concentrations of magnesium sulphate*. The possible effects produced by different concentrations of magnesium sulphate were also examined (Figure 3b). Magnesium sulphate at 0.1 g/l to 0.3 g/l in the basal medium showed a higher cell growth. Maximum biomass was observed at 0.2 g/l of magnesium sulphate. Increase in the concentrations (0 g/l – 0.2 g/l) of the magnesium sulphate in the media showed enhancement in the biosurfactant yield. Biosurfactant was produced initially at the late-exponential phase and maximum production was reached at the stationary phase. Higher concentrations, in excess of 0.2 g/l of magnesium sulphate considerably repressed the biosurfactant synthesis. The results were in agreement with Patel and Desai (1997), who showed that 0.2 g/l of magnesium sulphate was the optimum concentration for biosurfactant produced by *P. aeruginosa* GS3. Deziel *et al*. (2000) reported that optimum concentration of magnesium sulphate was 0.4 g /l for rhamnolipids produced by *P. aeruginosa* 57RP.

*Effect of different concentrations of calcium chloride*. This experiment was carried out by supplementing the basal medium with various concentrations of calcium chloride. The results indicated that bacterial growth and biosurfactant activity decreased dramatically in the absence of calcium chloride (Figure 3c). The calcium chloride at 0.02 g/l supported the highest growth and this was followed by 0.03 g/l and 0.01 g/l. Calcium chloride at 0.02 g/l yielded the highest biosurfactant production, reducing the surface tension to 41.2 dyne/cm and this was followed by 0.03 g/l and 0.01 g/l. The maximum emulsifying activity (62%) was obtained at 0.02 g/l of calcium chloride. A concentration of 0.03 g/l and 0.1 g/l gave 48% and 46% emulsifying activity, respectively. The biosurfactant activity was markedly inhibited by calcium chloride at a low concentration (0.1%) and completely inhibited at 3% level (Singh & Desai 1989). The effect of calcium is an important consideration for field applications because precipitation can cause major loss of surfactant which can in turn affect the performance of the surfactant system (Bai *et al*.1998).

*Effect of different concentrations of zinc sulphate and manganese sulphate*. Biosurfactant production was detected in media containing different individual concentrations of zinc sulphate and manganese sulphate. For the different concentrations of zinc sulphate tested, the highest bacterial growth was detected and gave relatively better results in medium incorporated with zinc sulphate at a concentration of 0.05 g/l, (Figure 3d). The surface tension activity in the presence of 0.05 g/l, 0.1 g/l and 0.5 g/l zinc sulphate were 41.6 dyne/cm, 47.8 dyne/cm and 48.8 dyne/cm, respectively. Lower levels of biosurfactant were observed when zinc sulphate and manganese chloride were used in the medium (Kosaric *et al*. 1990). The cell growth values obtained with various concentrations of manganese sulphate were considerably lower than those observed in basal medium (Figure 3e). The surface tension at different concentrations of manganese sulphate were 43.1 dyne/cm, 44.2 dyne/cm and 45.2 dyne/cm at 0.05 g/l, 0.1 g/l and 0.5 g/l; respectively. Deziel *et al*. (2000) demonstrated that maximum rhamnolipids production by *P. aeruginosa* 57RP was obtained in the absence of zinc and manganese salts. This observation indicated that zinc and manganese sulphate were not essential for growth and biosurfactant production by *P. aeruginosa* 181. It is well established that manganese acts as a 'key' metal for the production of other secondary metabolites by *Bacillus species* without having an effect on the cell growth (Weinberg 1970).

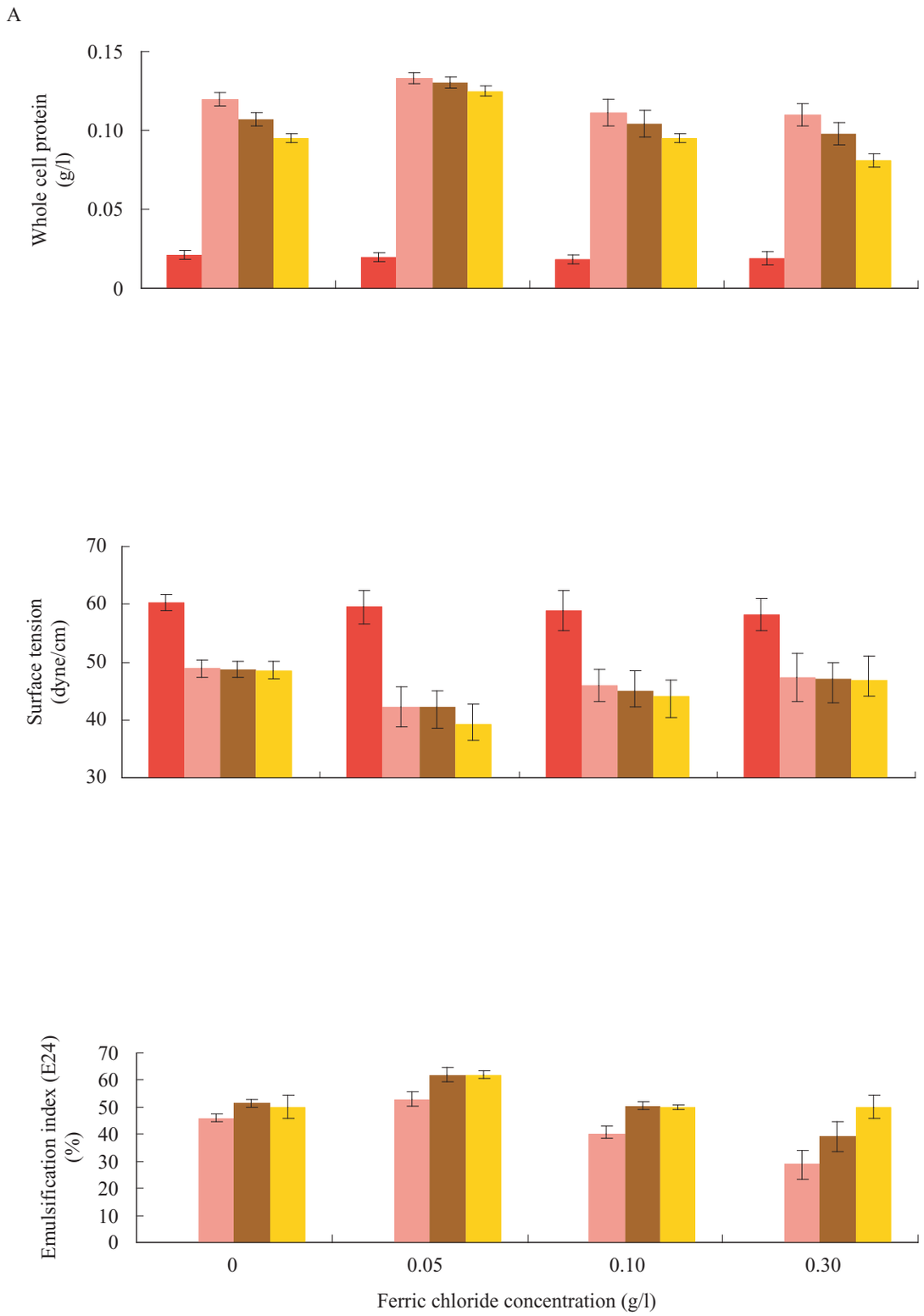


Figure 3a. Effect of different metal ions on bacterial growth and biosurfactant production by *P. aeruginosa* 181 as determined by whole cell protein, surface tension reduction and emulsification index (E24). Casamino acid, was added into basal media at pH 7.0, 37°C for 0 day ( ), 7 days ( ), 14 days ( ) and 21 days ( ). (a) Ferric chloride; (b) Magnesium sulphate; (c) Calcium chloride; (d) Zinc sulphate and (e) Manganese sulphate.

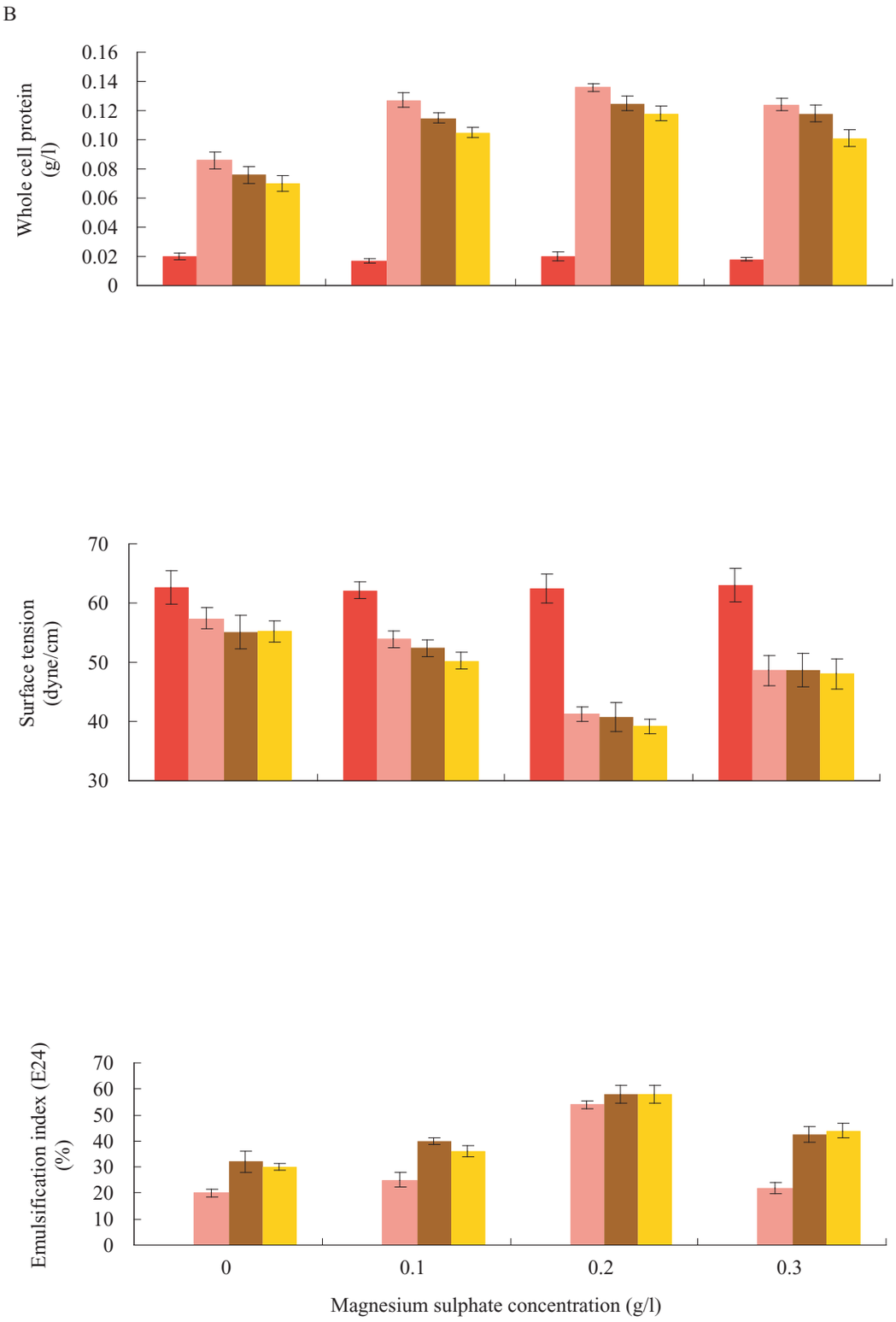


Figure 3b. Effect of different metal ions on bacterial growth and biosurfactant production by *P. aeruginosa* 181 as determined by whole cell protein, surface tension reduction and emulsification index (E24). Casamino acid, was added into basal media at pH 7.0, 37°C for 0 day ( ), 7 days ( ), 14 days ( ) and 21 days ( ). (a) Ferric chloride; (b) Magnesium sulphate; (c) Calcium chloride; (d) Zinc sulphate and (e) Manganese sulphate.

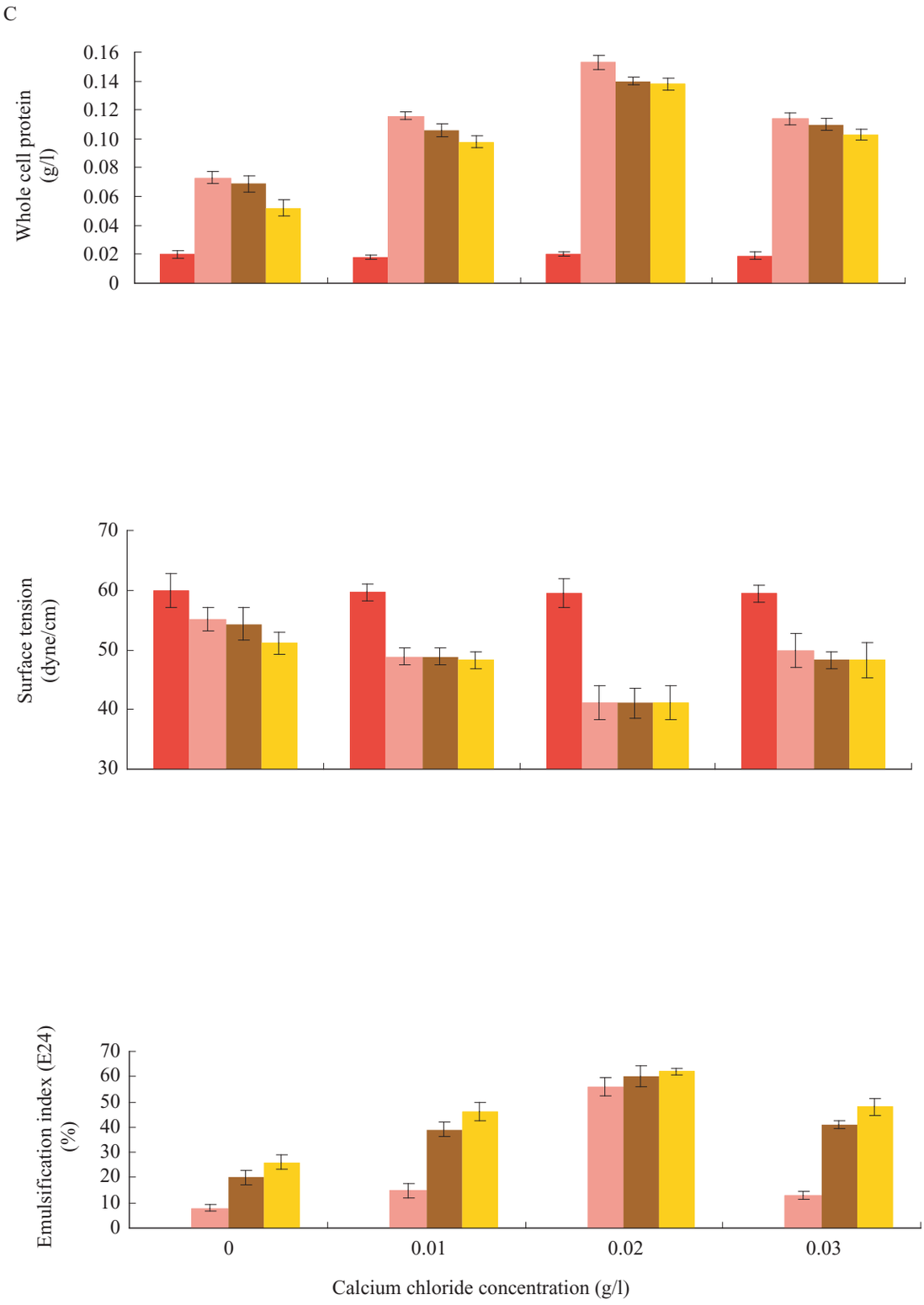


Figure 3c. Effect of different metal ions on bacterial growth and biosurfactant production by *P. aeruginosa* 181 as determined by whole cell protein, surface tension reduction and emulsification index (E24). Casamino acid, was added into basal media at pH 7.0, 37°C for 0 day ( ), 7 days ( ), 14 days ( ) and 21 days ( ). (a) Ferric chloride; (b) Magnesium sulphate; (c) Calcium chloride; (d) Zinc sulphate and (e) Manganese sulphate.

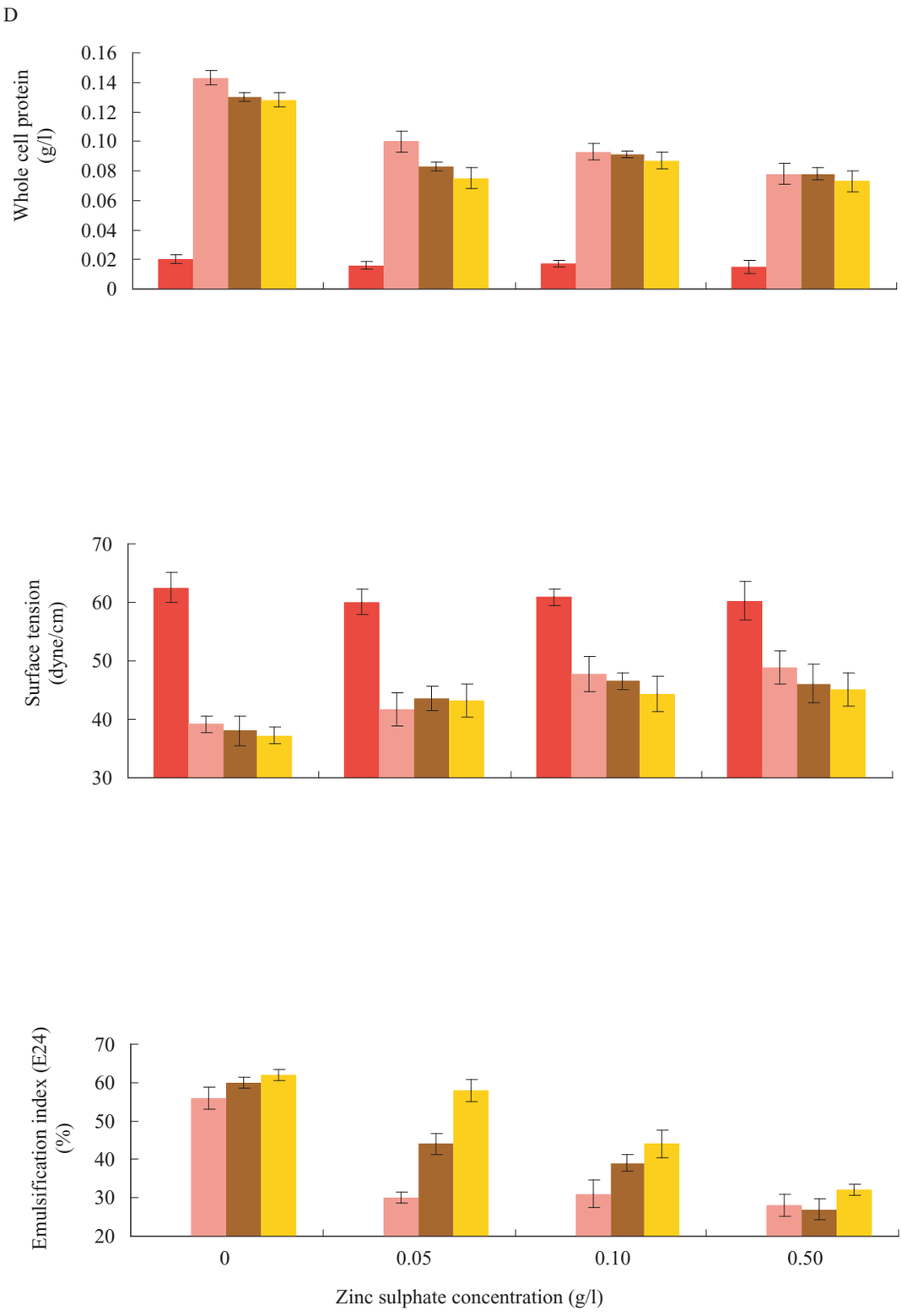


Figure 3d. Effect of different metal ions on bacterial growth and biosurfactant production by *P. aeruginosa* 181 as determined by whole cell protein, surface tension reduction and emulsification index (E24). Casamino acid, was added into basal media at pH 7.0, 37°C for 0 day ( ), 7 days ( ), 14 days ( ) and 21 days ( ). (a) Ferric chloride; (b) Magnesium sulphate; (c) Calcium chloride; (d) Zinc sulphate and (e) Manganese sulphate.

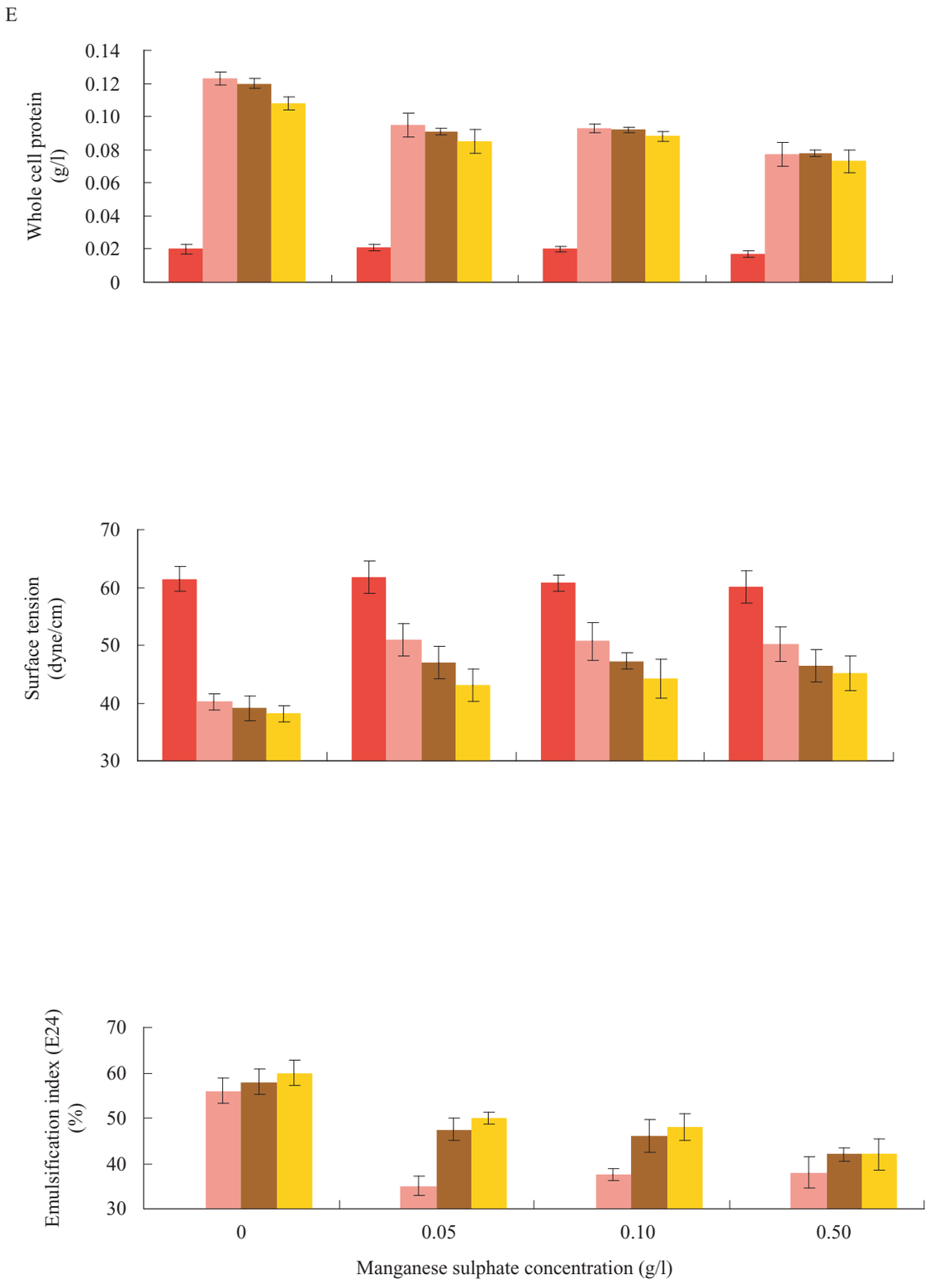


Figure 3e. Effect of different metal ions on bacterial growth and biosurfactant production by *P. aeruginosa* 181 as determined by whole cell protein, surface tension reduction and emulsification index (E24). Casamino acid, was added into basal media at pH 7.0, 37°C for 0 day ( ), 7 days ( ), 14 days ( ) and 21 days ( ). (a) Ferric chloride; (b) Magnesium sulphate; (c) Calcium chloride; (d) Zinc sulphate and (e) Manganese sulphate.

Our data indicate a medium composition and conditions for maximum biosurfactant production by *P. aeruginosa* 181. It was established specifically for optimum biosurfactant production by this strain and it might not be suitable for other strains or micro-organisms. Each organism or strain has its own defined medium and special conditions for maximum production.

## ACKNOWLEDGEMENT

The Ministry of Science Technology and Environmental Malaysia (IRPA No: 09 02 04 0184) and the Faculty of Nursing, International Islamic University Malaysia are acknowledged for funding this research.

*Date of submission: November 2006*
*Date of acceptance: June 2008*

## REFERENCES

Ali, FM 1998, 'Crude oil degrading bacteria: isolation, growth and biodegradation studies', MSc thesis, Universiti Putra Malaysia.

Bai, G, Brusseau, ML & Miller, RM 1998, 'Influence of cation type, ionic strength and pH on solubilization and mobilization of residual hydrocarbon by a biosurfactant', *Journal of Contaminant Hydrology*, vol. 30, no. 3, pp. 265–279.

Banat, IM 1995, 'Characterization of biosurfactants and their use in pollution removal-state of the art', *Acta Biotechnologica*, vol. 15, no. 5, pp. 251–267.

Banat, IM, Makkar, RS & Cameotra, SS 2000, 'Potential commercial applications of microbial surfactants', *Applied Microbiology and Biotechnology*, vol. 53, no. 5, pp. 495–508.

Bradford, MM 1976, 'Method of Bradford', *Analytical Biochemistry*, vol. 72, no. 7, pp. 248–254.

Cameotra, SS & Makkar RS 1998, 'Synthesis of biosurfactants in extreme conditions', *Applied Microbiology and Biotechnology*, vol. 50, pp. 520–529.

Cooper, DG & Goldenberg, BG 1987,'Surface-active agents from two *Bacillus* species', *Applied and Environmental Microbiology*, vol. 53, no. 2, pp. 224–229.

Cooper, DG, Akit, J & Kosaric, N 1981,'Surface activity of the cells and extracellular lipids of Corynebacterium fascians CF-15', *Journal of Fermentation Technology*, vol. 60, no. 1, pp. 19–24.

Deziel, E, Lepine, F, Milot, S & Villemur, R 2000,'Mass spectrometry monitoring of rhamnolipids from a growing culture of *Pseudomonas aeruginosa* Strain 57RP', *Biochimica et Biophysica Acta*, vol. 1485, no. 2–3, pp. 145–152.

Espuny, MN, Egido, S, Rodon, I, Manresa, A & Mercade, ME 1996, 'Nutritional requirements of a biosurfactant producing strain *Rhodococcus sp* 51T7', *Biotechnology Letters*, vol. 18, no. 5, pp. 521–526.

Finnerty, WR & Singer, ME 1983, 'Microbial enhancement of oil recovery', *Biotechnology*, vol. 1, no. 1, pp. 47–54.

Ghurye, GL, Vipulanandan, C & Willson, RC 1994,'A practical approach to biosurfactant production using non-aspetic fermentation of mixed cultures', *Biotechnology and Bioengineering*, vol. 44, no. 5, pp. 661–666.

Guerra-Santos, SL, Kappeli, O & Fiechter, A 1984, '*Pseudomonas aeruginosa* biosurfactant production in continuous culture with glucose as carbon source', *Applied and Environmental Microbiology*, vol. 48, no. 2, pp. 301–305.

Haba, E, Espuny, MJ, Busquets, M & Manresa, A 2000, 'Screening and production of rhamnolipids by *Pseudomonas aeruginosa* 47T2 NCIB 40044 from waste frying oils', *Journal of Applied Microbiology*, vol. 88, no. 3, pp. 379–387.

Jordan, NR, Nichols, PE & Cunningham, BA 1999, 'The role of (bio) surfactant sorption in promoting the bioavailability of nutrients localized at the solid-water interface', *Water Science and Technology*, vol. 39, no. 7, pp. 91–98.

Kim, H, Yoon, BD, Lee, CH, Suh, HH, Oh, HM, Katsuragi, T & Tani, Y 1997, 'Production and properties of lipopeptide biosurfactant from *Bacillus subtilis* C9', *Journal of Fermentation and Bioengineering*, vol. 84, no. 1, pp. 41–46.

Kosaric, N, Choi, HY & Bhaszczyk, R 1990, 'Biosurfactant production from *Nacardia* SFC-D', *Tenside Surfactant Detergent*, vol. 27, no. 1, pp. 294–297.

Malathi, S & Chakraborty, R 1991, 'Production of alkaline protease by a new *Aspergillus fiavus* isolate under solid-substrate fermentation conditions for use as a depilation agent', *Applied and Environmental Microbiology*, vol. 57, no. 3, pp. 712–716.

Marwick, JD, Wright, PC & Burgess, JG 1999, 'Bioprocess intensification for production of novel marine bacteria antibiotic through bioreactor operation and design', *Marine Biotechnology*, vol. 1, no. 5, pp. 495–507.

Mulligan, CN & Gibbs, BF 1993, 'Economics of biosurfactants' in N Kosaric, *Biosurfactants: production, properties, applications*, Mercel Dekker Inc., New York.

Patel, RM & Desai, AJ 1997,'Biosurfactant production by *Pseudomonas aeruginosa* GS3 from molasses', *Letters in Applied Microbiology*, vol. 25, no. 2, pp. 91–94.

Ramana, KV & Karanth, NG 1989, 'Production of Biosurfactants by the resting cells of *Pseudomonas aeruginosa* CFTR-6. *Biotechnology Letters*, vol. 11, no. 6, pp. 437–442.

Ron, EZ & Rosenberg, E 2002, 'Biosurfactants and oil bioremediation', *Current Opinion in Biotechnology*, vol. 13, no. 3, pp. 249–252.

Singh, M & Desai, JD 1989, 'Hydrocarbon emulsification by *Candida tropicalis* and *Debaryomyces polymorphosis', Indian Journal of Experimental Biology*, vol. 27, no. 3, pp. 224–226.

Tuleva, BK, Ivanov, GR & Christova, NE 2002, 'Biosurfactant production by a new *Pseudomonas putida* strain', *Zeitschrift für Naturforschung*, vol. 57, no. 3–4, pp. 356–360.

Weinberg, ED 1970, 'Biosynthesis of secondary metabolites: roles of trace metals', *Advances in Microbial Physiology*, vol. 4, no. 1, pp. 1–44.

Witholt, B, de Smet, MS, Kingma, S, van Beilen, IB, Kok, M, Lageveen, RO & Eggink, G 1990, 'Bioconversion of aliphatic compounds by *Pseudomonas oteovorans* in multiphase bioreactors: background and economic potential', *Trends in Biotechnology*, vol. 8, no. 2, pp. 46–52.

Yu-Hong, W & I-Ming, C 1998, 'Enhancement of surfactin production in iron-enriched media by *Bacillus subtilis* ATCC 21332', *Enzyme and Microbial Technology*, vol. 22, no. 8, pp. 724–728.

Zenaitis, MG & Cooper DG 1994, 'Antibiotic production by *Streptomyces aureofaciens* using self-cycling fermentation', *Biotechnology and Bioengineering*, vol. 44, no. 11, pp. 1331–1336.

ASM Sci. J., **2(1)**, 57–64

# Production of Carbon Nanotubes via Catalytic Decomposition of Methane

S.P. Chai[1], S.H.S. Zein[1] and A.R. Mohamed[1]*

Since the discovery of carbon nanotubes (CNTs) in 1991, a fundamental question still remained on how to control morphologically the synthesis of CNTs. This task has always been a challenge. In this paper, we report the results that we have published previously with the aim of sharing the possible controlled synthesis approach via this novel production method. Findings demonstrated that various CNTs could be synthesized by using specially developed supported catalysts from the catalytic decomposition of methane. These synthesized CNTs include carbon nanofibres, single-walled and multi-walled CNTs, Y-junction CNTs and CNTs with special morphologies. It was also revealed that catalyst composition and reaction parameters played an important role in controlling the morphology and type of CNTs formed. The synthesis of CNTs with various morphologies is important because this can enrich the nanostructures of the carbon family. This finding also provides useful data for better understanding of the parameters that govern the growth mechanism of CNTs which may be required in the near future for enhanced controlled synthesis of CNTs.

**Key words:** carbon nanotubes; carbon nanostructures; catalytic decomposition; methane; catalysts; morphology; production; carbon nanofibres

In the early 1990s, tubular carbon structures with diameter in the range order of the nanometer were first observed and they have been called carbon nanotubes (CNTs) (Iijima 1991). The first observed CNTs were multi-walled carbon nanotubes (MWNTs). Two years later, single-walled carbon nanotubes (SWNTs) were successfully synthesized (Iijima & Ichihashi 1993). In general, CNTs are unique nanostructures possessing extraordinary mechanical, electrical and thermal properties while providing strong, light and high toughness characteristics (Lau & Hui 2002; Reich *et al*. 2004). It is of importance to note that the most striking part of this material is that the properties can either be semiconducting or metallic depending on their geometrical characteristics. This uniqueness leads CNTs to a variety of new important applications such as the quantum wires, field-effect transistors, field emitters, diodes, gas sensors, electric power storage, and the like (Baughman *et al.* 2002).

To date, many methods for CNTs synthesis have been developed. Among them laser ablation, electric-arc-discharge and catalytic growth are the three most popular methods which are widely being used. Arc-discharge and laser ablation methods are efficient in synthesizing SWNTs. However, both methods require very high temperature (>3000ºC) and are subject to lower CNTs yield (Dai 2001) which limit the possibility of up-scaling both to industrial scale production. By comparison, the catalytic growth method has been appreciated as the best method to produce CNTs at a lower synthesis temperature, high yield and at relatively low cost (Yacaman *et al.* 1993; Ivanov *et al.* 1994). Consequently, this method has attracted the immense attention of scientists around the world who are studying and developing high-selectivity catalytic materials for growing CNTs with desirable structures and morphologies. Generally, synthesis of CNTs by the catalytic growth method means adopting the principle of decomposition of carbon-containing gases over catalytic material. In this aspect, supported transition metals, especially metals from group VIII (Fe, Co, Ni) in the periodic table, are extensively being used (Chai *et al*. 2006c; Zein *et al.* 2006). The main challenge of the catalytic method is the control of type and morphology of CNTs synthesized. Thus, we intend to report in this paper the findings that we have published in scientific literature, disclosing the factor and the criteria that govern the formation of CNTs of different type and morphology.

## MATERIALS AND METHODS

All the catalysts tested in this study were prepared using the conventional impregnation method as reported elsewhere (Mohamed 2006). Metals in nitrate form were used as a precursor for preparing monometallic, bimetallic and trimetallic catalysts. The total metal loading was adjusted to be 10 wt% for all catalysts. The desired amount of the metal nitrate was first dissolved in distilled water and then

[1] School of Chemical Engineering, Engineering Campus, Universiti Sains Malaysia, Seri Ampangan, 14300 Nibong Tebal, S.P.S. Pulau Pinang, Malaysia

* Corresponding author (e-mail: chrahman@eng.usm.my)

impregnated on the support powder. The resulting paste was dried at 105ºC for 12 h, calcined at 600ºC or 700ºC for 5 h and sieved into 425 µm – 600 µm particles. The synthesis of CNTs were carried out at atmospheric pressure in a stainless-steel fixed-bed reactor (length and diameter of the reactor were 600 mm and 20 mm, respectively) as shown in Figure 1, using methane as carbon feedstock. High purity methane (99.999% supplied by Malaysian Oxygen Bhd) was mixed with nitrogen (99.999% purity, supplied by Sitt Tatt Industrial Gases Sdn Bhd) with ratio 1:1 (v/v) before entering the reactor. For synthesizing nanotube material, 200 mg of catalyst was distributed in the middle part of the reactor for each run and the reaction temperature was varied from 550ºC to 800ºC. The carbon deposited on the catalyst was analyzed using a transmission electron microscope (TEM) (Philips, CM12). In preparation for TEM analysis, a few samples of the used catalyst were dispersed in acetone (99.9% purity), and then a drop was deposited on a coated copper grid.

## RESULTS AND DISCUSSION

### Formation of Carbon Nanofibres

Figure 2 shows the TEM images of typical carbon nanofilaments with solid cores or with insignificant hollow cores, known as carbon nanofibres (CNFs). This type of carbon nanostructure has great potential applications as catalyst support and reinforcement material. CNFs as shown in Figures 2a and 2b were grown from methane decomposition at 550ºC on $CoO_x/SiO_2$ and $NiO/SiO_2$ catalysts, respectively (Chai *et al.* 2006a; Chai *et al.* 2007d). The diameter of distributions of CNFs grown on $CoO_x/SiO_2$ catalyst was 27.0 ± 5.8 nm and 44.4 ± 18.4 nm for those grown on $NiO/SiO_2$ catalyst. In Figure 2a, it can be noticed that the diameter of CNFs grown on $CoO_x/SiO_2$ catalyst was more uniform as compared to those shown in Figure 2b. To explain why the $CoO_x/SiO_2$ catalyst grew CNFs with narrower diameter distribution than those on $NiO/SiO_2$ catalyst, we have to comprehend the effect of metal-support interaction (MSI) of a catalyst. In the case of $NiO/SiO_2$ catalyst, NiO particles attached weakly on $SiO_2$ support. Under the reaction conditions, NiO migrated and recombined with the adjacent NiO particles, agglomerating to form larger non-uniform NiO clusters. These clusters led to the growth of CNFs of larger and non-uniform diameters. On the other hand, the $CoO_x/SiO_2$ catalyst possesses a stronger MSI effect than that of the $NiO/SiO_2$ catalyst. The stronger MSI of $CoO_x/SiO_2$ catalyst assisted the formation of $CoO_x$ with more uniform and of a smaller size on $SiO_2$ support and these $CoO_x$ particles played a significant role in growing CNFs with comparatively uniform diameter and of a smaller size (Chai *et al.* 2007d).

### Formation of Multi-walled Carbon Nanotubes

Figures 3a and 3b show the TEM images of MWNTs grown on $CoO_x$-$MoO_x$(8:2)(w/w)/$Al_2O_3$ catalyst via decomposition of methane at 700ºC (Chai *et al.* 2007a; Chai *et al.* 2007b). The high degree of diameter control and uniformity of the synthesized MWNTs can be seen

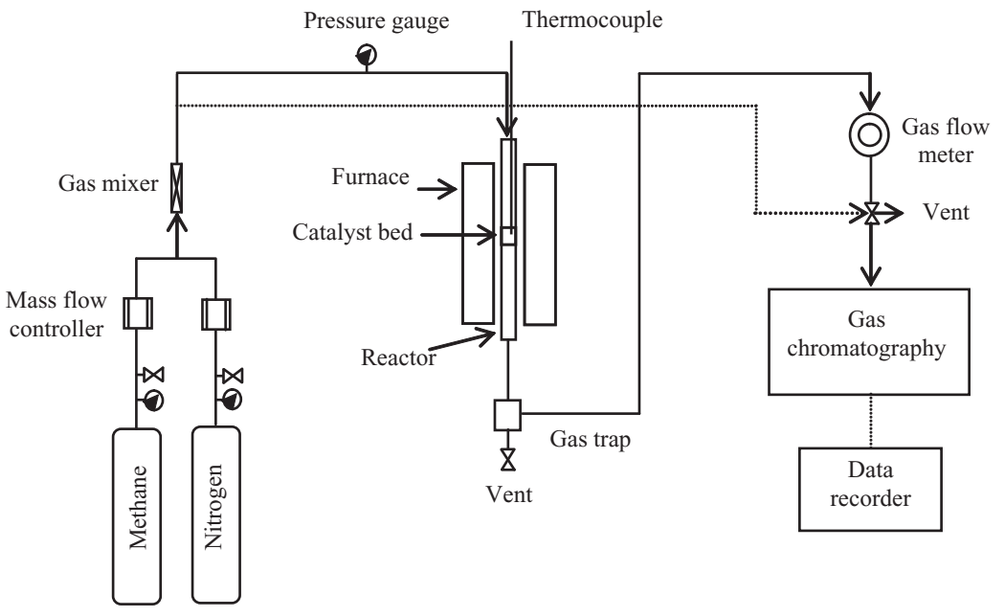


Figure 1. Schematic diagram of the experimental setup.

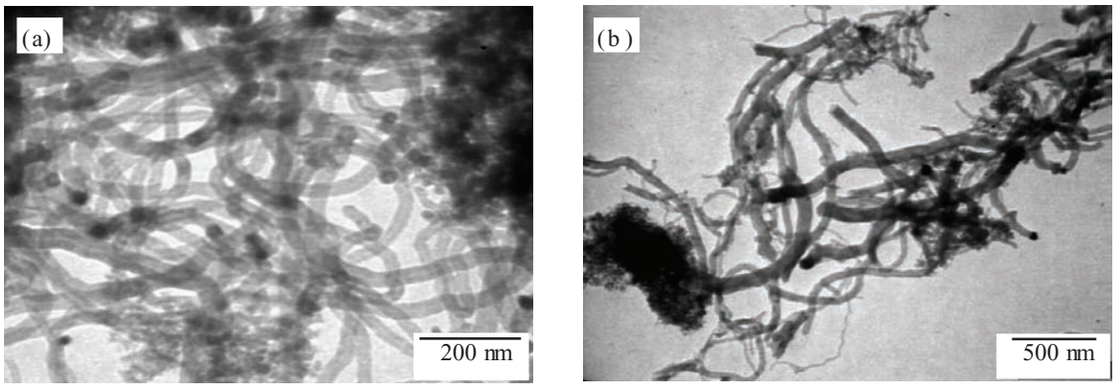


Figure 2. TEM images of CNFs grown on (a) $CoO_x/SiO_2$, and (b) $NiO/SiO_2$ catalysts.

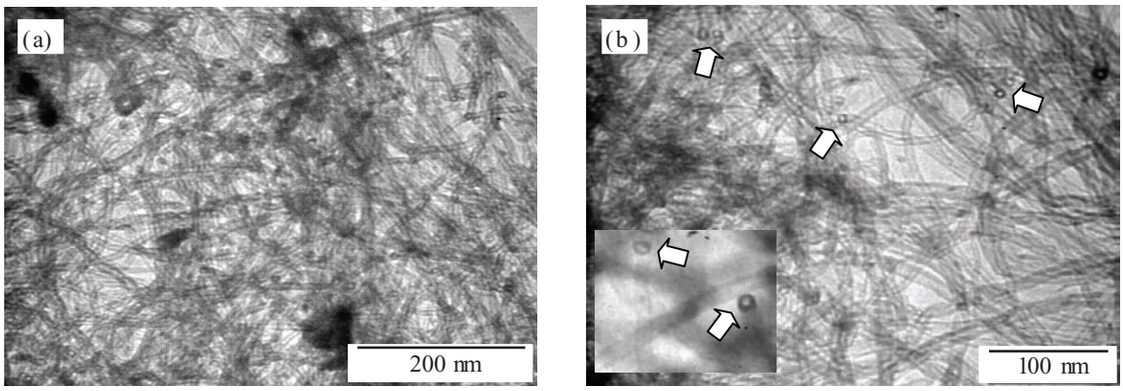


Figure 3. (a) Low-magnification, and (b) high-magnification TEM images of MWNTs grown on $CoO_x$-$MoO_x$(8:2)(w/w)/$Al_2O_3$ catalyst. Inset: TEM image of the open-tips.

clearly in the TEM images. The TEM analysis shows that out of a total of 156 MWNTs measured, more than 98% had diameters ranging from 6 nm to 12 nm. The calculated average diameter and standard deviation were 9.0 nm and 1.4 nm, respectively. The formation of MWNTs with nearly uniform diameters on $CoO_x$-$MoO_x$(8:2)(w/w)/$Al_2O_3$ was principally due to the added molybdenum which stabilized the cobalt species and $Al_2O_3$ that provided a suitable support for better dispersion of both cobalt and molybdenum particles (Chai *et al.* 2006c; Chai *et al*. 2007a). The ultimate goal for both catalyst components is to prevent the intense agglomeration of cobalt particles from forming larger clusters under the reaction conditions, in which these clusters would lead to the formation of CNTs of larger and non-uniform diameter. It was also noted that the MWNTs grew densely on all surfaces of the catalyst particles, forming an interwoven covering. Figure 3b shows the high-magnified TEM image of the produced CNTs. Significant hollow cores could be observed for the produced MWNTs. Furthermore, no catalyst particles were present at the tips of the nanotubes. This indicated that the nanotubes were grown following the base-growth model on $CoO_x$-$MoO_x$(8:2)(w/w)/$Al_2O_3$ catalyst, where the cobalt particles attached on alumina support were active in growing them. In most cases, openings at the tips, marked by arrows, were observed. CNTs with open-tips have more advantages than the enclosed-tips CNTs because the former provide the hollow parts which can be readily utilized for filling and adsorption purposes. Although many effective ways of producing CNTs with nearly uniform diameters have been suggested in literature, this study represents a simple and convenient way to achieve this objective. This also reflects a real possibility to produce CNTs of uniform diameter by means of a simpler and cheaper approach in the near future (Chai *et al.* 2007a).

The physical and chemical properties of MWNTs are sophisticated especially for CNTs with thicker wall

structure. This is due to the coupling effect between the constituent graphene layers. As a consequence, MWNTs with a smaller diameter and thinner wall structure are needed in miniaturized electronic applications because of their better electronic and electrical properties. In this study, thin-walled CNTs were synthesized using $CoO_x$-$Fe_2O_3$(8:2) (w/w)/$Al_2O_3$ as catalyst for methane decomposition at 700ºC, shown in Figure 4 (Chai *et al.* 2006d). We believe that the growth of thin-walled CNTs on $CoO_x$-$Fe_2O_3$ based catalysts was mainly induced by the $CoO_x$-$Fe_2O_3$ alloy formed on $Al_2O_3$ support. This conclusion was made after considering the findings which showed that $CoO_x$ supported on $Al_2O_3$ could not grow CNTs with thin-walled structure, whereas $Fe_2O_3$ supported on $Al_2O_3$ was not active in methane decomposition at 700ºC. Taking the thickness of each graphene layer and the spacing of the graphitic interplanar to be 0.1421 nm and 0.3354 nm, respectively (Liu *et al.* 2003), the number of graphene layers could be estimated using the following equation:

$$\tau = 0.142 + 0.335\ (n - 1) \quad (1)$$

where,

$\tau$ = Thickness of nanotube wall (each side), nm

$n$ = Number of graphine lyers

Based on this equation, we could estimate that the thin-walled CNTs consisted of only 2 – 5 graphene layers. However, the detailed wall structure of nanotubes still needs further characterization using high-resolution TEM (HRTEM) as to confirm the number of graphene layers.

## Formation of Single-walled Carbon Nanotubes

Figures 5a and 5b show the high-magnification and low-magnification TEM images of CNTs grown on NiO/$Al_2O_3$ catalyst via decomposition of methane at 700ºC (Chai *et al.* 2007c). Two types of CNTs were grown on the said catalyst, i.e. SWNTs and MWNTs, as indicated by arrow A and arrow B, respectively. From the TEM analysis, we could notice that the synthesized SWNTs appeared in two forms, i.e. isolated (arrow A1) and bundles (arrow A2). The Raman spectrum (not shown in this paper) shows strong intensity at the radial breathing mode (RBM), indicating that the occurrence of SWNTs was dominant. The RBM in the low frequency region shows five components at 123 $cm^{-1}$, 188 $cm^{-1}$ and 260 $cm^{-1}$. The frequency of these modes is known to be inversely proportional to the diameter of SWNTs. For calculating the diameter of SWNTs, we adopted the dependence of the RBM frequency on the diameter proposed by Bachilo *et al*. (2002):

$$\omega_{RBM} = 12.5 + \frac{223.5}{d} \quad (2)$$

Where,

$\omega$ = Peak position in the RBM region ($cm^{-1}$)

$d$ = Diameter of SWNTS (nm)

Based on this equation, the diameters of the SWNTs were calculated as $d$ = 2.02 nm, 1.27 nm and 0.90 nm, respectively (Chai *et al.* 2007c). Nevertheless, the RMB also discloses that the synthesized SWNTs were not mono-dispersed in diameter. To arrive at the understanding on why SWNTs were formed on NiO/$Al_2O_3$ catalyst, we have to know the nature of the catalyst structure. It is well accepted that the formation of CNTs is governed by the size of the metallic catalyst particles. In this case, if we are able to reduce the size of NiO particles to some extent, SWNTs can be grown. The formation of SWNTs on NiO/$Al_2O_3$ catalyst did reveal that very small sized NiO were formed on $Al_2O_3$ support and this size was small enough for growing SWNTs. As what we believe, the formation of these ultra-small NiO nanoparticles was mainly induced by the strong MSI effect between the NiO and the $Al_2O_3$ support. The catalyst with strong MSI allowed high NiO dispersion and prevented NiO from agglomerating and forming larger clusters. Probably, some adjacent NiO particles might combine/sinter during the calcination and reaction stages to form larger NiO particles and these particles led to the formation of MWNTs as indicated by arrow B in the TEM image.

## Formation of Y-junction Carbon Nanotubes

Figure 6 shows the TEM images of Y-junction CNTs grown on NiO-CuO-$MoO_x$(7:2:1)(w/w/w)/$SiO_2$ catalyst from methane decomposition at 700ºC. The joints of the branches were marked by arrows in the TEM image. Y-junction CNTs, a structure composing three joining tubes, were first observed in the carbon soot produced from arc-discharge method (Zhou & Seraphin 1995). The discovery of Y-junction CNTs brings a new hope to the development of CNTs-based nanoscale devices, especially nanoscale three-terminal devices such as three-terminal transistors, amplifiers and switches. In this study, it was found that $SiO_2$ supported NiO, CuO and NiO-CuO catalysts grew only straight CNTs, and no Y-junction structures were observed on these catalysts. However, by adding a small amount of $MoO_x$ to NiO-CuO, Y-junction CNTs were grown. It seems that molybdenum species acted as the nucleation sites in this case, seeding the growth of Y-junction CNTs. The detailed growth mechanism for this structure has been reported previously (Chai *et al.* 2006b). However, the yield of Y-junction CNTs obtained in this study was still low as it was only the by-product obtained from this process. We believe that through proper adjustment of the ratio of NiO, CuO and $MoO_x$, it was possible to increase the selectivity of the catalyst towards the formation of Y-junction CNTs.

## Formation of Carbon Nanotubes of Special Morphologies

In addition to ordinary morphology, several unique ones have been observed in our research work (Mohamed 2006). Some morphologies are very attractive which may have

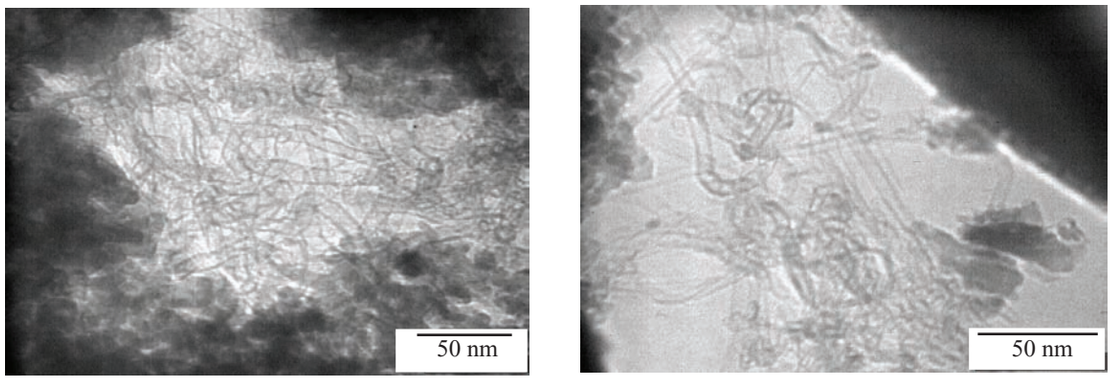


Figure 4. TEM images of thin-walled CNTs grown on $CoO_x$-$Fe_2O_3$(8:2)(w/w)/$Al_2O_3$ catalyst.

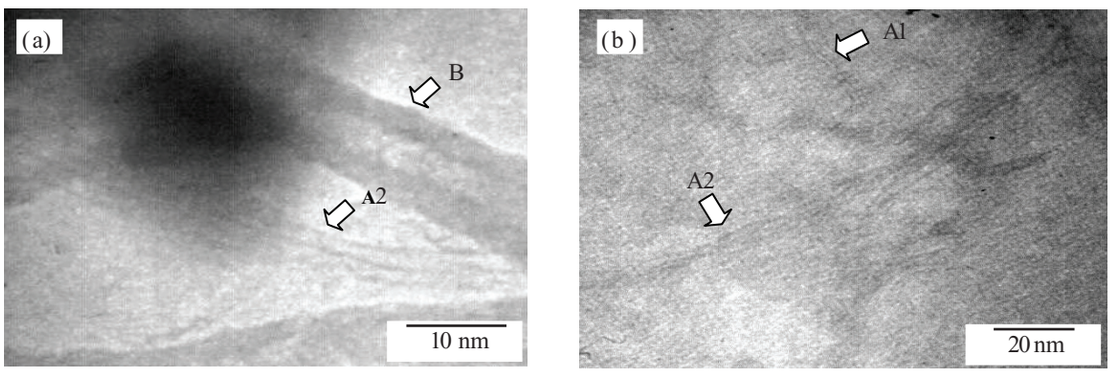


Figure 5. (a) High-magnification, and (b) low-magnification TEM images of SWNTs and MWNTs grown on NiO/$Al_2O_3$ catalyst.

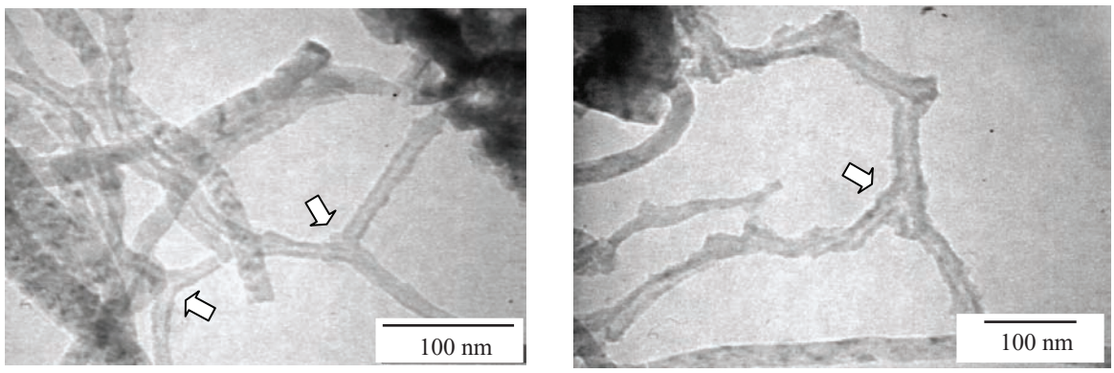


Figure 6. TEM images of Y-junction CNTs grown on NiO-CuO-$MoO_x$(7:2:1)(w/w/w)/$SiO_2$ catalyst.

some special advantages in certain applications. Figure 7a shows the bamboo-like CNTs. These nanostructures were grown on $NiO/CeO_2$ catalyst at 700ºC. Several compartments can be observed along the nanotubes axis, providing many unique chambers for gas storage when they are used as gas sensors. Another type of CNTs was grown from methane decomposition at 800ºC on $NiO/CeO_2$ catalyst and the respective TEM image is shown in Figure 7b. These carbon nanostructures were named as encapsulated type of CNTs. One can observe that the metallic parts of the catalyst were encapsulated within the tubes, as indicated by an arrow. We believe that nickel was in a quasi-liquid state at 800ºC. This condition allowed them to be elongated and segregated during the growth of CNTs, and finally trapped within the nanotubes, forming an encapsulated structure. Figures 7c and 7d show the helix-shaped CNTs and chain-like CNTs, respectively. Both nanostructures were observed on the $CoO_x$-$MoO_x$(8:2)(w/w)/$Al_2O_3$ and $CoO_x/Al_2O_3$ catalysts after methane decomposition at 800ºC. The formation of helix-shaped CNTs was reported by Amelinckx *et al*. (1994). According to the authors, the helix-shape is formed due to the eclipse shaped active sites of cobalt which determine the initial geometry of this structure. In detail, this may be due to the violation of the continuity condition for growing straight nanotubes because of the disparity of the carbon extrusion velocity and the rate of carbon deposition (Amelinckx *et al.* 1994). In most cases, only mixtures of CNTs with unique morphologies were obtained. The study describes the production of various structures of CNTs through selection of the catalyst components and reaction parameters.

## CONCLUSION

Various types of filamentous carbon, including CNFs, MWNTs, SWNTs, Y-junction CNTs and others with special morphologies, have been grown by supported catalysts via catalytic decomposition of methane. The types of filamentous carbons formed with respect to the catalysts and reaction temperatures employed are summarized in Table 1. Various CNTs synthesized in this study have enriched the nanostructure of the carbon family, providing more unique material which may be needed in future applications. Furthermore, this finding is important because it shows that synthesizing CNTs with desirable morphologies could be achieved through manipulating the catalyst components and reaction parameters. This does provide useful information towards the next level of controlled synthesis of CNTs for future needs.

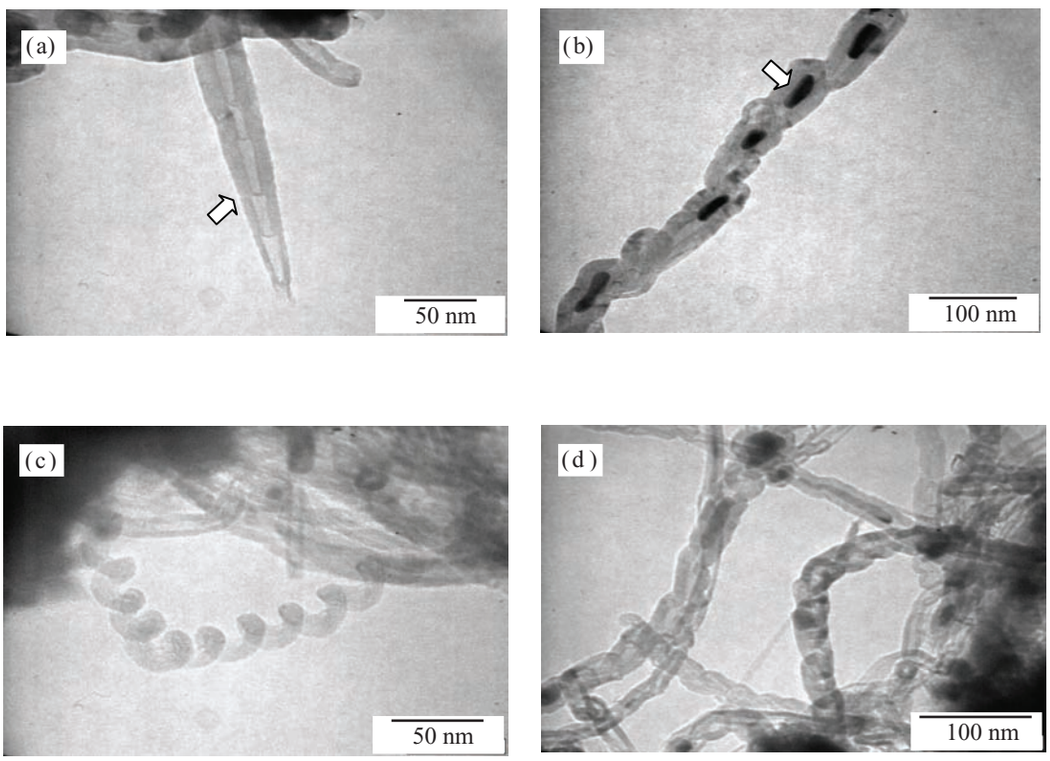


Figure 7. TEM images of carbon nanostructures synthesized over various supported catalysts via decomposition of methane: (a) bamboo-like CNTs; (b) encapsulated type CNTs; (c) helix-shaped CNTs and (d) chain-like CNTs.

Table 1. A summary of the types of filamentous carbon formed with respect to the catalysts used and reaction temperatures employed.

| Catalyst | Temperature | Findings |
|---|---|---|
| $CoO_x/SiO_2$ | 550ºC | Formation of CNFs with narrower diameter distribution |
| $NiO/SiO_2$ | 550ºC | Formation of CNFs with wider diameter distribution |
| $CoO_x$-$MoO_x$(8:2)(w/w)/$Al_2O_3$ | 700ºC | Formation of CNTs with good control in diameter uniformity |
| $CoO_x$-$Fe_2O_3$(8:2)(w/w)/$Al_2O_3$ | 700ºC | Formation of thin-walled CNTs with 2 – 5 layers of graphene |
| $NiO/Al_2O_3$ | 700ºC | Formation of single-walled CNTs |
| NiO-CuO-$MoO_x$(7:2:1)(w/w/w)/$SiO_2$ | 700ºC | Formation of Y-junction CNTs |
| $NiO/CeO_2$ | 700ºC | Formation of bamboo-like CNTs |
| $NiO/CeO_2$ | 800ºC | Formation of encapsulated type CNTs |
| $CoO_x$-$MoO_x$(8:2)(w/w)/$Al_2O_3$ | 800ºC | Formation of helix-shaped CNTs |
| $CoO_x/Al_2O_3$ | 800ºC | Formation of chain-like CNTs |

## ACKNOWLEDGEMENT

The authors gratefully acknowledge the financial support provided by the Academy of the Sciences Malaysia under the Scientific Advancement Grant Allocation (SAGA) (Project: A/C No. 6053001).

*Date of submission: March 2008*
*Date of acceptance: June 2008*

## REFERENCES

Amelinckx, A, Zhang, XB, Bernerts, D, Zhang, XF, Ivanov, V & Nagy, JB 1994, 'A Formation mechanism for catalytically grown helix-shaped graphite nanotubes', *Science*, vol. 265, no. 5172, pp. 635–639.

Bachilo, SM, Strano, MS, Kittrell, C, Hauge, RH, Smalley, RE & Weisman, RB 2002, 'Structure-assigned optical spectra of single-walled carbon nanotubes', *Science*, vol. 298, no. 5602, pp. 2361–2366.

Baughman, RH, Zakhidov, AA & De Heer, WA 2002, 'Carbon nanotubes — the route toward applications', *Science*, vol. 297, no. 5582, pp. 787–792.

Chai, SP, Zein, SHS & Mohamed, AR 2006a, 'COx-free hydrogen and carbon nanofibers produced from direct decomposition of methane on nickel-based catalysts', *Journal of Natural Gas Chemistry*, vol. 15, no. 4, pp. 253–258.

Chai, SP, Zein, SHS & Mohamed, AR 2006b, 'Formation of Y-junction carbon nanotubes by catalytic CVD of methane', *Solid State Communications*, vol. 140, no. 5, pp. 248–250.

Chai, SP, Zein, SHS & Mohamed, AR 2006c, 'Preparation of carbon nanotubes over cobalt-containing catalysts via catalytic decomposition of methane', *Chemical Physics Letters*, vol. 426, nos. 4–2, pp. 345–350.

Chai, SP, Zein, SHS & Mohamed, AR 2006d, 'The synthesis of thin-walled carbon nanotubes over CoO-$Fe_2O_3$ based catalysts', *Journal of Solid State Science and Technology Letters*, vol. 13, no. 2, pp. 66–68.

Chai, SP, Zein, SHS & Mohamed, AR 2007a, 'The effect of catalyst calcination temperature on the diameter of carbon nanotubes synthesized by the decomposition of methane', *Carbon*, vol. 45, no. 7, pp. 1535–1541.

Chai, SP, Zein, SHS & Mohamed, AR 2007b, 'The effect of reduction temperature on Co-Mo/$Al_2O_3$ catalysts for carbon nanotubes formation', *Applied Catalysis A: General*, vol. 326, no. 2, pp. 173–179.

Chai, SP, Zein, SHS & Mohamed, AR 2007c, 'Moderate temperature synthesis of single-walled carbon nanotubes on alumina supported nickel oxide catalyst', *Materials Letters*, vol. 61, no. 16, pp. 3519–3521.

Chai, SP, Zein, SHS & Mohamed, AR 2007d, 'Synthesizing carbon nanotubes and carbon nanofibers over supported-nickel oxide catalysts via catalytic decomposition of methane', *Diamond and Related Materials*, vol. 16, no. 8, pp. 1656–1664.

Dai, H 2001, 'Nanotube growth and characterization', in *Carbon nanotubes synthesis, structure, properties and applications,* eds, MS Dresselhaus, G Dresselhaus and P Avouris, Springer-Verlag, New York.

Iijima, S 1991, 'Helical microtubules of graphitic carbon', *Nature*, vol. 354, no. 6348, pp. 56–58.

Iijima, S & Ichihashi, T 1993, 'Single-shell carbon nanotubes of 1-nm diameter', *Nature*, vol. 363, no. 6340, pp. 603–605.

Ivanov, V, Nagy, JB, Lambin, P, Lucas, A, Zhang, XB, Zhang, XF, Bernaerts, D, Van Tendeloo, G, Amelinckx, S & Van

Landuyt, J 1994, 'The study of carbon nanotubules produced by catalytic method', *Chemical Physics Letters*, vol. 223, no. 4, pp. 329–335.

Lau, AKT & Hui, D 2002, 'The revolutionary creation of new advanced materials-carbon nanotube composites', *Composites Part B: Engineering*, vol. 33, no. 4, pp. 263–277.

Liu, BC, Lyu, SC, Lee, TJ, Choi, SK, Eum, SJ, Yang, CW, Park, CY & Lee, CJ 2003, 'Synthesis of single- and double-walled carbon nanotubes by catalytic decomposition of methane', *Chemical Physics Letters*, vol. 373, no. 5–6, pp. 475–479.

Mohamed, AR 2006, *Nanotiub karbon: penemuan sains yang merevolusikan nanoteknologi*, Universiti Sains Malaysia, Penang, Malaysia.

Reich, S, Thomsen, C & Maultzsch, J 2004, *Carbon nanotubes: basic concepts and physical properties*, Wiley-VCH, Germany.

Yacaman, MJ, Yoshida, MM, Rendon, L & Santiesteban, JG 1993, 'Catalytic growth of carbon microtubules with fullerene structure', *Applied Physics Letters*, vol. 62, no. 2, pp. 202–204.

Zein, SHS, Mohamed, AR & Chai, SP 2006, 'Screening of metal oxide catalysts for carbon nanotubes and hydrogen production via catalytic decomposition of methane', *Studies in Surface Science and Catalysis*, vol. 159, pp. 725–728.

Zhou, D & Seraphin, S 1995, 'Complex branching phenomena in the growth of carbon nanotubes', *Chemical Physics Letters*, vol. 238, nos. 4–6, pp. 286–289.

ASM Sci. J., **2(1)**, 65–73

# Ultrastructural Assessment of Fresh, Capacitated and Acrosome-reacted Jermasia Goat Sperm by Electron Microscopy

N.H. Hashida[1] and R.B. Abdullah[2*]

This study was carried out to compare the ultrastructure of fresh, capacitated and acrosome-reacted sperm. The sperm was treated with heparin for capacitation and calcium ionophore for acrosome reaction induction. Sperm samples were then prepared for ultrastructural studies and examined by transmission electron microscopy (TEM). Ultrastructural changes in plasma and acrosomal membranes, shape of the mitochondria and outer dense fibres, in capacitated and acrosome-reacted sperm were evident. The plasma membrane of fresh sperm was loosely fitted around the sperm head and the acrosomal membrane was closely opposed to the nucleus. The plasma and acrosomal membranes of the capacitated sperm were expanded, but disintegrated in the acrosome-reacted sperm. Mitochondria of fresh sperm appeared to be rounded in shape with plasma membrane closely opposed to it and the nine outer dense fibres were almost regular rounded in shape. However, in both capacitated and acrosome-reacted sperm, the mitochondria were almost regular and elongated in shape whilst the outer dense fibres were irregular in shape in the capacitated and acrosome-reacted sperm. There were no noticeable morphological changes found in the axonemal complexes in fresh, capacitated and acrosome-reacted sperm. Ultrastructural studies are able to provide detailed information on sequential events involving numerous physiological changes during fertilization.

**Key words:** goat sperm; sperm ultrastructures; capacitation; acrosome reaction; TEM; plasma membranes; mitochondria; axonemal complexes

It has been reported that during the movement of sperm through the epididymis there are changes in sperm morphology (Suzuki 1981), ion transport (Babcock & Lardy 1982) and also in cyclic nucleotides (Hoskins & Casillas 1975).

Sperm morphology has been widely described both in humans and animals (Cancel *et al*. 2000) since the detailed sperm cytology was described by Mac Leod (1965). It has been reported as the most significant prognostic factor for fertilization and pregnancy outcome in gamete intrafallopian transfer (GIFT), intrauterine transfer (IUT), *in vitro* fertilization (IVF) and male fertility potential; thus outweighing other conventional semen analysis parameters (Liu & Baker 1992; Yue *et al.* 1995).

Austin (1951) and Chang (1951) independently demonstrated that a sperm cell requires a period of time before it is able to fertilize an oocyte in the uterus. The incubation period required by sperm, termed as 'capacitation' (Austin 1952) is a collection of changes (a series of membrane-architectural and metabolic changes) before the sperm acquire the ability to bind to the zona pellucida and fertilize an oocyte.

The acrosome is a membrane bound vesicle forming a cap-like covering for the anterior part of the nucleus. It consists of two parts, an outer acrosomal membrane which lies close to the plasma membrane and an inner acrosomal membrane which is associated with the nucleus (Fawcett 1975). Inside these membranes are the acrosomal matrix which contains various hydrolytic enzymes (Friend 1977). There are two major enzymes, hyaluronidase and acrosin, which are released during the acrosome reaction. The acrosome reaction is an exocytotic secretory event involving the fusion of the plasma and outer acrosomal membranes and the release of the acrosomal contents prior to fertilization.

The present study was undertaken to compare the ultrastructural changes in the plasma and acrosomal membranes, mitochondria and axonemal complexes of the fresh, capacitated and acrosome-reacted Jermasia goat sperm.

[1]Centre for Foundation Studies in Science, University of Malaya, 50603 Kuala Lumpur, Malaysia
[2]Institute of Biological Sciences, Faculty of Science, University of Malaya, 50603 Kuala Lumpur, Malaysia
* Corresponding author (e-mail: nhhpasum@um.edu.my)

## MATERIALS AND METHODS

Jermasia goats reared at the Institute of Biological Sciences farm of the University of Malaya were used as semen donors. All goats used in the study (n = 15) had good reflexes, normal gait, firm testes, good libido and good erection of penis.

Freshly ejaculated semen samples were collected from mature Jermasia goats (1.0–2.5 years' old). Five bucks were used each morning (between 8.00 am – 9.00 am) for semen collection. The semen was collected before the bucks were fed and when the farm temperature ranged between 28ºC – 30ºC. The collected semen sample was stored in a wide-mouth thermos flask containing warm water at 37ºC. All semen samples were then immediately sent to the laboratory and transferred to a 37ºC water bath for further analysis.

All semen samples were washed twice with Toyoda-Yokojama-Hoshi (TYH) medium by spinning at 500 r.p.m. in a centrifuge for 5 min at 30ºC. The supernatant was then drained off leaving the sediment containing the sperm. The washed semen were subjected to swim-up procedure. Sperm suspension of 500 µl was placed at the bottom of a 50 ml conical tube containing 5 ml TYH medium. The preparation was incubated for 1 h at 37ºC under 5% $CO_2$. This technique allowed the good sperm to swim up to the top layer of the medium, leaving the dead or non-viable sperm at the bottom.

Heparin 0.05 g was dissolved in 1 ml modified TYH medium (BSA–free) giving a 3 mM concentration. The washed and swim-up sperm were subjected to heparin induction. The Heparin stock solution of 10 µl was added to 990 µl ($10^6$ sperm/ml) of the prepared sperm suspension giving 30.1 µM heparin challenge (Vendrell *et al*. 1998). The sperm suspension was incubated for 1 h at 37ºC under 5% $CO_2$.

Calcium ionophore A23187 of 1 mg was dissolved in 1.9 ml of DMSO and ethanol at a volume ratio of 3:1 (DMSO: ethanol) giving 1 mM concentration, according to Nurture Protocol (Rosliah 1997). For the induction of sperm, about 1 µl of calcium ionophore stock solution was added to 999 µl ($10^6$ sperm/ml) of the capacitated sperm suspension giving 1 µM ionophore challenge. The sperm suspension was then incubated for 1 h at 37ºC under 5% $CO_2$.

At the end of the incubation time, the sperm were then centrifuged at 2000 r.p.m. for 15 min at 30ºC. The sperm pellet was primarily fixed with 4% (v/v) glutaraldehyde and post-fixed with 1% (w/v) osmium tetroxide in 0.1 M sodium cacodylate buffer (pH 7.4). The samples were then dehydrated with ascending percentages of ethanol and embedded in epoxy resin. The specimen blocks were trimmed into trapezium shape and sectioned ultrathin. The ultrathin sections were then stained with uranyl acetate and lead citrate prior to examination in Philips CM 12 TEM operated at 80 kV (Zubaidah *et al*. 1999).

## RESULTS

### Sperm Head

In the longitudinal section of the fresh sperm head, the acrosomal membrane was closely opposed to the nucleus and the plasma membrane was loosely fitted around the sperm head (Figure 1).

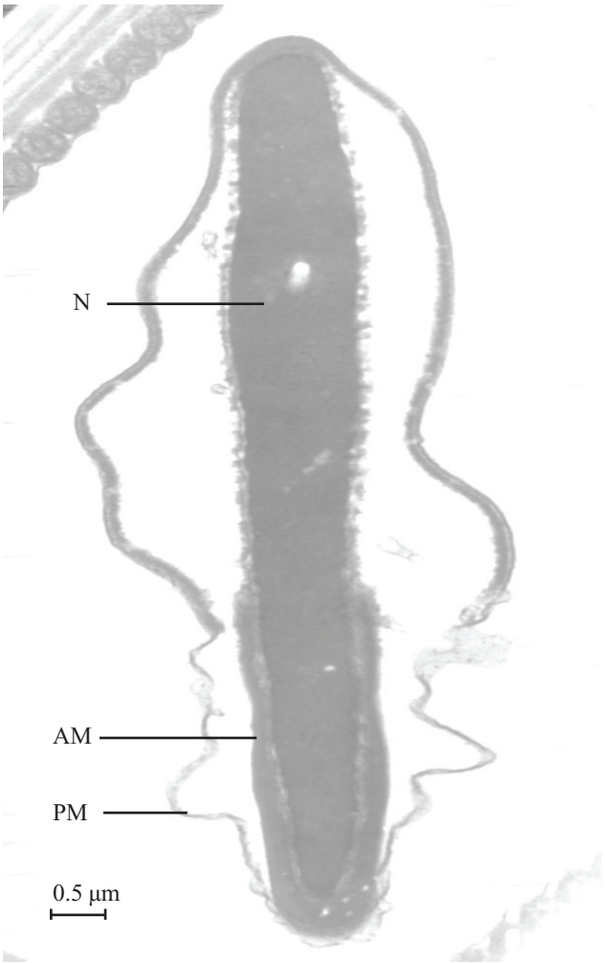


Figure 1. Longitudinal section of the fresh sperm head with intact acrosome. The nucleus (N) is covered with an acrosomal membrane (AM) that encloses a homogeneous acrosomal matrix and is bounded by the plasma membrane (PM). The plasma membrane loosely fits around the sperm head.

The longitudinal section of the capacitated sperm head showed that the acrosomal cap covered the dense nucleus. The plasma and acrosomal membranes were expanded.

Patches in the plasma membrane indicated the beginning of disintegration process, the dissolution of the plasma membrane prior to acrosome reaction (Figure 2). The longitudinal section of the acrosome-reacted sperm head showed the disintegration of the plasma and acrosomal membranes in the form of circular to irregular shaped profiles. Formation of acrosomal vesicles after the fusion of the plasma and outer acrosomal membranes and the exposure of inner acrosomal membrane were also observed in the longitudinal section of the acrosome-reacted sperm head (Figure 3).

### Longitudinal Section of the Sperm Midpiece

The longitudinal section of sperm midpiece showed mitochondria, outer dense fibres and axonemal complex. This complex running throughout the centre of the tail, originates in the neck. The mitochondria are ovoid in profiles and form a continuous spiral around the outer dense fibres.

The mitochondria of fresh sperm appeared to be rounded in shape and hooded with plasma membrane which is closely opposed to it (Figure 4). The plasma membrane of capacitated sperm was closely opposed to the mitochondria. The mitochondria were almost regular and elongated in shape (Figure 5). Vacuoles were observed in almost all the mitochondria in capacitated sperm. Gradual dissolution of the plasma membrane and elongated mitochondria were observed in the acrosome-reacted sperm (Figure 6).

### Transverse Section of the Sperm Midpiece

Transverse section of the sperm midpiece showed mitochondria, outer dense fibres and axonemal complex. The axonemal complex which consists of axoneme doublets and the central pair, extends the full length and is surrounded by nine outer dense fibres and mitochondria.

The plasma membrane of the fresh (Figure 7) and capacitated sperm (Figure 8) was usually intact and closely opposed to the underlying structures. The midpiece of the fresh sperm showed that the nine outer dense fibres were almost regular rounded in shape. The nine outer dense fibres were irregular in shape for capacitated sperm. Vacuoles were observed in the mitochondria in capacitated sperm. The plasma membrane of acrosome-reacted sperm was disrupted and the nine outer dense fibres were irregular in shape (Figure 9). No noticeable difference in the axonemal complex arrangement was observed in any of the samples.

## DISCUSSION

The ejaculated sperm head consists of the nucleus surrounded by plasma membrane containing the apical body, the acrosome and the acrosomal cap. The whole head is ensheathed within the plasma membrane. In this study, the plasma and acrosomal membranes were more sensitive to capacitation and acrosome-reaction induction treatments than the nucleus and locomotive (midpiece) parts of the sperm. The acrosomal membrane was closely juxtaposed to the nucleus which was similar to that observed by Nath (1972). Furthermore, the mitochondria were found to be rounded and hooded in the longitudinal section of the sperm midpiece and hooded mitochondria are believed to increase the surface area of mitochondria which subsequently enhanced the lipid peroxidation process (Nath 1972). The lipid peroxidation system which is located in the mitochondrial sheath is associated with sperm motility (Rao *et al.* 1989). Woolley and Richardson (1978) observed that the mitochondria were ovoid in shape and lying against the outer dense fibres of the axonemal complex. Transverse section of the sperm midpiece showed that the nine outer dense fibres were almost rounded in shape, which is similar to that reported by Tingari (1991) who indicated that the outer dense fibres were almost of the same size.

Our results showed that the plasma and outer acrosomal membranes of the capacitated sperm head have expanded compared with that of the freshly collected samples. Patches were observed in the plasma membrane which probably indicated that the sperm were in the process of capacitation. The current study on the longitudinal section of the capacitated sperm midpiece showed that the mitochondria were regular elongated in shape. This was supported by the regular thickness of mitochondria observed in transverse section, although the nine outer dense fibres were irregular in shape which is probably due to sperm hyperactivation. Kumar *et al*. (2006) reported that, activity of pyruvate dehydrogenase A (PDHA) in hamster sperm correlates positively with hyperactivation and is associated with sperm capacitation. Hamster sperm PDHA is a testis-specific phosphotyrosine that is associated with the fibrous sheath of hamster sperm. In both sections, the plasma membrane of the capacitated sperm was closely juxtaposed to the mitochondria. The fragility of the plasma membrane after capacitation probably explained the role of various surface molecules. In several mammals, hyperactivated motility of sperm has been found to be associated with capacitation (Yanagimachi 1994; Kumar *et al*. 2006).

The longitudinal section of the acrosome-reacted sperm head in the current research revealed ruptured and dissolved plasma, and acrosomal membranes. Dispersion of the acrosomal matrix was also observed in this section. Fusion of the plasma and outer acrosomal membranes formed acrosomal vesicles which were found to be identical to that reported by VandeVoort *et al*. (1997). The plasma and outer acrosomal membranes of sperm head in the present study had disintegrated from circular to irregular profiles which were also reported by Hadek (1969). The author

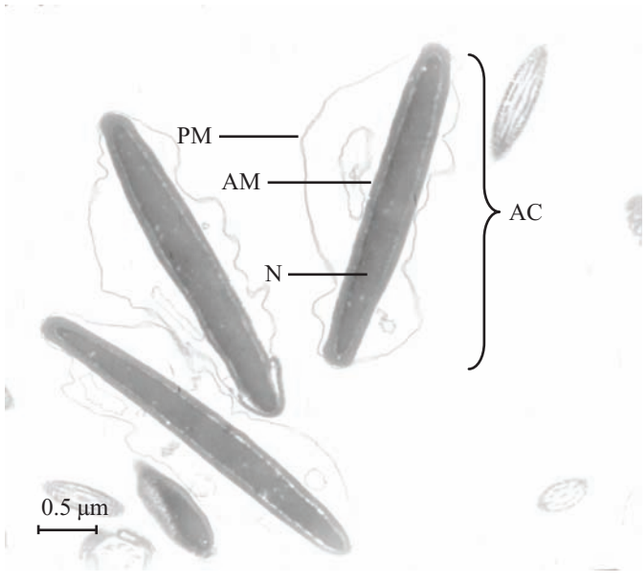


Figure 2. Longitudinal section of the capacitated sperm head. The nucleus (N) is surrounded by the acrosomal cap (AC). The plasma (PM) and acrosomal membranes (AM) are swollen.

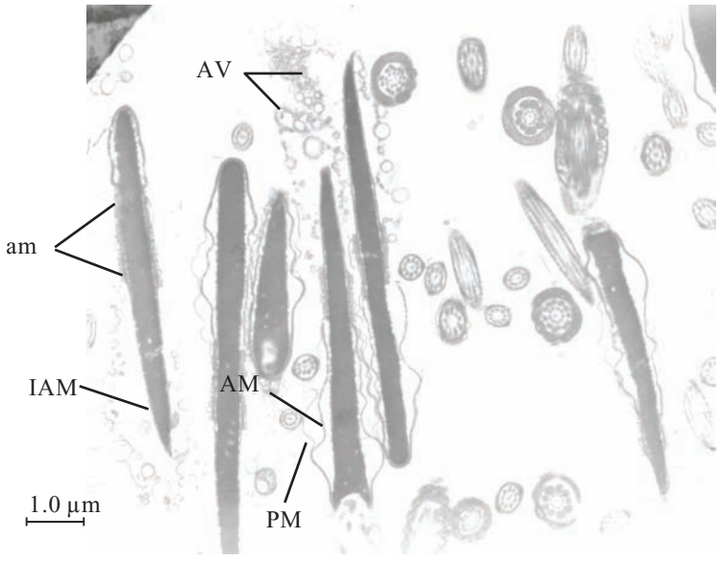


Figure 3. Longitudinal section of the acrosome-reacted sperm head showing dispersion of the acrosomal matrix (am), ruptured plasma (PM) and acrosomal membranes (AM). The inner acrosomal membrane (IAM) is exposed. Acrosomal vesicles (AV) are formed following fusion of the plasma and acrosomal membranes.

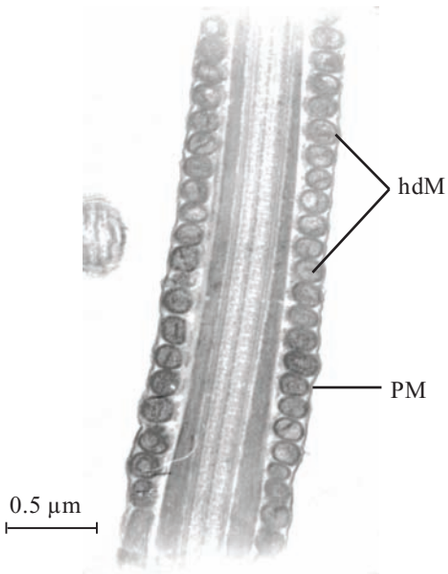


Figure 4. Longitudinal section of the fresh sperm midpiece showing rounded and hooded mitochondria (hdM) with plasma membrane (PM) closely juxtaposed to them.

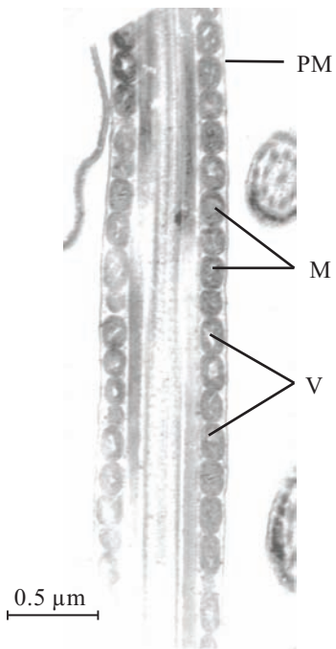


Figure 5. Longitudinal section of the capacitated sperm midpiece showing plasma membrane (PM) closely juxtaposed to mitochondria (M) which is almost elongated in shape. Vacuoles (V) are observed in almost all the mitochondria.

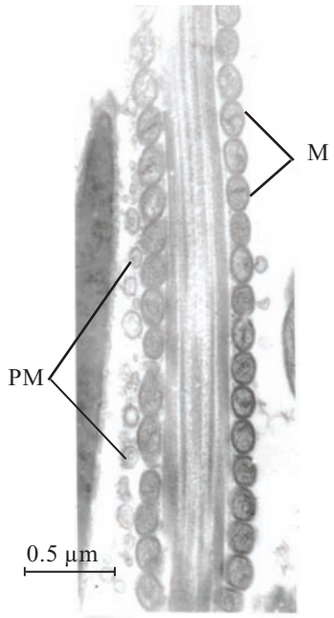


Figure 6. Longitudinal section of the acrosome-reacted sperm midpiece showing elongated mitochondria (M). The plasma membrane (PM) is disrupted.

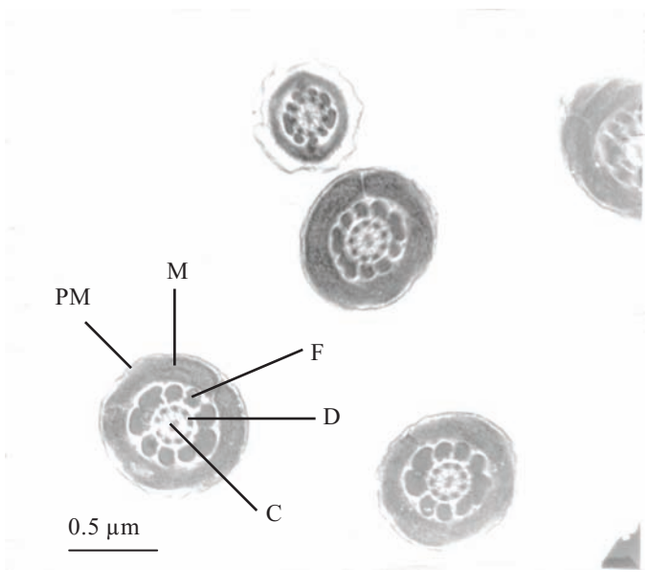


Figure 7. Transverse section of the fresh sperm midpiece showing the plasma membrane (PM) closely juxtaposed to the mitochondria (M). The nine outer dense fibres (F) are almost regular in shape. There is no noticeable difference in the arrangement of the axonemal complex (C and D).

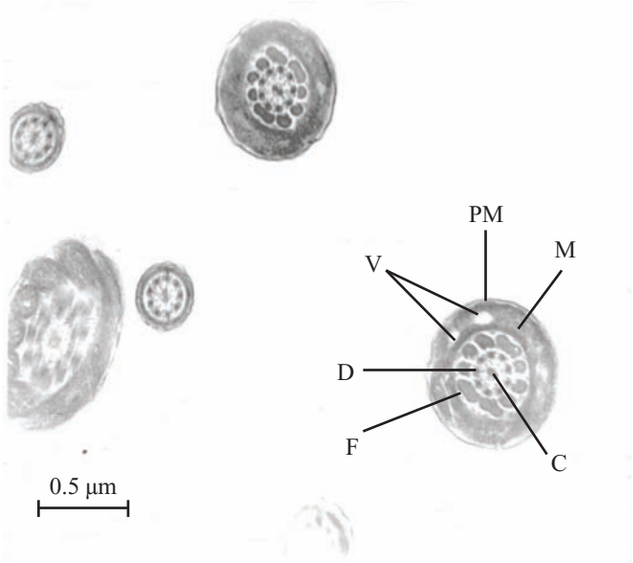


Figure 8. Transverse section of the capacitated sperm midpiece showing the plasma membrane (PM) closely juxtaposed to the mitochondria (M). The nine outer dense fibres (F) are almost irregular in shape. There is no noticeable difference in the arrangement of the axonemal complex (C and D). Vacuoles (V) are observed in the mitochondria.

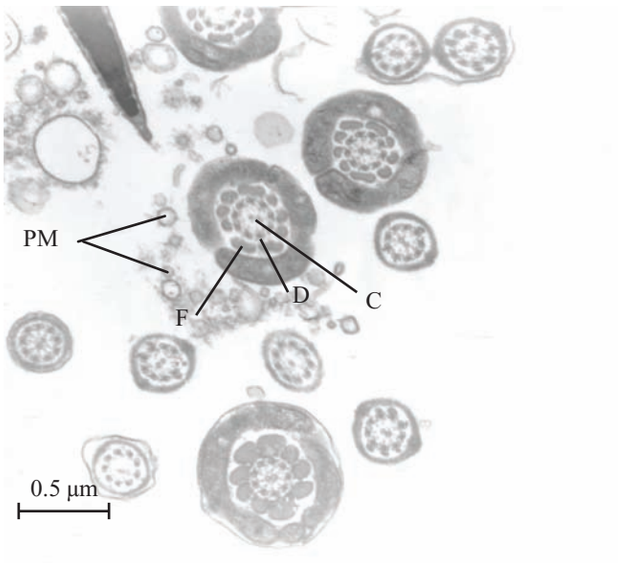


Figure 9. Transverse section of the acrosome-reacted sperm midpiece showing some disrupted plasma membrane (PM). The nine outer dense fibres (F) are irregular in shape. There is no noticeable difference in the arrangement of the axonemal complex (C and D).

suggested that the phenomenon occured when the sperm penetrated the oocyte's zona pellucida. This particular stage of gamete interaction has been studied extensively in the golden hamster, a species in which the acrosomal shroud appears to anchor the sperm to the zona surface (Cherr *et al*. 1986), after which the penetrating sperm may push through the remnant of the shroud to enter the zona substrate (Drobnis *et al*. 1988). A similar sequence of events have been observed in rabbit (Esaguy *et al*. 1988). This phenomenon may also take place before fertilization in cattle (Crozet 1984), sheep (Crozet & Dumont 1984) and in the goat (Crozet *et al*. 1987). In these animals, remnants of acrosomal shrouds have been detected on the zonae pellucidae of oocytes that were fertilized in vivo. The acrosomal shroud is associated with strong acrosin activity (Richardson *et al*. 1991). Accumulation of acrosin has also been observed on the surface of the human zona pellucida after *in vitro* sperm penetration (Tesarik *et al.* 1988).

Sperm heads which were observed in areas wherein zona pellucida has been dissolved, showed that the acrosomal membrane is in the process of disintegration. By the time the sperm has reacted with the vicinity of the vitelline membrane, the acrosomal cap has disappeared (Piko & Tyler 1964). As a result, the sperm nucleus is covered only by the inner acrosomal membrane. The plasma membrane is absent and the acrosomal cap is represented only in the equatorial region.

The longitudinal section of sperm midpiece showed similar mitochondrial structure which were rounded in shape. Transverse and longitudinal sections of sperm midpiece showed similar results, the dissolution of the plasma membrane. The nine outer dense fibres were irregular in shape. However, no morphological changes were observed in the mitochondria.

## CONCLUSION

Our study has enabled us to understand how sperm and oocyte interact normally during fertilization and how the relevant changes could be optimized in *in vitro* preparation. These results might however be used for providing a general understanding of the complex interrelationships between the sperm movement characteristic with fertilization rate and could possibly provide a good guide to the fertilizability of the sperm.

*Date of submission: December 2007*
*Date of acceptance: June 2008*

## REFERENCES

Austin, CR 1951, 'Observations on penetration of the sperm into the mammalian egg', *Aust. Journal Sci. Res.*, vol. 4, pp. 581–596.

Austin, CR 1952, 'The "capacitation" of the mammalian sperm', *Nature*, vol. 170, pp. 326.

Babcock, DF & Lardy, HA 1982, 'Alteration of membrane permeability to calcium-ion and their consequences during maturation of bovine spermatozoa', in *Membrane and Transport*, ed AN Martonosi, Plenum Publication, New York, pp. 671–675.

Cancel, A, Lobdell, D, Mendola, P & Perreault, SD 2000, 'Objective evaluation of hyperactivated motility in rat spermatozoa using computer-assisted sperm analysis', *Hum. Reprod.*, vol. 15, pp. 1322–1328.

Chang, MC 1951, 'Fertilizing capacity of spermatozoa deposited into the fallopian tubes', *Nature*, vol. 168, pp. 697–698.

Cherr, GN, Lambert, H, Meizel, S & Katz, DE 1986, '*In vitro* studies of the golden hamster sperm acrosome reaction: completion on the zona pellucida and induction by homologous soluble zonae pellucidae', *Dev. Biol.*, vol. 114, pp. 119–131.

Crozet, N 1984, 'Ultrastructure aspects of in vivo fertilization in the cow', *Gamete Res*, vol. 10 pp. 241–251.

Crozet, N & Dumont, M 1984, 'The site of acrosome reaction during in vivo penetration of the sheep oocyte', *Gamete Res.*, vol. 10, pp. 97–105.

Crozet, N, Theron, MC & Chemineau, P 1987, 'Ultrastructure of in vivo fertilization in the goat', *Gamete Res.*, vol. 18, pp. 191– 99.

Drobnis, EZ, Yudin, AI, Cherr, GN & Katz, DF 1988, 'Hamster sperm penetration of the zona pellucida: kinematic analysis and mechanical implications', *Dev. Biol.*, vol. 130, pp. 311–323.

Esaguy, N, Welch, JE & O'Rand, MG 1988, 'Ultrastructural mapping of a sperm plasma membrane autoantigen before and after the acrosome reaction', *Gamete Res.*, vol. 19. pp. 387–399.

Fawcett, DW 1975, 'Morphogenesis of the mammalian sperm acrosome in new perspective', in *The Functional Anatomy of the Spermatozoon*, ed BA Afzelius, Pergamon Press, Oxford, pp. 199–210.

Friend, DS 1977, 'The organization of the spermatozoon membrane', in *Immunobiology of Gametes*, ed M Edidin & M Johnson, Cambridge University Press, New York, pp. 5–30.

Hadek, R (eds) 1969, 'Mammalian fertilization', in *An Atlas of Ultrastructure*, Academic Press, New York.

Hoskins, DD & Casillas, ER 1975, 'Function of cyclic nucleotides in mammalian spermatozoa', in *Handbook of Physiology*, eds RO Greep & EB Estwood, American Physiological Society, Bethesda.

Kumar, V, Rangaraj, N & Shivaji, S 2006, 'Activity of pyruvate dehydrogenase A (PDHA) in hamster spermatozoa correlates positively with hyperactivation and is associated with sperm capacitation', *Biol. Reprod.*, vol. 75, pp. 767–777.

Liu, DY & Baker, HWG 1992, 'Morphology of spermatozoa bound to the zona pellucida of human oocytes that failed to fertilize *in vitro*' *J. Reprod. Fertil.*, vol. 94, pp. 71–84.

Mac Leod, J 1965, 'The semen examination', *Clin. Obstet. Gynecol.*, vol. 8, pp. 115–127.

Nath, J 1972, 'Correlative biochemical and ultrastructural studies on the mechanism of freezing damage to ram semen', *Cryobiology*, vol. 9, pp. 240–246.

Piko, L & Tyler, A 1964, 'Fine structural studies of sperm penetration in the rat' in *Proceedings of the 5th International Congress of Animal Reproduction*, vol. 2, Trento, pp. 372–377.

Rao, B, Soufir, JC, Martin, M & David, G 1989, 'Lipid peroxidation in human spermatozoa as related to midpiece abnormalities and motility', *Gamete Res*., vol. 24, pp. 127–134.

Richardson, RT, Nikolajezyk, BS, Abdullah, J, Beavers, JC & O'Rand, MG 1991, 'Localization of rabbit sperm acrosin during the acrosome reaction induced by immobilized zona matrix', *Biol. Reprod.*, vol. 45, pp. 20–26.

Rosliah, H 1997, 'Effect of cryopreservation on sperm morphology and acrosome', MMSc thesis, University of Nottingham, UK.

Suzuki, F 1981, 'Changes in intermembranous particle distribution in epididymal spermatozoa of the boar', *Anat. Rec.*, vol. 199, pp. 361–376.

Tesarik, J, Drahorad, J & Peknicova, J 1988, 'Subcellular immunochemical localization of acrosin in human spermatozoa during the acrosome reaction and zona pellucida penetration', *Fertil. Steril.*, vol. 50, pp. 133–141.

Tingari, MD 1991, 'Studies on camel semen. III. Ultrastructure of the spermatozoon', *Anim. Reprod. Sci.*, vol. 26, pp. 333–344.

VandeVoort, CA, Yudin, AI & Overstreet, JW 1997, 'Interaction of acrosome-reacted Macaque sperm with the Macaque zona pellucida', *Biol. Reprod.*, vol. 56, pp. 1307–1316.

Vendrell, FJ, Rubio, C & Tarín, JJ 1998, 'The heparin-glutathione test: an alternative to the hypo-osmotic swelling test to select viable sperm for intracytoplasmic sperm injection', *Fertil. Steril.*, vol. 70, no. 6 pp. 1156–1161.

Woolley, DM & Richardson, DW 1978, 'Ultrastructural injury to human spermatozoa after freezing and thawing', *J. Reprod. Fertil.*, vol. 53, pp. 389–394.

Yanagimachi, R 1994, 'Mammalian fertilization', in *The Physiology of Reproduction*, eds E Knobil & JD Neill, vol. 1, Raven Press, New York.

Yue, A, Meng, FJ, Jorgensen, N, Ziebe, S & Nyboe, AA 1995, 'Sperm morphology using strict criteria after Percoll density separation', *Hum. Reprod.*, vol. 10, pp. 781–1785.

Zubaidah, AH, Norehan, A, Wong, MH, Zulkifli, I & Abdullah, O 1999, *Laboratory Manual*, Electron Microscope Unit, Faculty of Medicine, University of Malaya, Kuala Lumpur.

ASM Sci. J., **2(1)**, 75–81

# Robust Digit Recognition with Dynamic Time Warping and Recursive Least Squares

S.A.R. Al-Haddad[1]*, S.A. Samad, A. Hussain[1], K.A. Ishak[1] and A.O.A. Noor[1]

Robustness is a key issue in speech recognition. A speech recognition algorithm for Malay digits from zero to nine and an algorithm for noise cancellation by using recursive least squares (RLS) is proposed in this article. This system consisted of speech processing inclusive of digit margin and recognition using zero crossing and energy calculations. Mel-frequency cepstral coefficient vectors were used to provide an estimate of the vocal tract filter. Meanwhile dynamic time warping was used to detect the nearest recorded voice with appropriate global constraint. The global constraint was used to set a valid search region because the variation of the speech rate of the speaker was considered to be limited in a reasonable range which meant that it could prune the unreasonable search space. The algorithm was tested on speech samples that were recorded as part of a Malay corpus. The results showed that the algorithm managed to recognize almost 80.5% of the Malay digits for all recorded words. The addition of a RLS noise canceller in the preprocessing stage increased the accuracy to 94.1%.

**Key words:** Robustness; speech; algorithm; Malay digits; noise; cancellation; processing; digit margin; recognition; vocal tract; filter; time warping; voice

This study used the Malay language which is a branch of the Austronesian (Malayo-Polynesian) language family, spoken as a native language by more than 33 000 000 people distributed over the Malay Peninsula, Sumatra, Borneo and the numerous smaller islands of the area, and widely used in Malaysia and Indonesia as a second language (Britannica 2007).

Speech recognition (SR) is a technique aimed at converting a speaker's spoken utterance into a text string. SR is still far from a solved problem. It has been quoted that the best reported word-error rates on English broadcast news and conversational telephone speech were 10% and 20%, respectively (Le 2003). Meanwhile error rates on conversational meeting speech were about 50% higher, and much more under noisy conditions (Le *et al.* 2002). However, these error rates decrease every year, as speech recognition performance has improved quite steadily. Deng and Huang (2004) estimated that performance has improved roughly 10% a year over the last decade due to a combination of algorithmic improvements and Moore's Law.

Recursive least squares (RLS) algorithm is used to improve the presence of speech in a background of noise. The RLS algorithm provides good performance for models with accurate initial information on a parameter or a state to be estimated (Park 2008). In many applications of noise cancellation, the changes in signal characteristics can be quite fast. This requires the utilization of adaptive algorithms which converge rapidly. From this perspective the best choice is the RLS (Vijayakumar 2007). The beginning and end of a word could be detected by the system that processes the word after noise cancellation had been done.

This paper proposes a speech recognition algorithm for Malay digits from zero to nine. This system consisted of speech processing inclusive of digit margin and recognition which used zero crossing and energy calculation techniques. Mel-frequency cepstral coefficients (MFCC) vectors were used to provide an estimate of the vocal tract filter. Meanwhile dynamic time warping (DTW) was used to detect the nearest recorded voice.

## METHODOLOGY

The system consisted of speech processing and recognition phases as shown in Figure 1. The speech processing phase began with recording the voice, RLS filtering, endpoint detecting, blocking into frames, frame windowing and MFCC. MFCC was chosen because of the sensitivity of the low order cepstral coefficients to overall spectral slope and the sensitivity properties of the high-order cepstral coefficient (Sheikh *et al.* 2002).

[1] Department of Electrical, Electronic and Systems Engineering, Faculty of Engineering, Universiti Kebangsaan Malaysia, Bangi, Selangor, Malaysia

* Corresponding author (e-mail: sar_upm@yahoo.com)

The recognition phase created a word dictionary or a template of words which was used for the recognition. At the recognition phase the required speech was recorded and processed to detect the speech period and to reduce noise. The spoken speech was processed while the word template was made. The words used in this experiment were Malay isolated digits from zero to nine spoken as 'Kosong', 'Satu', 'Dua', 'Tiga', 'Empat', 'Lima', 'Enam', 'Tujuh', 'Lapan' and 'Sembilan'.

The RLS was used in preprocessing for noise cancellation as shown in Figure 2 (Ifeachor 2004). The parameters for Figure 2 are as follows:

$n$ is the background noise of any type
$\hat{}$ is a noise correlated to $n$
$s$ is a speech signal
$d$ is the desired signal
$W$ is the optimum filter weight matrix
$y$ is the output of adaptive process
$e$ is the error signal in ideal case (clean speech).

Figure 3 shows the result after using the RLS adaptive filtering on the noisy signal. Figure 3a, shows the amplitude of a noisy speech and Figure 3b shows the amplitude after processing using RLS.

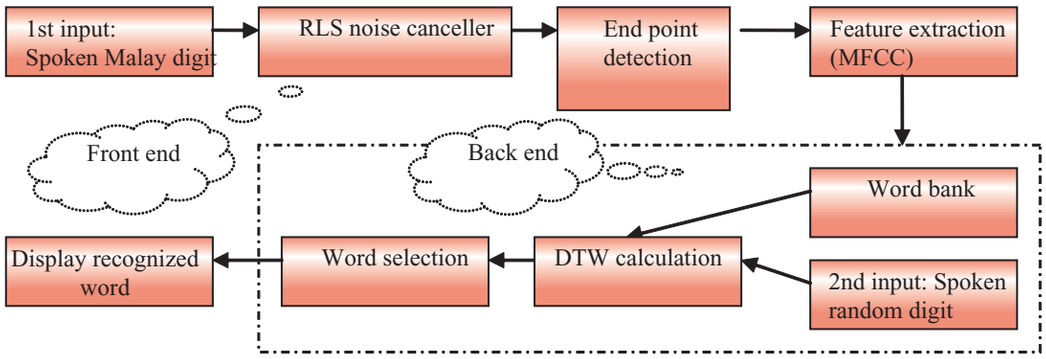


Figure 1. A block diagram of Malay digit recognition.

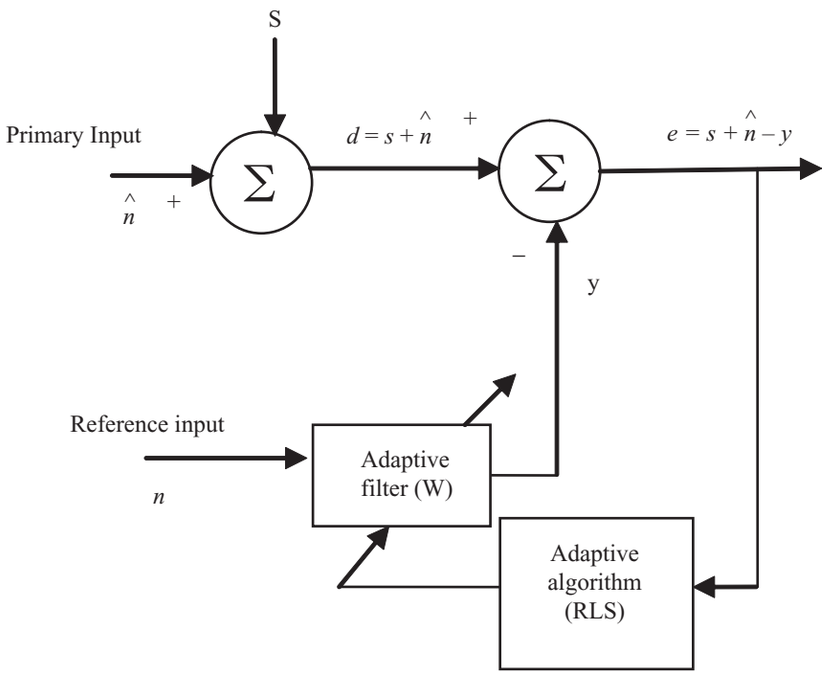


Figure 2. Adaptive noise canceling concept.

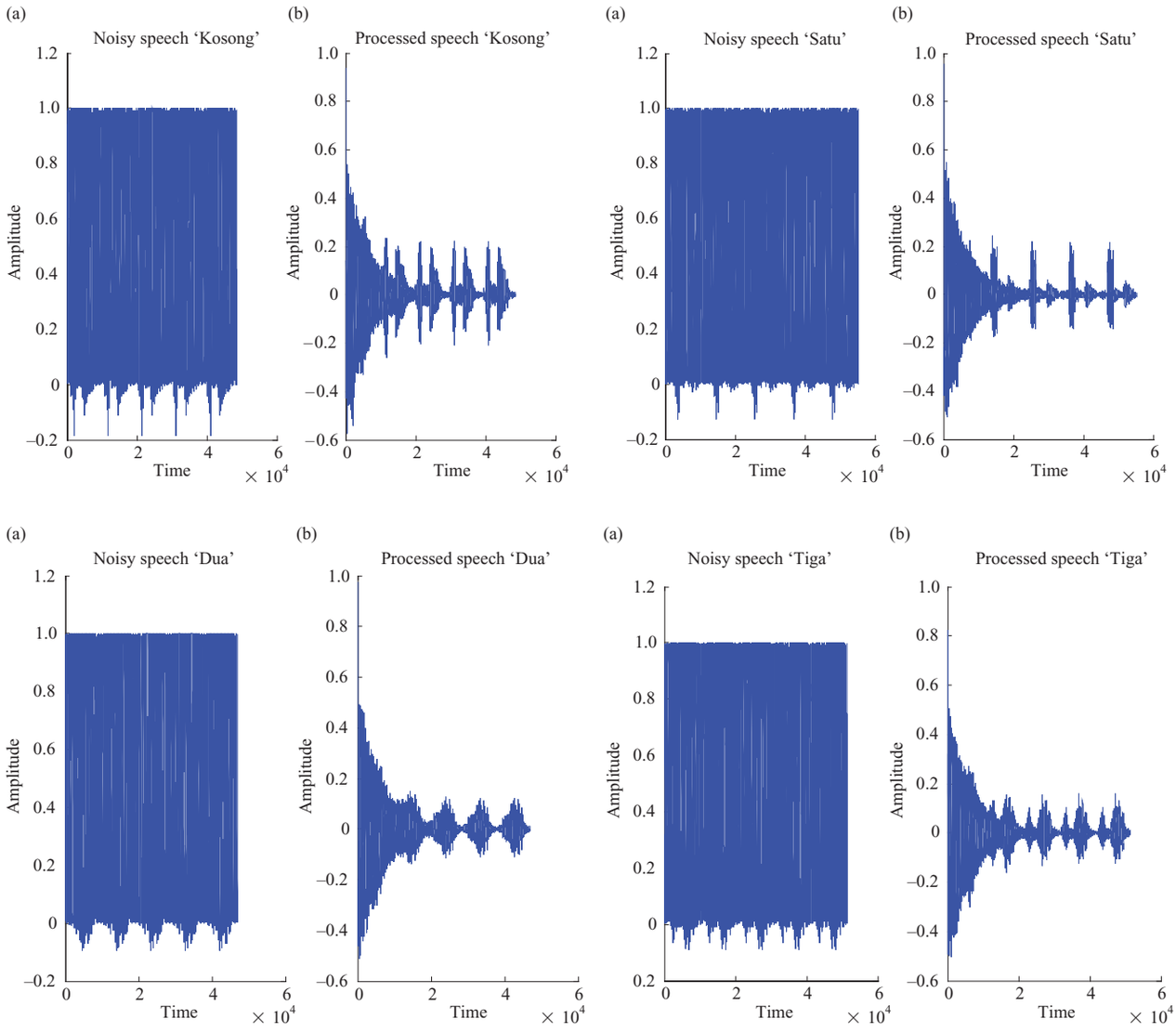


Figure 3. (a) Noisy speech; (b) Signal processed by adaptive noise canceller.

After the RLS noise canceller process, zero crossings were calculated which were 10% of the maximum zero crossing rate (ZCR). Next, log energy allowed us to calculate the amount of energy at a specific instance. For a given window size there were no standard values of energy. Log energy depended on the energy in the signal, this changed on how the sound was recorded. In a clean recording of speech, log energy was higher for voiced speech and zero or close to zero for silence.

Next the program found the endpoint upper level by searching from the first point until the energy crossed the upper level energy threshold. It deleted short sound clips by eliminating sound lengths that were less than a certain value. After that, it expanded the endpoint lower level by reversing the sound index until it reached the first point's energy which fell below the low level energy threshold. Next it expanded the endpoint for the high ZCR area where, if the ZCR index was greater than the ZCR threshold, then it was moved to the first point. Lastly it transformed a sample point-based index for the beginning and ending indices.

This endpoint technique managed to show the voiced speech and unvoiced speech (including silence) segments. Furthermore, this endpoint detection algorithm had been tested for various kinds of real noise recorded at various places (Al-Haddad *et al*. 2006a) and also on Malay digits (Al-Haddad *et al*. 2006b) which give good segmentation for male and female speakers with a reasonable accuracy rate of 87.5%. For voiced speech, the energy was high and

the zero crossing rates were low. On the other hand, for unvoiced speech the energy was low and the zero crossing rates were high.

For labeling the segmented speech frame, the ZCR and energy were applied to the frame. Unfortunately it contained some level of background noise due to the fact that energy for breath and surroundings could quite easily be confused with the energy of a fricative sound (Gold & Morgan 2000). Figure 4 shows the waveform, ZCR and energy for continuous digits recorded from a male speaker. Also as shown in Figure 4, voiced speech could be distinguished from unvoiced speech as it had much greater amplitude displacement when the speech was viewed as a waveform. It also showed a margin line for the beginning and endpoint for each segment.

As a result, this algorithm performed an almost perfect segmentation for voices recorded by male speakers. For recordings done at noisy places, segmentation problems happened because in some cases the functions produced different values caused by background noise. This caused the cutoff for silence to be raised as it might not be quite zero due to noise being interpreted as speech by the functions. On the other hand under clean speech both the ZCR and short-term energy should be zero for silent regions.

Furthermore, the way people talk, the volume and speed also caused problems in detecting the endpoints. This is because the ZCR had a low value for silence and voiced speech, therefore there was more chance of an error between these values, but energy was only high when voiced speech occured.

It was necessary then to filter the signal from unwanted noise. Before the signal could be made into a template, the signal had to be normalized so that the volume of the speech would not become a factor in the speech recognition. The normalization was done by dividing the signal with the maximum absolute value of the signal. The speech signal was then processed in 20 msec (256 point) frames which were stepped by 10 msec (128 points) between processing frames. Figure 4 shows the stages through which a speech signal passed to be transformed into an MFCC vector as simplified by Milner and Shao (2002). This conformed to the MFCC standard proposed by the European Telecommunications Standards Institute (ETSI). A few standards for an Automatic Speech Recognition feature extraction are available from ETSI (ETSI 2002). The framing method used is Hamming.

After the MFCC process, the results were saved in the sound word bank. Here we used 'MalayDigit' as the directory for saving. Then it was tested by using Dynamic Time Warping (DTW). DTW was the main algorithm in this system for recognition. Due to the wide variation in speech between different instances for the same speaker, it was necessary to apply some type of non-linear time warping prior to the comparison of two speech instances. DTW was the preferred method for doing this, whereby the principles of dynamic programming could be applied to optimally align the speech signals.

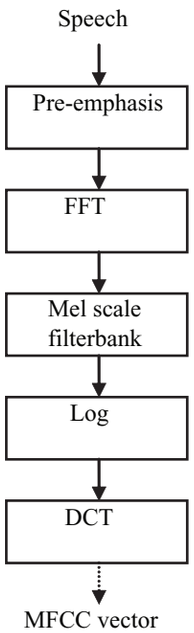


Figure 4. Procedure for calculating MFCC vectors.

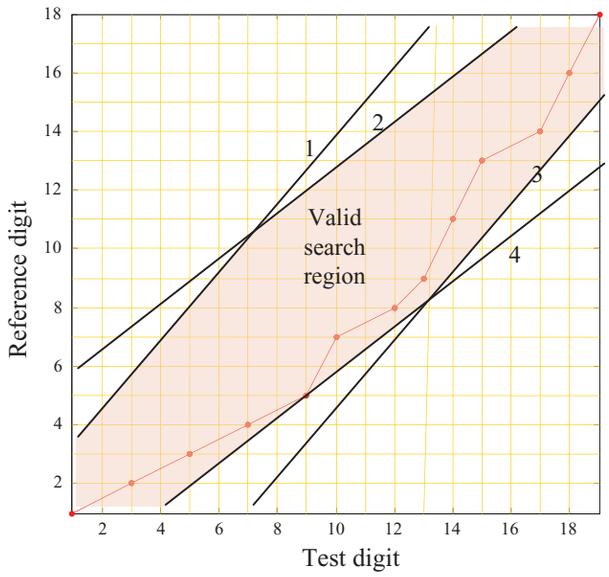


Figure 5. DTW path taken for recognition of utterance of 'Dua'.

The application of DTW to isolated digit recognition could be visualized by aligning the processing frames of a reference digit along the y-axis and a test digit along the x-axis as shown in Figure 5. The distance metric was then computed between the frames of the test and reference digit while progressing from the origin at the left bottom corner, up and to the right.

The principles of dynamic programming could be applied to find the path, which had the minimum accumulated distance metric. After this test was performed using the entire reference vocabulary digit for each test digit, the reference digit with the minimum accumulated distance metric was deemed to be a match. For a speech signal, there were a number of constraints on the search path which could be applied to decrease the complexity of the search.

The primary constraint was that the search should be monotonic, meaning that the path chosen could not be in negative $y$ or $x$ direction and could only increase one step at a time. The distance metric was formed by using Euclidean distance for the cepstral coefficients over all the frames, after DTW was applied to align the frames optimally. All paths were given a transition cost of 1. The metric distance between frames $i$ of the test digit $T$ and frame $j$ of the reference digit $R$ was calculated as follows:

$$d(x,y) = \sqrt{\Sigma_j (x_j - y_j)^2} \quad (1)$$

Another constraint, which was the global constraint, was used to restrict the extent of compression or expansion of speech signals over long ranges of time. The variation of the speech rate of a speaker was considered to be limited in a reasonable range which meant that it could prune unreasonable search space and limit the search to the valid region. In order to get the best recognition, the global constraint had to be set to an optimum level; however, this was not always possible except on an experimental state. To further improve recognition accuracy, the starting point of the search should not be set at the point of origin but at a minimum pre-defined margin value of the set.

## RESULT AND DISCUSSION

The results obtained after running the algorithm are shown in Figure 6. The system required the user to record numbers 1 until 10 in the Malay language. After that the system

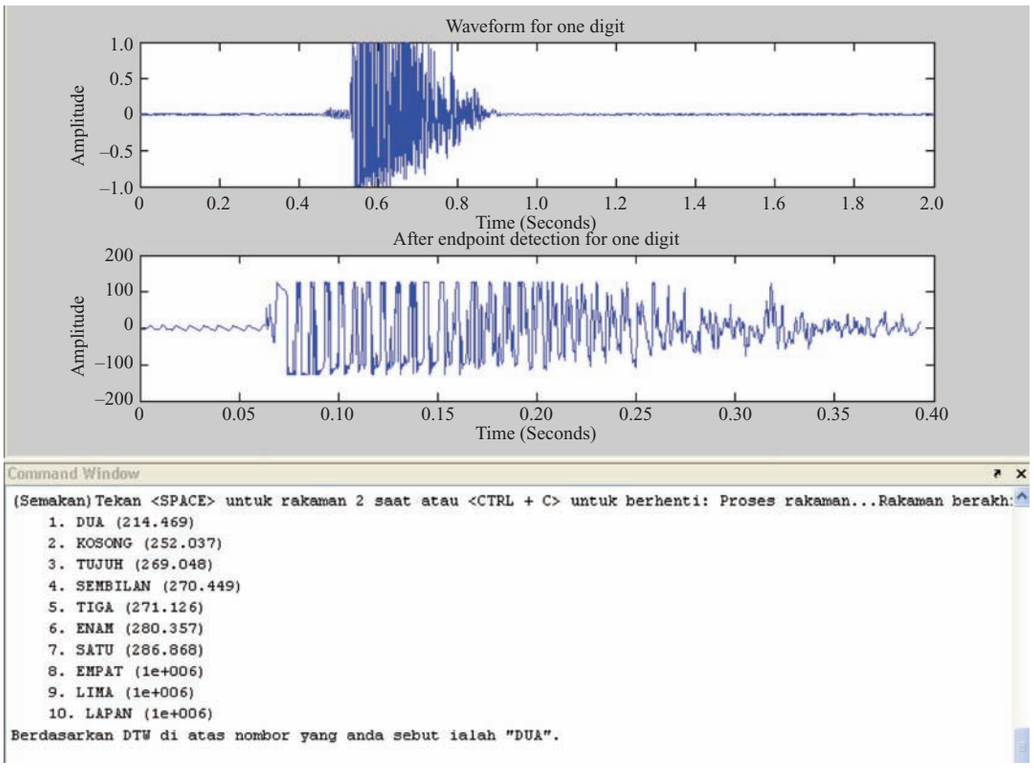


Figure 6. Screenshot of output after recording digit number 2 (pronounced in Malay as 'Dua') where the system will choose the nearest digit inside the storage.

saved the recorded voice into a Malay digit directory. Then, the user was required to record any single number between zero and nine as shown in Figure 6. The input word was then recognized as the word corresponding to the template with the lowest matching score. As an example, in Figure 6 it showed that the word number 2 ('Dua') had the lowest matching score.

The recognition was implemented using DTW where the distance calculation was done between the tested speech and the reference word bank. After the distance was obtained, the path cost was calculated by getting the cheapest path cost with reference to global and local constraints. Recognition accuracy is found to be greatly increased by the implementation of the global constraint and further increased by the application of the local constraint. Figure 5 is a sample of the recognition result of the DTW path cost of the utterance 'Dua'. The shaded area in the figure shows the global constraint (or the valid search area). To increase the accuracy of the recognition after implementation, the appropriate global constraint was found to be as follows:

(1) $y = 1.61x + 3.84$
(2) $y = 0.93x + 9.07$
(3) $y = 0.86x - 3$
(4) $y = 1.08x - 0.5$

The reason behind setting this global path (from the above equations) was to prepare a valid search region because the variation of the speech rate of the speaker was considered to be limited in a reasonable range, which meant that it could prune the unreasonable search space. The local constraint was monotonicity as discussed in the methodology section. Another local constraint applied which had been proven to improve the accuracy, was the starting point of the path search.

Table 1 shows the score results of recognition of the utterance 'Dua' which had the corresponding lowest path score and the path taken was as in Figure 6. Table 1 shows that the word 'Dua' had the lowest score of 214.469, which meant that it was recognized as the correct word. The closest score to that is the word 'Kosong'. A limit has to be set in order not to recognize the wrong word. The limit set in this case was a path score of 450 because most of the time the result was a path score of about 400, depending on the recording condition of the speech.

The recognition algorithm was then tested for accuracy. The test was limited to digits from zero to nine. Random utterance of numbers was done and the accuracy of 100 sample numbers were analyzed. The results obtained were about 80.5% accurate. The results obtained were as displayed in Table 2. Most of the time, the inaccuracy of recognition was due to sudden impulses of noise or a sudden drastic change in the voice tone.

Meanwhile for the robustness test, the RLS noise canceller was used and the result is as shown in Table 3. The accuracy was improved to 94.1%.

Table 1. Results of the utterance 'Dua'.

| Word | Score |
|---|---|
| Dua | 214.469 |
| Kosong | 252.037 |
| Tujuh | 269.048 |
| Sembilan | 270.449 |
| Tiga | 271.126 |
| Enam | 280.357 |
| Satu | 286.868 |
| Empat | 1E+006 |
| Lima | 1E+006 |
| Lapan | 1E+006 |

Table 2. Accuracy test results without RLS noise canceller.

| Word | Accuracy |
|---|---|
| Satu | 65% |
| Dua | 80% |
| Tiga | 65% |
| Empat | 100% |
| Lima | 75% |
| Enam | 100% |
| Tujuh | 65% |
| Lapan | 95% |
| Sembilan | 95% |
| Sepuluh | 65% |
| Average | 80.5% |

Table 3. Accuracy test results with RLS noise canceller.

| Word | Accuracy |
|---|---|
| Kosong | 87% |
| Satu | 86% |
| Dua | 100% |
| Tiga | 86% |
| Empat | 100% |
| Lima | 94% |
| Enam | 100% |
| Tujuh | 88% |
| Lapan | 100% |
| Sembilan | 100% |
| Average | 94.1% |

## CONCLUSION

This paper has shown that the accuracy of speech recognition algorithm for Malay digits had increased after using the RLS noise canceller. MFCC vectors provided an estimate of the vocal tract filter. Meanwhile, DTW was used to detect the nearest recorded voice with appropriate global constraint to set a valid search region because the variation of the speech rate of the speaker was considered to be limited in a reasonable range, which meant that it could prune the unreasonable search space. The results showed a promising Malay digit speech recognition module. Recognition with about 80.5% accuracy could be achieved using this method (without the RLS noise canceller). Impressively, the accuracy increased to 94.1% after being filtered by RLS noise canceller.

*Date of submission: March 2007*
*Date of acceptance: June 2008*

## REFERENCES

Al-Haddad, SAR, Samad, SA & Hussain, A (2006a), 'Automatic digit boundary segmentation recognition', in *MMU International Symposium on Information and Communication Technology (M2USIC)*, Petaling Jaya, Selangor, Malaysia, pp. 280–283.

Al-Haddad, SAR, Samad, SA & Hussain, A (2006b), 'Automatic segmentation for Malay speech recognition', in *Proceedings of Post-graduate Research Seminar 2006*, Bangi, Selangor, Malaysia, pp. 235–239.

Analog Devices Inc, 1992, *Digital signal processing applications using the ADSP-2100 Family*, vol. 2, Prentice-Hall Inc., Englewood Cliffs, NJ, USA.

Encyclopedia Britannica Online, 2007, <http://www.britannica.com/eb/article-9050292>, viewed 8 August 2007.

Deng, L & Huang, X 2004, 'Challenges in adopting speech recognition', *Communications of the ACM*, vol. 47, no. 1, pp. 69–75.

European Telecommunications Standards Institute, 2002, *Speech processing, transmission and quality aspects (STQ); Distributed speech recognition; Advanced front-end feature extraction algorithm; Compression algorithm* (ETSI Standard Document—ES 201 108), Sophia Antipolis, France.

Gold, B & Morgan, N 2000, *Speech and audio signal processing*, 1st edn, John Wiley and Sons, New York, USA.

Ifeachor, EC & Jervis, BW 2004, *Digital signal processing — a practical approach*, Pearson Education, Delhi.

Kim, DS, Lee, SY & Kil, RM 1999, 'Auditory processing of speech signals for robust speech recognition in real world noisy environments', *IEEE Trans. Speech and Audio Proc.*, vol. 7, no. 1, pp. 55–69.

Le, A 2003, 'Rich transcription 2003: spring speech-to-text transcription evaluation results, in *Proc. RT03 Workshop,* Boston, MA, USA, viewed 25 October 2007, <http://www.nist.gov/speech/tests/rt/rt2003/spring/presentations/rt03s-stt-results-v9.pdf>.

Le, A, Fiscus, J, Garofolo, J, Przybocki, M, Martin, A, Sanders, G & Pallet, D 2007, 'The 2002 NIST RT evaluation speech-to-text results', in *Proc. RT02 Workshop,* Vienna, Va, USA, viewed 25 October 2007, <http://www.nist.gov/speech/tests/rt/rt2002/presentations/rt02_stt_results_v5.pdf>.

Milner, B.P., and Shao, X 2002, 'Speech reconstruction from mel-frequency cepstral coefficients using a source-filter model', in *7th International Conference on Spoken Language Processing (ICSLP) 2002*, Denver, Colorado, USA, pp. 2421–2424.

Park, JH, Quan, ZH, Han, S & Kwon, WH 2008, 'New recursive least squares algorithms without using the initial information, *IEICE Trans. Commun*., vol. E91–B, no. 3, pp. 968–971.

Rabiner, LR & Sambur, MR 1975, 'An algorithm for determining the endpoints of isolated utterances', *The Bell System*, *Technical Journal*, vol. 54, no. 2, pp. 297 & 315.

Rabiner, LR & Schafer, RW 1978, *Digital processing of speech signals*, 1st edn, Prentice-Hall Inc., Englewood Cliffs, NJ, USA.

Sheikh, HS, Hong, KS, Tan, TS 2002, 'Design and development of speech-control robotic manipulator arm', in *Proceedings of 7th International Conference on Control Automation, Robotics and Vision (ICARCV 2002)*, Singapore, pp. 459–463.

Vijayakumar, VR & Vanathi, PT 2007, 'Modified adaptive filtering algorithm for noise cancellation in speech signals, Electronics and Electrical engineering', *Kaunas Technologija*, vol. 2, no. 74, pp. 17–20.

ASM Sci. J., **2(1)**, 83–92

# Kinetic Resolution of Complexity of Reaction Paths in the Alkaline Hydrolysis of *N*-(2'-Hydroxyphenyl) phthalimide in Mixed $H_2O$-$CH_3CN$ Solvent

Y.L. Sim[1], A. Ariffin[1] and M.N. Khan[1*]

The rate of aqueous cleavage of *N*-(2'-hydroxyphenyl)phthalimide (A), monitored at 320 nm, $1.0 \times 10^{-3}$ M NaOH, 35ºC and within $CH_3CN$ content range 1% – 80% v/v in mixed aqueous solvents, follows the reaction scheme: $A + HO^-/H_2O \xrightarrow{k_1} B + HO^-/H_2O \xrightarrow{k_2} P_1 + P_2$ where B, $P_1$ and $P_2$ represent *N*-(2'-hydroxyphenyl)phthalamic acid, phthalic acid and 2-hydroxyaniline, respectively. The values of $k_1$ and $k_2$ at different content of $CH_3CN$ have been calculated from a kinetic equation based upon a reaction scheme with two irreversible pseudo-first-order consecutive reaction paths. The values of $k_1/k_2$ are $> 10^4$ within $CH_3CN$ content range 1% – 80% v/v in mixed aqueous solvents. The intermediate hydrolysis product (B) exists in 72% dianionic, 27.9% monoanionic and 0.1% nonionic form under the present experimental conditions. Both dianionic and monoanionic forms of B are non-reactive while the nonionic form of B is reactive towards hydrolysis under such conditions.

**Key words:** *N*-(2'-Hydroxyphenyl)phthalimide; *N*-(2'-hydroxyphenyl)phthalamic acid; 2-hydroxyaniline; phthalic acid; base; hydrolysis; kinetics; reaction scheme; irreversible; consecutive reaction paths

One of the most important classes of biological polymeric compounds is coined as protein. All the protein molecules are formed from monomers (known as amino acids) through strong covalent secondary amide bond as shown in **1** (*Scheme 1*) and this specific secondary amide bond is widely known as peptide bond. The half-life period for hydrolytic cleavage of a secondary amide bond, under physiological pH, temperature and reaction medium is ~ 20 years (Kahne & Still 1988). Perhaps it is worth mentioning that the kinetic study of a reaction with a half-life of a few weeks is not an attractive area of research because of the various unavoidable practical problems associated with such studies. As such, studies are generally carried out at high temperature and [$HO^-$] values. The rate constant values under such conditions are then used to estimate rate constant values at physiological conditions. Thus, in the absence of enzymatic catalytic processes, it would have been impossible for any living creature/species to survive because digestion processes require ~ 20 years to digest half of the amount of protein eaten/taken at a time in the life span. The specific enzyme (s), through its catalytic action, reduced the half-life period from ~ 20 years to less than a second (Hirohara *et al*. 1977; Brot & Bender 1969). Perhaps, a relatively more thoroughly understood mechanism, by which an enzyme increases the reaction rate, involves the ability of the enzyme to approximate an intermolecular bimolecular reaction into an intramolecular reaction as shown by (*Scheme 2* (Jencks 1969; Jencks 1975; Kanamori & Roberts 1983).

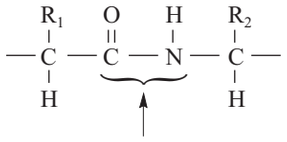

A secondary amide bond

**1**

Scheme 1

Awareness of this fact in some enzyme-catalyzed reactions in 1969 (Blow *et al*. 1969) led to a surge of study on the mechanistic diagnosis of rate enhancement (~ $10^2$ to $10^{14}$ – fold) due to intramolecularity over an analogous intermolecularity of the reactions (Page *et al*. 1987; Milstein & Cohen 1972; Menger 1985; Menger & Ladika 1988; Shashidhar *et al*. 1997; Zhou *et al*. 1998). Bender (1957) and Bender *et al*. (1958) in a seminal paper, reported, perhaps for the first time, an efficient rate enhancement in the hydrolytic cleavage of a primary amide bond, under mild acidic aqueous solvent, of phthalamic acid **(2)** compared to that of benzamide **(3)** and terephthalamic acid **(4)** as shown in *Scheme 3*. Bender (1957) showed, through an ingeneous isotopic labelling technique, the presence of a symmetric

[1] Department of Chemistry, Faculty of Science, University of Malaya, 50603 Kuala Lumpur, Malaysia
* Corresponding author (e-mail: niyaz@um.edu.my)

reactive intermediate (most likely phthalic anhydride) as shown in *Scheme 4*. Subsequent studies on mild acidic aqueous hydrolysis of phthalamic acid and its derivatives provided UV spectrophotometric evidence for intermediacy of phthalic anhydride in these reactions (Blackburn *et al*. 1977; Khan 1996; Khan & Ariffin 2003). Today, several related studies (Milstein & Cohen 1972; Menger & Ladika 1988; Kirby & Lancaster 1972; Kirby *et al*. 1974; Kluger & Lam 1975; Kluger & Lam 1978; Granados & de Rossi 2001; Hawkins 1976; Sim *et al*. 2004; Sim *et al.* 2006) show rate enhancements due to neighboring COOH group assistance in the mild acidic aqueous cleavage of amide which vary in the range of $10^2$ to $10^{14}$-fold. The upper limit of rate enhancement of $10^{14}$-fold is equivalent to α-chymotripsin (an enzyme) catalyzed aqueous cleavage of the peptide bond (Hirohara *et al*. 1977).

Reaction medium or solvent significantly affects the catalytic efficiency of various enzymes including α-chymotripsin. The effects of aqueous-organic solvents on the reaction rates are generally rationalized qualitatively in terms of empirical approaches. The reason for this fact is the lack of a perfect and general theoretical model to deal with such extremely complex and highly dynamic structural features of such solvent systems. Despite this fact, a huge amount of kinetic data on the effects of pure and mixed solvents on the reaction rates are available and they provide some very useful insights regarding the mechanistic aspects of these reactions. However, the kinetic data on the effects of mixed aqueous-organic solvents on the intramolecular assisted-reaction rates are relatively rare (Khan & Ariffin 2003; Sim *et al*. 2004; Sim *et al.* 2006; Khan 1993; Ariffin & Khan 2005; Khan 1998).

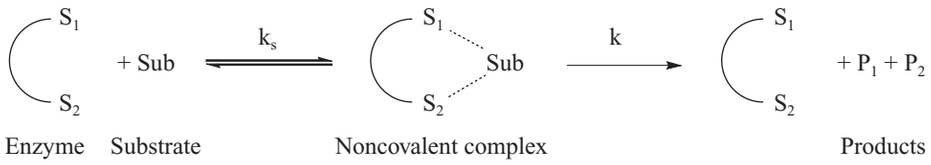


Scheme 2

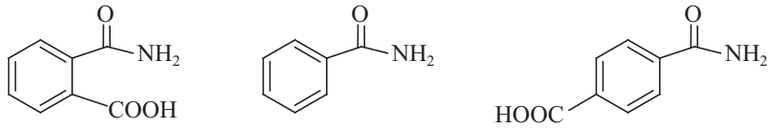


Scheme 3

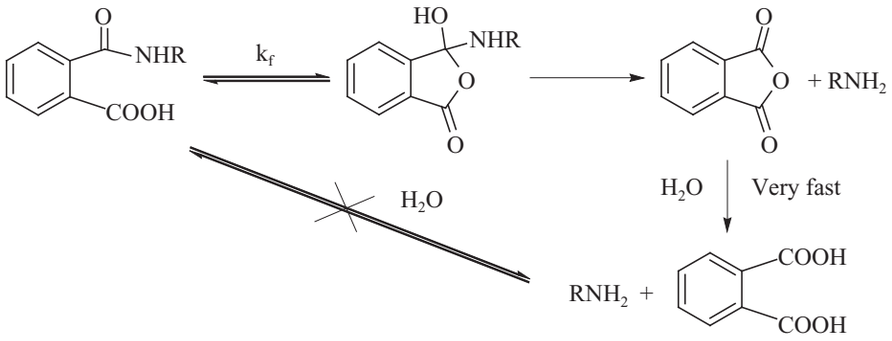


Scheme 4

The use of kinetics in the diagnosis of the fine detailed reaction mechanisms has been the most important and useful aspect of such research studies. Ironically, a majority of the solution phase reactions either obey or are made to obey first-order kinetics under pseudo-first-order kinetic conditions. Kinetic studies on the rate of two or more than two step reactions (i.e. consecutive reactions) are relatively limited partly because of the complex kinetic equations produced by solving the rate laws of such reactions. Generally, these complex kinetic equations are transcendental equations whose exact solutions are almost impossible to achieve, and hence they are difficult to solve for intended rate constants by the use of any conventional mathematical technique (Frost & Pearson 1961). With the easy access to computers and software programs in various computer languages, the kinetics of consecutive reactions can be studied rather easily (Khan & Khan 1975).

Phthalamic and N-substituted phthalamic acids, under mild aqueous acidic solutions, undergo product formation as shown by *Scheme 5*.

Depending upon the reaction conditions, the rate of hydrolysis of phthalamic acid (R = H) has been found to follow simple first-order rate law (Bender 1957) and two complex irreversible consecutive reaction paths (Blackburn *et al*. 1977; Khan 1996). The aim of the present work is to study the rate of mild alkaline hydrolysis of *N*-(2'-hydroxyphenyl)phthalimide under the reaction conditions where the reaction kinetics follow the complex consecutive reaction paths. The observed kinetic data and their kinetic interpretation are described in this article.

## EXPERIMENTAL

### Materials

Synthesis of *N*-(2'-hydroxyphenyl)phthalimide **(5)** and *N*-(2'-hydroxyphenyl)phthalamic acid **(6)** are described elsewhere (Sim *et al.* 2007). All other chemicals used were of reagent grade commercial products of highest available purity. Standard solutions of (0.03 M) was prepared in acetonitrile.

### Kinetic Measurements

The rate of alkaline hydrolysis of 5 was conveniently studied spectrophotometrically by monitoring the product formation at 320 nm. The details of the kinetic procedure are described elsewhere (Sim *et al.* 2006).

### Product Characterization

Authentic samples of **6**, 2-hydroxyaniline and phthalic acid were used to show that the alkaline hydrolysis of 5 involves **6** as an intermediate as well as 2-hydroxyaniline and phthalic acid as the immediate final products.

### Kinetic Data Analysis

The kinetic data (absorbance, $A_{obs}$ versus reaction time, $t$) for a few typical kinetic runs have been shown in Figure 1. These observed data show that the intermediate product **(6)** of hydrolysis of **5**, which absorbs strongly at 320 nm, converts to hydrolysis products, 2-hydroxyaniline

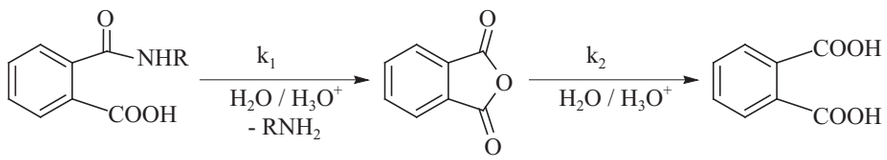


Scheme 5

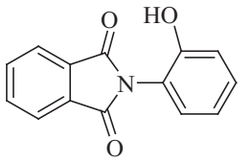


**5**

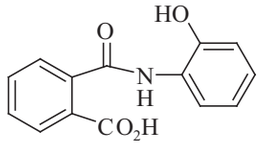


**6**

and phthalic acid. The main overall reaction steps in the cleavage of **5** at 1.0 × $10^{-3}$ M NaOH and within $CH_3CN$ content range 1% – 80% v/v in mixed aqueous solvents may be represented by *Scheme 6*.

In view of *Scheme 6*, it follows readily that:

$$[\mathbf{5}] = [R_0] \exp(-k_{obs}\, t) \quad (1)$$

$$[\mathbf{6}] = \frac{k_{1obs}\,[R_0]}{(k_{2obs} - k_{1obs})}\,[\exp(-k_{1obs}\, t) - \exp(-k_{2obs}\, t)] \quad (2)$$

$$[\mathbf{5}] + [6] + [P_1] = [R_0] \quad (3)$$

and $[P_1] = [P_2] = [R_0] - [\mathbf{5}] - [\mathbf{6}]$ (4)

where $[R_0]$ represents the initial concentration of **5**, i.e. $[\mathbf{5}_0] = [R_0]$ at $t = 0$, [**5**], [**6**], $[P_1]$ and $[P_2]$ represent concentration of corresponding reaction species at any $t$. The observed absorbance ($A_{obs}$) at 320 nm and at any reaction time ($t$) may be given as:

$$A_{obs} = \delta_5\,[\mathbf{5}] + \delta_6\,[\mathbf{6}] + \delta_{P1}\,[P_1] + \delta_{P2}\,[P_2]$$
$$= \delta_5\,[\mathbf{5}] + \delta_6\,[\mathbf{6}] + (\delta P_1 + \delta_{P2})\,([R_0] - [\mathbf{5}] - [\mathbf{6}]) \quad (5)$$

where, $\delta_x$ stands for molar extinction coefficient of compound '$x$'. Equations 1, 2 and 5 can easily lead to Equation 6:

$$A_{obs} = A_1\,[R_0]\,[\exp(-k1_{obs}\, t) - 1] + \frac{A_2\,[R_0]}{k_{2obs} - k_{1obs}}\,[\exp(-k_{1obs}\, t) - \exp(-k_{2obs}\, t)] + [R_0]\,\delta_5 \quad (6)$$

where $A_1 = \delta_5 - \delta P_1 - \delta P_2$,
$A_2 = (\delta_6 - \delta P_1 - \delta P_2)\, k_{1obs}$
$[R_0]\,\delta_5 = A_0$ (absorbance at $t = 0$).

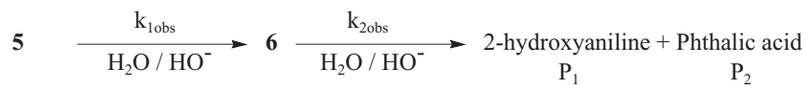


Scheme 6

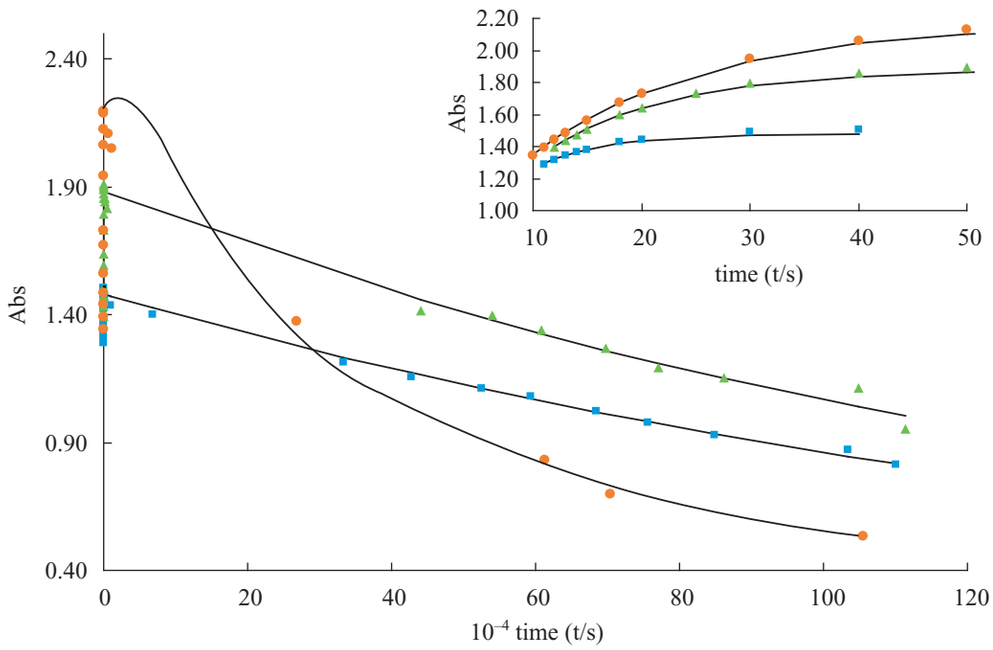


Figure 1. Plots showing the dependence of absorbance, Abs (at 320 nm), versus $t$ for alkaline hydrolysis of **5** at 1.0 × $10^{-3}$ M NaOH, 3.0 × $10^{-4}$ M **5**, 35°C and $CH_3CN$ content 1% v/v (■), 50% v/v (▲) and 80% v/v (●). The solid lines are drawn through the least-squares calculated data points using Equation 6 and parameters listed in Table 2.

## RESULTS AND DISCUSSION

In principle, observed data ($A_{obs}$ versus $t$) can be used to calculate $k_{1obs}$, $k_{2obs}$, $A_1$, $A_2$ and $A_0$ (= $\delta_5$ [$R_0$]) from Equation 6 using the non-linear least-squares (NLS) technique. An approximate technique is now normally used to get approximate solutions of equations such as Equation 6. It is well known that in the use of NLS technique, the reliability of the calculated values of the unknown parameters decreases with the increase in the number of unknown parameters. Hence, it is advisable in such data analysis to reduce the number of unknown parameters to a minimum possible value (≥ 2). In the present reacting system, the value of $A_0$ can be easily and accurately obtained from extrapolation of $A_{obs}$ values to $t$ = 0. Thus, the observed data fit to Equation 6 was carried out by the use of NLS considering $k_{1obs}$, $k_{2obs}$, $A_1$ and $A_2$ as four unknown parameters.

The rate of alkaline hydrolysis of intermediate **(6)** was found to be extremely slow and as a consequence only a few kinetic runs were carried out at 1.0 × $10^{-3}$ M NaOH, 35ºC and within $CH_3CN$ content range 1% – 80% v/v in mixed aqueous solvent for the reaction periods of ~ 300 h which could be equivalent to ~ 1 half-life for kinetic runs at ≤ 50 % v/v $CH_3CN$. The nature of Equation 6 is such that the use of NLS technique cannot give reliable values of all or some of the kinetic parameters ($k_{1obs}$, $k_{2obs}$, $A_1$, $A_2$) if the kinetic run was monitored for the reaction period of ≤ 1 half-life (Khan 2006). Thus, in order to get the relatively more reliable values of kinetic parameters, the value of $A_{obs}$ at $t \geq 10$ half-lives should be known (Khan 2006). The expected hydrolysis products of **6** are 2-hydroxyaniline and phthalic acid. The authentic samples of phthalic acid and 2-hydroxyaniline were used to obtain δ for these compounds under the reaction conditions of kinetic runs which in turn gave $A_\infty^{est}$ as summarized in Table 1 where $A_\infty^{est} = A_{obs}$ at $t$ > 15 half-lives. The use of $A_{obs} = A_\infty^{est}$ at $t$ > 15 half-lives yielded the values of $k_{1obs}$, $k_{2obs}$, $A_1$ and $A_2$ as shown in Table 1. The reliability of the data fit to Equation 6 is evident from the standard deviations associated with the calculated kinetic parameters (Table 1) and from a few typical plots of Figure 1 where solid lines are drawn through the least-squares predicted absorbance values.

The values of $k_{1obs} / k_{2obs} > 10^4$ (Table 1), and consequently the values of $k_{1obs}$, $\delta_{app}$ (apparent molar extinction coefficient of the reaction mixture) where $\delta_{app} = \delta_6 - \delta_5$ and $A_0$ were also calculated from Equation 7 using the observed data points in the initial phase of the reaction. The calculated values of $k_{1obs}$, $\delta_{app}$ and $A_0$ are shown in Table 2. The values of $k_{1obs}$ are comparable with the corresponding values of $k_{1obs}$ calculated from Equation 6 (Table 1). The values of $\delta_{app}$ (= $\delta_6 - \delta_5$) and $A_0$ (= $\delta_5$ [$R_0$]) were used to calculate $\delta_5$ and $\delta_6$ values as shown in Table 1 and Table 2, respectively.

$$A_{obs} = \delta_{app} [R_0] [1 - \exp(-k_{obs} t)] + A_0 \quad (7)$$

The values of $A_1$, $A_2$, $k_{1obs}$, $\delta_5$ (Table 1) and $\delta_6$ (Table 2) can be used to calculate $\delta_{P1} + \delta_{P2}$ from the relationships: $A_1 = \delta_5 - (\delta_{P1} + \delta_{P2})$ and $A_2 = (\delta_6 - \delta_{P1} - \delta_{P2})\ k_{1obs}$ and these calculated values of $(\delta_{P1} + \delta_{P2})$ are shown in Table 1. The values of $(\delta_{P1} + \delta_{P2})$ obtained from authentic samples of

Table 1. Least-Squares Calculated Values of $k_{1obs}$, $k_{2obs}$, $A_1$ and $A_2$ from Equation 6.[a]

| $CH_3CN$ % (v/v) | $\delta_5$[b] $M^{-1}$ $cm^{-1}$ | $10^3\ k_{1obs}$ $s^{-1}$ | $10^8\ k_{2obs}$ $s^{-1}$ | $A_1$ $M^{-1}$ $cm^{-1}$ | $A_2$ $M^{-1}$ $cm^{-1}$ $s^{-1}$ | $10^2$ $A_\infty^{est}$[c] | $Z_1$[d] $M^{-1}$ $cm^{-1}$ | $Z_2$[e] $M^{-1}$ $cm^{-1}$ |
|---|---|---|---|---|---|---|---|---|
| 1 | 1713 | 150 ± 5[f] | 58.9 ± 1.4[f] | 1421 ± 59[f] | 699 ± 24[f] | 8.6 | 292 | 360 |
| | | 154 ± 7 | 95.0 ± 18.0 | 57 ± 414 | 503 ± 70 | [g] | | |
| | | 149 ± 5 | 66.4 ± 1.8 | 1038 ± 61 | 639 ± 23 | 0.200[h] | 675 | 731 |
| | | 149 ± 5 | 74.2 ± 2.1 | 706 ± 59 | 587 ± 20 | 0.300[h] | 1007 | 1080 |
| | | 147 ± 5 | 96.2 ± 3.2 | 53 ± 57 | 487 ± 17 | 0.500[h] | 1660 | 1707 |
| 10 | 1740 | 154 ± 6 | 67.2 ± 1.9 | 1394 ± 73 | 768 ± 29 | 10.1 | 346 | 433 |
| 20 | 1790 | 129 ± 5 | 72.3 ± 2.3 | 1393 ± 85 | 683 ± 26 | 11.7 | 397 | 532 |
| 30 | 1830 | 113 ± 3 | 67.7 ± 2.0 | 1386 ± 85 | 612 ± 19 | 13.2 | 444 | 590 |
| 40 | 1877 | 92.7 ± 2.1 | 111 ± 3 | 1376 ± 75 | 519 ± 13 | 14.7 | 501 | 627 |
| 50 | 1890 | 84.2 ± 2.6 | 64.7 ± 2.2 | 1318 ± 99 | 480 ± 16 | 17.1 | 572 | 695 |
| 60 | 1827 | 75.2 ± 1.9 | 114 ± 3 | 1154 ± 83 | 439 ± 12 | 19.7 | 673 | 764 |
| 70 | 2100 | 70.3 ± 1.4 | 191 ± 5 | 1294 ± 62 | 424 ± 9 | 23.1 | 806 | 871 |
| 80 | 2130 | 62.7 ± 1.6 | 212 ± 8 | 1082 ± 86 | 387 ± 10 | 31.4 | 1048 | 1194 |

[a] [$R_0$] = 3.0 × $10^{-4}$ M, [NaOH] = 1.0 × $10^{-3}$ M, λ = 320 nm, $T$ = 35ºC. [b] $\delta_5$ values were obtained from Equation 7 as described in the text. [c] Observed absorbance (= $A_\infty^{est}$) at 320 nm of mixed $H_2O$-$CH_3CN$ solvent containing 3.0 × $10^{-4}$ M 2-hydroxyaniline, 3.0 × $10^{-4}$ M phthalic acid and 1.0 × $10^{-3}$ M NaOH. [d] $Z_1 = \delta_{P1} + \delta_{P2} = \delta_5 - A_1$. [e] $Z_2 = \delta_{P1} + \delta_{P2} = \delta_6 - (A_2 / k_{1obs})$. [f] Error limits are standard deviations. [g] Final $A_{obs}$ value (= 0.813), included in the data treatment, was obtained at 306 h. [h] These are the presumed values of $A_\infty^{est}$ just to determine the effects of possible uncertainty in the experimentally determined values of $A_\infty^{est}$ on the calculated values of kinetic parameters, $k_{1obs}$, $k_{2obs}$, $A_1$ and $A_2$ as described on p.88.

Table 2. Least-Squares calculated values of $k_{1obs}$, $\delta_{app}$ and $A_0$ from Equation 7.

| $CH_3CN$ % (v/v) | $10^3\ k_{1obs}$ $s^{-1}$ | $\delta_{app}$ $M^{-1}\ cm^{-1}$ | $10^2\ A_0$ | $\delta_6$ [a] $M^{-1}\ cm^{-1}$ |
|---|---|---|---|---|
| 1 | 139 ± 1 [b] | 3307 ± 27 [b] | 51.4 ± 0.8 [b] | 5020 |
| 10 | 140 ± 3 | 3681 ± 127 | 52.2 ± 3.9 | 5420 |
| 20 | 117 ± 2 | 4037 ± 83 | 53.7 ± 2.6 | 5827 |
| 30 | 105 ± 1 | 4176 ± 43 | 54.9 ± 1.4 | 6006 |
| 40 | 87.2 ± 0.5 | 4349 ± 24 | 56.3 ± 0.8 | 6226 |
| 50 | 78.9 ± 0.9 | 4506 ± 45 | 56.7 ± 1.5 | 6396 |
| 60 | 72.0 ± 0.7 | 4776 ± 34 | 54.8 ± 1.1 | 6602 |
| 70 | 68.3 ± 0.6 | 4802 ± 31 | 63.0 ± 1.0 | 6902 |
| 80 | 59.5 ± 0.3 | 5236 ± 15 | 63.9 ± 0.5 | 7366 |

[a] $\delta_6 = A_\infty / [R_0]$ where $A_\infty = \delta_{app}\ [R_0] + A_0$, $[R_0] = 3.0 \times 10^{-4}$ M. [b] Error limits are standard deviations.

2-hydroxyaniline and phthalic acid ($\delta_{P1} + \delta_{P2} = A_\infty^{est} / [R_0]$, Table 1) may be compared with the corresponding values of ($\delta_{P1} + \delta_{P2}$) obtained from the relationships: ($\delta_{P1} + \delta_{P2}$) = $\delta_5 - A_1$ and ($\delta_{P1} + \delta_{P2}$) = $\delta_6 - (A_2 / k_{1obs})$.

## Aqueous Alkaline Degradation of 2-Hydroxyaniline

Perhaps it is worth mentioning that 2- and 4-hydroxyanilines undergo a rather complex oxidative degradation process under alkaline medium (Sim *et al*. 2008). Satisfactory observed data fit to Equation 6 indicates that the pseudo-first-order rate constant for the alkaline degradation of 2-hydroxyaniline must be either faster or slower than $k_{2obs}$ by > 10-fold. In order to assess this possibility, a single kinetic run was carried out for the aqueous degradation of 2-hydroxyaniline at 300 nm, 35ºC, $1.0 \times 10^{-3}$ M NaOH in aqueous solvent containing 1% v/v $CH_3CN$ and $3.0 \times 10^{-4}$ M 2-hydroxyaniline. The plot of $A_{obs}$ versus $t$, as shown in Figure 2, shows the presence of a maximum. But the rate of the degradation of the initial phase appeared to be much faster than that of final phase and as a consequence, the observed data for initial and final degradation were treated with Equations 7 and 8, respectively. The least-squares calculated values of kinetic parameters are as follows: $10^4\ k'_{1obs} = 2.11 \pm 0.46\ s^{-1}$, $\delta_{app} = 787 \pm 74\ M^{-1}\ cm^{-1}$ and $A_0 = 1.01 \pm 0.01$ for initial phase and $10^6\ k'_{2obs} = 4.91 \pm 0.76\ s^{-1}$, $\delta'_{app} = 442 \pm 27\ M^{-1}\ cm^{-1}$ and $A'_\infty = 1.05 \pm 0.01$ for final phase of degradation.

$$A_{obs} = \delta'_{app}\ [R_0] \exp(-k'_{2obs}\ t) + A'_\infty \qquad (8)$$

The value of $k'_{2obs}$ ($= 491 \times 10^{-8}\ s^{-1}$) is more than 8 - fold larger than $k_{2obs}$ ($= 58.9 \times 10^{-8}\ s^{-1}$, Table 1) which explains why the alkaline degradation of immediate final product, 2-hydroxyaniline, of alkaline hydrolysis of **6** could not complicate the kinetics of the alkaline hydrolysis of **5**. However, the data treatment to Equation 6 requires the use of the value of $A_\infty^{est}$ as the absorbance at 320 nm due to final alkaline degradation product of 2-hydroxyaniline in the presence of $3.0 \times 10^{-4}$ M phthalic acid which is not known. The values of $A_{obs}$ for kinetic run at 1% v/v $CH_3CN$ are 0.870 and 0.813 at respective t = $103.5 \times 10^4$ and $110.0 \times 10^4$ s which show that $A_{obs}$ value at t ≥ 10 half-lives should be significantly smaller than 0.813. It should be noted that the effective hydroxide ion concentration, $[HO^-]_{eff}$, for the reaction step: **5** → **6** is $7.0 \times 10^{-4}$ M (= [NaOH] – $[R_0]$) because of the presence of acidic group in 2-hydroxyaniline moiety of **5**, while the value of $[HO^-]_{eff}$ is $4.0 \times 10^{-4}$ M for the reaction step: **6** → $P_1 + P_2$ in *Scheme 2* because of the presence of two acidic groups in **6**.

Although the values of $\delta_{P1} + \delta_{P2}$, obtained from kinetic data, are comparable with the corresponding values of $\delta_{P1} + \delta_{P2}$, obtained from authentic samples of $P_1$ and $P_2$ i.e. $A_\infty^{est}$ (Table 1), a skeptic might suspect the reliability of $A_\infty^{est}$ values because of the fact that product $P_1$ is unstable under alkaline medium (Figure 2). In order to evaluate the effects of presumed uncertainty associated with $A_\infty^{est}$ values, the observed data at 1% v/v $CH_3CN$ were treated with Equation 6 at different given values of $A_\infty^{est}$ and the calculated results obtained are summarized in Table 1. It is apparent from these results that at 1% v/v $CH_3CN$, the increase in $A_\infty^{est}$ from $8.6 \times 10^{-2} - 50 \times 10^{-2}$ has the following consequences: (i) the value of $k_{1obs}$ remains unchanged, (ii) $k_{2obs}$ value increases by 63%, (iii) $A_1$ value decreases by ~ 27-fold, (iv) $A_2$ value decreases by ~ 1.44-fold and (v) although the increase in the residual errors (= $A_{obsi} - A_{calcdi}$ where $A_{obsi}$ and $A_{calcdi}$ represent respective observed and least - square calculated absorbance values at $i$th reaction time $t$) and standard deviations associated with the calculated values of $k_{2obs}$ and $A_2$ are modest, the increase of the standard deviation of $A_1$ is large. The standard deviation of $A_1$ value at $A_\infty^{est} = 0.50$ is > 100% and as a consequence, the $A_1$ value is unreliable. The observed data could not fit to Equation 6 at $A_\infty^{est} > 0.50$.

It is known that $CH_3CN$ molecules hydrolyze to produce acetamide under alkaline medium and the value of hydoxide ion-catalyzed second-order rate constant ($k_{OH}$) for this reaction is $4.6 \times 10^{-6}\ M^{-1}\ s^{-1}$ at 35ºC (Widegrist 1956). The value of $k_{OH}$ of $4.6 \times 10^{-6}\ M^{-1}\ s^{-1}$ shows that the value of pseudo-first-order rate constant by alkaline hydrolysis of $CH_3CN$ is $4.6 \times 10^{-9}\ s^{-1}$ at $1.0 \times 10^{-3}$ M NaOH which

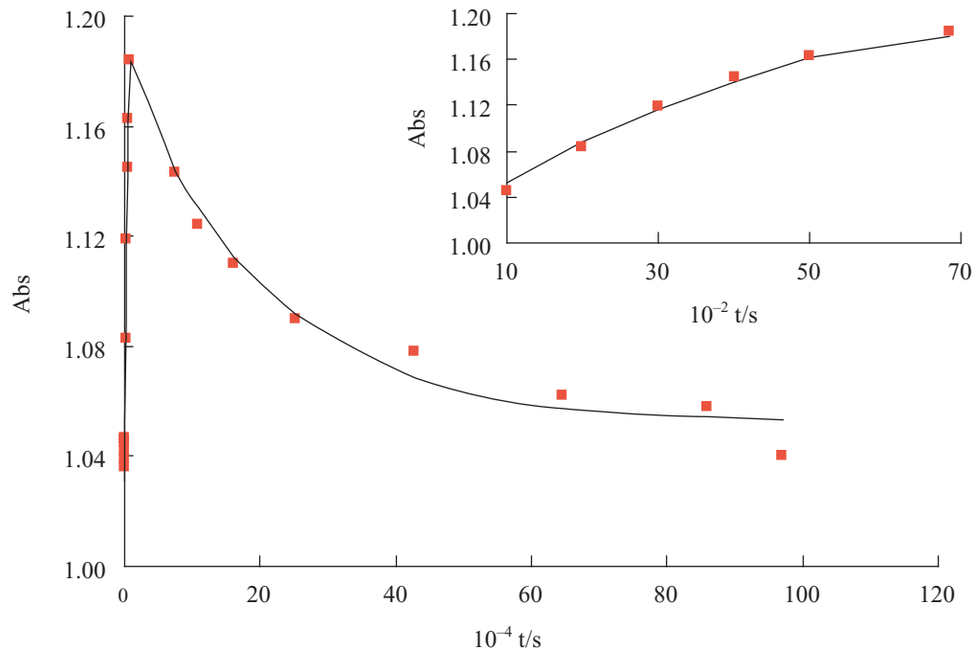


Figure 2. Plots showing the dependence of absorbance, Abs (at 300 nm), versus *t* for aqueous degradation of 2-hydroxyaniline at $1.0 \times 10^{-3}$ M NaOH, $3.0 \times 10^{-4}$ M 2-hydroxyaniline, 35ºC and 1% v/v $CH_3CN$. The solid lines is drawn through the least-squares calculated data points using Equation 7 and 8.

is more than 100-fold smaller than the lowest value of $k_{2obs}$ and as a consequence, the rate of alkaline hydrolysis of $CH_3CN$ could be considered as insignificant during the aqueous alkaline degradation of **5**.

The effects of mixed $H_2O$ – $CH_3CN$ solvents were also studied at 35ºC in the presence of $1.0 \times 10^{-3}$ M NaOH by monitoring the reaction rate at 300 nm (Sim *et al.* 2006) where the consecutive nature of the reaction was not as distinct as at 320 nm in the present study. The reason for this observation is the large difference in the relative values of $\delta_6$ / $\delta_5$ at 300 and 320 nm ($\delta_6$ / $\delta_5$ range 0.61 – 0.57 at 300 nm and $\delta_6$ / $\delta_5$ range 2.93 – 3.46 at 320 nm within $CH_3CN$ content range 1% – 80% v/v in mixed aqueous solvent). However, the values of $k_{1obs}$ were 10% – 40% higher than the corresponding $k_{obs}$ obtained at 300 nm where observed data were treated with first-order rate law. Although the values of $k_{1obs}$ / $k_{2obs}$ > $10^4$ (Table 1), the values of $k_{1obs}$ (from Equation 6) / $k_{obs}$ (from Equation 7) varied from 1.03 – 1.10 (Table 2) which show the amount of errors produced when the consecutive nature of the reaction (Equation 6) is approximated to simple one step reaction (Equation 7) for the observed data treatment. The physico-chemical explanation for the effects of mixed $H_2O$ – $CH_3CN$ solvents on $k_{1obs}$ remained essentially the same as described elsewhere (Sim *et al.* 2006).

The values of $k_{2obs}$ are almost independent of the content of $CH_3CN$ within its range 1% – 60% v/v followed by a moderate increase with its increase at ≥ 70% v/v (Table 1). These observations are considered to be unusual if the alkaline hydrolysis of **6** involves ionized **6** and $HO^-$ as the reactants. The rate of alkaline hydrolysis of *N*-(2'-methoxyphenyl)phthalimide **(7)** has been shown to involve **7** and $HO^-$ as the reactants and pseudo-first-order rate constants ($k_{obs}$) for alkaline hydrolysis of **7** at $1.0 \times 10^{-3}$ M NaOH decreased nonlinearly by ~ 17-fold with the increase in the $CH_3CN$ content from 2% to 70% v/v followed by ~ 1.2 - fold increase in $k_{obs}$ at 80% v/v $CH_3CN$ (Sim *et al.* 2006). A recent study on the rate of hydrolysis of **6** at 35ºC in aqueous solvent containing 1% v/v $CH_3CN$ and [NaOH] ≥ 1.2 M shows that the hydrolysis involves **6** and $HO^-$ as the reactants and the value of second-order rate constant ($k_{OH}$) for the reaction of $HO^-$ with **6** is $4.73 \times 10^{-8}$ $M^{-1}$ $s^{-1}$ at 35ºC (Sim *et al*. 2008). In view of this reported value of $k_{OH}$, the value of $k_{2obs}$ at $1.0 \times 10^{-3}$ M NaOH should be $4.7 \times 10^{-11}$ $s^{-1}$ at 1% v/v $CH_3CN$. This predicted value of $k_{2obs}$ is $1.3 \times 10^4$ - fold smaller than experimentally observed $k_{2obs}$ value (= $5.89 \times 10^{-7}$ $s^{-1}$, Table 1). Thus, it is apparent that the $k_{2obs}$ values summarized in Table 1 do not conform to the expectation that the hydrolysis of **6** at $1.0 \times 10^{-3}$ M NaOH involves **6** and $HO^-$ as the reactants.

An alternative reaction mechanism for the hydrolysis of **6** at $1.0 \times 10^{-3}$ M NaOH may be described as follows. The reported respective values of $pK_{a1}$ and $pK_{a2}$ for **6** are 3.33 and 9.52 at 35ºC as well as the respective values of $\delta_{NE}$[6], $\delta_{MA}$[6] and $\delta_{DA}$[6] at 300 nm are $2.00 \times 10^3$, $1.64 \times 10^3$ and

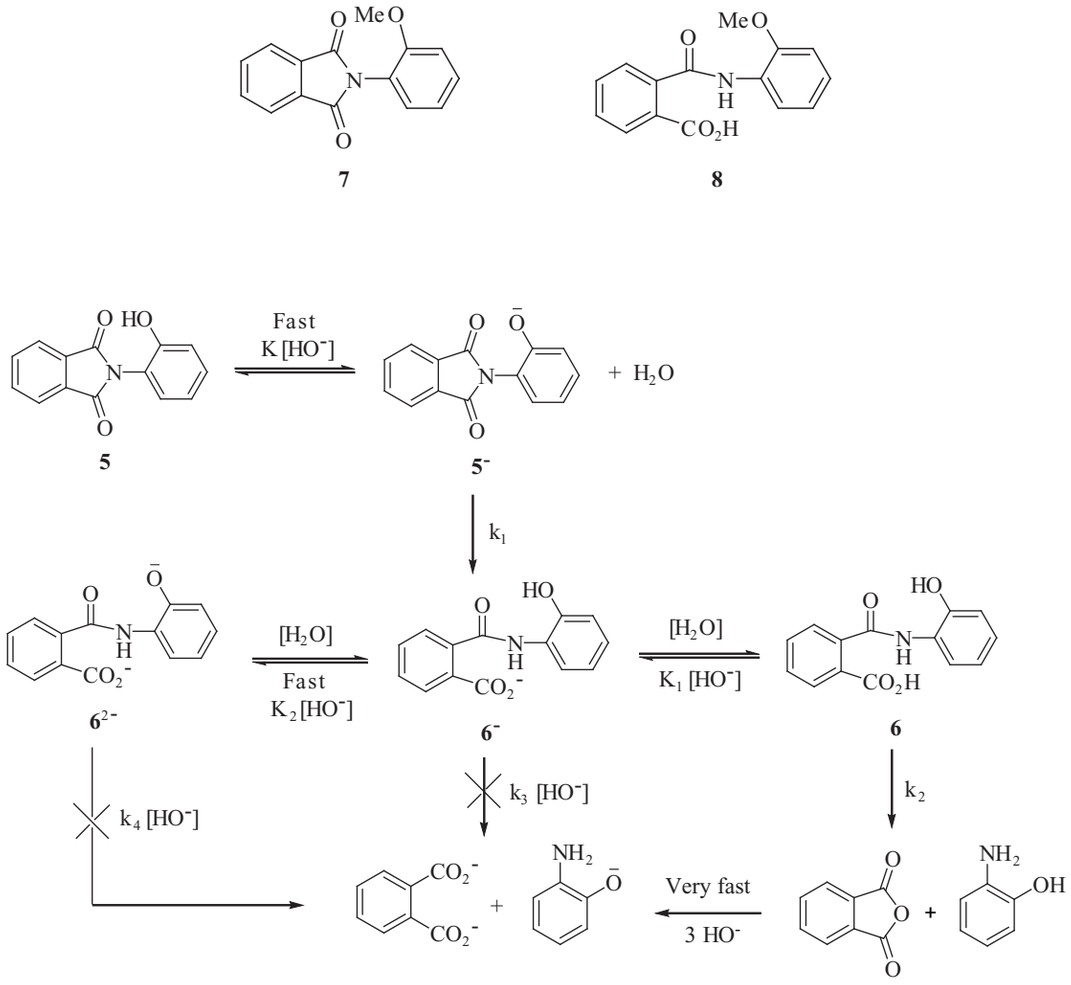


Scheme 7

$5.60 \times 10^3$ $M^{-1}$ $cm^{-1}$ where $\delta_{NE}^{6}$, $\delta_{MA}^{6}$ and $\delta_{DA}^{6}$ represent molar extinction coefficient of neutral, monoanionic and dianionic **6**, respectively (Sim *et al*. 2008). These results and the values of $A_\infty$, calculated from equation similar to Equation 8 for alkaline hydrolysis of **5** at 300 nm, $1.0 \times 10^{-3}$ M NaOH and within $CH_3CN$ content range 1% – 80% v/v, were used to obtain $F_{DA}^{6}$ from the relationship: $F_{DA}^{6} = (A_\infty - \delta_{AV}^{6}[S]_T) / (\delta_{DA}^{6} - \delta_{AV}^{6})[S]_T$ where $\delta_{AV}^{6} = (\delta_{NE}^{6} + \delta_{MA}^{6}) / 2$, $F_{DA}^{6} = [S^{2-}] / [S]_T$ and $[S]_T = [S^{2-}] + [SH^-] + [SH_2] = 3.0 \times 10^{-4}$ M with $S^{2-}$, $SH^-$ and $SH_2$ representing dianionic (DA) **6**, monoanionic (MA) **6** and nonionic (NE) **6**, respectively. The calculated values of $F_{DA}^{6}$ within $CH_3CN$ range 1% – 80% v/v give average value of $F_{DA}^{6}$ as 0.72 ± 0.02 which reveals that ~ 28% **6** molecules exist in neutral and monoanionic forms. Although the initial concentration of NaOH was kept constant at $10 \times 10^{-4}$ M, the respective effective values of [NaOH] became $7 \times 10^{-4}$ M and $4 \times 10^{-4}$ M at the beginning and the end of first step of *Scheme 6* because of the presence of one acidic group in **5** and two acidic groups in **6**. Thus, under such experimental conditions, the expected reaction paths for aqueous degradation of **5** may be shown by *Scheme 7* where the mechanistic details of $k_1$-, $k_2$- and $k_4$-step have been described elsewhere (Sim *et al*. 2006; Sim *et al*. 2007). The mechanistic details of alkaline hydrolysis of **6** may be considered to be similar to the alkaline hydrolysis of *N*-(2'-methoxyphenyl)phthalamic acid **(8)** and the mechanistic details of alkaline hydrolysis of **8** are discussed in the recent report (Sim *et al*. 2008).

The reported values of $k_2$, $k_3$ and $k_4$ are $66.9 \times 10^{-5}$ $M^{-1}$ $s^{-1}$ (at 0.049 M HCl, 35ºC for **6**)24, $22.0 \times 10^{-8}$ $M^{-1}$ $s^{-1}$ (at 35ºC for 8) (Sim *et al*. 2008) and $4.73 \times 10^{-8}$ $M^{-1}$ $s^{-1}$ (at 35ºC for $6^{2-}$) (Sim *et al*. 2008), respectively. In view of these reported results, the rate of hydrolysis of **6** through $k_3$- and $k_4$-steps should be insignificant compared to $k_2$-step. The value of $k_2$ is unusually very large because of the involvement of the uncatalyzed intramolecular carboxylic group (COOH) assistance in the cleavage of amide bond (Sim *et al*. 2006). The calculated values of $k_{2obs}$ of the order

of $10^{-7}$ $s^{-1}$ (Table 1) reveal that the values of the fraction of **6** {$F_{NE} = F_6 = [\mathbf{6}] / ([\mathbf{6}] + [\mathbf{6}^-] + [\mathbf{6}^{2-}])$} are of the order of $10^{-3}$. As concluded earlier that $F_{NE} + F_{MA} = 0.28$ and $F_{DA} = 0.72$, it readily follows that $F_{MA} = 0.279$ because $F_{NE} = 0.001$. The extremely low value of $F_6 \equiv F_{NE}$ ($= 10^{-3}$) seems plausible in the sense that (i) the expected values of the effective concentration of NaOH at the start and the end of $k_2$-step of *Scheme 2* should be $\sim 4 \times 10^{-4}$ M and $\sim 1 \times 10^{-4}$ M, respectively, and (ii) kinetics were carried out for the reaction period of $> 12$ days without any protection device of the possible effects of atmospheric carbon dioxide on the pH of the reaction medium.

## ACKNOWLEDGEMENT

The authors thank the National Scientific Research and Development Council of Malaysia for ScienceFund (Grant No.: 14-02-03-4014) for financial support.

*Date of submission: May 2008*
*Date of acceptance: November 2008*

## REFERENCES

Ariffin, A & Khan, MN 2005, 'Unexpected rate retardation in the formation of phthalic anhydride from N-methylphthalamic acid in acidic $H_2O$-$CH_3CN$ medium', *Bull. Korean Chem. Soc*., vol. 26, no. 7, pp. 1037–1043.

Bender, ML 1957, 'General Acid-Base Catalysis in the Intramolecular Hydrolysis of Phthalamic Acid', *J. Am. Chem. Soc*., vol. 79, pp. 1258–1259.

Bender, ML, Chow, Y-L & Chloupek, F 1958, 'Intramolecular catalysis of hydrolytic reactions. ii. the hydrolysis of phthalamic acid', *J. Am. Chem. Soc*., vol. 80, pp. 5380–5384.

Blackburn, RAM, Capon, B & McRitchie, AC 1977, 'The mechanism of hydrolysis of phthalamic and N-phenylphthalamic acid. The spectrophotometric detection of phthalic anhydride as an intermediate', *Bioorg. Chem*., vol. 6, no. 1, pp. 71–78.

Blow, DM, Birktoft, JJ & Hartley, BS 1969, 'Role of a buried acid group in the mechanism of action of chymotrypsin', *Nature*, vol. 221, no. 5178, pp. 337–340.

Brot, FE & Bender, ML 1969, 'Use of the specificity constant of alpha-chymotrypsin', *J. Am. Chem. Soc*., vol. 91, no. 25, pp. 7187–7191.

Frost, AA & Pearson, RG 1961, *Kinetics and mechanism*, 2nd Edn, John Wiley & Sons, New York.

Granados, AM & de Rossi, RH 2001, 'Effect of cyclodextrin on the intramolecular catalysis of amide hydrolysis', *J. Org. Chem*., vol. 66, no. 5, pp. 1548–1552.

Hawkins, MD 1976, 'Intramolecular catalysis. Part III. Hydrolysis of 3'- and 4'-substituted phthalanilic acids [o-(*N*-phenylcarbamoyl)benzoic acids]', *J. Chem. Soc. Perkin Trans.* vol. 2, pp. 642–647.

Hirohara, H, Philipp, M & Bender, ML 1977, 'Binding rates, oxygen-sulfur substitution effects, and the pH dependence of chymotrypsin reactions', *Biochemistry*, vol. 16, no. 8, pp. 1573–1580.

Jencks, WP 1969, *Catalysis in chemistry and enzymology*, McGraw-Hill, New York, USA.

Jencks, WP 1975, 'Binding energy, specificity, and enzymic catalysis: the circe effect', *Adv. Enzymol*., vol. 43, pp. 219–410.

Kahne, D & Still, WC 1988, 'Hydrolysis of a peptide bond in neutral water', *J. Am. Chem. Soc*., vol. 110, no. 22, pp. 7529–7534.

Kanamori, K & Roberts, JD 1983, 'Nitrogen-15 NMR Studies of biological systems', *Acc. Chem. Res*., vol. 16, no. 2, pp. 35–41.

Khan, MN 1993, 'Kinetics and mechanism of the aqueous cleavage of phthalic anhydride (PAn)', *Indian J. Chem. Section A*, vol. 32, no. 5, pp. 387–394.

Khan, MN 1996, 'Suggested improvement in the Ing-Manske Procedure and Gabriel synthesis of primary amines: kinetic study on alkaline hydrolysis of *N*-phthaloylglycine and acid hydrolysis of *N*-(o-carboxybenzoyl)glycine in aqueous organic solvents', *J. Org. Chem*., vol. 61, no. 23, pp. 8063–8068.

Khan, MN 1998, 'Unexpected rate enhancement in the intramolecular carboxylic acid-catalyzed cleavage of o-carboxybenzohydroxamic acid', *J. Phys. Org. Chem*., vol. 11, no. 3, pp. 216–222.

Khan, MN 2006, 'Micellar Catalysis', In *Surfactant science series*, CRC Press, Taylor & Francis Group, LLC, Boca Raton, FL., U.S.A.

Khan, MN & Ariffin, A 2003, 'Kinetics and mechanism of intramolecular carboxylic acid participation in the hydrolysis of *N*-methoxyphthalamic acid', *Org. Biomol. Chem*., vol. 1, no. 8, pp. 1404–1408.

Khan, MN & Khan, AA 1975, 'Kinetics and mechanism of hydrolysis of succinimide in highly alkaline medium', *J. Org. Chem*., vol. 40, no. 12, pp. 1793–1794.

Kirby, AJ & Lancaster, PW 1972, 'Structure and efficiency in intramolecular and enzymic catalysis. Catalysis of amide hydrolysis by the carboxy-group of substituted maleamic acids', *J. Chem. Soc. Perkin Trans. 2*, pp. 1206–1214.

Kirby, AJ, McDonald, RS & Smith, CR 1974, 'Intramolecular catalysis of amide hydrolysis by two carboxy-groups', *J. Chem. Soc. Perkin Trans. 2*, pp. 1495–1504.

Kluger, R & Lam, C-H 1975, 'Effects of leaving group basicity on the hydrolysis of aryl-substituted maleanilinic acids', *J. Am. Chem. Soc*., vol. 97, no. 19, pp. 5536–5540.

Kluger, R & Lam, C-H 1978, 'Carboxylic acid participation in amide hydrolysis. External general base catalysis and general acid catalysis in reactions of norbornenylanilic acids', *J. Am. Chem. Soc*., vol. 100, no. 7, pp. 2191–2197.

Menger, FM 1985, 'On the source of intramolecular and enzymatic reactivity', *Acc. Chem. Res*., vol. 18, no. 5, pp. 128–134.

Menger, FM & Ladika, M 1988, 'Fast hydrolysis of an aliphatic amide at neutral pH and ambient temperature. A peptidase model', *J. Am. Chem. Soc*., vol. 110, no. 20, pp. 6794–6796.

Milstien, S & Cohen, LA 1972, 'Stereopopulation control. I. Rate enhancement in the lactonizations of o-hydroxyhydrocinnamic acids', *J. Am. Chem. Soc*., vol. 94, no. 26, pp. 9158–9165.

Page, MI & Jencks, WP 1987, 'In defense of entropy and strain as explanations for the rate enhancement shown in intramolecular reactions', *Gazzetta Chimica Italiana*, vol. 117, no. 8, pp. 455–460.

Shashidhar, MS, Rajeev, KG & Bhatt, MV 1997, 'Methanolysis of ortho- and para-formylbenzenesulfonates in basic media: evidence for the intramolecular nucleophilic catalysis by the carbonyl group', *J. Chem. Soc. Perkin Trans. 2*, pp. 559–562.

Sim, Y-L, Ahmad, WHW, Ariffin, A & Khan, MN 2008, 'Determination of $pK_a$ of ammonium and phenolic groups: evidence of intramolecular hydrogen bonding in aqueous solution', *Indian J. Chem. Section A*, vol. 47A, no. 2, pp. 240–245.

Sim, Y-L, Ariffin, A & Khan, MN 2004, 'Effects of mixed aqueous-organic solvents on the rate of intramolecular carboxylic group-catalyzed cleavage of *N*-(4'-Methoxyphenyl)phthalamic acid', *Int. J. Chem. Kinet*., vol. 36, pp. 316–325.

Sim, Y-L, Ariffin, A & Khan, MN 2006, 'Intramolecular carboxylic group – assisted cleavage of N-(2-hydroxyphenyl)phthalamic acid (7) and N-(2-methoxyphenyl)phthalamic acid (8): absence of intramolecular general acid catalysis due to 2-OH in 7', *Int. J. Chem. Kinet*., vol. 38, pp. 746–758.

Sim, Y-L, Ariffin, A & Khan, MN 2007, 'Efficient rate enhancement due to intramolecular general base (IGB) assistance in the hydrolysis of *N*-(o-hydroxyphenyl)phthal imide', *J. Org. Chem*., vol. 72, no. 7, pp. 2392–2401.

Sim, Y-L, Damit, EF, Ariffin, A & Khan, MN 2008, 'Kinetics and mechanism of hydrolysis of *N*-(2'-hydroxyphenyl)phthalamic acid (1) and *N*-(2'-methoxyphenyl)phthalamic acid (2) in a highly alkaline medium', *Int. J. Chem. Kinet*., in press.

Widequist, S 1956, 'Alkaline hydrolysis of acetonitrile', *Arkiv. Foer Kemi*., vol. 10, pp. 265–270.

Zhou, D-M & Taira, K 1998, 'The Hydrolysis of RNA: from theoretical calculations to the hammerhead ribozyme-mediated cleavage of RNA', *Chem. Rev*., vol. 98, no. 3, pp. 991–1026.

ASM Sci. J., **2(1)**, 93–100

# Sandwich Theorem for Analytic Functions Involving a Fractional Operator

R.W. Ibrahim[1] and M. Darus[1]*

We have considered a fractional integral operator in this study. By using this integral operator we obtained a Briot-Bouquet superordination and sandwich theorem.

**Key words:** fractional calculus; univalent solution; subordination; superordination; sandwich theorem; AMS Mathematics Subject Classification: 34G10, 26A33, 30C45

## INTRODUCTION AND PRELIMINARIES

Let $A$ be the class of all normalized analytic functions

$$f(z) = z + \sum_{n=2}^{\infty} a_n z^n$$

in the open unit disk $U := \{z \in \mathbb{C} : |z| < 1\}$ satisfying $f(0) = 0$ and $f'(0) = 1$. Let $\mathcal{H}$ be the class of analytic functions in $U$ and for any $a \in \mathbb{C}$ and $n \in \mathbb{C}$, $\mathcal{H}[a, n]$ be the subclass of $\mathcal{H}$ consisting of functions of the form $f(z) = a + a_n z^n + \ldots$ .

Let $F$ and $G$ be analytic in the unit disk $U$. The function $F$ is *subordinate* to $G$ written $F \prec G$, if $G$ is univalent, $F(0) = G(0)$ and $F(U) \subset G(U)$. Alternatively, given two functions $f(z)$ and $G(z)$ which are analytic in $U$ the function $F(z)$ is said to be subordinate to $G(z)$ in $U$ if there exists a function $h(z)$ analytic in $U$ with:

$h(0) = 0$ and $|h(z)| < 1$ for all $z \in U$

and

$F(z) = G[h(z)]$ for all $z \in U$.

**Definition 1.1.** (Miller & Mocanu 2003) Denote by $Q$ the set of all functions $f(z)$ that are analytic and injective on $\overline{U} - E(f)$ where $E(f) : \{\zeta \in \partial U : lim_{z \to \zeta} f(z) = \infty\}$ and are such that $f'(\zeta) \neq 0$ for $\zeta \in \partial U - E(f)$. The subclass of $Q$ for which $f(0)$ is denoted by $Q(a)$.

Let $\beta$ and $\gamma$ be complex numbers. Let $\Omega_2$ and $\triangle_2$ be sets in the complex plane, and let $p$ be analytic in the unit disc $U$. Miller and Mocanu (2000), determined conditions so that

$$\{p(z) + \frac{zp'(z)}{\beta p(z) + \gamma} \; | z \in U\} \subset \Omega_2 \Rightarrow p(U) \subset \triangle_2 .$$

The differential operator on the left is known as the *Briot – Bouquet* differential operator. Miller and Mocanu (1997), considered the dual problem of determining conditions so that

$$\Omega_1 \subset \{p(z) + \frac{zp'(z)}{\beta p(z) + \gamma} \; | z \in U\} \Rightarrow \triangle_1 \subset p(U).$$

If the sets $\Omega_1$ and $\triangle_1$ are simply connected domains not equal to $\mathbb{C}$, then it is possible to rephrase expressions in terms of subordination and superordination in the forms:

$$p(z) + \frac{zp'(z)}{\beta p(z) + \gamma} \prec h_2(z) \Rightarrow p(z) \prec q_2(z).$$

This is called *Briot – Bouquet* differential subordination and the function $q_2$ is called a dominant of the differential subordination. The best dominant which provides a sharp result, is the dominant that is subordinant to all other dominants.

$$h_1(z) \prec p(z) + \frac{zp'(z)}{\beta p(z) + \gamma} \Rightarrow q_1(z) \prec p(z).$$

This is called *Briot – Bouquet* differential superordination and the function $q_1$ is called a subordinant of the differential superordination. The best subordinant which provides a sharp result, is the subordinant that is superordinate to all other subordinants. Miller and Mocanu (2007) combined them and obtained a condition such that the *Briot – Bouquet* sandwich

$$h_1(z) \prec p(z) + \frac{zp'(z)}{\beta p(z) + \gamma} \prec h_2(z)$$

implies that $q_1(z) \prec p(z) \prec q_2(z)$.

In this article, we assumed that $\beta = 0$ and $\gamma = 1$. We needed the following results in the sequel.

[1] School of Mathematical Sciences, Faculty of Science and Technology, Universiti Kebangsaan Malaysia, 43600 Bangi, Selangor, Malaysia
* Corresponding author (e-mail: maslina@ukm.my)

**Lemma 1.1.** (Miller & Mocanu 2000) Let $\Omega \subset \mathbb{C}$, $q \in \mathcal{H}[q(0), 1]$, $\varphi : \mathbb{C}^2 \times \overline{U} \to \mathbb{C}$ and $\varphi(q, tzq'; \zeta) \in \Omega$ for $z \in U$ and $\zeta \in \partial U$ and $0 < t \leq \frac{1}{n} < 1$. If $p \in Q(a)$ and $\varphi(p, zp'; z)$ is univalent in $U$ then

$$\Omega \subset \{\varphi(p, zp'; z) | z \in U\} \Rightarrow q(z) \prec p(z).$$

**Lemma 1.2.** (Antonino 2008) Let $p$ and $q$ be analytic in $U$, with $p(0) = q(0)$, let $M$ be an analytic function in a domain $D$ that contains $p(U) \cup q(U)$ and let $N$ be an analytic function in $U \times D$. If $M[q(z)]$ is convex and $\Re\{N[z, p(z)]\} > 0$, then

$$M[p(z)] + zp'(z)\, M'[p(z)]\, N[zp'(z)] \prec M[q(z)] \Rightarrow p(z) \prec q(z).$$

Srivastava and Owa (1989) gave definitions for fractional operators (derivative and integral) in the complex-z-plane $\mathbb{C}$ as follows:

**Definition 1.2**. The fractional derivative of order $\alpha$ is defined, for a function $f(z)$ by

$$D_z^{\alpha} f(z) := \frac{1}{\Gamma(1-\alpha)} \frac{d}{dz} \int_0^z \frac{f(\zeta)}{(z-\zeta)^{\alpha}} d\zeta;\ 0 \leq \alpha < 1,$$

where the function $f(z)$ is analytic in a simply-connected region of the complex z-plane $\mathbb{C}$ containing the origin and the multiplicity of $(z-\zeta)^{-\alpha}$ is removed by requiring $log\,(z-\zeta)$ to be real when $(z-\zeta) > 0$.

**Definition 1.3**. The fractional integral of order $\alpha$ is defined, for a function $f(z)$ by

$$I_z^{\alpha} f(z) := \frac{1}{\Gamma(\alpha)} \int_0^z f(\zeta)\, (z-\zeta)^{\alpha-1} d\zeta;\ 0 \leq \alpha < 1,$$

where the function $f(z)$ is analytic in a simply-connected region of the complex z-plane $\mathbb{C}$ containing the origin and the multiplicity of $(z-\zeta)^{\alpha-1}$ is removed by requiring $log\,(z-\zeta)$ to be real when $(z-\zeta) > 0$.

Note that, $I_z^{\alpha} f(z) : f(z) \times \frac{z^{\alpha-1}}{\Gamma(\alpha)}$, for $z > 0$ and 0 for $z \leq 0$ (Miller & Ross 1993).

**Remark 1.1**. From Definition 1.2, we had $D_z^0 f(z) = f(z)$, $lim_{\alpha \to 0} I_z^{\alpha} f(z) = f(z)$ and $lim_{\alpha \to 0} D_z^{1-\alpha} f(z) = f'(z)$. Moreover,

$$D_z^{\alpha}\{z^{\mu}\} = \frac{\Gamma(\mu+1)}{\Gamma(\mu-\alpha+1)}\{z^{\mu-\alpha}\},\ \mu > -1;\ 0 \leq \alpha < 1$$

and

$$I_z^{\alpha}\{z^{\mu}\} = \frac{\Gamma(\mu+1)}{\Gamma(\mu+\alpha+1)}\{z^{\mu+\alpha}\},\ \mu > -1;\ 0 \leq \alpha < 1,\ z > 0.$$

Our work was organized as follows: In section 2, we would derive a sandwich result, combining inequalities and subordination, for normalized analytic functions involving fractional integral in the open unit disk $U$

$$\left[\frac{zI_z^{\alpha} g_1(z)}{\rho_{\alpha}(z)}\right]^{\mu} \prec \left[\frac{zI_z^{\alpha} f(z)}{\rho_{\alpha}(z)}\right]^{\mu} \prec \left[\frac{zI_z^{\alpha} g_2(z)}{\rho_{\alpha}(z)}\right]^{\mu}.$$

In section 3, we studied the existence of locally univalent solution for the fractional differential equation

$$D_z^{\alpha} \rho_{\alpha}(z) u(z) = f[z, u(z)],\ 0 \leq \alpha < 1 \qquad (1)$$

subject to the initial condition $u(0) = 0$, where $u : U \to \mathbb{C}$ was an analytic function for all $z \in U$ and $f : U \times \mathbb{C} \to \mathbb{C}$, $\rho : U \to \mathbb{C}\backslash\{0\}$ were analytic functions in $z \in U$. The existence was shown by using Schauder fixed point theorem while the uniqueness was verified by using the Banach fixed point theorem. For that purpose, we needed to the following definitions and results.

Let $M$ be a subset of Banach space $X$ and $A : M \to M$ an operator. The operator $A$ is called compact on the set $M$ if it carries every bounded subset of $M$ into a compact set. If $A$ is continuous on $M$ (that is, it maps bounded sets into bounded sets) then it is said to be completely continuous on $M$. A mapping $A : X \to X$ is said to be a contraction if there exists a real number $\rho$, $0 \leq \rho < 1$ such that $\|Ax - Ay\| \leq \rho\|x - y\|$ for all $x, y \in X$.

**Theorem 1.1**. Arzela-Ascoli (see Curtain & Pritchard 1997) Let $E$ be a compact metric space and $C(E)$ be the Banach space of real or complex valued continuous functions normed by

$$\|f\| := sup_{t\in E}|f(t)|.$$

If $A = \{f_n\}$ is a sequence in $C(E)$ such that $f_n$ is uniformly bounded and equi-continuous, then $\overline{A}$ is compact.

**Theorem 1.2**. (Schauder) (see Balachandar & Dauer 1999) Let $X$ be a Banach space, $M \subset X$ a nonempty closed bounded convex subset and $P : M \to M$ is compact. Then $P$ has a fixed point.

**Theorem 1.3**. (Banach) (see Balachandar & Dauer 1999) If $X$ is a Banach space and $P : X \to X$ is a contraction mapping then $P$ has a unique fixed point.

## SOME PROPERTIES

In this section, some preliminary properties of the fractional integral operators $I_z^{\alpha}$ given by Ibrahim and Darus (2008, p. 872–873) will be used in the next results.

**Theorem 2.1**. For $\alpha, \in (0,1)$ and $f$ is a continuous function, then

$$1 - DI_z^{\alpha} f(z) = \frac{(z)^{\alpha-1}}{\Gamma(\alpha)} f(0) + I_z^{\alpha} Df(z); D = \frac{d}{dz}.$$

$$2 - I_z^{\alpha} D_z^{\alpha} f(z) = D_z^{\alpha} I_z^{\alpha} f(z) = f(z).$$

**Lemma 2.1**. Let $f(z)$ be a non-decreasing function then for $z_1 \leq z_2$ and $z_1 > 0, z_2 > 0$ we had $I_{z_1}{}^{\alpha} f(z_1) \leq I_{z_2}^{\alpha} f(z_2)$. We gave our first result on subordination between two fractional integral operators of the same order.

**Theorem 2.2**. Let $f, g$ be analytic functions in $U$. Assume that $[\frac{zI_z^{\alpha} f(z)}{\rho\alpha^{(z)}}]^{\mu}$ is a convex analytic function in $U$, $[\frac{zI_z^{\alpha} g(z)}{\rho\alpha^{(z)}}]^{\mu}$ is analytic in $U$. If the subordination

$$[\frac{z^{\alpha-1}}{\Gamma(\alpha)}]^{\mu}[(\frac{zf(z)}{\rho_{\alpha}(z)})^{\mu}][1 + \mu(1 + \frac{zf'(z)}{f(z)} - \frac{z\rho'_{\alpha}(z)}{\rho_{\alpha}(z)})] \prec [\frac{z^{\alpha-1}}{\Gamma(\alpha)}]^{\mu}[(\frac{zg(z)}{\rho_{\alpha}(z)})^{\mu}][1 + \mu(1 + \frac{zg'(z)}{g(z)} - \frac{z\rho'_{\alpha}(z)}{\rho_{\alpha}(z)})]$$

holds. Then

$$[\frac{zI_z^{\alpha} f(z)}{\rho_{\alpha}(z)}]^{\mu} \prec [\frac{zI_z^{\alpha} g(z)}{\rho_{\alpha}(z)}]^{\mu}.$$

**Proof**. Setting

$$p(z) := [\frac{zI_z^{\alpha} f(z)}{\rho_{\alpha}(z)}]^{\mu}, q(z) := [\frac{zI_z^{\alpha} g(z)}{\rho_{\alpha}(z)}]^{\mu}.$$

We used Lemma 1.2. Assume that $M[q(z)] := q(z)$ and $N[z,p(z)] := 1$. It is clear that $M$ and $N$ are analytic functions in $U$ and $U \times U$, respectively. Moreover, $\Re\{N[z,p(z)]\} = 1 > 0$ and $p(0) = q(0) = 0$. We showed that $p(z) + zp'(z) \prec q(z) + zq^1(z)$.

Through a simple computation we showed that

$$p(z)+zp'(z)=[\frac{z^{\alpha-1}}{\Gamma(\alpha)}]^{\mu}[(\frac{zf(z)}{\rho_{\alpha}(z)})^{\mu}][1+\mu(1+\frac{zf'(z)}{f(z)}-\frac{z\rho'_{\alpha}(z)}{\rho_{\alpha}(z)})]$$
$$\prec[\frac{z^{\alpha-1}}{\Gamma(\alpha)}]^{\mu}[(\frac{zg(z)}{\rho_{\alpha}(z)})^{\mu}][1+\mu(1+\frac{zg'(z)}{g(z)}-\frac{z\rho'_{\alpha}(z)}{\rho_{\alpha}(z)})]$$
$$=q(z)+zq'(z).$$

Thus in view of Lemma 1.2, we obtained the result $p(z)\prec q(z)$.

In the next theorem, we established the superordination result by using Lemma 1.1.

**Theorem 2.3**. Let $f, g$ be analytic in $U$. Assume that $[\frac{zI_z^{\alpha}g(z)}{\rho_{\alpha}(z)}]^{\mu}\in\mathcal{H}[0,1]$, $[\frac{zI_z^{\alpha}f(z)}{\rho_{\alpha}(z)}]^{\mu}\in Q$, and

$$[\frac{z^{\alpha-1}}{\Gamma(\alpha)}]^{\mu}[(\frac{zf(z)}{\rho_{\alpha}(z)})^{\mu}][1+\mu(1+\frac{zf'(z)}{f(z)}-\frac{z\rho'_{\alpha}(z)}{\rho_{\alpha}(z)})]$$

is univalent in $U$. If,

$$|g(z)|^{\mu}\{1+\mu[1+\frac{|\rho_{\alpha}(z)|}{|\rho_{\alpha}(z)|}+\frac{|g'(z)|}{|g(z)|}]\}<|f(z)|^{\mu}\{1+\mu[1+\frac{|\rho_{\alpha}(z)|}{|\rho_{\alpha}(z)|}+\frac{|f'(z)|}{|f(z)|}]\}$$

then,

$$[\frac{zI_z^{\alpha}g(z)}{\rho_{\alpha}(z)}]^{\mu}\prec[\frac{zI_z^{\alpha}f(z)}{\rho_{\alpha}(z)}]^{\mu}.$$

**Proof**. Setting:

$$p(z):=[\frac{zI_z^{\alpha}f(z)}{\rho_{\alpha}(z)}]^{\mu},\ q(z):=[\frac{zI_z^{\alpha}g(z)}{\rho_{\alpha}(z)}]^{\mu}.$$

We used Lemma 1.1. Assume that $\varphi[q(z), tzq'(z); \zeta]:=q(z)+ztq'(z)$ and defining the set

$$\Omega:=\{z\in\mathbb{C}:\ |z|\le\frac{|g(z)|^{\mu}}{[\Gamma(\alpha)]^{\mu}|\rho_{\alpha}(z)|^{\mu}}\{1+\mu[1+\frac{|g'(z)|}{|g(z)|}+\frac{|\rho'_{\alpha}(z)|}{|\rho_{\alpha}(z)|}]\}\}$$

thus for $z\in U$, we obtain that

$$|\varphi(g(z), tzq'(z); \zeta)|\le|q(z)|+|z||t||q'(z)|$$
$$<|q(z)|+|q'(z)|$$
$$<\frac{|g(z)|^{\mu}}{[\Gamma(\alpha)]^{\mu}|\rho_{\alpha}(z)|^{\mu}}+\frac{\mu|g(z)|^{\mu}}{[\Gamma(\alpha)]^{\mu}|\rho_{\alpha}(z)|^{\mu}}\ |[1+\frac{g'(z)}{g(z)}+\frac{\rho'_{\alpha}(z)}{\rho_{\alpha}(z)}]|$$
$$=\frac{|g(z)|^{\mu}}{[\Gamma(\alpha)]^{\mu}|\rho_{\alpha}(z)|^{\mu}}\{1+\mu|[1+\frac{g'(z)}{g(z)}+\frac{\rho'_{\alpha}(z)}{\rho_{\alpha}(z)}]|\}$$
$$\le\frac{|g(z)|^{\mu}}{[\Gamma(\alpha)]^{\mu}|\rho_{\alpha}(z)|^{\mu}}\{1+\mu|[1+\frac{g'(z)}{|g(z)|}+\frac{\rho'_{\alpha}(z)}{|\rho_{\alpha}(z)|}]|\}.$$

Hence $\varphi[q(z), tzq'(z); \zeta]\in\Omega$, for $z\in U$. By the assumption of the theorem $\varphi[p(z), zp'(z); z]:=p(z)+zp'(z)$ is univalent in $U$. Further, let $z\in\Omega$, then we had

$$|z|\le\frac{|g(z)|^{\mu}}{[\Gamma(\alpha)]^{\mu}|\rho_{\alpha}(z)|^{\mu}}\{1+\mu[1+\frac{|g'(z)|}{|g(z)|}+\frac{|\rho'_{\alpha}(z)|}{|\rho_{\alpha}(z)|}]\}$$
$$<\frac{|f(z)|^{\mu}}{[\Gamma(\alpha)]^{\mu}|\rho_{\alpha}(z)|^{\mu}}\{1+\mu[1+\frac{|f'(z)|}{|f(z)|}+\frac{|\rho'_{\alpha}(z)|}{|\rho_{\alpha}(z)|}]\},$$

which implied that $\Omega\subset\{\varphi(p, zp'; z)|\ z\in U\}$. Thus in view of Lemma 1.1, we obtained that $q(z)\prec p(z)$.

The next result shows the conditions for the sandwich theorem such that these conditions combine the inequalities and the subordination of analytic functions.

**Theorem 2.4**. Let $f, g_1, g_2$ be analytic in $U$. Assume that $[\frac{zI_z^{\alpha} g_1(z)}{\rho_\alpha(z)}]^{\mu} \in \mathcal{H}[0,1]$, $[\frac{zI_z^{\alpha} f(z)}{\rho_\alpha(z)}]^{\mu} \in Q$, is a convex analytic function in $U$, $[\frac{zI_z^{\alpha} g_2(z)}{\rho_\alpha(z)}]^{\mu}$ is analytic in $U$ and

$$[\frac{z^{\alpha-1}}{\Gamma(\alpha)}]^{\mu}[\frac{(zf(z)}{\rho_\alpha(z)})^{\mu}][1+\mu(1+\frac{zf'(z)}{f(z)}-\frac{z\rho'_\alpha(z)}{\rho_\alpha(z)})]$$

is univalent in $U$. If

$$|g_1(z)|^{\mu}\{1+\mu(1+\frac{|\rho'_\alpha(z)|}{|\rho_\alpha(z)|}+\frac{|g'_1(z)|}{|g_1(z)|}]\} < |f(z)|^{\mu}\{1+\mu(1+\frac{|\rho'_\alpha(z)|}{|\rho_\alpha(z)|}+\frac{|f(z)|}{|f(z)|}]\}$$

and the subordination

$$[\frac{z^{\alpha-1}}{\Gamma(\alpha)}]\mu[\frac{(zf(z)}{\rho_\alpha(z)})^{\mu}][1+\mu(1+\frac{zf'(z)}{f(z)}-\frac{z\rho'_\alpha(z)}{\rho_\alpha(z)})] \prec [\frac{z^{\alpha-1}}{\Gamma(\alpha)}]^{\mu}[\frac{(zg_2(z)}{\rho_\alpha(z)})^{\mu}][1+\mu(1+\frac{zg'_2(z)}{g_2(z)}-\frac{z\rho'_\alpha(z)}{\rho_\alpha(z)})]$$

holds, then

$$[\frac{zI_z^{\alpha} g_1(z)}{\rho_\alpha(z)}]^{\mu} \prec [\frac{zI_z^{\alpha} f(z)}{\rho_\alpha(z)}]^{\mu} \prec [\frac{zI_z^{\alpha} g_2(z)}{\rho_\alpha(z)}]^{\mu}.$$

## Univalent Solution for Fractional Differential Equation

In this section we established the existence and uniqueness solution for the differential Equation 1 and applied the results in the previous section to obtain the relation of univalent solutions for problem (1). Let $\mathcal{B} := C[U, \mathbb{C}]$ be a Banach space of all continuous functions on $U$ endowed with the sup. norm

$$\|u\| := sup_{z \in U}|u(z)|.$$

By using the properties in Theorem 2.1, we easily obtained the following result.

**Lemma 3.1**. If the function $h$ is analytic, then the initial value problem (1) is equivalent to the nonlinear integral equation

$$u(z) = \frac{1}{\rho\alpha(z)} \int_0^z \frac{(z-\zeta)^{\alpha-1}}{\Gamma(\alpha)} f[\zeta, u(\zeta)]\, d\,\zeta;\ \alpha \in (0,1). \tag{2}$$

In other words, every solution of Equation 2 is also a solution of the initial value problem (1) and vice versa.

The following assumptions are needed in the next theorem:

(**H1**) There exists a continuous function $\gamma : U \to \mathbb{R}_+$ and increasing positive function $\Psi \in C[\mathbb{R}_+, \mathbb{R}_+]$ such that

$$|f(z,u)| \leq \gamma(z)\ \Psi\ (\|u\|).$$

Denotes $\overline{\gamma} := sup_{z \in U}\{\gamma(z)\}$ and $\overline{\Psi} := sup_{u \in B}\Psi(\|u\|)$. Further, assume that $\|f\| > 0$.

Note that $C[\mathbb{R}_+, \mathbb{R}_+]$ is the Banach space of all continuous positive functions.

(**H2**) There exists a positive constant $M$ such that $|\frac{1}{\rho_\alpha(z)}| \leq M$.

**Theorem 3.1**. Let the assumptions (H1) and (H2) hold. Then Equation 1 has a univalent solution $u(z)$ in $U$.

**Proof**. Define an operator $P : \mathcal{B} \to \mathcal{B}$ as follows

$$(Pu)(z) : = \frac{1}{\rho_\alpha(z)} \int_0^z \frac{(z-\zeta)^{\alpha-1}}{\Gamma(\alpha)} f[\zeta, u(\zeta)]\, d\,\zeta. \tag{3}$$

In order to show that Equation 1 had a solution we have to show that the operator (3) had a fixed point.

$$\begin{aligned}
|(Pu)(z)| : &= |\frac{1}{\rho_\alpha(z)} \int_0^z \frac{(z-\zeta)^{\alpha-1}}{\Gamma(\alpha)} f[\zeta, u(\zeta)]\, d\,\zeta| \\
&\leq |\frac{1}{\rho_\alpha(z)}|| \int_0^z \frac{(z-\zeta)^{\alpha-1}}{\Gamma(\alpha)} f[\zeta, u(\zeta)]\, d\,\zeta| \\
&\leq \frac{M\| f\|}{\Gamma(\alpha)} | \int_0^z (z-\zeta)^{\alpha-1}\, d\,\zeta| \\
&= \frac{M\| f\|}{\Gamma(\alpha+1)} |z|^\alpha \\
&\leq \frac{M|\gamma(z)|\Psi(\|u\|)}{\Gamma(\alpha+1)} |z|^\alpha \\
&< \frac{M\gamma\Psi}{\Gamma(\alpha+1)}
\end{aligned}$$

Thus we obtained that

$$\| P \| < \frac{M\bar{\gamma}\bar{\Psi}}{\Gamma(\alpha+1)} = : r$$

that $P : B_r \to B_r$ Then $P$ maped $B_r$ into itself. We proceeded to prove that $P$ was equicontinuous. For $z_1, z_2 \in U$ such that $z_1 \neq z_2, |z_2 - z_1| < \delta, \delta > 0$. Then for all $u \in S$ where

$$S : = \{u \in \mathbb{C} \ , : |u| \leq \frac{M\bar{\gamma}\bar{\Psi}}{\Gamma(\alpha+1)}\},$$

we obtained

$$\begin{aligned}
|(Pu)(z_1) - (Pu)(z_2)| &\leq |\frac{1}{\rho_\alpha(z)}|| \int_0^{z_1} \frac{(z_1-\zeta)^{\alpha-1}}{\Gamma(\alpha)} f[\zeta, u(\zeta)]\, d\,\zeta - \int_0^{z_2} \frac{(z_2-\zeta)^{\alpha-1}}{\Gamma(\alpha)} f[\zeta, u(\zeta)]\, d\,\zeta| \\
&\leq \frac{M\| f\|}{\Gamma(\alpha)} | \int_0^{z_1} [(z_1-\zeta)^{\alpha-1} - (z_2-\zeta)^{\alpha-1}]\, d\zeta + \int_{z_1}^{z_2} (z_2-\zeta)^{\alpha-1} d\zeta| \\
&< 3\frac{M\bar{\gamma}\bar{\Psi}}{\Gamma(\alpha+1)} |z_2 - z_1|^\alpha \\
&< 3\frac{M\bar{\gamma}\bar{\Psi}}{\Gamma(\alpha+1)} \delta^\alpha,
\end{aligned}$$

which was independent of $u$.

Hence $P$ is an equicontinuous mapping on $S$. Under the assumption (H1), we showed that $P$ was a univalent function (see Goodman 1983). The Arzela-Ascoli theorem yields that every sequence of functions $\{u_n\}$ from $P(S)$ has a uniformly convergent subsequence $\{\overline{u_n}\}$, and therefore $P(S)$ is relatively compact. Schauder's fixed point theorem asserts that $P$ has a fixed point. By construction, a fixed point of $P$ is a univalent solution (in view of H1) of the initial value problem (1).

Now we discuss the uniqueness solution for the problem (1). For this purpose, let us state the following assumption:

(**H3**) The function $f$ satisfies that there exists a positive number $L$ such that for each $u,v \in \mathcal{B}$, we have

$$|f[z, u(z)] - f[z, v(z)]| \leq L\|u - v\|.$$

**Theorem 3.2**. Let the hypotheses (H2) and (H3) hold. If $\frac{ML}{\Gamma(\alpha + 1)} < 1$, then (1) admits a unique univalent solution $u(z)$.

**Proof**. Assume the operator $P$ defined in equation (3), we only need to show that $P$ is a contraction mapping, that is $P$ has a unique fixed point which is corresponding to the unique solution of the Equation 1. Let $u,v \in \mathcal{B}$ then for all $z \in U$ we obtain that

$$\begin{aligned}
|(Pu)(z) - (Pv)(z)| &= |\frac{1}{\rho_\alpha(z)}\|\int_0^z \frac{(z-\zeta)^{\alpha-1}}{\Gamma(\alpha)} f[\zeta, u(\zeta)]\, d\zeta - \frac{1}{\rho_\alpha(z)}\int_0^z \frac{(z-\zeta)^{\alpha-1}}{\Gamma(\alpha)} f[\zeta, v(\zeta)]\, d\zeta| \\
&\leq |\frac{1}{\rho_\alpha(z)}\|\int_0^z \frac{(z-\zeta)^{\alpha-1}}{\Gamma(\alpha)} \{f[\zeta, u(\zeta)]\, d\zeta - f[\zeta, v(\zeta)]\}\, d\zeta| \\
&\leq \frac{M\|f(z,u) - f(z,v)\|}{\Gamma(\alpha)}|\int_0^z (z-\zeta)^{\alpha-1} d\zeta| \\
&\leq \frac{ML\|u - v\|}{\Gamma(\alpha + 1)}|z^\alpha| \\
&\leq \frac{ML\|u - v\|}{\Gamma(\alpha + 1)}|z|^\alpha \\
&< \frac{ML}{\Gamma(\alpha + 1)}\|u - v\|.
\end{aligned}$$

Thus by the assumption of the theorem, we have that $P$ is a contraction mapping. Then in view of Banach fixed point theorem, $P$ has a unique fixed point which is corresponding to the univalent solution (Theorem 3.1) of Equation 1. Hence the proof.

Next we provide two remarks that show the relation of univalent solutions for problem (1).

**Remark 3.1**. Let the assumption of Theorem 2.4 be satisfied. Then univalent solutions $u_1$, $u$, $u_2$, of the problem (1) satisfy the subordination $u_1 \prec u \prec u_2$.

**Proof**. Setting $f[z, u(z)] := f(z), f[z, u_1(z)] := g_1(z), f[z, u_2(z)] := g_2(z)$ and $\mu = 1$.

**Remark 3.2**. Let the assumption of Theorem 2.4 be satisfied. Then univalent solutions $u_1$, $u$, $u_2$, of the problem

$$D_z^\alpha \rho_\alpha(z)[\mu(z)]^{\frac{1}{\mu}} = f[z, u(z)], \mu > 1,$$

subject to the initial condition $u(0) = 0$, where $u : U \to \mathbb{C}$ is an analytic function for all $z \in U$ and $f : U \times \mathbb{C} \to \mathbb{C}$, $\rho : U \to \mathbb{C}\backslash\{0\}$ are functions as in Theorem 3.1 which satisfy the subordination $u_1 \prec u \prec u_2$.

**Proof**. Setting $f[z, u(z)] := f(z), f[z, u_1(z)] := g_1(z), f[z, u_2(z)] := g_2(z)$.

## ACKNOWLEDGEMENT

The work presented here was supported by SAGA GRANT:STGL-012-2006, Academy of Science Malaysia, Malaysia.

*Date of submission: March 2008*
*Date of acceptance: November 2008*

## REFERENCES

Antonino, J 2008, 'Strong subordination to a class of first order differential equations', (in press).

Balachandar, K & Dauer, JP 1999, *Elements of control theory*, Narosa Publishing House, New Delhi.

Curtain, RF & Pritchard, AJ 1977, *Functional analysis in modern applied mathematics*, Academic Press, London.

Goodman, AW 1983, *Univalent function*, Mariner Publishing Company, Inc., Tampa, Florida, USA.

Ibrahim, RW & Darus, M 2008, 'Subordination and superordination for univalent solutions for fractional differential equations', *J. Math. Anal. Appl*., vol. 345, no. 2, pp. 871–879.

Miller, SS & Mocanu, PT 1997, 'Briot-Bouquet differential equations and differential subordinations', *Complex Variables*, vol. 33, nos. 1–4, pp. 217–237.

Miller, SS & Mocanu, PT 2000, '*Differential subordinants*', *Theory and applications, monographs and texbooks in pure and applied mathematics*, vol. 225, Marcel Dekker, New York.

Miller, SS & Mocanu, PT 2003, 'Subordinants of differential superordinations', *Complex Variables*, vol. 48, no. 10, pp. 815–826.

Miller, SS & Mocanu, PT 2007, 'Briot-Bouquet differential subordinations and sandwich theorem', *J. Math. Anal. Appl*., vol. 327, no. 1, pp. 327–335.

Miller, KS & Ross, B 1993, *An introduction to the fractional calculus and fractional differential equations*, JohnWiley and Sons, Inc.

Srivastava, HM & Owa, S 1989, *Univalent functions, fractional calculus, and their applications*, Halsted Press, John Wiley and Sons, New York, Chichester, Brisbane, and Toronto.

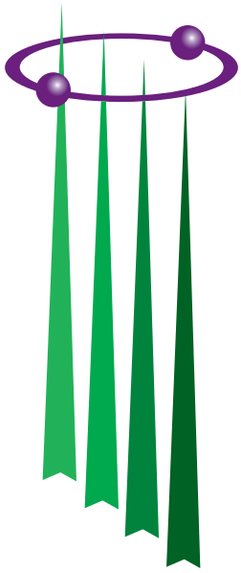

# MAHATHIR SCIENCE AWARD 2009

## Invitation for Nominations

The Academy of Sciences Malaysia (ASM) is a body set up with a mission that encompasses pursuit, encouragement and enhancement of excellence in the fields of science, engineering and technology for the development of the nation and the benefit of mankind. The Academy has instituted the Mahathir Science Award (Formerly Known as ASM Award For Scientific Excellence in Honour of Tun Dr Mahathir Mohamad) in recognition of scientists/institutions who have contributed to cutting-edge tropical research that have had an impact on society.

This Award is Malaysia's most prestigious Science Award for tropical research launched in honour of Tun Dr Mahathir Mohamad who promoted and pursued with great spirit and determination his convictions in science and scientific research in advancing the progress of mankind and nations. Tun Dr Mahathir was the major force and the man who put into place much of the enabling mechanisms for a scientific milieu in our country.

This Award will be given to researchers who have made internationally recognised breakthroughs in pioneering tropical research in the fields of Tropical Medicine, Tropical Agriculture, Tropical Architecture and Engineering, and Tropical Natural Resources.

One Award will be conferred in 2009 covering any of the above four fields. The Award carries a cash prize of RM100 000, a gold medal and a certificate.

### NOMINATION CRITERIA

- Awards will be given to researchers who have made internationally recognised breakthroughs in pioneering tropical research that have brought greater positive impacts on the well-being of society.
- Nominations can be made by individuals or institutions.
- A recipient could be an individual or an institution.

Nomination forms may be downloaded from the Academy's website:
www.akademisains.gov.my

**Closing date: 31 March 2009**

For more information, please contact:
Academy of Sciences Malaysia
902-4, Jalan Tun Ismail, 50480 Kuala Lumpur
Tel : 603-2694 9898; Fax : 603-2694 5858
E-mail: seetha@akademisains.gov.my
admin@akademisains.gov.my

# 4th Malaysian International Seminar on Antartica 2009 (MISA4 2009)

1–3 April 2009
Venue: Cyberjaya, Selangor

**Theme:**

"Legacy of International Polar Year to the Tropics"

**Scientific Programme**

Sessions on:

| | | | |
|---|---|---|---|
| 1) | Physical Sciences | : | Antarctic meteorology and climatology |
| | | : | Geological and Geophysical study at the Poles |
| | | : | Paleogeography |
| | | : | Status and change in Cryosphere |
| | | : | Remote sensing and communication radio science at the Poles |
| | | : | Hydrocarbon deposition, vertical transport and mobilization in Artartica |
| 2) | Biological Sciences | : | Biodiversity and Adaptation |
| | | : | Response of Life to Change |
| 3) | Policy, Heritage and Legacy | | |

**Workshop 1 – Recent Antarctic Climate Change and its Implications on the Marine and Terrestrial Biota**

Objectives:

- To develop an understanding of the mechanics of climate variability, causes and impacts on the terrestrial and marine ecosystems
- To understand the relative contribution of atmospheric and oceanographic forcing on the climate system of the Antarctic and begin to link these changes to global scale phenomena such as E1 Ni no Southern Oscilation (ENSO) fluctuations, anthropogenic greenhouse gases, internal instability in the ocean system and impact on Antarctic species; and
- To develop better links between teh scientists working in the physical and life sciences.

**Workshop 2 – Molecular Markers and Environmental Forensic Techniques for the Identification of the Transport Pathways of Organic Pollutants in Extreme Marine Environment**

Objectives:

- To provide a platform for local scientists to get involved in hydrocarbon pollution and to learn the latest development of the research and to establish an international link with foreign experts
- To present the latest findings and case studies in hydrocarbon pollution derived from transboundary transport using the latest fingerprinting techniques; and
- To chart the future vision and quality of polar research in the topic of "transboundary pollution"; in a clear manner and use the method as a 'tool' for 'source identification' of pollutants in Antarctica.

**Enquiries:**

Academy of Sciences Malaysia
902-4, Jalan Tun Ismail
50480 Kuala Lumpur
Tel: 03-2694 9898; Fax: 03-2694 5858
E-mail: talhady@gmail.com
misa4.um@gmail.com

# ASM Publications

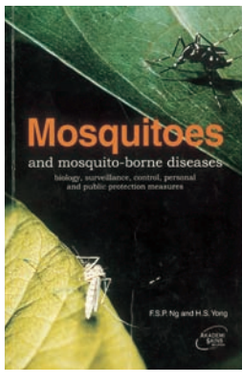


**Mosquitoes and Mosquito-borne Diseases: Biology, Surveillance, Control, Personal and Public Protection Measures**

*F.S.P. Ng* and *H.S. Yong (Editors)*
(2000)

ISBN 983-9445-05-7
Price: RM60.00 / USD20.00

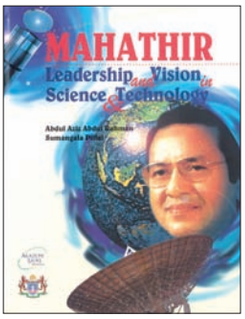


**Mahathir: Leadership and Vision in Science and Technology**

*Abdul Aziz Abdul Rahman* and *Sumangala Pillai*
(1996)

ISBN 983-9319-09-4
Price: RM100.00 / USD30.00

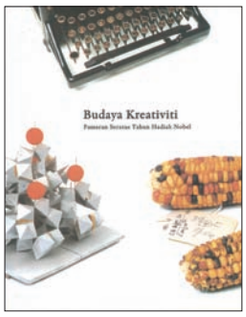


**Budaya Kreativiti: Pameran Seratus Tahun Hadiah Nobel**

*Ulf Larsson (Editor)*
(2004)

ISBN 983-9445-09-X
Price: RM50.00 / USD15.00


**CD Kompilasi *Estidotmy***

Edisi 1 – 70, 2002–07
Price: RM30.00 / USD10.00

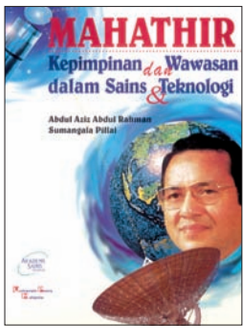


**Mahathir: Kepimpinan dan Wawasan dalam Sains dan Teknologi**

*Abdul Aziz Abdul Rahman*
dan *Sumangala Pillai*
(1996)

ISBN 983-9319-09-4
Price: RM100.00 / USD30.00

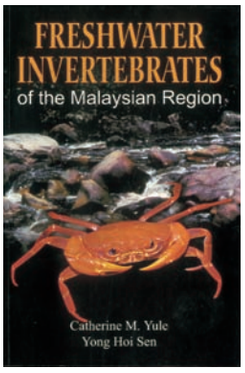


**Freshwater Invertebrates of the Malaysian Region**

*Catherine M. Yule* and *Yong Hoi Sen*
(2004)

ISBN 983-41936-0-2
Price: RM180.00 / USD52.00

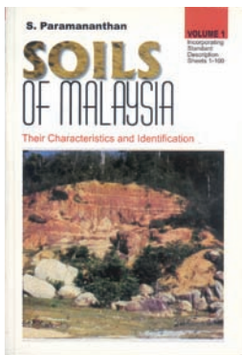


**Soils of Malaysia: Their Characteristics and Identification (Vol. 1)**

*S. Paramananthan*
(2000)

ISBN 983-9445-06-5
Price: RM100.00 / USD30.00


**Bencana Tsunami 26.12.04 di Malaysia: Kajian Impak Alam Sekitar, Sosio-Ekonomi dan Kesejahteraan Masyarakat**

*Ibrahim Komoo (Editor)*
(2005)

ISBN 983-9444-62-X
Price: RM100.00 / USD30.00

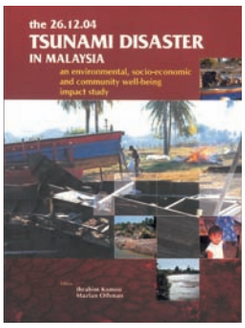


**The 26.12.04 Tsunami Disaster in Malaysia: An Environmental, Socio-Economic and Community Well-being Impact Study**

*Ibrahim Komoo* and *Mazlan Othman (Editors)*
(2006)

ISBN 983-9444-62-X
Price: RM100.00 / USD30.00

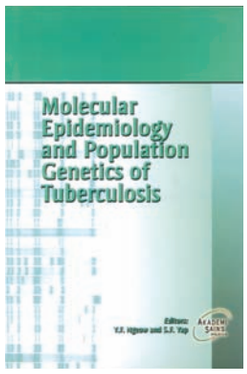


**Molecular Epidemiology and Population Genetics of Tuberculosis**

*Y.F. Ngeow* and *S.F. Yap (Editors)*
(2006)

ISBN 983-9445-14-6
Price: RM40.00 / USD12.00

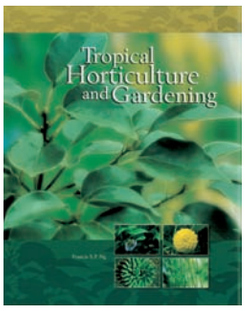


**Tropical Horticulture and Gardening**

*Francis S.P. Ng*
(2006)

ISBN 983-9445-15-4
Price: RM260.00 / USD75.00

**Kecemerlangan Sains dalam Tamadun Islam: Sains Islam Mendahului Zaman Scientific Excellence in Islamic Civilization: Islamic Science Ahead of its Time**

*Fuat Sezgin*
(2006)

ISBN 983-9445-14-6
Price: RM40.00 / USD12.00

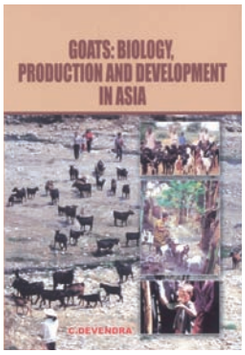


**Goats: Biology, Production and Development in Asia**

*C. Devendra*
(2007)

ISBN 978-983-9445-18-3
Price: RM180.00 / USD52.00


**Proceedings: Seminar on Antarctic Research, 27–28 June 2005, University of Malaya, Kuala Lumpur, Malaysia**

*Irene K.P. Tan* et al. *(Editors)*
(2006)

ISBN 978-983-9445-17-6
Price: RM40.00 / USD12.00

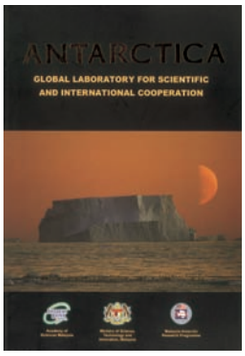


**Antarctica: Global Laboratory for Scientific and International Cooperation**

*Aileen Tan Shau-Hwai* et al. *(Editors)*
(2005)

ISBN 983-9445-13-8
Price: RM40.00 / USD12.00

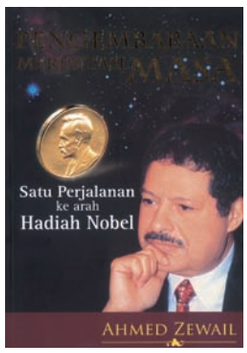


**Pengembaraan Merentasi Masa: Satu Perjalanan ke Arah Hadiah Nobel**

*Ahmed Zewail*
(2007)

ISBN 978-9445-20-6
Price: RM40.00 / USD12.00

# ASM Publications

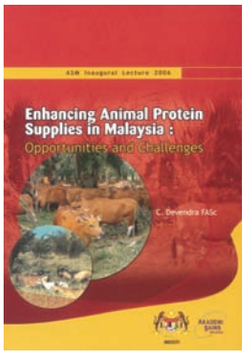


**Enhancing Animal Protein Supplies in Malaysia: Opportunities and Challenges**

*C. Devendra*
(2007)

ISBN 983-9444-62-X

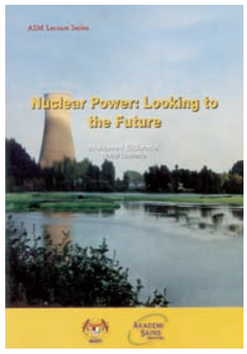


**Nuclear Power: Looking to the Future**

*Mohamed ElBaradei*
(2008)

ISBN 983-9445-14-6

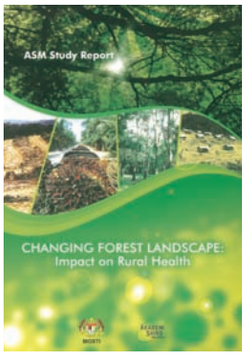


**Changing Forest Landscape: Impact on Rural Health**
(2007)

ISBN 983-9445-15-4

**Dunia Sains**
Vol. 5, No. 4, Oktober – Disember 2007
(2008)

A World of Science
Vol. 5, No. 4
October – December 2007

**http://portal.unesco.org/science/en/ev.php-URL ID=5572&URL DO=DO TOPIC&URL SECTION=201.html**

**http://www. akademisains.gov.my/unesco/ dunia_sains/okt_dis_2007.pdf**


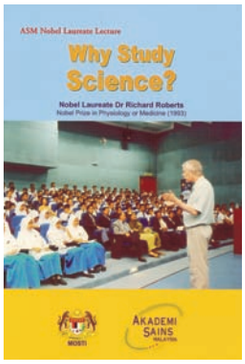


**Why Study Science?**

*Richard Roberts*
(2008)

ISBN 978-983-9445-18-3

**Dunia Sains**
Vol. 6, No. 1, Januari – Mac 2008
(2008)

A World of Science
Vol. 6, No. 1
January – March 2008



**ASM Science Journal**
Vol. 1, No. 1, June 2007

ISSN : 1823-6782

Price: RM100.00 / USD 50.00 (Individual)
RM200.00 / USD 100.00 (Institution)


**ASM Science Journal**
Vol. 1, No. 2, December 2007

ISSN : 1823-6782

Price: RM100.00 / USD 50.00 (Individual)
RM200.00 / USD 100.00 (Institution)

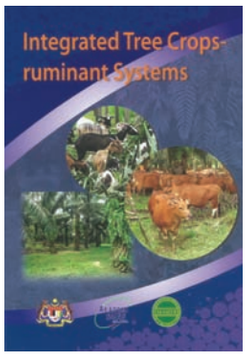


**Integrated Tree Crops-ruminant Systems (Proceedings)**

*C. Devendra, S. Shanmugavelu* and *Wong Hee Kum (Editors)*
(2008)

ISSN : 983-9445-24-3

Price: RM40.00 / USD 12.00

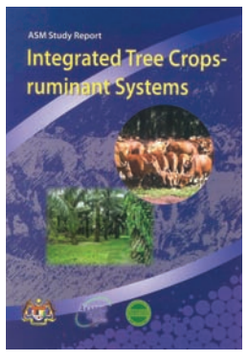


**ASM Study Report: Integrated Tree Crops-ruminant Systems**

ISSN : 983-9445-24-4

Price: RM30.00 / USD 9.00

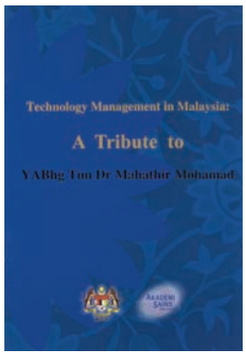


**Technology Management in Malaysia: A Tribute to YABhg Tun Dr Mahathir Mohamad**

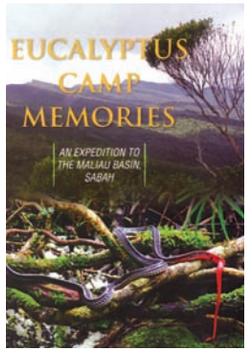


**Eucalyptus Camp Memories: An Expedition to the Maliau Basin, Sabah**

ISSN : 978-983-9445-25-1

Price: RM220.00 / USD 61.00 (Hard cover)
RM160.00 / USD 42.00 (Soft cover)

For purchasing, please access:
http://www.akademisains.gov.my

# About the Journal

**Mission Statement**

To serve as the forum for the dissemination of significant research, S&T and R&D policy analyses, and research perspectives.

**Scope**

The ASM Science Journal publishes advancements in the broad fields of medical, engineering, earth, mathematical, physical, chemical and agricultural sciences as well as ICT. Scientific articles published will be on the basis of originality, importance and significant contribution to science, scientific research and the public.

Scientific articles published will be on the basis of originality, importance and significant contribution to science, scientific research and the public. Scientists who subscribe to the fields listed above will be the source of papers to the journal. All articles will be reviewed by at least two experts in that particular field. The journal will be published twice in a year.

The following categories of articles will be considered for publication:

**Research Articles**

Each issue of the journal will contain no more than 10 research articles. These are papers reporting the results of original research in the broad fields of medical, engineering, earth, mathematical, physical, chemical and life sciences as well as ICT. The articles should be limited to 6000 words in length, with not more than 100 cited references.

**Short Communications**

These are articles that report significant new data within narrow well-defined limits or important findings that warrant publication before broader studies are completed. These articles should be limited to 2000 words and not more that 40 cited references. Five (5) Short Communications will be accepted for publication in each issue of the journal.

**Research Perspectives**

These are papers that analyse recent research in a particular field, giving views on achievements, research potential, strategic direction etc. A Research Perspective should not exceed 2000 words in length with not more than 40 cited references.

**Reviews/Commentaries**

Each issue of the journal will also feature Reviews/ Commentaries presenting overviews on aspects such as Scientific Publications and Citation Ranking, Education in Science and Technology, Human Resources for Science and Technology, R&D in Science and Technology, Innovation and International Comparisons or Competitiveness of Science and Technology etc. Reviews/Commentaries will encompass analytical views on funding, developments, issues and concerns in relation to these fields and not exceed 5000 words in length and 40 cited references.

**Science Forum**

Individuals who make the news with breakthrough research or those involved in outstanding scientific endeavours or those conferred with internationally recognised awards will be featured in this section. Policy promulgations, funding, science education developments, patents from research, commercial products from research, and significant scientific events will be disseminated through this section of the journal. The following will be the categories of news:

- Newsmakers
- Significant Science Events
- Patents from Research
- Commercial Products from Research
- Scientific Conferences/Workshops/Symposia
- Technology Upgrades
- Book Reviews.

# Instructions to Authors

The ASM Science Journal will follow the Harvard author-date style of referencing examples of which are given below.

In the text, reference to a publication is by the author's name and date of publication and page number if a quote is included, e.g. (Yusoff 2006, p. 89) or Yusoff (2006, p. 89) 'conclude.....' as the case may be. They should be cited in full if less than two names (e.g. Siva & Yusoff 2005) and if more than two authors, the work should be cited with first author followed by *et al*. (e.g. Siva *et al*. 1999).

All works referred to or cited must be listed at the end of the text, providing full details and arranged alphabetically. Where more than one work by the same author is cited, they are arranged by date, starting with the earliest. Works by the same author published in the same year are ordered with the use of letters a, b, c, (e.g. Scutt, 2003a; 2003b) after the publication date to distinguish them in the citations in the text.

**General Rules**

*Authors' names:*

- Use only the initials of the authors' given names.
- No full stops and no spaces are used between initials.

*Titles of works:*

- Use minimal capitalisation for the titles of books, book chapters and journal articles.
- In the titles of journals, magazines and newspapers, capital letters should be used as they appear normally.
- Use italics for the titles of books, journals and newspapers.
- Enclose titles of book chapters and journal articles in single quotation marks.

*Page numbering*

- Books: page numbers are not usually needed in the reference list. If they are, include them as the final item of the citation, separated from the preceding one by a comma and followed by a full stop.
- Journal articles: page numbers appear as the final item in the citation, separated from the preceding one by a comma and followed by a full stop.

  Use the abbreviations p. for a single page, and pp. for a page range, e.g. pp. 11–12.

*Whole citation*

- The different details, or elements, of each citation are separated by commas.
- The whole citation finishes with a full stop.

**Specific Rules**

Definite rules for several categories of publications are provided below:

*Journal*

Kumar, P & Garde, RJ 1989, 'Potentials of water hyacinth for sewage treatment', *Research Journal of Water Pollution Control Federation*, vol. 30, no. 10, pp. 291–294.

*Monograph*

Hyem, T & Kvale, O (eds) 1977, *Physical, chemical and biological changes in food caused by thermal processing*, 2nd edn, Applied Science Publishers, London, UK.

*Chapter in a monograph*

Biale, JB 1975, 'Synthetic and degradative processes in fruit ripening', eds NF Hard & DK Salunkhe, in *Postharvest biology and handling of fruits and vegetables*, AVI, Westport, CT, pp. 5–18.

*Conference proceedings*

Common, M 2001, 'The role of economics in natural heritage decision making', in *Heritage economics: challenges for heritage conservation and sustainable development in the 21st century: Proceedings of the International Society for Ecological Economics Conference, Canberra, 4th July 2000*, Australian Heritage Commission, Canberra.

*Report*

McColloch, LP, Cook, HT & Wright, WR 1968, *Market diseases of tomatoes, peppers and egg-plants*, Agriculture Handbook no. 28, United States Department of Agriculture, Washington, DC.

*Thesis*

Cairns, RB 1965, 'Infrared spectroscopic studies of solid oxygen', PhD thesis, University of California, Berkeley, CA.

*Footnotes, spelling and measurement units*

If footnotes are used, they should be numbered in the text, indicated by superscript numbers and kept as brief as possible. The journal follows the spelling and hyphenation of standard British English. SI units of measurement are to be used at all times.

**Submission of Articles**

*General*. Manuscripts should be submitted (electronically) in *MS Word* format. If submitted as hard copy, two copies of the manuscript are required, double-spaced throughout on one side only of A4 (21.0 × 29.5 cm) paper and conform to the style and format of the *ASM Science Journal*. Intending contributors will be given, on request, a copy of the journal specifications for submission of papers.

*Title.* The title should be concise and descriptive and preferably not exceed fifteen words. Unless absolutely necessary, scientific names and formulae should be excluded in the title.

*Address*. The author's name, academic or professional affiliation, e-mail address, and full address should be included on the first page. All correspondence will be only with the corresponding author (should be indicated), including any on editorial decisions.

*Abstract*. The abstract should precede the article and in approximately 150–200 words outline briefly the objectives and main conclusions of the paper.

*Introduction*. The introduction should describe briefly the area of study and may give an outline of previous studies with supporting references and indicate clearly the objectives of the paper.

*Materials and Methods*. The materials used, the procedures followed with special reference to experimental design and analysis of data should be included.

*Results*. Data of significant interest should be included.

*Figures*. If submitted as a hard copy, line drawings (including graphs) should be in black on white paper. Alternatively sharp photoprints may be provided. The lettering should be clear. Halftone illustrations may be included. They should be submitted as clear black and white prints on glossy paper. The figures should be individually identified lightly in pencil on the back. All legends should be brief and typed on a separate sheet.

*Tables*. These should have short descriptive titles, be self explanatory and typed on separate sheets. They should be as concise as possible and not larger than a Journal page. Values in tables should include as few digits as possible. In most cases, more than two digits after the decimal point are unnecessary. Units of measurements should be SI units. Unnecessary abbreviations should be avoided. Information given in tables should not be repeated in graphs and vice versa.

*Discussion*. The contribution of the work to the overall knowledge of the subject could be shown. Relevant conclusions should be drawn, and the potential for further work indicated where appropriate.

*Acknowledgements*. Appropriate acknowledgements may be included.

*Reprints*. Twenty copies of reprints will be given free to all the authors. Authors who require more reprints may obtain them at cost provided the Editorial Committee is informed at the time of submission of the manuscript.

**Correspondence**

All enquiries regarding the ASM Science Journal, submission of articles, including subscriptions to it should be addressed to:

The Editor-in-Chief
*ASM Science Journal*
Academy of Sciences Malaysia
902-4, Jalan Tun Ismail
50480 Kuala Lumpur, Malaysia.
Tel: 603-2694 9898; Fax: 603-2694 5858
E-mail: sciencejournal@akademisains.gov.my

**ASM SCIENCE JOURNAL**
**(ASM Sc. J.)**

**ORDER FORM**

**Subscription (Two issues per year)**

| | Malaysia | Other Countries |
|---|---|---|
| **Individual** | **RM100** | **USD50** |
| **Institution** | **RM200** | **USD100** |

1. Complete form and return.

Name/Institution: .....
(Please print)
.....
.....

Street Address: .....
.....
.....

City, Region: .....

Country, Postal Code: .....

2. Payment method: Cheque/Bank Draft/Postal Order/ Money Order No.: .....
   Payable to **"Akademi Sains Malaysia"**
   (Please include bank commission, if applicable)
   RM/USD: .....

3. For on-line purchasing, please access:
   http://www.akademisains.gov.my

Date: ..... Signature: .....

**Please send to:**
Academy of Sciences Malaysia
902-4, Jalan Tun Ismail
50480 Kuala Lumpur, Malaysia
Tel: 03-2694 9898; Fax: 03-26945858
E-mail: sciencejournal@akademisains.gov.my

ASM Science JOURNAL

In Pursuit of Excellence in Science

Affix
stamp
here

**Academy of Sciences Malaysia**
902-4, Jalan Tun Ismail
50480 Kuala Lumpur
Malaysia

## RESEARCH ARTICLES



## ANNOUNCEMENTS